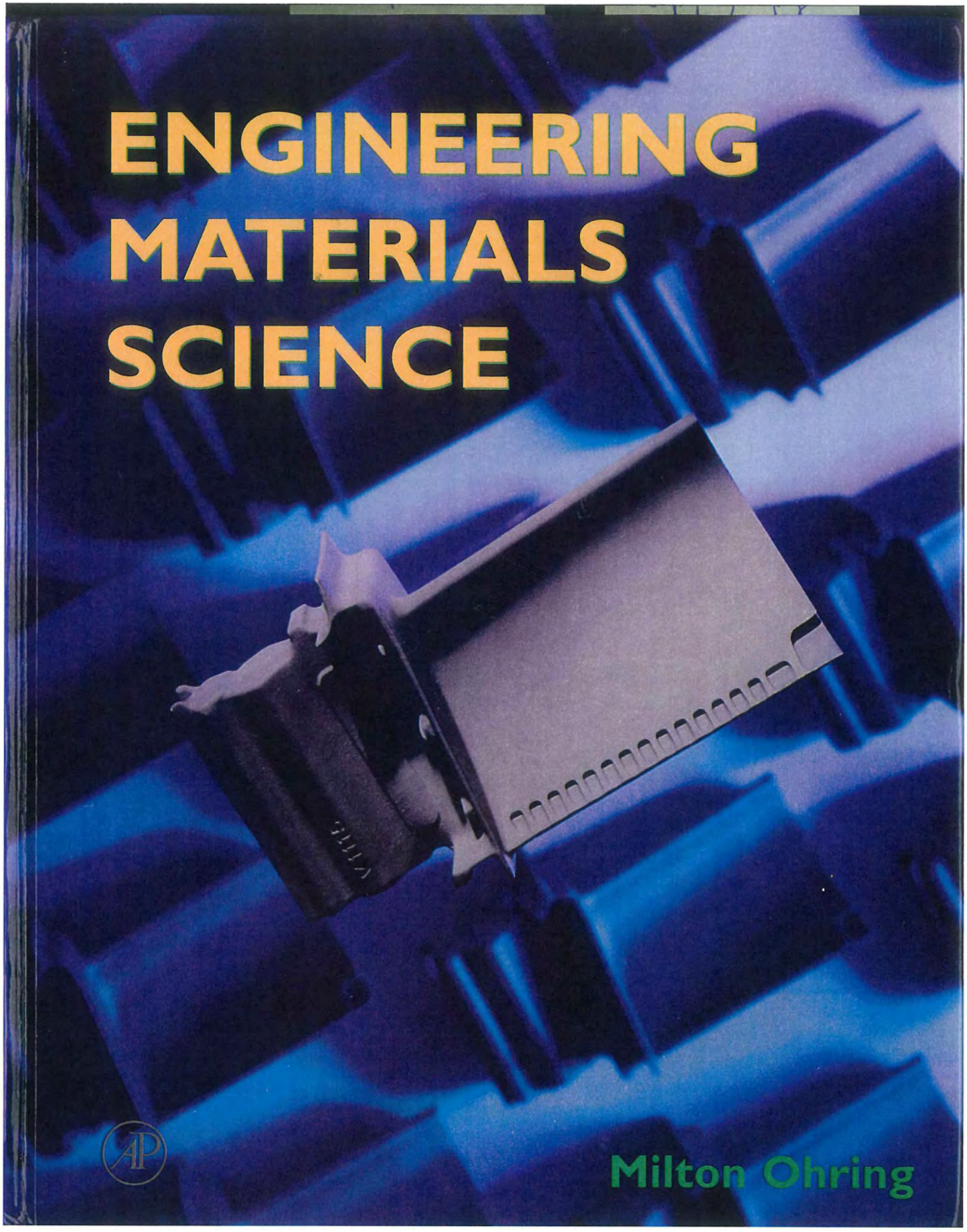

ENGINEERING MATERIALS SCIENCE

Milton Ohring

Department of Materials Science and Engineering
Stevens Institute of Technology
Hoboken, New Jersey

ACADEMIC PRESS

San Diego New York Boston London Sydney Tokyo Toronto

Front Cover Photograph: Single crystal superalloy turbine blades used in a jet aircraft engine (courtesy of Howmet Corporation).
Back Cover Photograph: Pentium microprocessor integrated circuit chip (courtesy of INTEL Corporation).
Both products rank among the greatest materials science and engineering triumphs of the 20th century.

This book is printed on acid-free paper. ♾

Academic Press, Inc.
A Division of Harcourt Brace & Company
525 B Street, Suite 1900, San Diego, California 92101-4495

United Kingdom Edition published by
Academic Press Limited
24-28 Oval Road, London NW1 7DX

Library of Congress Cataloging-in-Publication Data

Ohring, Milton, date.
Engineering materials science / by Milton Ohring.
p. cm.
Includes index.
ISBN 0-12-524995-0
1. Materials science. 2. Materials. I. Title.
TA403.037 1995
620.1'1--dc20 94-40228
CIP

PRINTED IN THE UNITED STATES OF AMERICA
95 96 97 98 99 00 DO 9 8 7 6 5 4 3 2 1

2 ELECTRONS IN ATOMS AND SOLIDS: BONDING

2.1. INTRODUCTION

It is universally accepted that atoms influence materials properties, but which subatomic portions of atoms (e.g., electrons, nuclei consisting of protons, neutrons) influence which properties is not so obvious. Before addressing this question it is necessary first to review several elementary concepts introduced in basic chemistry courses. Elements are identified by their atomic numbers and atomic weights. Within each atom is a nucleus containing a number of positively charged protons that is equal to the atomic number (Z). Circulating about the nucleus are Z electrons that maintain electrical neutrality in the atom. The nucleus also contains a number of neutrons; these are uncharged.

Atomic weights (M) of atoms are related to the sum of the number of protons and neutrons. But this number physically corresponds to the actual weight of an atom. Experimentally, the weight of Avogadro's number ($N_A = 6.023 \times 10^{23}$) of carbon atoms, each containing six protons and six neutrons, equals 12.00000 g, where 12.00000 is the atomic weight. One also speaks about **atomic mass units** (amu): 1 amu is one-twelfth the mass of the most common isotope of carbon, ^{12}C. On this basis the weight of an electron is 5.4858×10^{-4} amu and protons and neutrons weigh 1.00728 and 1.00867 amu, respectively. Once the atomic weight of carbon is taken as the standard, M values for the other elements are ordered relative to it. A mole of a given element weighs M grams and contains 6.023×10^{23} atoms. Thus, if we had

only 10^{23} atoms of copper, by a simple proportionality they would weigh $1/6.023 \times 63.54 = 10.55$ g (0.01055 kg). Note that the atomic weight of Cu, as well as most of the other elements in the Periodic Table including carbon, is not an integer. The reason for this is that elements exist as isotopes (some are radioactive, most are not), with nuclei having different numbers of neutrons. These naturally occurring isotopes are present in the earth's crust in differing abundances, and when a weighted average is taken, nonintegral values of M result. If compounds or molecules (e.g., SiO_2, GaAs, N_2) are considered, the same accounting scheme is adopted except that for atomic quantities we substitute the corresponding molecular ones.

EXAMPLE 1-1

a. What weights of gallium and arsenic should be mixed together for the purpose of compounding 1.000 kg of gallium arsenide (GaAs) semiconductor?

b. If each element has a purity of 99.99999 at.%, how many impurity atoms will be introduced in the GaAs?

Note: $M_{Ga} = 69.72$ g/mol, $M_{As} = 74.92$ g/mol, $M_{GaAs} = 144.64$ g/mol.

ANSWER a. The amount of Ga required is $1000 \times (69.72/144.64) = 482$ g. This corresponds to 482/69.72 or 6.91 mol Ga or, equivalently, to $6.91 \times 6.023 \times 10^{23} = 4.16 \times 10^{24}$ Ga atoms. Similarly, the amount of As needed is also 6.91 mol, or 518 g. The equiatomic stoichiometry of GaAs means that 4.16×10^{24} atoms of As are also required.

b. Impurity atoms introduced by Ga + As atoms number $2 \times (0.00001/100) \times 6.91 \times 6.023 \times 10^{23} = 8.32 \times 10^{17}$. Because the total number of Ga + As atoms is 8.32×10^{24}, the impurity concentration corresponds to 10^{-7}, or 1 part in 10 million.

Returning to the subatomic particles, we note that electrons carry a negative charge of -1.602×10^{-19} coulombs (C); protons carry the same magnitude of charge, but are positive in sign. Furthermore, an electron weighs only 9.108×10^{-28} g, whereas protons and neutrons are about 1840 times heavier. In a typical atom in which $M = 60$, the weight of the electrons is not quite 0.03% of the total weight of the atom. Nevertheless, when atoms form solids, it is basically the electrons that control the nature of the bonds between the atoms, the electrical conduction behavior, the magnetic effects, the optical properties, and the chemical reactions between atoms. In contrast, the subnuclear particles and even nuclei, surprisingly, contribute very little to the story of this book. Radioactivity, the effects of radiation, and the role of high-energy ion beams in semiconductor processing (ion implantation) are exceptions. One reason is that nuclear energies and forces are enormous compared with what

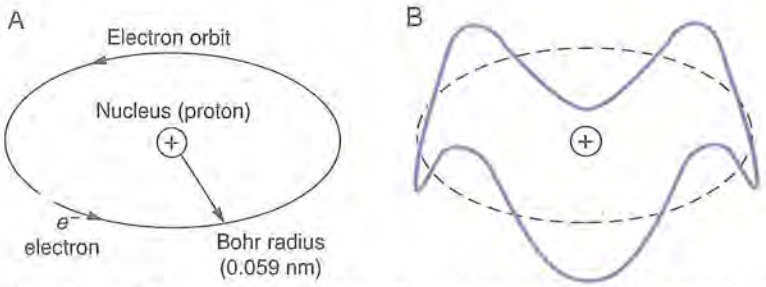

FIGURE 2-1 (A) Model of a hydrogen atom showing an electron executing a circular orbit around a proton. (B) De Broglie standing waves in a hydrogen atom for an electron orbit corresponding to $n = 4$.

atoms experience during normal processing and use of materials. Another reason is that the nucleus is so very small compared with the extent to which electrons range. For example, in hydrogen, the smallest of the atoms (Fig. 2-1A), the single electron circulates around the proton in an orbit whose radius, known as the Bohr radius, is 0.059 nm long [1 nm = 10^{-9} m = 10 Å (angstroms)]. The radius of a proton is 1.3×10^{-6} nm, whereas nuclei, typically $\sim M^{1/3}$ times larger, are still very much smaller than the Bohr radius. Before a pair of atomic nuclei move close enough to interact, the outer electrons have long since electrostatically interacted and repelled each other. The preceding considerations make it clear why the next topic addressed is the atomic electrons.

2.2. ATOMIC ELECTRONS IN SINGLE ATOMS

Before the role of electrons in solids can be appreciated it is necessary to understand their behavior in single isolated atoms. The simplest model of an atom assumes it to be a miniature solar system at whose center is a positively charged nucleus (the sun) surrounded by a cloud of orbiting negatively charged atomic electrons (the planets). Charge is distributed so that the atom is electrically neutral. We now know these atomic electrons display a complex dynamical behavior (the larger the Z, the more complex the behavior) governed by the laws of quantum mechanics. The underlying philosophy and mathematical description of quantum theory are quite involved. Nevertheless, the resulting concepts and laws that derive from them can be summarized for our purposes in terms of a few relatively simple equations and rules that are discussed in turn.

2.2.1. Wave/Particle Duality

The term *wave/particle duality* suggests that both particles and waves have a dual nature. For the most part particles (a baseball, a stone, an electron) obey the classical Newtonian laws of mechanics. Occasionally, however, they

reveal another, mysterious side of their character and behave like waves. An electron speeding down the column of an electron microscope produces such wavelike diffraction effects upon interaction with materials. Similarly, waves that exhibit standard optical effects like refraction and diffraction can surprisingly dislodge electrons from metals by impinging on them under certain conditions. Our first instinct is to attribute this **photoelectric effect** to a mechanical collision, attesting to the particle-like nature of waves. Wave/particle duality is expressed by the well-known de Broglie relationship

$$\lambda = h/p = h/mv. \tag{2-1}$$

In this important formula λ is the effective wavelength, and p is the momentum of the associated particle whose mass is m and velocity v. Planck's constant h ($h = 6.62 \times 10^{-34}$ J-s) bears witness to the fact that quantum effects are at play here.

The de Broglie relationship provides a way to rationalize the stability of electron orbits in atoms. Classically, circulating electrons ought to emit electromagnetic radiation, lose energy in the process, and spiral inward finally to collapse into the nucleus. But this does not happen and atoms survive in so-called **stationary states**. Why? If the de Broglie waves associated with the electron in hydrogen were **standing waves**, as shown in Fig. 2-1B, they would retain their phase, and orbits would persist intact despite repeated electron revolutions. But, if the waves did not close on themselves, they would increasingly interfere destructively with one another and, with each revolution, move more and more out of phase. Electron orbit disintegration would then be inevitable. This same notion of standing waves is used again later in the chapter (Section 2.4.3.2) to derive the energies of electrons in metals.

2.2.2. Quantized Energies

We know from experience that both particles (objects) and waves possess energy. The kinetic energies of gas molecules and the heating effects of laser light are examples. It outwardly appears that the energies can assume any values whatever. But this is not true. A fundamental law of quantum theory holds that energies of particles and waves, or more appropriately **photons**, can assume only certain fixed or quantized values. For photons, the energy is given by Planck's formula

$$E = h\nu = hc/\lambda. \tag{2-2}$$

Here ν is the frequency of the photon which travels at the speed of light c, where $c = \nu\lambda$ ($c = 2.998 \times 10^8$ m/s). Interestingly, the vibrations of atoms in solids give rise to waves or **phonons**, whose energies are given by a similar formula:

$$E = (n + \tfrac{1}{2})h\nu, \qquad n = 1, 2, 3, \ldots. \tag{2-3}$$

In this expression n is a quantum number that assumes integer values. This means that solids absorb and emit thermal energy in discrete quanta of $h\nu$ when their atoms vibrate with frequency ν. In solids, ν is typically 10^{13} Hz.

More relevant to our present needs is the fact that the energies of electrons in atoms are also quantized, meaning that they can assume only certain discrete values. The case of the single electron in the hydrogen atom may be familiar to readers. Here the energy levels (E) are given by the Bohr theory as

$$E = \frac{-2\pi^2 m_e q^4}{h^2 n^2} = \frac{-13.6}{n^2} \text{ eV}, \qquad n = 1, 2, 3, \ldots. \tag{2-4}$$

The electron mass and charge are m_e and q, respectively. Again, n is an integer known, in this case, as the principal quantum number. The closer they are to the nucleus, the lower the energies of the electrons. And because the electron energy inside the atom is less than that outside it (where the zero-energy-level reference is assumed), a negative sign is conventionally used. Resulting energy levels are enumerated in Fig. 2-2. At any given time only one level can be occupied. In an unexcited hydrogen atom the electron resides in the ground state ($n = 1$) while the other levels or states are vacant. Absorption of 13.6 eV of energy (1 eV/atom = 1.60×10^{-19} J/atom = 96,500 J/mol) will excite the electron sufficiently to eject it and thus ionize the hydrogen atom.

For other atoms a very crude estimate of the electron energies is given by

$$E = -13.6 Z^2/n^2 \text{ eV}, \qquad n = 1, 2, 3, \ldots, \tag{2-5}$$

where Z, the atomic number, serves to magnify the nuclear charge. The effect of core electron screening of the nuclear charge is neglected in this formula.

2.2.3. The Pauli Principle

In reality, multielectron atoms and hydrogen as well are more complicated than the simple Bohr model of Fig. 2-1. Electrons orbiting closer to the nucleus shield outer electrons from the pull of the nuclear charge. This complicates their motion sufficiently that different electrons are not at the same energy level; furthermore, electron energies are not easily calculated. In general, more advanced theories indicate that the electron dynamics within all atoms is characterized by four quantum numbers n, l, m, and s. These arise from solutions to the celebrated Schrödinger equation, a cornerstone of the modern quantum description of atoms. Specifically, the three-dimensional motion of electrons is embodied in the quantum numbers n, l, and m.

The **principal quantum number** is still n and it can assume only integer values 1, 2, 3, ..., as before. Electrons are now organized into shells. When $n = 1$ we speak of the K electron shell, while for the L and M shells, $n = 2$ and $n = 3$, respectively. As will become evident after introduction of the other quantum numbers, there are 2 electrons in the K shell, 8 in the L shell, 18 in the M shell, and so on.

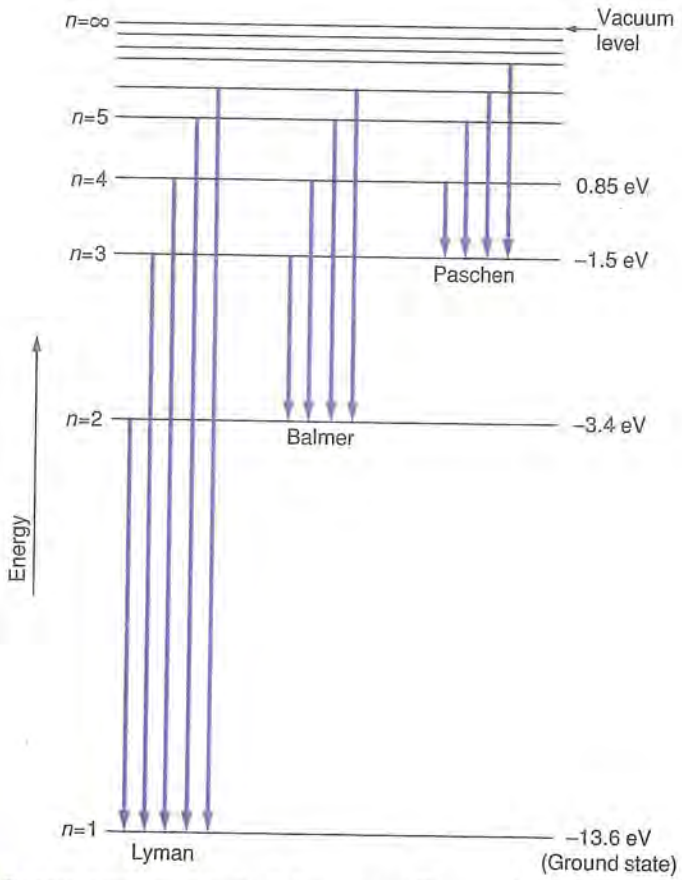

FIGURE 2-2 Electron energy levels in the hydrogen atom. The ground state corresponds to the electron level $n = 1$, with $E = -13.6$ eV. For the $n = \infty$ level, corresponding to $E = 0$, the electron has gained the 13.6 eV energy needed to ionize hydrogen. Electron transitions from upper levels to the $n = 1$ level are known to spectroscopists as the Lyman series; to the $n = 2$ level, the Balmer series; to the $n = 3$ level, the Paschen series.

The angular momentum arising from the rotational motion of orbiting electrons is also quantized or forced to assume specific values which are in the ratio of whole numbers. Recognition of this fact is taken by assigning to the **orbital quantum number** l values of 0, 1, 2, ..., $n - 1$. The shape of electron orbitals is essentially determined by the l quantum number. When $l = 0$ we speak of s electron states. These electrons have no net angular momentum, and as they move in all directions with equal probability, the charge distribution is spherically symmetrical about the nucleus. For $l = 1, 2, 3, \ldots$, we have corresponding p, d, f, ... states.

A third quantum number, m, specifies the orientation of the angular momen-

tum along a specific direction in space. Known as the **magnetic quantum number,** m takes on integer values between $+l$ and $-l$, that is $-l, -l+1, \ldots, +l-1, +l$.

Lastly there is the **spin quantum number,** s, in recognition of the fact that electrons spin as they simultaneously orbit the nucleus. Because there are only two orientations of spin angular momentum, up or down, m assumes $-\frac{1}{2}$ and $+\frac{1}{2}$ values. We return to electron spin in Chapter 14 in connection with ferromagnetism.

The Pauli principle states that no two electrons in an atom can have the same four quantum numbers.

Let us apply the Pauli principle to an atom of sodium. As $Z = 11$ we have to specify a tetrad of quantum numbers (n, l, m, s) for each of the 11 electrons:

$1s$ states (K shell)	$(1, 0, 0, +\frac{1}{2})$ and $(1, 0, 0, -\frac{1}{2})$;
$2s$ states (L shell)	$(2, 0, 0, +\frac{1}{2})$ and $(2, 0, 0, -\frac{1}{2})$;
$2p$ states (L shell)	$(2, 1, 0, +\frac{1}{2})$, $(2, 1, 0, -\frac{1}{2})$, $(2, 1, 1, +\frac{1}{2})$, $(2, 1, 1, -\frac{1}{2})$, $(2, 1, -1, +\frac{1}{2})$, and $(2, 1, -1, -\frac{1}{2})$;
$3s$ state (M shell)	$(3, 0, 0, +\frac{1}{2})$.

Another way to identify the electron distribution in sodium is $1s^2\,2s^2\,2p^6\,3s^1$ and similarly for other elements. In shorthand notation the integers and letters are the principal and orbital quantum numbers, respectively, and the superscript number tells how many electrons have the same n and l values.

2.2.4. Electron Energy Level Transitions

The atomic model that has emerged to this point includes a set of electrons, each having a unique set of numbers that distinguishes it from others of the same atom. Furthermore, the energies of the electrons depend primarily on n and, to a lesser extent, on l. This means that an electron energy level scheme like that for hydrogen (Fig. 2-2) exists for every element. In the case of hydrogen the electron in the ground state ($n = 0$) can make a transition to an excited state provided (1) the state is vacant, and (2) the electron gains enough energy. The energy needed is simply the difference in energy between the two states.

Likewise, energy is released from a hydrogen atom when it is deexcited, a process that occurs when an electron descends from an occupied excited state to fill an unoccupied lower-energy state. Photons are frequently involved in both types of transitions as schematically indicated in Fig. 2-3. If the energy levels in question are E_1 and E_2, such that $E_2 > E_1$, then

$$E_2 - E_1 = \Delta E = h\nu_{12} = hc/\lambda. \tag{2-6}$$

As a computational aid, if ΔE is expressed in electron volts and λ in micrometers, then

$$\Delta E \text{ (eV)} = 1.24/\lambda \text{ } (\mu\text{m}). \tag{2-7}$$

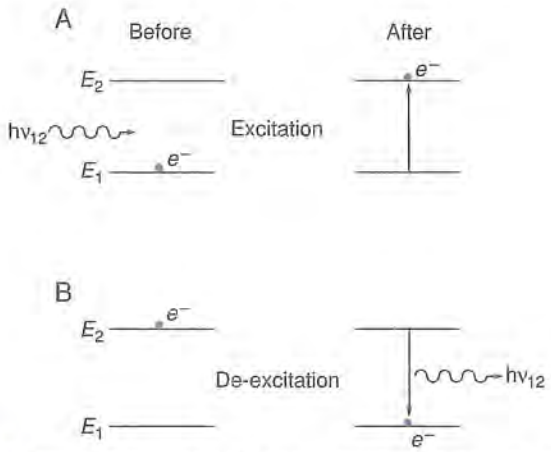

FIGURE 2-3 Schematic representation of electron transitions between two energy levels: (A) Excitation. (B) Deexcitation.

EXAMPLE 2-2

What is the wavelength of the photon emitted from hydrogen during an $n = 4$ to $n = 2$ electron transition?

ANSWER Using Eq. 2-4, $\Delta E = E_4 - E_2 = -13.6\ (1/4^2 - 1/2^2) = 2.55$ eV. From Eq. 2-7, $\lambda = 1.24/\Delta E = 1.24/2.55 = 0.486\ \mu$m. This wavelength of 486 nm, or 4860 Å, falls in the blue region of the visible spectrum.

2.2.5. Spatial Distribution of Atomic Electrons

It makes a big difference whether electrons move freely in a vacuum as opposed to being confined to orbit atoms. For one thing, in the former case electron motion is usually viewed in classical terms. This means that the electron can have any energy; there is no quantum restriction that limits energies to only certain fixed values as is the case for electrons confined to atoms. We also imagine that the actual location of classical electrons is very precisely limited to coincide within their intrinsic dimensions. According to quantum mechanics and, in particular, the Heisenberg uncertainty principle,

$$\Delta p \cdot \Delta x = h/2\pi, \tag{2-8}$$

this view is too simplistic. Rather, Eq. 2-8 suggests that the more precisely the electron momentum p is known, the less we know about its position x, and vice versa. The Δ's in Eq. 2-8 represent the uncertainties in p and x.

A cardinal feature of the wave mechanics approach in quantum theory is the notion that electron waves can have a presence or time-averaged charge

density that extends in space, sometimes well beyond atomic dimensions. We speak of wave functions that mathematically describe the regions where the electronic charge can most probably be found. If they could be observed with a microscope, the picture would be strange and bewildering. For example, pictorial representations of the geometrically complex charge distributions in hydrogen-like *s, p,* and *d* states are shown in Fig. 2-4. It takes some doing to imagine that a single electron can split its existence between two or more distinct locations simultaneously.

2.3. FINGERPRINTING ATOMS

The previously described electronic theory of atoms is not only the substance of textbooks and the culture of science. A number of very important and sophisticated commerical instruments have appeared in recent years that capitalize on the very concepts just introduced. Their function is to perform qualitative as well as quantitative analysis of atoms in very localized regions of solids. Developed largely for the semiconductor industry to characterize the composition of electronic materials and devices, their use has spread to include the analysis of all classes of inorganic and organic, as well as biological, materials. In this section we focus on the emission of both X rays and electrons and learn how to fingerprint or identify the excited atoms from which they originate. **Optical spectroscopy**, a science that has been practiced for a long time, also fingerprints atoms but by measuring the wavelength of visible light derived from low-energy, *outer*-electron-level transitions. In contrast **X-ray spectroscopy**, which we consider next, relies on emission of X rays from the deeper, high-energy **core** electron levels.

2.3.1. X-Ray Spectroscopy

There is hardly a branch of scientific and engineering research and development activity today that does not make use of a **scanning electron microscope** (SEM), shown in Fig. 2-5; many examples of remarkable SEM images are found throughout this book and others have been widely reproduced in the printed and electronic media. The SEM is more fully discussed in Section 3.6.3. Our interest in the SEM here is as a source of finely focused electrons that impinge on a specimen under study. This causes electronic excitations within a volume that typically extends 1000 nm deep and measures about 10^8 nm^3. Typical bacteria and red blood cells are considerably larger. Within the volume probed the chemical composition of impurity particles, structural features, and local regions of the matrix can be analyzed. The incident (~30-keV) electrons are sufficiently energetic to knock out atomic electrons from previously occupied levels as schematically indicated in Fig. 2-6. An electron from a more

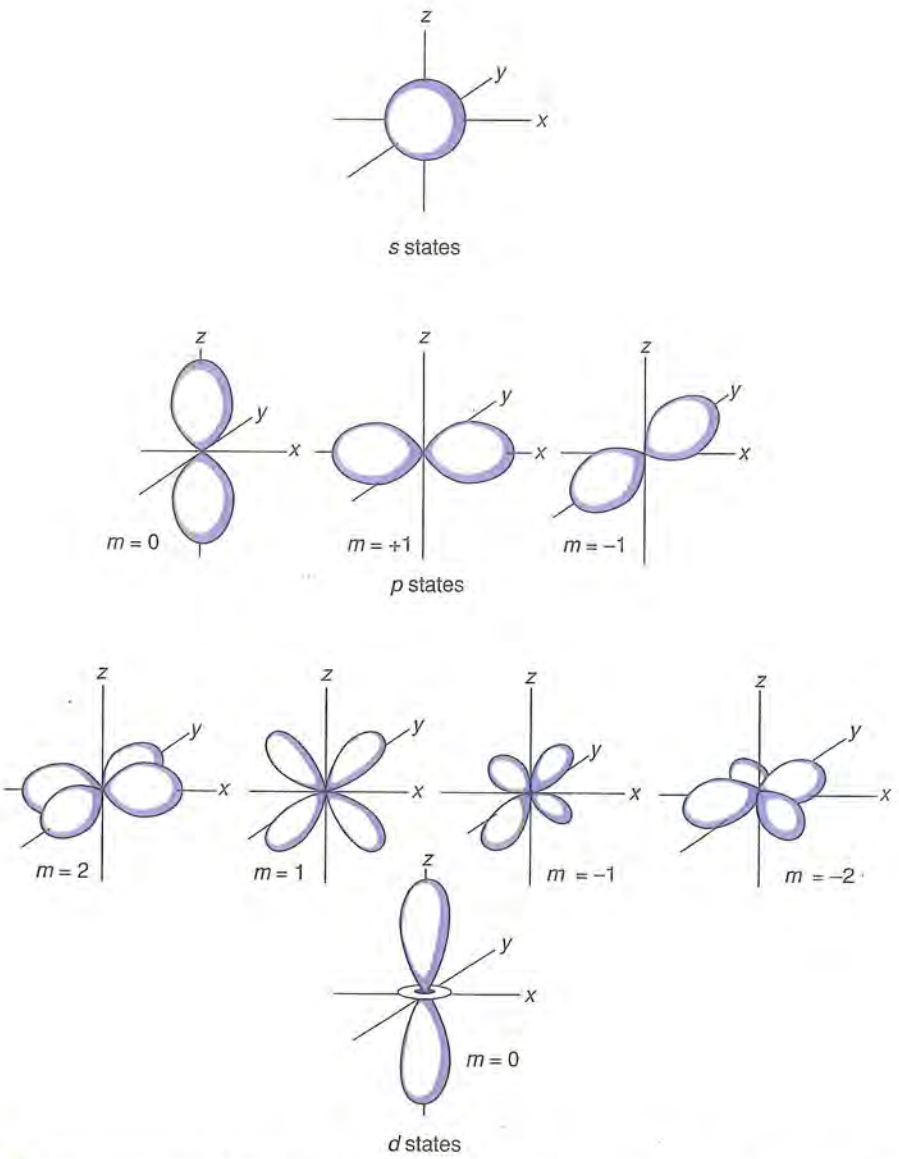

FIGURE 2-4 Pictorial representation of the charge distribution in hydrogen-like *s*, *p*, and *d* wavefunctions. *s* states are spherically symmetrical, whereas *p* states have two charge lobes, or regions of high electron density extending along the axes of a rectangular coordinate system. *d* states typically have four charge lobes.

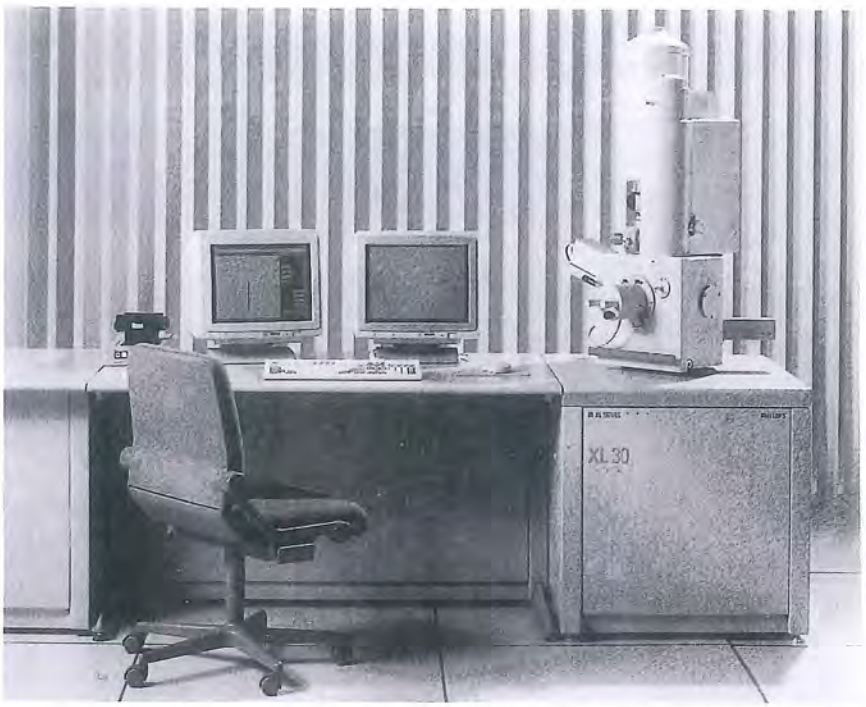

FIGURE 2-5 Photograph of a modern scanning electron microscope with X-ray energy dispersive analysis detector. The left- and right-hand monitors display the X-ray spectrum and specimen image, respectively. Operation of the SEM is controlled by a personal computer. Courtesy of Philips Electronic Instruments Company, a Division of Philips Electronics North America Corporation.

energetic level can now fall into the vacant level, a process accompanied by the emission of a photon.

To see how this works in practice, consider the electron energy level diagram for titanium metal depicted in Fig. 2-7A, where values for the energies of *K*, *L*, and *M* electrons are quantitatively indicated.

EXAMPLE 2-3

If an electron vacancy is created in the *K* shell of Ti and an L_3 electron fills it, what are the energy and wavelength of the emitted photon?

ANSWER This problem is identical in spirit to Example 2-2. The energy of the photon is $E_{L_3} - E_K = [-455.5 - (-4966.4)] = 4510.9$ eV. By Eq. 2-7, this corresponds to a wavelength of 2.75×10^{-4} μm, or 0.275 nm. Therefore, the photon is an X ray spectrally identified as K_α. The X-ray emission spectrum diagram for Ti is shown in Fig. 2-7B.

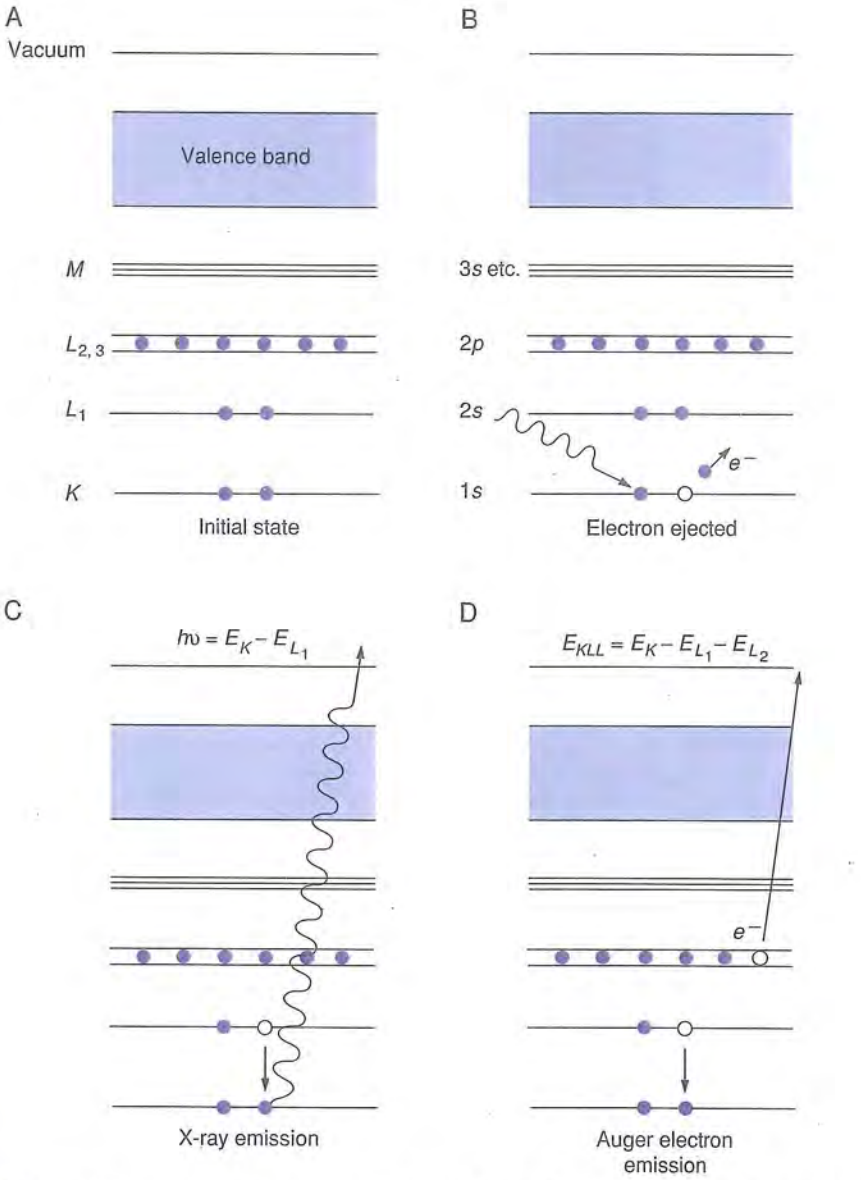

FIGURE 2-6 Schematic representation of electron energy transitions: (A) Initial state. (B) Incident photon or electron ejects *K*-shell electron. (C) X-ray emission when 2*s* electron fills vacant level. (D) Auger electron emission process.

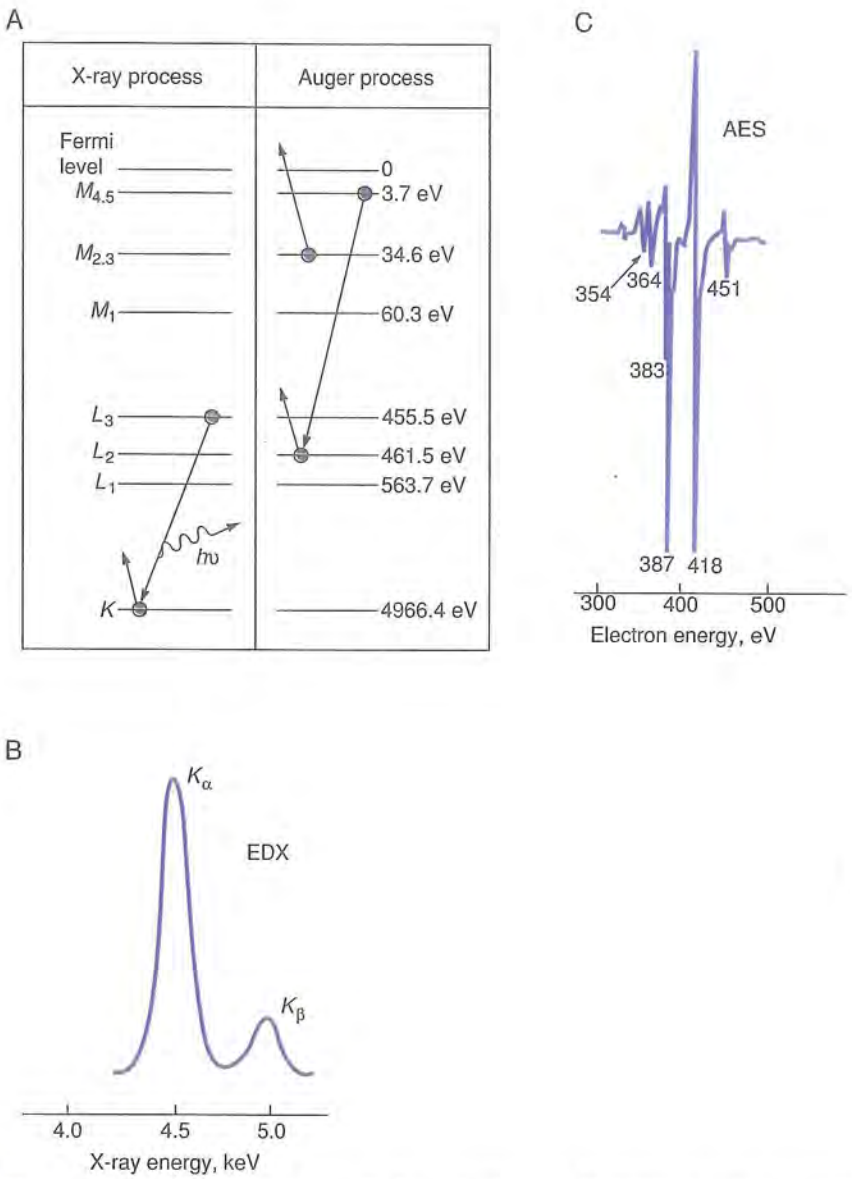

FIGURE 2-7 Electron excitation processes in titanium. (A) Energy level scheme. All electron energies are negative in magnitude. (B) X-ray emission spectrum of Ti. Only the K_α and K_β lines are shown. (C) Auger electron spectral lines for Ti.

During analysis, the electron beam actually generates electron vacancies in all levels. Therefore, many transitions occur simultaneously, and instead of a single X-ray line there is an entire spectrum of lines. Each element has a unique X-ray spectral signature that can be used to identify it unambiguously. Importantly, high-speed pulse processing electronics enables multielement analysis to be carried out simultaneously and in a matter of seconds. X rays emitted from the sample are sensed by a nearby cryogenically cooled semiconductor photon detector attached to the evacuated SEM column and analyzed to determine their energy spectrum. Results are displayed as a spectrum of signal intensity versus X-ray energy, hence the acronym **EDX** (Energy Dispersive X ray) for the method. For multielectron atoms, Eq. 2-5 suggests that core levels for many useful elements can be expected to have X-ray energies of tens of kilo-electron volts. Extensive tables of the X-ray emission spectra of the elements exist to aid in materials identification.

An allied technique makes use of incident energetic X-ray or gamma ray photons, rather than electrons. They also induce identical electron transitions and X-ray emission, so that from the standpoint of identification of atoms, there is no difference. This so-called **X-ray fluorescence** technique is used when the specimen cannot withstand electron bombardment or when it is not feasible to place it into the vacuum chamber of an SEM. Chemical analyses of pigments in oil paintings and inks in paper currency have been made this way to expose forgeries.

2.3.2. Auger Electron Spectroscopy

Electron transitions within and between outer and core electrons are involved in the technique of Auger electron spectroscopy (AES), as indicated in Fig. 2-6D. But, unlike EDX where X-ray photons are emitted, so called Auger (pronounced oh-zhay) electrons are released in AES. A low-energy electron beam (~2 keV) impinges on the specimen and creates the initial vacancy that is filled by an outer electron; however, the photon that is normally created never exits the atom. Instead, it transfers its energy to another electron, the Auger electron. A collection of Auger electrons with varying intensity and unique energies does emerge to establish the wiggly spectrum that is the unambiguous signature of the atom in question. The AES spectrum for Ti is shown in Fig. 2-7C. Because core and not valence (or chemical bonding) electrons are involved in both EDX and AES, it makes little difference in which chemical state the Ti atoms exist: pure Ti, $TiAl_3$, TiO_2, $(C_5H_5)_2$ TiI_2, and so on. Titanium is detected independently of the other elements to which it is bonded.

What makes AES so special is that the low-energy Auger electrons can penetrate only ~1–2 nm (10–20 Å) of material. This means that AES is limited to detection of atoms located in the uppermost 1- to 2-nm-thick surface layers of the specimen. Because it is a surface-sensitive technique, extreme cleanliness and a very high vacuum environment are required during analysis to prevent

FIGURE 2-8 Photograph of an Auger electron spectrometer. Courtesy of Perkin–Elmer Physical Electronics Division.

further surface contamination. The atomic detection limit of both EDX and AES techniques is about 1%. In the case of AES where the incident electron beam spot size is ~100 nm, the volume sampled for analysis is $[\pi\ (100)^2/4] \times 1 = 7850\ \text{nm}^3$, which corresponds to about 400,000 atoms. Thus, under optimum conditions it is possible to detect about 4000 impurity atoms in the analysis. This astounding capability does not come cheaply, however. The commercial AES spectrometer shown in Fig. 2-8 costs more than half a million dollars. Auger analysis is used to determine the composition of surface films and contaminants in semiconductors, metals, and ceramics. An example of its use is shown in Fig. 2-9.

Despite the fact that sophisticated analytical methods have been introduced here, both EDX and AES rely on energy transitions involving core electron levels. In closing, our debt to the framers of the quantum theory of electrons in atoms should be appreciated.

2.4. ELECTRONS IN MOLECULES AND SOLIDS

2.4.1. Forming a Hydrogen Molecule

What happens to the atomic electrons when two or more widely separated atoms are brought together to form a molecule? This is an important question

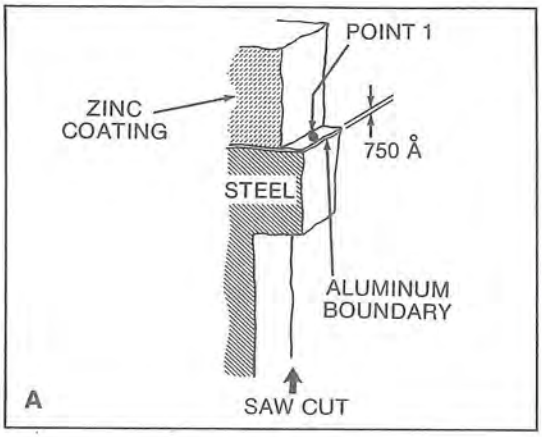

C

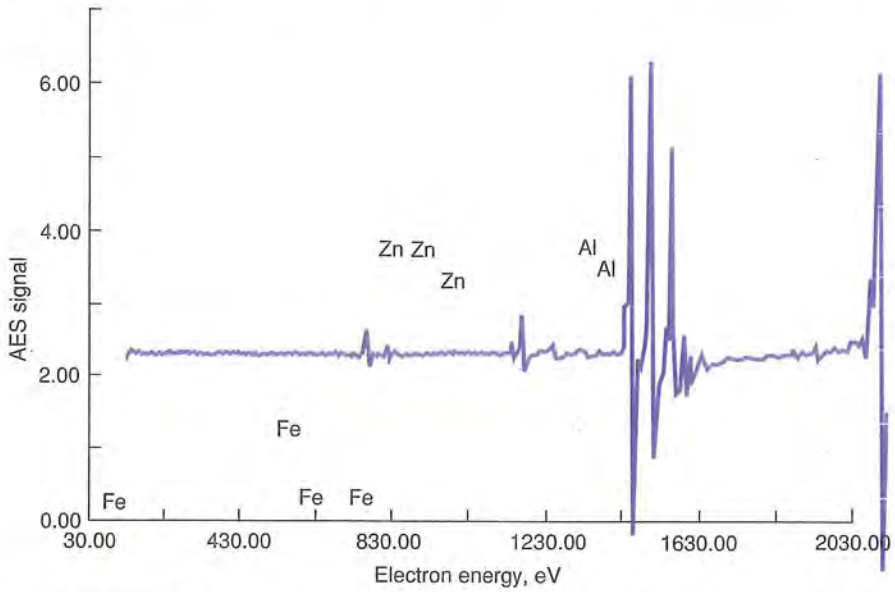

FIGURE 2-9 Case study involving AES. In hot-dip galvanizing, steel acquires a protective zinc coating after being dipped into a molten Zn bath. The iron and zinc react to form a compound that sometimes flakes off during fabrication. To prevent Fe–Zn reaction, 0.10% aluminum is added to the Zn bath. The very thin Al-rich layer that forms prevents the two metals from reacting. (A) The test specimen in this application shown schematically. (B) A magnified image of the Al-rich layer is analyzed at point 1. (C) The resulting AES spectrum detected at point 1 reveals the presence of Al. Courtesy of Perkin–Elmer Physical Electronics Division.

because by extension to many atoms, we can begin to understand condensation to the solid state. Whatever else happens, however, there must be a final overall reduction in the total energy of individual atoms when they interact and form stable molecules or solids. The quantum theories involved are very complex. One approach stresses replacement of **atomic orbitals** or wavefunctions by an equal number of **molecular orbitals.** To see how this works, let us consider two distant atoms of hydrogen (H) that are brought together to form a hydrogen molecule (H_2). Focusing only on the spherically symmetric 1*s* charge distribution, we note little change in each atom as long as they are far apart. But when they move close enough so that the two 1*s* charge clouds overlap, the rules of quantum chemistry suggest two new molecular charge distributions. In the first of these, the electron density is enhanced in the region between the nuclei (Fig. 2-10A). This preponderance of negative charge binds the positively charged nuclei together; an energy reduction occurs in this so-called **bonding orbital.** In Fig. 2-10B the second possibility is shown. Here the electron charge density is enhanced on the side of each nucleus away from the other nucleus. Because little negative charge is left between the positive nuclei, the latter strongly repel each other on approach, and the energy rises. This is the case of the **antibonding orbital.** The overall electron energy versus distance of approach for both orbitals is shown in Fig. 2-10C. Of note are the energy minimum and stable molecular configuration for the bonding orbital. But when the nuclei move too close, their mutual electrostatic repulsion begins to exceed the attraction caused by the electron density between them, and the energy rises.

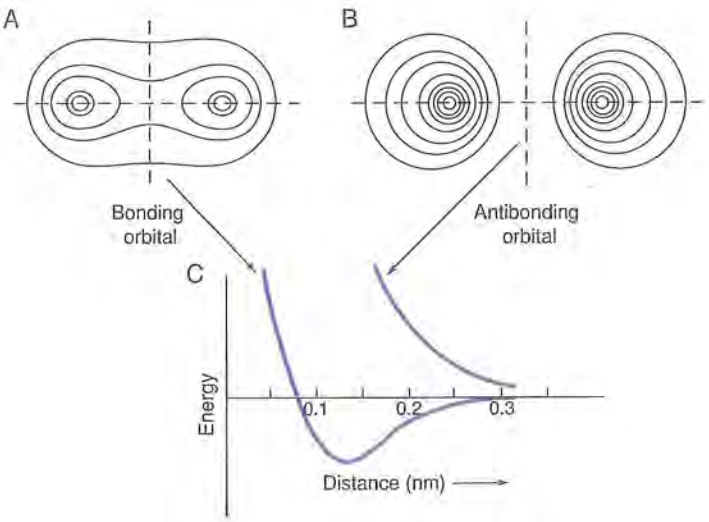

FIGURE 2-10 (A) Representation of electron cloud contours in the two-hydrogen-atom **bonding** orbital. There is a high electron density between the protons. (B) Representation of electron cloud contours in the two-hydrogen-atom **antibonding** orbital. The electron density between the protons is low. (C) Electron energies of the bonding and antibonding orbitals as a function of the internuclear distance.

In summary, recurring themes in the remainder of this chapter are:

1. The splitting of one energy level into two (or more generally, N levels for N electrons)
2. The minimum in the energy at an interatomic distance corresponding to the stable molecule (or solid)
3. The rise in energy when the nuclei approach too closely.

2.4.2. Electron Transfer in Ionic Molecules

At a higher level of complexity consider the formation of a LiF molecule through interaction between initially distant and neutral lithium and fluorine atoms (Fig. 2-11). As we all know, Li is extremely reactive chemically (especially with water) because of the strong tendency to shed its $2s$ valence electron. But this does not happen normally because Li can be stored as metal. An **ionization energy** of 5.4 eV is required to remove the electron and create a Li^+ ion. Similarly, the F atom exhibits a strong **electron affinity**, meaning that incorporation of an electron into its incomplete $2p$ shell is encouraged because it leads to an energy reduction of 3.6 eV. Interestingly, during ionization, the Li atom radius shrinks from 0.157 to 0.078 nm as it becomes a Li^+ ion. The reason is that the higher effective charge on the nucleus in the ion causes it to draw the remaining electrons toward it. Alternately, a lower effective nuclear charge in F^- causes the ion to expand to 0.133 nm from the initially uncharged F atomic radius of 0.071 nm. Information on atomic and ionic radii of the elements is given in Appendix A. Unlike the symmetrical electronic charge distribution in the hydrogen molecule, the electron density in the bonding orbital is large close to F^- and small near Li^+. The reverse is true for the antibonding orbital.

It should be noted that during electron transfer between these atoms as they draw close, there is actually a surprising *increase* in energy of 5.4 eV − 3.6 eV = 1.8 eV! Why do they then react to form molecules? The answer is that the ions are not as close to each other as they could be. Account must be taken of the electrostatic force of attraction between the ions, which falls off with the distance (r) between them as r^{-2}. The potential energy of interaction (U) associated with the force between these point charges is given by

$$U = \frac{-q^2}{4\pi\varepsilon_0 r}, \tag{2-9}$$

where ε_0 is a constant (known as the permittivity of vacuum) that has a value of 8.85×10^{-12} C/V-m. As r shrinks, Eq. 2-9 reveals that a point is reached where $U = -1.8$ eV, and the energy is recovered; bringing the ions closer together lowers the energy further, leading to the net energy reduction required for bonding. But, if the Li and F ions are squeezed together even more tightly, the energy rises. This time the negatively charged, core electron clouds begin to repel each other. These repulsive forces have a very short range and hence their contribution to U is assumed to vary with r as $+Br^{-n}$, where both B and

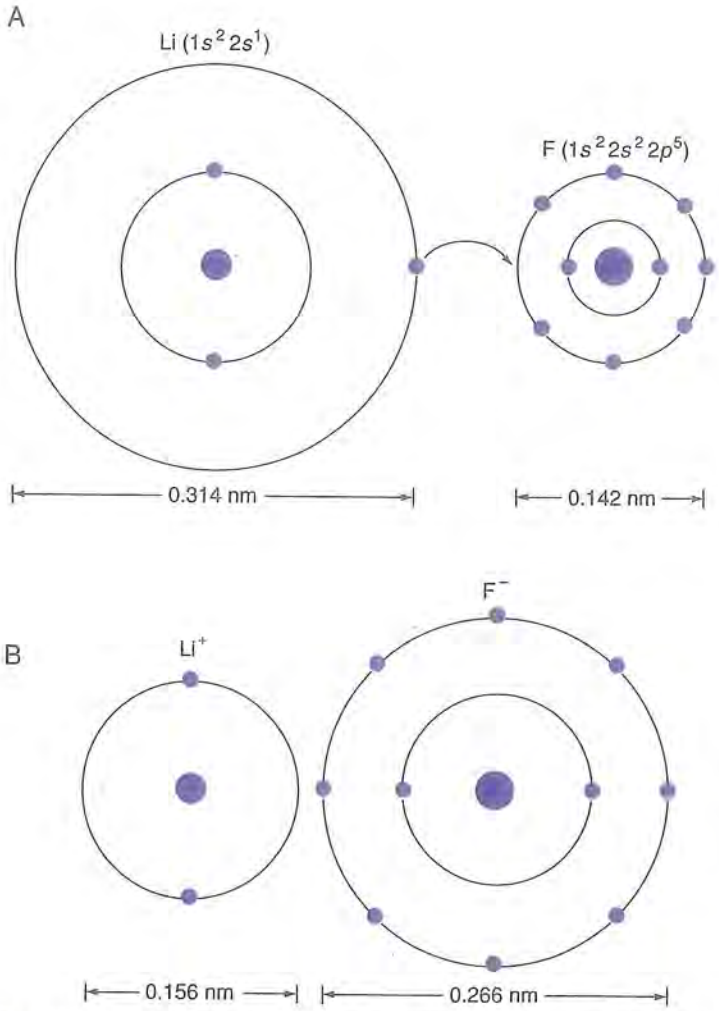

FIGURE 2-11 Formation of a LiF molecule. (A) Electronic structure and size of the isolated lithium and fluorine atoms. (B) Electron transfer from Li to F creating an ionic bond between Li^+ and F^- ions.

n are constants. Because n typically ranges from 5 to 10, as r shrinks r^{-n} rises very rapidly, as seen in Fig. 2-12. Therefore, by adding attractive and repulsive components

$$U = -q^2/4\pi\varepsilon_0 r + Br^{-n}. \tag{2-10}$$

Nature knows how to strike a compromise, however, and the equilibrium distance r_0 prevails in the molecule when the attractive and repulsive forces balance; r_0 can be calculated by minimizing U with respect to r. Simple differen-

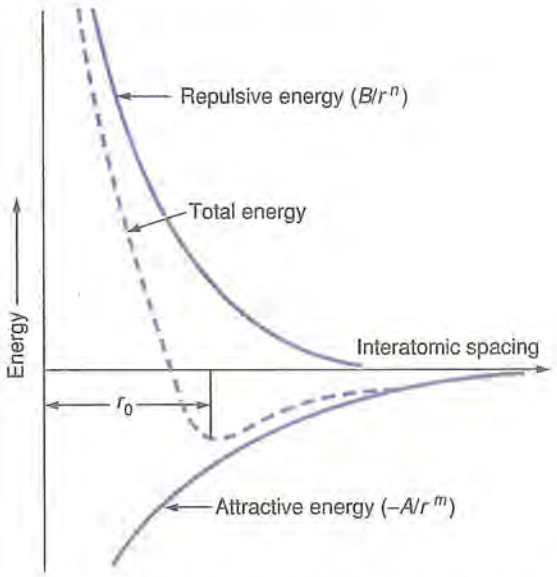

FIGURE 2-12 Potential energy of interaction between two ions or atoms as a function of interatomic spacing. For two monovalent ions of opposite charge, $A = q^2/4\pi\varepsilon_0$, and $m = 1$.

tiation and solving for r yields $r_0 = (4\pi\varepsilon_0 nB/q^2)^{1/(n-1)}$, when $dU/dr = 0$. The quantity $q^2/4\pi\varepsilon_0$ is evaluated to be 2.30×10^{-28} N-m^2, a number that will be useful in Example 2-5.

The model just presented is essentially classical in that quantum theory was not used in any significant way. Nevertheless, a simple extension of these ideas is all that is needed to quantitatively describe the bonding of electropositive and electronegative ions, not in a single molecule, but in alkali halide solids containing huge numbers of atoms. This is done in Section 2-5.

2.4.3. Electrons in Metals

2.4.3.1. Core Electrons

Electrons in metals experience a fate different from that of electrons in ionic materials. Neutral metal atoms have electron complements like those shown for Ti (Fig. 2-7). As the individual metal atoms approach each other they do not transfer electrons, one to the other—alkali halide style—because this is not profitable energetically. Rather, both the core and the outer electrons begin to interact because of electrostatic effects, At any distance of approach the $1s$ electrons of a given atom will interact less with the core $1s$ electrons of surrounding atoms than will the corresponding pairs of $2s$ electrons. The reason, of course, is that the outer $2s$ electrons will be closer to each other. And similarly, $2p$ and $3s$ electrons will interact even more strongly than $2s$ electrons.

Their charge clouds extend further from the nucleus, allowing greater overlap with the electron clouds of the neighboring atoms. As the interatomic separation distance is reduced, the strength of the electronic interactions intensifies in proportion to the extent of overlap.

The resultant alteration of individual electron levels is shown for sodium metal in Fig. 2-13. Broadening of initially discrete levels is the key feature of this figure; it occurs as a consequence of the Pauli principle. Atomic electrons within the interaction volume are forbidden to have the same four quantum numbers n, l, m, and s. Instead, the quantum numbers for each electron assume slightly different values. This changes the overall electron energy in the process; in fact, energies are split into as many levels as there are electrons. Some new levels are higher than the original one, elevating the energy and contributing to antibonding effects; but importantly, new lower energy levels are produced and they are in the majority. As a reuslt, atoms are bound together in the solid because a net energy reduction is achieved.

What emerges are **energy bands**, one for each of the original discrete atomic electron levels, that now contain enormous numbers of very closely spaced energy levels. The highest and lowest of these energy levels define the bandwidth, which changes as a function of interatomic spacing (Fig. 2-13). As before, very complex compromises are made to offset the attractive and repulsive interactions between electrons and ion cores. In sodium and metals of higher Z, the lower-energy core level bandwidths are narrow and do not overlap. It

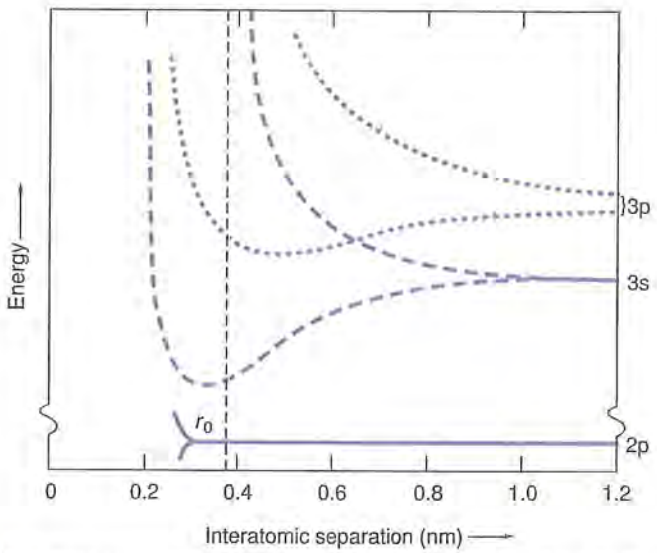

FIGURE 2-13 Calculated overlapping 3*s* and 3*p* energy levels in sodium metal as a function of interatomic separation. After J. C. Slater.

is only the high-energy atomic electron levels that tend to be broadly split and experience overlap at the equilibrium spacing in the solid.

2.4.3.2. Conduction Electrons

The outermost valence electrons of metal atoms undergo similar, but even more extensive splitting than the core electrons. Because the properties of these electrons are so critical to the bonding, chemical, and electrical properties of metals as well as semiconductors, they are variably known as **valence** or **conduction** electrons. They have been the subject of much theoretical and experimental study and a simplified description of their properties is presented here.

One may imagine that a well or box of length L with impenetrable walls, shown in Fig. 2-14A, encloses this dense collection of electrons (e.g., one per atom) that are totally **delocalized** from the atoms. It is the nature of metals not to tolerate voltage differences or gradients across them but to develop a short circuit instead. Therefore, it is reasonable to assume that these electrons only see a constant electric potential (V), whose magnitude we may take to be zero everywhere. But electrons at zero potential are, by definition, free, and the de Broglie relationship implies they ought to have waves associated with them. If an electron moving in the x direction is considered, the longest wavelength (λ) it can have is $2L$. Because the electron changes velocity (v) as it reflects from each wall, all of its possible associated waves have nodes there. The amplitude of these waves must vanish at the walls because electrons can never extend past them. This is a consequence of the essentially infinite value of V outside the well.

In order of decreasing wavelength, the allowable values of λ are

$$\lambda = 2L/1,\quad 2L/2,\quad 2L/3,\quad 2L/4,\quad 2L/5, \ldots, 2L/n_x \qquad (n_x = \text{integer}), \qquad (2\text{-}11)$$

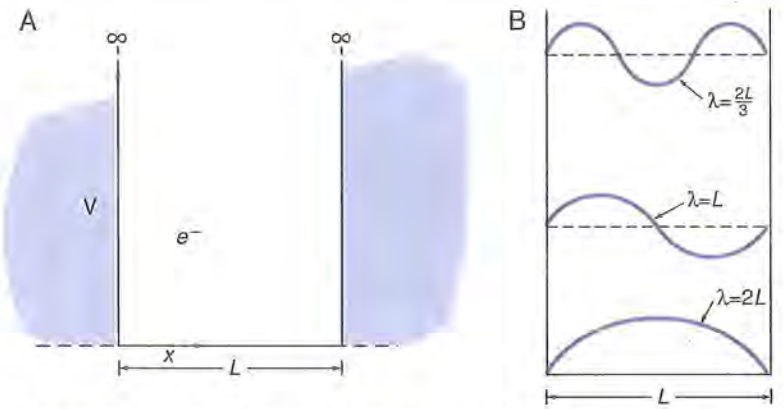

FIGURE 2-14 (A) An electron *particle* in a cubic box that has impenetrable walls. (B) Allowed electron wavefunctions for the particle in the box.

as indicated in Fig. 2-14B. Mathematically they can be represented as sine waves of the form $A \sin 2\pi x/\lambda$, where x is the distance from the left wall and A is a constant. The kinetic energy of these electrons is given by

$$E = \tfrac{1}{2} m_e v^2 = \frac{p^2}{2m_e}. \tag{2-12}$$

As $\lambda = h/p$ (Eq. 2-1), combination of Eqs. 2-1, 2-11, and 2-12 yields

$$E = \frac{h^2 n_x^2}{8m_e L^2}. \tag{2-13}$$

In this formula n_x is an effective quantum number that describes electron motion or wave propagation in the x direction. If account is taken of similar behavior in the y and z directions by including quantum numbers n_y and n_z in Eq. 2-13, the result is simply

$$E = h^2 (n_x^2 + n_y^2 + n_z^2)/8m_e L^2. \tag{2-14}$$

As with atoms, four quantum numbers are still involved but the rules for selecting them are much simpler. Each electron state is defined by a triad of integer quantum numbers (n_x, n_y, n_z) and contains two electrons with antiparallel spins, $+\frac{1}{2}$ and $-\frac{1}{2}$. Conduction electrons must also obey the Pauli principle; therefore, no two electrons can have the same four quantum numbers.

EXAMPLE 2-4

a. How many conduction electron states are there in a cube of gold 1.0 cm^3 in volume?

b. Identify the 10 lowest quantum states.

c. What is the energy spacing between the two lowest levels?

d. Suppose that one of the states having the highest energy has quantum numbers $n_x = 3.83 \times 10^7$, $n_y = 0$, and $n_z = 0$. What is the highest occupied energy level?

ANSWER a. Each Au atom contributes one $6s$ conduction electron. Dimensional analysis shows that the number of Au atoms per cubic centimeter is $N_{Au} = N_A$ (atoms/mol) $\times \rho$ (g/cm^3)/M_{Au} (g/mol). For Au, $M_{Au} = 197$ and ρ (the density) = 19.3 g/cm^3. After substitution, $N_{Au} = 6.023 \times 10^{23} \times 19.3/(197) = 5.90 \times 10^{22}$ cm^{-3}. This number of electrons can be accommodated in half as many, or 2.95×10^{22} states, because of the two spin orientations.

b. The 10 lowest quantum states are [100], [010], [001], [110], [101], [011], [111], [200], [020], and [002]. Only 20 electrons can occupy these 10 states as each state accommodates two electrons. Equation 2-14 indicates that many of these different states (e.g., the first three) have the same energy. This phenomenon, known as *degeneracy*, is common for large values of E because there are many equivalent combinations of the sums of squares of three numbers. It is obvious that the conduction electron distribution is highly degenerate.

c. The lowest energy is $E_{100} = h^2\{1 + 0 + 0\})/8m_eL^2$. After substitution, $E_{100} = (6.62 \times 10^{-34}\ \text{J-s})^2 \times 1/[8 \times (9.11 \times 10^{-31}\ \text{kg}) \times (10^{-2}\ \text{m})^2] = 6.01 \times 10^{-34}\ \text{J} = 3.75 \times 10^{-15}$ eV. The next higher energy level is E_{110} with twice the energy or 7.50×10^{-15} eV. Therefore, the spacing between levels is 3.75×10^{-15} eV.

d. After substitution in Eq. 2-14, $E = \{(6.62 \times 10^{-34})^2 \times [(3.83 \times 10^7)^2 + 0 + 0]\}/[8 \times (9.11 \times 10^{-31}) \times (10^{-2})^2] = 8.82 \times 10^{-19}$ J, or 5.51 eV. The width of the band is the difference in energy between highest and lowest levels, or 5.51 eV.

This illustrative example is instructive for a number of reasons. From it one can appreciate the sort of numbers that describe electrons in metals. In even a tiny specimen there are huge numbers of them and they populate an extremely densely spaced set of discrete states. Because 10^{22} to 10^{23} electrons per cubic centimeter are compressed into a band that has an energy spread of only ~5 eV, the conduction electrons are imagined to populate a continuum of states and described in such terms as free electron gas or sea.

The elementary picture of metals that emerges views the ion cores as being immersed within a conduction electron sea. The latter also serves as a kind of glue that binds the nuclei together in the solid. Electrons move readily in response to very small applied dc voltages or electric fields, and this accounts for the high electrical conductivity of metals. High reflectivity of metals is also a consequence of the free electrons. When visible light shines on a metal the electromagnetic radiation excites these electrons to higher energy levels. But, as they fall back to lower levels, photons are reemitted as reflected light. The role of the free electrons in electrical conduction and other electronic and optical phenomena within metals and semiconductors is addressed again in Chapters 11, 12, and 13.

In real metals, electrons are not so hopelessly confined to the impenetrable well of the above example. It is possible to transfer some electrons from metals into an adjacent vacuum by heating them to a sufficiently high temperature. The operation of vacuum tubes, including the TV picture tube, depends on this **thermionic emission** of electrons. As noted earlier, incident photons will also remove electrons provided they have sufficient energy. In both cases "sufficient" means the **work function energy** ($q\Phi$), a kind of electrostatic barrier that prevents conduction electrons from leaving the metal. A frequently assumed model for the electron structure of metals is depicted in Fig. 2-15, where the work function is typically 2–5 eV. Values for the highest occupied electron energy level (**Fermi energy**) and work function distinguish different metals.

2.4.4. Electrons in Covalent Materials

2.4.4.1. Nonmetals

Electrons in many important engineering materials like diamond, Si, GaAs, polymers, and SiC participate in covalent bonding effects. But substances like

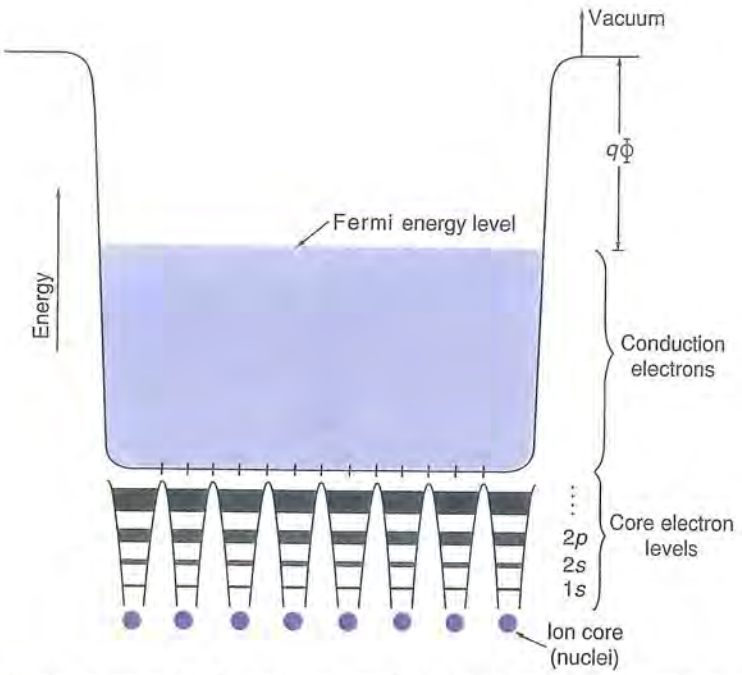

FIGURE 2-15 Simple electron model of a metal consisting of individual unbroadened and broadened atomic core levels, surmounted by a distribution of conduction electrons.

H_2, which was treated above, F_2, and CH_4, together with hundreds of thousands of organic molecules, also exhibit covalent bonding. This type of bonding relies on neighborly sharing of electrons. Bond energies and lengths have been determined for a great number of covalently bonded atomic pairs and are listed in Table 2-1.

For elements to bond covalently they must have at least a half-filled outer electron shell, for example, half of eight or four electrons in outer s plus p electron states. In the case of a chlorine atom there are seven such electrons (two $3s$ plus five $3p$). Two Cl atoms share one electron between them and thus attain the eight necessary to fill each outer shell and achieve a stable Cl_2 bonding configuration. To generally account for the number of covalent bonds required between elements a rule has been formulated: *If the group number of the Periodic Table in which the element falls is N, then 8 − N covalent bonds are necessary to complete the outer electron shell.* On this basis, Cl ($N = 7$) requires one and C($N = 4$) requires four covalent bonds.

2.4.4.2. Semiconductors

Elements in the fourth column of the Periodic Table are the most important examples of covalent solids from an engineering standpoint. For this reason

TABLE 2-1 COVALENT BOND ENERGIES[a] AND LENGTHS

Bond	Energy (kcal/mol)	Energy (kJ/mol)	Bond length (nm)
C—C	81	340	0.154
C=C	148	620	0.134
C≡C	194	810	0.120
C—H	100	420	0.109
C—N	69	290	0.148
C—O	84	350	0.143
C=O	172	720	0.121
C—F	105	440	0.138
C—Cl	79	330	0.177
O—H	110	460	0.097
O—O	33	140	0.145
O=O	96	400	0.121
O—Si	103	430	0.16
N—O	43	180	0.12
N—H	103	430	0.101
H—H	105	440	0.074
Cl—Cl	57	240	0.199
H—Cl	103	430	0.127

[a] Energy values are approximate as they depend on chemical environment. All values are negative for bond formation (energy is released) and positive for bond breaking (energy is absorbed).
Source: J. Waser, K. N. Trueblood, and C. M. Knobler, *Chem One*, 2nd ed., McGraw–Hill, New York (1980).

let us consider what happens to the electrons when silicon atoms are brought close together to form the solid. At first, electrons stemming from the same energy level (e.g., $3s$–$3s$ and $3p$–$3p$) overlap and split as described previously. But as atoms draw even closer electrons do not solely overlap with electrons of the same orbit. Rather, $3s$ and $3p$ electrons overlap or mix in a significant way to yield the energy band structure shown in Fig. 2-16. This phenomenon is known as **hybridization** and leads to four hybridized electron orbitals that radiate outwardly from each silicon atom in a manner suggested by Fig. 2-17A for diamond (which has the same structure) and explicitly in Fig. 3-6A. Each of these electrons pairs off with another like itself from neighboring silicon atoms to cement strongly directed covalent bonds. Complete electron sharing means that eight electrons will now surround each silicon atom and totally fill all of its four valence band states. There are no more electrons to go around and, therefore, the conduction band is empty. Unlike the situation for Na (Fig. 2-13) at the equilibrium distance (r_0), there is now a gap in the electron energy levels. There are no electron states and, therefore, no electrons possessing energies within the span defined by the energy gap, E_g.

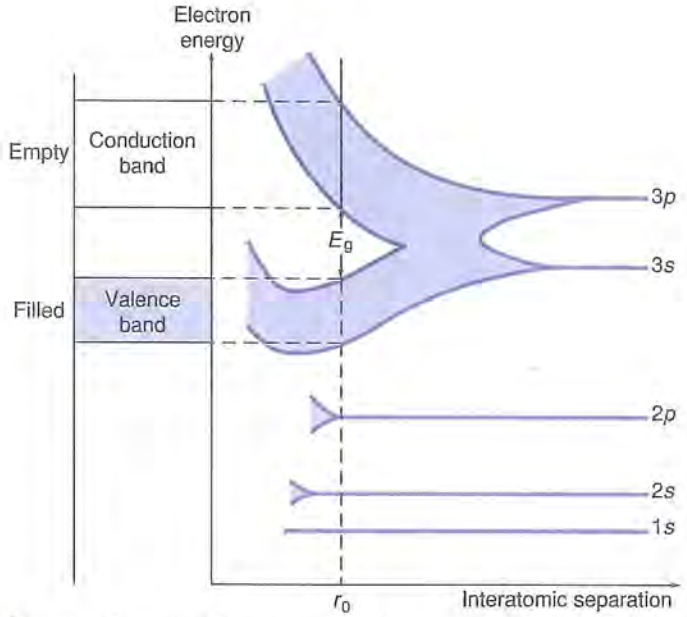

FIGURE 2-16 Formation of energy bands in silicon as isolated atoms are brought together. The admixture or hybridization of the 3*s* and 3*p* electrons leaves an energy gap in the bands at the equilibrium spacing.

In order of increasing electron energy the picture that emerges at 0 K is:

1. Unbroadened 1*s*, 2*s*, and 2*p*, core levels.
2. A much broadened, filled band of admixed 3*s*–3*p* states commonly known as the **valence band**
3. An **energy gap**
4. A broadened, empty **conduction band** of admixed 3*s*–3*p* states

Electrons in diamond and germanium have similar band structures and display comparable covalent bonding effects. One difference is that 2*s*–2*p* and 4*s*–4*p* hybridized states are involved respectively in C and Ge. And whereas the energy gap (E_g) is 1.12 eV in silicon, E_g = ~6 eV in C and E_g = 0.68 eV in Ge. The low expenditure of energy required to promote electrons into the conduction band facilitates charge motion and makes solid-state semiconductor devices possible. Further discussion of the implications of the electronic structure of semiconductors is deferred until Chapter 12.

2.4.4.3. Carbon

Carbon is a truly remarkable element that exists in a number of polymorphic forms, each possessing strikingly different structures and properties. It has already been noted that carbon atoms in diamond form covalent bonds with one another the way silicon atoms do. The four tetrahedral bonds reflect the

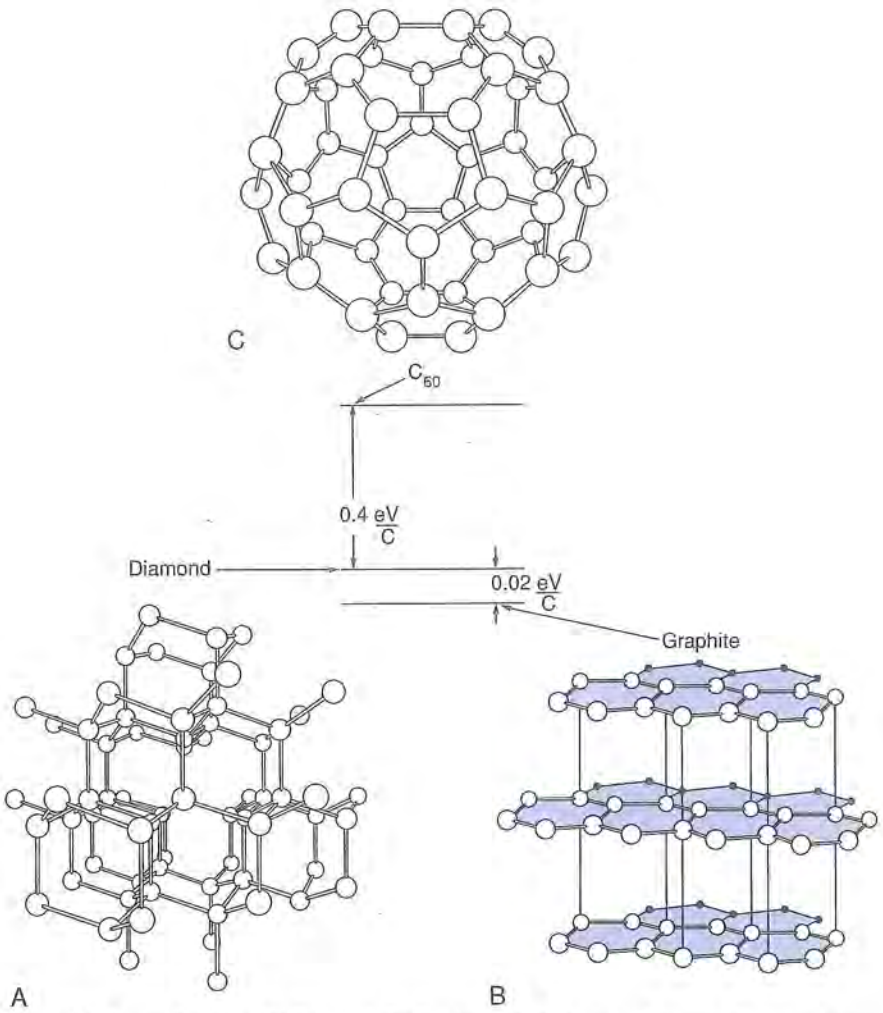

FIGURE 2-17 Polymorphic forms of carbon: (A) Diamond. (B) Graphite. (C) Buckminsterfullerenes. The inset shows that in order of increasing carbon bond stability are the polymorphs C_{60}, diamond, and graphite. After A. H. Hebard, AT&T Bell Laboratories.

geometric configuration; electronically, the bonds consist of four so-called sp^3 hybridized orbitals. The latter confer diamond's fabled hardness and high stiffness. With no conduction electrons, diamond is a poor conductor of electricity. Recent years have witnessed a plethora of new diamond materials that have been prepared in bulk and thin film form. Varied applications include abrasive grit for grinding, hard cutting tools for machining, and wear-resistant coatings on computer hard disk drives.

Graphite, another polymorphic form of carbon, consists of a hexagonal layered structure (Fig. 2-17B). Instead of three-dimensional tetrahedral bonding as in diamond, each carbon atom shares electrons with three other coplanar carbon atoms. In the planes or layers, strong covalent bonds hold atoms together. Weaker, so-called van der Waals forces (see Section 2.5.2) emanating from the fourth electron act normal to these layers. They serve to bond the layers to one another, but not strongly, accounting for the slippery, lubricated feel of graphite. This is the reason for the **anisotropic** behavior of graphite, meaning it exhibits different properties depending on direction. Desirable properties include chemical inertness, high electrical conductivity, stiffness, and temperature stability, as well as a low thermal expansion coefficient and density. These attributes are the basis of graphite use in furnace crucibles, large electrodes, electrical contacts, and engineering composites. Normally graphite is formed by subjecting carbon black particles, tar, pitch, resins, and other materials to the extremely high temperature of ~2500°C, where it is the stable form of carbon.

A last and intriguing polymorph of carbon was discovered in 1985 and has the structure shown in Fig. 2-17C. Years earlier Buckminster Fuller invented the geodesic dome. As this architectural structure bears a strong resemblance to the depicted molecules, the latter are known as *buckminsterfullerenes*; and because they resemble a soccer ball, they are also known as *bucky balls*. The molecule is composed of no fewer than 60 carbon atoms, and denoted by C_{60}. Each carbon atom bonds covalently to three others, forming both hexagonal and pentagonal rings. Presently a scientific curiosity, applications for C_{60} are being explored.

Unlike these polymorphs, carbon also bonds to elements other than carbon (e.g., H, O, N, S) in hydrocarbons and organic compounds. Polymeric materials are the most important engineering examples and they are introduced in Chapter 4.

2.5. BONDING IN SOLIDS

2.5.1. Interaction of Atomic Pairs

Until now a mostly microscopic view of solids has emerged in terms of behavior of individual atomic electrons. Next in the structural hierarchy are individual atoms. Interestingly, there is a way of differentiating solids based on *atomic* interactions that parallels interactions between *electrons*. The similarity lies in the nature of the potential energy of interaction (U) between electrons or atoms as their distance of separation (r) is reduced. Complexities of quantum electron levels, energies, and charge distributions are replaced in favor of the integrated response of a pair of atoms. These are assumed to interact in a classical manner that can be described in mathematically simple

ways. We have already considered bonding in an ionic **molecule** using this approach in Section 2.4.2. Additionally, Figs. 2-10, 2-12, 2-13, and 2-16 should be contrasted for their distinctions and compared for their similarities.

The huge collection of atoms that condense to form a solid is very different from an interacting pair of atoms that form a molecule. But there still are attractive and repulsive forces exerted by neighboring atoms. With little loss in generality, what is true for a pair of interacting atoms can be extended to the entire solid. A commonly employed expression for U, applicable to atoms in solids, is given by

$$U = -A/r^m + Br^{-n}, \tag{2-15}$$

where A, B, m, and n are constants. As before, the second term represents the repulsive interaction between atoms while the first term is the corresponding attractive contribution to binding. If $m = 1$ we have the case of the alkali halide solid. Although A, B, and n generally have different values in the ionic solid compared with the molecule (Eq. 2-10), a plot of Eq. 2-15 resembles that of Fig. 2-12. In condensed materials with weaker secondary bonds that keep molecules attached to one another (e.g., polymers, ice, liquid gases), m and n are frequently taken as 6 and 12, respectively. A number of physical associations can then be made using Eq. 2-15 and they are considered in turn.

2.5.1.1. Equilibrium Distance of Atomic Separation (r_0)

The equilibrium distance of atomic separation (r_0) was considered previously in Section 2.4.1. Differentiating U with respect to r yields $dU/dr = mA/r^{m+1} - nB/r^{n+1}$. At the equilibrium separation, $dU/dr = 0$, and solving yields for the critical value of r ($=r_0$),

$$r_0 = (nB/mA)^{1/(n-m)}. \tag{2-16}$$

In crystalline solids r_0 can be associated with the lattice parameter a, of which more will be said in the next chapter.

2.5.1.2. Binding Energy (U_0)

In forming a solid, N widely spaced atoms in a gas phase can be imagined to condense according to the chemical reaction

$$NG \rightarrow NS + U_0,$$

where G and S refer to the gas and solid atoms. In the process there is an energy reduction of amount U_0. Usually known as the **binding** or **bonding** energy, it is given by the depth of the energy trough. If generalized to a mole of atoms, U_0 would refer to the molar energy to break bonds and decompose the solid. The reason can be seen by considering the reverse chemical reaction where input of (thermal) energy U_0 would cause S to convert to G, and atoms to separate from r_0 to $r = \infty$. A practical measure of the magnitude of U_0 is the heat liberated when elements react to form the solid. The sublimation

energy of the solid (energy to transfer atoms from the solid to the vapor) is another widely used measure of U_0. Both measures of U_0 are entered in Table 2-2 for selected solids. Experimentally, U_0 is generally proportional to the melting temperature of the solid. Substitution of r_0 (Eq. 2-16) into Eq. 2-15 yields a theoretical estimate of U_0, provided A and B are known.

2.5.1.3. Forces between Atoms

In mechanical systems the force F is often equivalent to $-dU/dr$. But this quantity was already calculated above and is given by

$$F = -dU/dr = -a/r^M + br^{-N}, \tag{2-17}$$

where $a = mA$, $b = nB$, $M = m + 1$, and $N = n + 1$. The equations repesenting F and U are thus algebraically similar. So is the plot of F versus r (Fig. 2-18A), but it is shifted to the right of the U–r curve. This curve must cross the axis, or be zero at $r = r_0$, the equilibrium spacing, because the forces of atomic attraction balance those of repulsion at this critical distance. If the F–r curve is flipped over (as in Fig. 2-18B), it is now consistent with easy-to-visualize force displacement behavior; more importantly, it resembles the stress–strain curve, a representation used in Chapter 7.

TABLE 2-2 VALUES OF MELTING POINT (T_M), BINDING ENERGY (U_0), YOUNG'S MODULUS (E_y), AND COEFFICIENT OF THERMAL EXPANSION (α) FOR SELECTED MATERIALS

Material	T_M (°C)	U_0 (kJ/mol)[a]			E_y (GPa)	α (10^{-6} °C^{-1})
NaCl	801	765*	413**	211***	49	40
KCl	776	688*	436**	198***		100
LiF	842	988*	612**	269***	112	
MgO	2800	3891*	603**		293	13.5
SiO_2	1710		879**		94	0.5
Al_2O_3	2980		1674**		379	8.8
Si_3N_4	1900		749**		310	2.5
WC	2776				720	4.0
Diamond	~4350			713***	1050	1
Si	1415			366***	166	3
Ge	937			384***	129	
Al	660			319***	70	22
Cu	1083			338***	115	17
Fe	1534			398***	205	12
W	3410			~770***	384	4.4
Polyethylene					~0.35	~150
Nylon					~2.8	~100

[a] The three measures of U_0 are physically different: * Energy liberated upon formation from the ions at 298 K. ** Heat liberated upon formation from the elements (atoms) at 298 K. *** Heat of sublimation.
Data were taken from various sources.

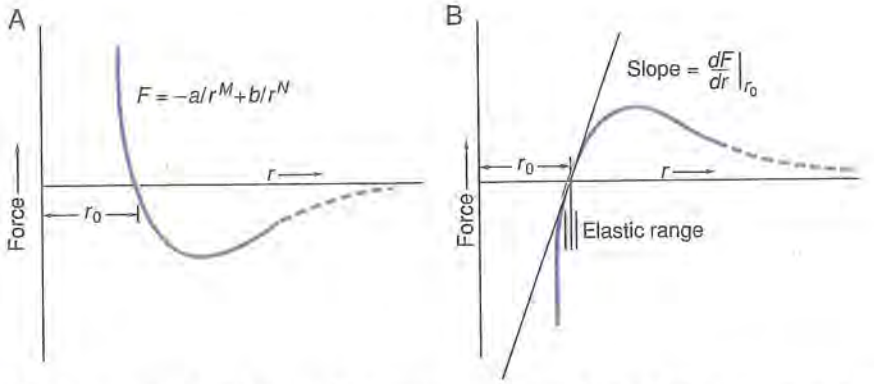

FIGURE 2-18 Force between atoms as a function of the interatomic spacing. (A) Plot of $F = -dU/dr$ versus r. (B) Plot of $F = +dU/dr$ versus r. The range of elastic response is indicated.

Let us focus our attention on the unloaded solid, that is, $F = 0$, $r = r_0$. If the solid is extended by pulling or applying a tensile load, atomic bonds are stretched and $r > r_0$. And similarly, if the solid is compressed, atoms are squeezed together and the bonds contract. If these loads are not too high and then removed, the solid snaps back elastically like a spring. In fact, atomic bonds are often thought of as springs whose dynamical behavior is familiar. For an atomic displacement of $\delta = r - r_0$, the force on the atomic bonds is given by $F = -k_S(r - r_0)$, where k_S is the spring constant. The negative sign means that a positive δ establishes an oppositely directed restoring force. A mathematical definition of the spring constant is $k_S = -(dF/dr)_{r=r_0}$, and this is equivalent to $k_S = (d^2U/dr^2)_{r=r_0}$. For a given δ, atomic forces between atoms are large when k_S is large; this is the case in stiff solids. For example, average atomic bonds in bronze (a copper–tin alloy) are stiffer than those in lead, and this is reflected in the choice of the former metal in bells.

2.5.1.4. Young's Modulus

Solids are placed in a state of **stress** by applying external loads to their surfaces, in which case they **strain**. Just how these loads are transmitted through the solid to exert forces on and stretch individual atomic bonds is not obvious. Nevertheless, extending the spring analogy, we may write a similar relationship between the stress and strain. Although these terms are defined more precisely in Chapter 7, stress is defined here as $-F/r_0^2$ (or bond force per unit *atomic* area). Similarly, the dimensionless strain is assumed to be defined by δ/r_0. **Hooke's law** expresses the fact that stress is linearly proportional to strain, that is, $-F/r_0^2 = E_y\delta/r_0$. The constant of proportionality, E_y, is known as the elastic or **Young's modulus** and is given by $-r_0^{-1}F/\delta$. But $F = -dU/dr$ and $\delta \sim dr$, so that E_y can be approximately expressed as $E_y \sim -r_0^{-1}(dF/dr)_{r_0}$ or

$$E_y \sim r_0^{-1}(d^2U/dr^2)_{r_0}. \tag{2-18}$$

Materials whose U vs r curves are deeply set (large U_0) and highly curved at r_0 tend to be stiff and have high elastic moduli. Physically, strains are small in high-E_y materials because the steep U vs r walls imply a sharp energy increase with r.

Young's moduli of selected materials are listed in Table 2-2. In general the higher the melting point of the solid, the larger the modulus of elasticity.

EXAMPLE 2-5

a. How does Young's modulus depend on r_0 in alkali halide solids?

b. If the equilibrium distance between Na and Cl ions in rocksalt is 0.282 nm (2.82×10^{-10} m), estimate the binding energy of a single NaCl molecule if it is assumed that $n = 9.4$.

ANSWER a. Young's modulus is given by $E_y \sim -(1/r_0)\,(dF/dr)_{r_0}$. Differentiation of Eq. 2-17 with respect to r_0 yields $(dF/dr)r_0 = m(m+1)A/r_0^{m+2} - n(n+1)B/r_0^{m+2}$. Through Eq. 2-16, the constants B and A are related by $B = (mA/n)r_0^{(n-m)}$. Substituting for B yields $(dF/dr)r_0 = m(m-n)A/r_0^{m+2}$, or $E_y = -m(m-n)A/r_0^{m+3}$.

In alkali halides $m = 1$ and, therefore, E_y varies as $\sim 1/r_0^{1+3} = r_0^{-4}$. The predicted dependence of E on the inverse fourth power of r_0 has been observed.

b. In NaCl, $m = 1$ and $A = q^2/4\pi\varepsilon_0 = 2.30 \times 10^{-28}$ N − m^2. Simple substitution of the expression for r_0 (Eq. 2-16) into Eq. 2-15 yields $U_0 = -Ar_0^{-m}\,(1 - m/n)$ after a bit of algebra. Upon evaluation, $U_0 = -2.30 \times 10^{-28}\,(2.82 \times 10^{-10})^{-1}\,(1 - 1/9.4) = 7.29 \times 10^{-19}$ N − m (J). For a mole of Na^+–Cl^- ion interactions, $U_0 = -6.02 \times 10^{23} \times 7.29 \times 10^{-19} = -439$ kJ.

A value of U_0 for *solid* NaCl based on experiment is −765 kJ/mol. The cause of the discrepancy is the neglect of an exactly calculable factor known as the *Madelung constant*. This constant, related to the geometry of the electrostatic interaction of all the Na^+ and Cl^- ions in the ordered solid state, has a value of 1.748 in the rocksalt structure (See Fig. 3-7). Multiplying by this factor yields $U_0 = -1.748 \times 439 = -767$ kJ/mol, in excellent agreement with experiment. Note that U_0 refers here to the energy reduction when *ions* (not *atoms*) condense to a solid (see Table 2-2).

2.5.1.5. Thermal Expansion

When atoms in a solid vibrate they undergo displacements that are limited by the walls of the U versus r potential well. Imagine a perfectly *symmetrical* or parabolic well; the thermally induced atomic motion in the positive and negative r directions will always average to $r = r_0$. And as the temperature is raised the amplitude of vibration increases but the average value of r is still r_0. Hence there is no thermal expansion.

Consider, however, what happens when the potential well is *asymmetrical*, as shown in Fig. 2-19. At temperature T_1 the average displacement or midpoint between the well walls falls slightly to the right of r_0. And at T_2 ($T_2 > T_1$) the average position lies even further to the right of r_0, and so on. In this case the material thermally expands.

All materials expand to one extent or another when heated and the coefficient of thermal expansion (α) is the material property that measures this tendency. By definition

$$\alpha = \frac{1}{L}\frac{dL}{dT}, \tag{2-19}$$

where L is a unit length of material. Because the attractive portion of the U vs r curve is less steep than the repulsive component, the displacement of the mean equilibrium position relative to r_0 increases with T, and α has a positive value. Thermal expansion coefficients for selected materials are listed in Table 2-2. In general, small coefficients of thermal expansion are observed in high-melting-point materials and vice versa.

EXAMPLE 2-6

Show that Young's modulus decreases with temperature, i.e., $dE_y/dT < 0$.

ANSWER To demonstrate this we use the formula $E_y = (-m(m-n)A)/r_0^{m+3}$ from illustrative problem Example 2-5. Differentiating, $dE_y/dT = +[m(m-n)A(m+3)/r_0^{m+4}]\,(dr_0/dT)$. If r_0 is substituted for L, then by Eq. 2-19, $\alpha = (1/r_0)(dr_0/dT)$. Finally, $dE_y/dT = +[m(m-n)A(m+3)/r_0^{m+3}]\,\alpha$. Because $n > m$, and all other terms are positive including α, the sign of dE_y/dT is negative.

The decline in E_y with a rise in T is indeed observed in materials. This subject is addressed again in Section 7.2.4.

2.5.2. Bonding Classifications

In Chapter 1 it was mentioned that metals, ceramics, semiconductors, and polymers constitute our engineering materials. Indeed, the remainder of the book is devoted to their properties. But from a scientific standpoint there are other ways to classify solids. Of the main bonding categories in this new classification scheme—**metallic, covalent,** and **ionic**—three have already been introduced. But nature only broadly tolerates classification schemes, the less so when so few categories are available to compartmentalize so much phenomena.

Metals like Au, Ag, and Cu, covalent solids like diamond, and ionic materials like NaCl and other alkali halides are reasonably pure exemplars of the three

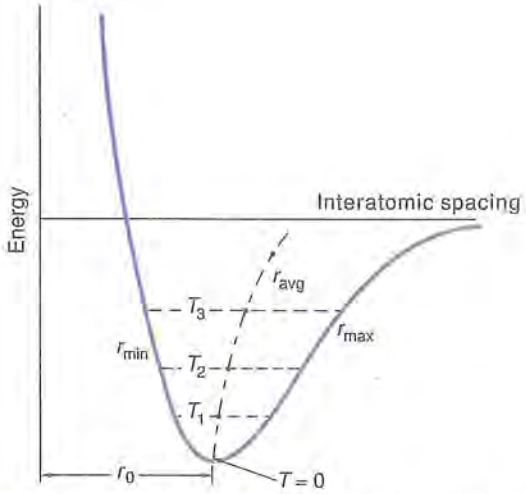

FIGURE 2-19 Schematic representation of atom vibrating in an asymmetrical well defined by the U vs r potential. In this case the average displacement increases with temperature and there is thermal expansion.

distinct bonding mechanisms; however, atoms in most materials are bonded by an admixture of mechanisms. Transition metals with incomplete inner shells (e.g., Fe, Ni, W, etc.) have some covalent character through nearest-atomic-neighbor sharing of core electrons. This gives metallic bonds a directional character that strengthens them, resulting in high melting points. Metals whose core electron complement is complete (e.g., Zn, Mg) have no way to bond covalently and largely melt at lower temperatures. Compound semiconductors like GaAs have a small amount of ionic character, CdTe more so. Conversely, ionic solids like Al_2O_3 and SiO_2 have strong covalent character. Sorting it all out is nightmarish. The thing to remember is that these three bonding mechanisms cement strong **primary** bonds by **transferring** (ionic) and **sharing** (covalent, metallic) electrons. Primary bonds have energies ranging from ~1 to 10 eV/atom (~100 to 1000 kJ/mol).

The remaining bonding mechanisms establish weak **secondary** bonds typically possessing only a tenth (or less) of the energy of primary bonds. Although primary bonds largely originate from direct point charge interactions, secondary bonds stem from second-order coupling of weaker **dipole** charge distributions. A dipole consists of closely spaced positive and negative centers of charge. For example, in the water molecule oxygen is the seat of negative charge while an equal amount of positive charge is covalently shared with the two hydrogen atoms. The molecular geometry of water is V-shaped, with an effective dipole composed of the negative charge at the O apex and positive charge along the two legs set at an angle of 105°. The dangling H atoms or protons (as they have lost electrons to the oxygen) can couple to oxygen atoms of other water molecules in chains. In ice they polymerize into a three-dimensional array that

extends throughout the solid as shown in Fig. 2-20. **Hydrogen bonding** is the name given to this bonding mechanism because protons are the bridge that connects the anions of molecules together. This bonding mechanism is also operative between molecules containing **permanent** dipoles composed of hydrogen and strongly electronegative elements, for example, HF and HCl. Hydrogen bonds are appreciably weaker than chemical bonds but stronger than the **van der Waals** bonds considered next.

The most important examples of secondary bonding arise from van der Waals interactions. Dipoles are also involved here but they are not permanent in nature. The classic example of such bonding occurs in inert gases. Outer electron shells are completely filled and the molecule is not only electrically neutral, but the negative charge appears to be symmetrically distributed about the positive nucleus. What then is the mechanism that causes atoms of argon to condense, first as a liquid and then as a solid, as the temperature is successively reduced? Even in the vapor phase slight deviations in the perfect gas law for all kinds of gases were recognized by van der Waals because molecules weakly attracted one another. Apparently, weak dipole moments form and disappear as small electronic charge imbalances are continually created about the nucleus. The orientation of these fluctuating dipoles constantly changes in neighboring atoms or molecules. But on average, weak dipole–dipole interactions exert slight tugs of attachment and nondirectional bonds are produced. Such fluctuating dipole bonds are collectively known as van der Waals bonds. The attractive energy of interaction falls off rapidly with distance, that is, as r^{-6}, in

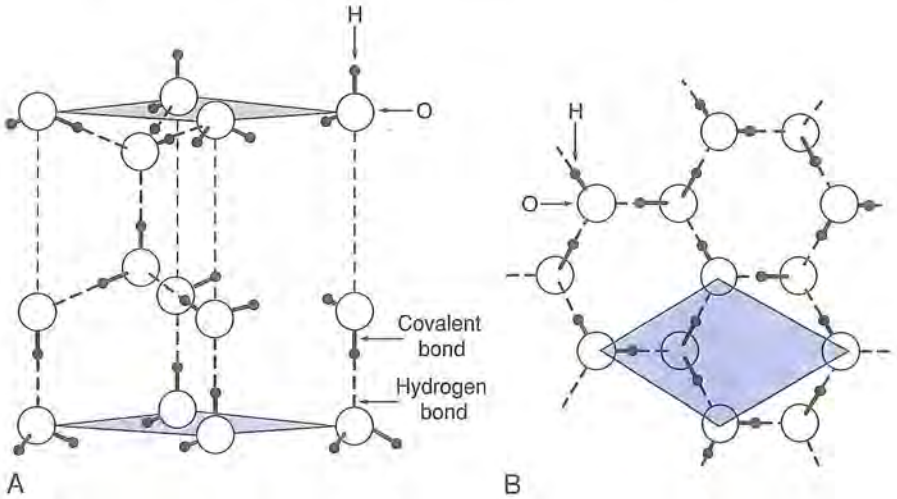

FIGURE 2-20 Structure of ice shown in (A) side and (B) top views. (Also see Fig. 3-22D.) Intramolecular covalent bonds exist within the H_2O molecule. Intermolecular hydrogen bonds link H_2O molecules together. From K. M. Ralls, T. H. Courtney, and J. Wulff, *Introduction to Materials Science and Engineering*, Wiley, New York (1976).

contrast to the slower r^{-1} decay in ionic bonding. Bonding energies of ~0.1 eV are typical.

To complicate bonding issues further there are materials that simultaneously possess both primary and secondary bonds. Nitrogen gas is an example. In a single molecule the atoms are covalently bound, but in liquid nitrogen at 77 K van der Waals forces hold the molecules together. Simply pouring the liquid gas on a warmer surface is sufficient to destroy the weak secondary bonding. Long-chain molecules in polymeric solids are very important engineering examples and are treated at length in Chapter 4. So-called **intramolecular** (within the molecule) carbon–carbon and carbon–hydrogen bonds are covalent and strong. Covalent C–C bonds along the spine are admixed with the far weaker **intermolecular** (between molecules) van der Waals bonds that link adjacent linear molecules together. Property admixtures can therefore be expected based on the proportion of intra- and intermolecular bonding.

Not only does van der Waals bonding occur in atoms and molecules of the same type, but it occurs across interfaces of dissimilar materials; indeed it is responsible for adhesion effects in films and coatings. For example, the molecular composition and nature of paint constituents (organic plus ionic) differ from those of the metal surface they coat. Primary chemical bonds across such interfaces do not form and adhesion is a problem that is overcome by weak van der Waals bonds. There are three categories of van der Waals bonds (London, Debye, and Keesom types) dependent on whether neither, one, or both of the paired atoms or molecules possess electric dipoles.

2.5.3. Material Properties

The chapter ends with a comparison among the different bonding mechanisms and the material property trends they foster. This is done in a self-explanatory way in Table 2-3, where assorted properties are compared. Because there are reasonably large property variations within particular bonding groups, comparisons are approximate.

2.6. PERSPECTIVE AND CONCLUSION

This chapter has provided a panoramic view of what materials are composed of and what holds them together. More than any other chapter in the book it enables distinctions to be drawn between materials and their properties. A dichotomy exists between the quantum description of solids in terms of atomic *electrons*, on the one hand, and classical models involving interacting pairs of *atoms* that attract and repel one another, on the other hand. In the former, the approach is to enumerate possible electron states (defined by quantum numbers) of individual atoms, their occupation by electrons, and their fate when atoms are brought together in solids. The latter assumes that whole

TABLE 2-3 BONDING TYPES AND PROPERTY TRENDS

	Bonding type			
Property	**Metallic**	**Ionic**	**Covalent**	**Secondary**
Magnitude of U_0	Large (3)[a]	Very large (1)	Very large (2)	Very small (4)
Melting point	High (3)	High (1, 2)	High (1, 2)	Very low (4)
Magnitude of E_y	High (2)	High (1)	High (1)	Very small (4)
Magnitude of α	Small (2)	Small (3, 4)	Small (3, 4)	Large (1)
Hardness (strength)	High (3)	High (2)	High (1)	Very low (4)
Toughness	High (1)	Low (4)	Low (2)	Low (3)
Density	High (l)	Medium (3)	Medium (2)	Low (4)
Electrical conductivity	High (1)	Low (3, 4)	Medium (2)	Low (3, 4)
Thermal conductivity	High (1)	Low (4)	Medium (2)	Low (3)
Optical reflectivity	High (1)	Low (3, 4)	Medium (2)	Low (3, 4)
Chemical reactivity	High (1)	Low (4)	Low (2, 3)	Low (3, 4)

[a] 1 = highest, 4 = lowest.

atoms, which integrate and smooth the complex behavior of subatomic particles, interact according to mathematically simple physical laws. A guiding operative principle in either case is that stable bonding configurations are the outcome of minimizing the energy that resides in electrons and atoms. In both cases compromises must be struck between attractive and repulsive forces, the resultant of which yields very precise solid-state atomic positions and well-defined bond energies.

Knowledge of atomic electron energy levels and transitions between them has been capitalized upon in assorted electron (AES) and X-ray spectrometers to identify atoms. These instruments have been indispensable tools in characterizing surface layers and interfaces in all classes of materials, particularly in microelectronics technology. Together with high-resolution electron microscopy (discussed in the next chapter), these methods have provided much of our information on the structural and bonding character of atoms within solids.

Generally speaking, hard, high-strength materials are the legacy of strong primary bonds. These are found particularly in ionic and covalent solids as well as in many metals. As we shall see later in the book, high electrical and thermal conduction and optical reflectivity go hand in hand with the availability of large numbers of mobile electrons, and metals have these in the greatest profusion.

There are, of course, materials that defy classification or exhibit anomalous behavior in particular composition and temperature ranges. Excellent examples are the high-temperature ceramic superconductors (e.g., $YBa_2Cu_3O_7$), which are outwardly ionic but behave as metals. They have a schizophrenic nature as do semiconductors that exhibit attributes of both ionic and metallic character. In design work, engineers must anticipate typical or expected property

trends within material categories. But one must also be particularly alert to deviations from expected behavior; for example, diamond, a covalent solid, conducts heat better than any metal. This is what imparts excitement to the subject of materials.

Additional Reading

R. J. Borg and G. J. Dienes, *The Physical Chemistry of Solids*, Academic Press, Boston (1992).
L. Smart and E. Moore, *Solid State Chemistry: An Introduction*, Chapman & Hall, London (1992).
J. Waser, K. N. Trueblood, and C. M. Knobler, *Chem One*, 2nd ed., McGraw–Hill, New York (1980).

QUESTIONS AND PROBLEMS

2-1. a. How many atoms are there in a pure silicon wafer that is 15 cm in diameter and 0.5 mm thick?
b. If the wafer is alloyed with 10^{16} phosphorus atoms per cubic centimeter what is the atomic fraction of phosphorus in silicon?

2-2. Aluminum has an atomic density of 6.02×10^{22} atoms/cm^3. What is the mass density?

2-3. How many grams of Ni and Al are required to make 1 kg of the compound Ni_3Al?

2-4. What energy is associated with the absorption of the smallest quantum of vibrational energy in a typical solid?

2-5. A helium–neon laser beam is rated at 0.005 W and emits light with a wavelength of 632.8 nm. How many photons are emitted per second?

2-6. a. What is the de Broglie wavelength associated with an electron traveling at 1×10^6 m/s?
b. What is the de Broglie wavelength associated with a 3000-lb car traveling at 55 mph?

2-7. a. The wavelength of a copper X ray is 0.154 nm. What is the momentum associated with it?
b. When an X ray is emitted, the Cu atom recoils much like a rifle discharging a bullet. What momentum would be imparted to a free Cu atom upon X-ray emission?
c. What is the recoil velocity of the atom?

2-8. a. What is the expected ionization energy of the $3s$ electron in Na?
b. The actual ionization energy of Na is 5.2 eV. How do you account for the difference between the two values?

2-9. Calculate the energy and wavelength of the photon emitted when an electron in a titanium atom falls from the $n = 3$ to the $n = 1$ state.

The next several problems are based on the electron energy levels (in eV) for the elements listed in the following table and identified in Fig. 2-7.

Element	K	L_1	L_2	L_3	M_1	$M_{2,3}$	$M_{4,5}$
Cr	5,989	695	584	575	74.1	42.5	2.3
Cu	8,979	1,096	951	931	120	73.6	1.6
Mo	20,000	2,865	2,625	2,520	505	400	229
W	69,525	12,100	11,544	10,207	2820		

2-10. a. Create an energy level diagram for Cu.
b. What is the energy of the photon emitted in the $M_3 \rightarrow K$ electron transition in Cu?
c. In what range of the electromagnetic spectrum (visible, infrared, X-ray, etc.) does this photon lie?
d. Repeat parts (b) and (c) for the $M_{4,5} \rightarrow M_{2,3}$ transition.

2-11. a. Will electrons that travel at velocities of 4.7×10^7 m/s have enough kinetic energy to eject the K electron from Cr? Can they eject Mo K electrons?
b. Does a photon with a wavelength of 0.161 nm have enough energy to eject a K electron from Cu? Can it eject the Cr K electron?

2-12. The metals listed in the previous problem are all used commercially as targets in X-ray generating tubes (see Section 3.4.1.).
a. What is the photon wavelength corresponding to the $L_3 \rightarrow K$ electron transition in each metal? This transition gives rise to the so-called K_{α_1} X ray.
b. X-ray tubes with Cu, Cr, Mo, and W targets were mixed up in a laboratory. To identify them they were operated sequentially and the K_{α_1} wavelengths were measured with an EDX system. The first tube tested yielded a wavelength of 0.0709 nm. What is the target metal?

2-13. Moseley's law of atomic physics suggests that the energy of K_{α_1} X rays varies as $(Z-1)^2$, where Z is the atomic number of the element. Plot the K_{α_1} X-ray energies for Ti, Cr, Cu, Mo, and W versus $(Z-1)^2$ so that a straight line results. Based on your plot what are the energy and wavelength of K_{α_1} X rays in Sn?

2-14. Fluorescent X-ray analysis from an automobile fender revealed a spectrum with lines at 5.41 keV (intense) and 5.95 keV (less intense) and a weaker line at 8.05 keV. Interpret these findings.

2-15. During the Renaisance the white pigment used in oil paints was lead oxide. In the 19th century zinc oxide was used as well. In more recent times titanium oxide has been the preferred choice. A painting suspected of being a forgery is examined by EDX methods and yielded 75-keV $K\alpha_1$ X rays from a region painted white. Pending further investigation what, if anything, can you infer about the painting's age? (*Hint*: See Problem 2-13.)

2-16. The chemical composition of a series of binary Cu–Ti alloys is calibrated by measuring the relative intensity of fluorescent X rays emitted. For pure Cu the rate of X-ray emission is measured to be 1562 (photon) counts per second (cps), whereas 2534 cps was detected from pure Ti. The alloy yields a rate of 656 cps for Cu plus 1470 cps for Ti X rays. What is the overall alloy composition? (In all cases the same sample and measurement geometry were employed and a

linear composition calibration is assumed.) Is the composition measured in weight or atomic percent?

2-17. Elemental analysis of the heavy metals by EDX methods is virtually independent of what phase (solid, liquid, gas) or state of chemical bonding (metallic, ionic, covalent) is involved. Why?

2-18. A common form of the potential energy of interaction between atoms is given by $U = -A/r^6 + B/r^{12}$, where A and B are constants.

a. Derive an expression for the equilibrium distance of separation in terms of A and B.

b. If $r_0 = 0.25$ nm, what is the ratio of B to A?

c. Derive an expression for the energy at the equilibrium separation distance in terms of A.

2-19. Consider a one-dimensional linear material consisting of ions of alternating charge separated by distance a as shown.

$$-\underline{\quad a \quad}+\underline{\quad a \quad}-\underline{\quad a \quad}+\underline{\quad a \quad}-\underline{\quad a \quad}+$$

Starting with any ion derive an expression for the electrostatic attractive energy between it and its two nearest-neighbor ions. Then add the repulsive energy between it and the two next nearest-neighbor ions. Continue in this manner and show that the sum of resulting terms is given by $U = (-2 \ln 2\, q^2)/(4\pi\varepsilon_0 a)$.

2-20. In cesium chloride the distance between Cs and Cl ions is 0.356 nm and $n = 10.5$. What is the molar energy of a solid composed of Avogadro's number of CsCl molecules?

2-21. For the Li–F molecule what is the magnitude of the force of attraction between the two ions if the equilibrium separation distance is 0.201 nm? What is the magnitude of the repulsive force between these ions?

2-22. Ionic solids LiF and NaBr have the same structure as NaCl. For LiF, $n = 5.9$ and $r_0 = 0.201$ nm, whereas for NaBr, $n = 9.5$ and $r_0 = 0.298$ nm.

a. Which of these materials is expected to have a higher modulus of elasticity?

b. Calculate the molar energy of ionic interactions for both materials.

2-23. A cation of Mg^{2+} and an anion of O^{2-} are brought together.

a. Write an expression for the Coulomb energy of attraction.

b. If these two ions come to rest at the equilibrium distance of 0.201 nm, what is the value of the Coulomb energy?

c. If MgO has a molar energy of 603 kJ calculate the values of both n and B.

2-24. a. Opposite sides of a rocksalt crystal are pulled to extend the distance between neighboring ions from $r_0 = 0.2820$ nm to $r = 0.2821$ nm. Similarly, during compression, ions are squeezed to within a distance of 0.2819 nm. Compare the value of the tensile (or extension) force developed with that of the compressive force reached. Are they the same?

b. Repeat the calculation if the final distances are 0.2920 nm for extension and 0.2720 nm in compression.

2-25. Atoms on the surface of a solid make fewer bonds with surrounding atoms

than do interior atoms. Sketch, in schematic fashion, the interatomic potential of surface and interior atoms as in Fig. 2-12.

2-26. Provide a reasonable physical argument for each of the following statements.
a. The higher the melting temperature of the solid, the greater the depth of the potential energy well.
b. Materials with deep energy wells are likely to have a more symmetrical potential energy curve.
c. Materials with high melting points tend to have low coefficients of thermal expansion.
d. Materials with high melting points tend to have large moduli of elasticity.

2-27. a. In a 1-cm^3 cube of Au metal what is the electron momentum in the x direction for the state $n_x = 3.83 \times 10^7$, $n_y = 1$, $n_z = 0$?
b. What is the electron momentum in the y direction?
c. How does the answer to (a) change for a 1000-cm^3 cube of Au?

2-28. Rationalize the decrease in magnitude of the energy band gap with increasing atomic number for elements in the fourth column of the Periodic Table.

2-29. In what ways are electrons in an isolated copper atom different from electrons in a copper penny?

2-30. Quantum well structures consisting of layers of very thin semiconductor films have been synthesized and used in advanced electronic devices. They have the property of trapping electrons in a well much like a "particle in a box." In a one-dimensional, infinitely high, 5-nm-wide well what is the electron energy for the $n = 1$ state?

2-31. How narrow would the quantum well in Problem 2-30 have to be before the electron energy for the $n = 1$ state were equal to that for the $n = 1$ ground state for the electron in the hydrogen atom? (Note that the electron energy is increased by squeezing its domain.)

2-32. What is so special about the electronic structure of carbon that enables it to form more than a million organic compounds with hydrogen, oxygen, nitrogen, and sulfur?

2-33. State whether ionic, covalent, metallic, or van der Waals bonding is evident in the following solids. (Where applicable distinguish between intramolecular and intermolecular bonding.)

a. Mercury b. KNO_3 c. Solder d. Solid nitrogen e. SiC
f. Solid CH_4 g. Aspirin h. Rubber i. Na_3AlF_6 j. PbTe k. Snow

2-34. Is it likely that a stable solid will have an interatomic potential energy of interaction where the attractive part of the potential is steeper than the repulsive part? Why?

5 THERMODYNAMICS OF SOLIDS

5.1 INTRODUCTION

The concept of equilibrium is an important one in science. Statics, a common course of study, deals with the balance of forces that prevails in mechanical structures and systems when they are in equilibrium. When such a state exists it means the structure or system has no tendency to move or change and, in effect, has minimized its mechanical or potential energy. We may view the materials we are concerned with in this book as chemical systems that are occasionally relatively pure, but more frequently contain two or more different elements. Several questions then arise with respect to chemical compared with mechanical systems: What do we mean by chemical equilibrium? Are there comparable forces that equilibrate in chemical equilibrium? Is there a corresponding energy that is minimized at equilibrium? Fully developed answers to these questions are given in chemistry and thermodynamics courses, but here we can only stress some highlights in a qualitative way.

A good place to start is with two famous quotations by the German physicist Clausius: "Die Energie der Welt ist konstant." "Die Entropie der Welt strebt einem maximum zu." (The energy of the world is constant. The entropy of the world strives toward a maximum.) Although Clausius had global notions in mind, what if the world we are interested in is some solid we deal with in this book? Energy in this sense deals broadly with the interactions between atoms and specifically with the bond energies discussed in Chapter 2. There

we noted that a balance of attractive and repulsive forces led to a minimum energy in a single bond. The concept of entropy is, however, more subtle. It is common to view entropy as a measure of the state of disorder or randomness in the system. A quantitative statistical measure of entropy is related to the number of possible configurations atoms can assume; the larger this number the greater the randomness and entropy. The creative synthesis of these opposing natural tendencies—of lowering internal energy by bringing atoms together, while simultaneously increasing entropy by randomizing their location—is a main cornerstone of thermodynamics. Here, we state without proof that a single function known as the free energy (G) combines both internal energy (E) and entropy (S) attributes within systems as

$$G = E + PV - TS, \tag{5-1}$$

where T is the temperature in degrees Kelvin. The additional term, a product of the pressure (P) and volume (V), is small in solids. G is temperature dependent, reflecting the strong influence of T in Eq. 5-1 and the generally slight temperature dependence of both E and S.

In this book we are always concerned with **changes** in energy between initial (i) and final (f) states that are at **constant** temperature and pressure. The latter conditions imply that enthalpy (H), defined as $H = E + PV$, rather than internal energy E, is strictly more appropriate; because the difference between E and H is small, we use both energy terms interchangeably. With these facts taken into consideration the equation of interest is

$$\Delta G = \Delta H - T\Delta S, \tag{5-2}$$

where ΔH and ΔS are the respective changes in enthalpy and entropy (usually on a molar basis).

A very important consequence of the laws of thermodynamics is that spontaneous reactions occur at constant T and P when $\Delta G = G_f - G_i$ is minimized, or when ΔG is negative. Note that neither the sign of ΔH nor the sign of ΔS taken individually determines reaction direction; rather it is the sign of the *combined* function ΔG that is crucial. For example, during the condensation of a vapor to form a solid there is a reduction in entropy ($\Delta S < 0$). This is due to the many atomic configurations in the vapor and the markedly reduced number in the ordered solid. But the enthalpy (energy) decrease on forming the solid more than offsets the entropy decrease, and the net change in ΔG is negative. Systems thus naturally proceed to reduce G_i successively to a still lower, more negative value G_f, until it is no longer possible to reduce G any further. When this happens, $\Delta G = 0$ and the system is at rest or in equilibrium; there is no longer a driving force for change.

Thermodynamic driving forces include the gradients or spatial derivatives of temperature, pressure, and chemical potential. When the temperature in all parts of the system is the same there are no temperature gradients or driving forces for heat flow. This constitutes a state of **thermal equilibrium.** Similarly,

mechanical equilibrium implies a balance of pressures. If pressure is not equilibrated there will be bulk flows and deformations of matter in parts of the system. **Chemical equilibrium** implies no tendency for chemical change. The chemical potential, a type of thermodynamic concentration, is the most difficult of the variables to understand. It is defined as the free energy per unit mass of a given atomic species. If there is a gradient in chemical potential (~ effective atomic concentration), then a driving force is established that causes individual atoms to diffuse. (The subject of diffusion is addressed in more detail in Chapter 6.) In summary, systems are only in true **thermodynamic equilibrium** when all gradients, and the driving forces they create, vanish.

The remainder of this chapter is devoted to a number of applications in which thermodynamic issues play a major role. Of these topics the greatest emphasis is placed on binary phase diagrams. To preview this important subject within the context of the above concepts it is instructive to consider Fig. 5-1. A binary system is schematically depicted in which there are a number of possible configurations of the same number of A and B atoms (components). What are the thermodynamic implications, if any, of these different physical distributions of atoms? In Fig. 5-1A initial blocks of pure A and B atoms are brought together. Next these atoms are allowed to mix together freely as they might do if they were melted together (Fig. 5-1B). The entropy of this randomly mixed system (or **liquid solution**) is larger relative to case A. Upon solidification of the melt one possible atomic configuration resembles that of the prior liquid solution. In this so-called **random solid solution** there does not appear to be any great tendency for A atoms to bond to A neighbors or for B atoms to couple to B neighbors (Fig. 5-1C). Rather, both A and B atoms show little preference in selecting their neighbors, but the energy of the solid is lower than that of the liquid. This state is completely different from the one shown in Fig. 5-1D. Here, A atoms clearly prefer to bond to A atoms, and likewise for B atoms. Relative to case B the entropy has fallen, but relative to case A it has risen. This segregation of A and B atoms into pure clusters is apparently due to A–A and B–B bonds having lower energies than A–B bonds. Rather than a solution, atoms have separated into a so-called **two-phase mixture.** Surprisingly, although concentration variations and gradients are evident, the system is actually in equilibrium. This is a case that shows the absence of any tendency toward homogenization by atomic diffusion. Although there are concentration gradients, there are, in fact, no chemical potential gradient driving forces. State D also has a somewhat higher surface energy than state A. This is due to the larger total perimeter length and interfacial surface area associated with clusters relative to the linear boundary separating A and B atoms in case A. Finally, in marked contrast to case D there is the solid-state configuration shown in Fig. 5-1E. It resembles a **compound**, but in comparison to case C we might also describe it as an **ordered solid solution.** In this configuration the energy reduction due to favored A–B bonds offsets the lowered entropy due to ordering.

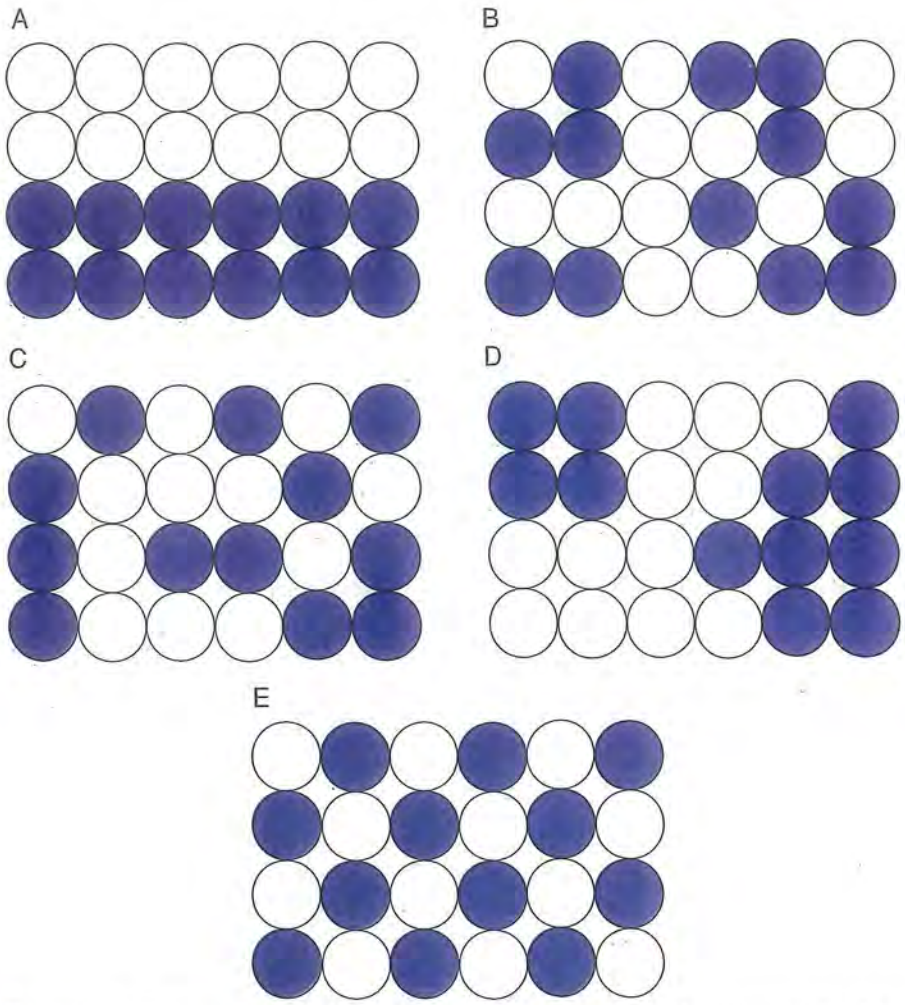

FIGURE 5-1 Illustration of differing configurations of A and B atoms within binary alloys. (A) Separate blocks of A and B atoms. (B) A melt of A and B randomly distributed. (C) Random solid solution of A and B. (D) Separation of A- and B-rich regions or phases. (E) Ordered compound of A and B.

It should be appreciated that interest in thermodynamics is wonderfully interdisciplinary in nature. There are many approaches to the subject and each can be understood on different levels. At the most fundamental level all of these approaches actually converge. Mechanical engineering stresses the **macroscopic** nature of matter and the thermodynamic approach taken makes no assumption about the atomic constitution of the working medium (e.g., steam) of the system. Electrical engineering frequently adopts this point of view in energy conversion applications. Materials science, physics, and chemistry, however,

usually stress the microscopic statistical nature of atomic phenomena, illustrated, for example, in Fig. 5-1. When binary atomic distributions exist in stable thermodynamic equilibrium, it is certain that the system has achieved minimum free energy. Chemical thermodynamics is also very much concerned with free energy as we shall see in the next section.

5.2. CHEMICAL REACTIONS

5.2.1. Oxide Formation Reactions

There are many instances where chemical reactions play an important role in materials science and engineering. The oxidation of metals, high-temperature reactions in polymer mixtures, corrosion, and the deposition of hard ceramic coatings from gases are but a small sample of the examples that can be profitably described by the thermodynamics of chemical reactions. According to the rules of thermochemistry that apply to chemical reactions at equilibrium, we recall that the energies (enthalpies, free energies) of reactants are additive when account is taken of the number of moles involved, and similarly for the products. The net energy difference (ΔH, ΔG) is what remains when the energies of the products are subtracted from those of the reactants. To see how this works, consider the oxidation of metal M by the reaction

$$M + O_2 = MO_2, \qquad \Delta G^\circ_{MO_2}. \tag{5-3}$$

If MO_2 is produced under standard conditions (e.g., pure M, 1 atm O_2), then the change in free energy of oxide formation per mole, ΔG°, is given by $\Delta G^\circ = G_{MO_2} - G_M - G_{O_2}$. In elementary chemistry it is shown that the equilibrium constant of a reaction (K_{eq}) is related to ΔG° through the important equation

$$K_{eq} = \frac{[MO_2]}{[M]P_{O_2}} = \exp(-\Delta G^\circ/RT). \tag{5-4}$$

The terms in brackets are the effective concentrations, P_{O_2} is the oxygen pressure, T is the absolute temperature, and R is the gas constant. (R = 8.314 J/mol-K or 1.987 cal/mol-K.)

Extensive tables of ΔG° values exist not only for oxides, but for other compounds formed from elemental constituents. Data for oxides have been conveniently graphed in Fig. 5-2, providing a handy collection of thermodynamic information which is used in the following illustrative problems.

EXAMPLES 5-1

a. Thin-film Al conducting stripes are brought into intimate contact with insulating layers of SiO_2 in integrated circuits. Is there a thermodynamic tendency for them to react at 400°C?

b. What is the maximum O_2 pressure to which a Ni melt at 1460°C can be exposed before it tends to oxidize?

c. What is the reason for the negative slope of ΔG^0 versus T for oxidation of carbon whereas the slope for the other metals is positive?

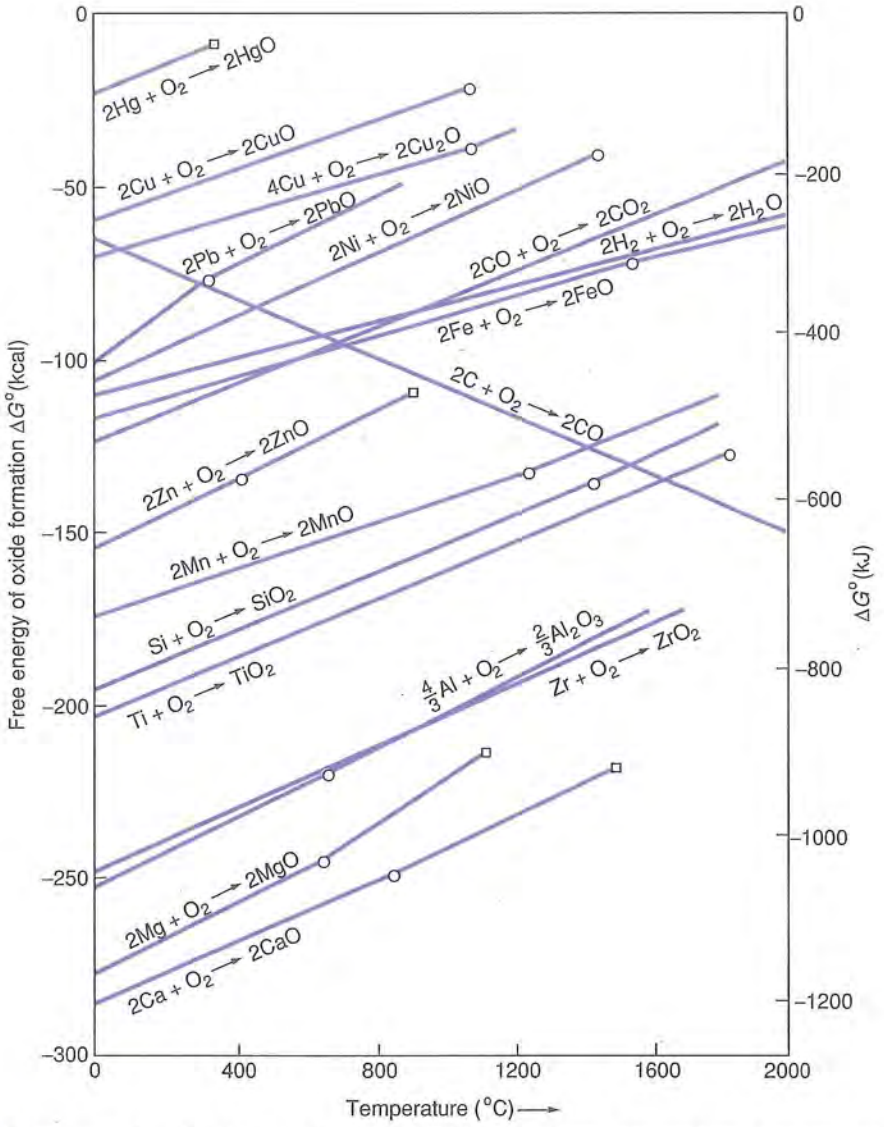

FIGURE 5-2 Free energy of metal oxide formation versus temperature. ○, Melting point; □ boiling point (1 atm). From A. G. Guy, *Introduction to Materials Science*, McGraw–Hill, New York (1972).

ANSWERS a. We must consider the reactions (from Fig. 5-2)

$$\tfrac{4}{3}Al + O_2 = \tfrac{2}{3}Al_2O_3 \qquad \Delta G^\circ_{Al_2O_3} = -235 \text{ kcal/mol at } 400^\circ C$$
$$Si + O_2 = SiO_2 \qquad \Delta G^\circ_{SiO_2} = -180 \text{ kcal/mol at } 400^\circ C$$

Eliminating O_2 through subtraction of these two equations yields

$$\tfrac{4}{3}Al + SiO_2 = \tfrac{2}{3}Al_2O_3 + Si$$
$$\Delta G^\circ = \Delta G^\circ_{Al_2O_3} - \Delta G^\circ_{SiO_2}$$
$$= -235 - (-180) = -55 \text{ kcal/mol (or } -230 \text{ kJ/mol).}$$

Because ΔG° is negative the reaction is thermodynamically favorable. Whether reaction will, in fact, occur is dependent on kinetic factors. In this case reaction rates are too sluggish to produce troublesome effects.

b. Assume that molten nickel oxidizes according to the reaction

$$2Ni + O_2 = 2\,NiO \qquad \text{and} \qquad \Delta G^\circ_{NiO} = -40 \text{ kcal/mol at } 1460^\circ C \text{ (1733 K).}$$

In Eq. 5-4 the effective standard concentrations of both metal and oxide are usually taken to be unity. If the same can also be assumed for Ni and NiO, then [NiO] = 1 and [Ni] = 1. Thus,

$$\ln P_{O_2} = \Delta G^\circ/RT = (-40{,}000 \text{ cal/mol})/(1.99 \text{ cal/mol K})(1733 \text{ K}) = -11.6.$$

Therefore, $P_{O_2} = \exp -11.6 = 9.17 \times 10^{-6}$ atm.

c. If Eq. 5-2 is plotted as ΔG versus T, a straight line results provided ΔH and ΔS are not temperature dependent but constant. This generally appears to be the case in Fig. 5-2. The slope of ΔG versus T is $-\Delta S$. In the case of carbon two molecules of CO form for each O_2 consumed. This corresponds to a gas volume expansion and an entropy *increase* ($\Delta S > 0$). During oxidation of all the metals there is a *reduction* in gas volume as O_2 reacts and is consumed. Therefore, $\Delta S < 0$, and the slopes are positive.

Because its free energy will fall below that for any metal, provided the temperature is high enough, carbon is a universal reducing agent. In the form of charcoal it has enabled metals to be extracted from oxide ores since antiquity.

As a generalization, the metal of an oxide that has a more negative ΔG° than a second oxide will reduce the latter, and be oxidized in the process.

5.2.2. Chemical Vapor Deposition Reactions

There are a number of important applications in which thin films or coatings are synthesized from high-temperature gas mixtures. The objective of these chemical vapor deposition (CVD) processes is to coat selected substrates with the required materials. As an example consider the TiN, TiC, and Al_2O_3 compound coatings deposited on tungsten carbide metal machining and cutting

tools. (The gold color commonly seen on cutting tools and on tungsten carbide tool inserts is due to a TiN coating.) Hundreds of millions of tool bits worldwide have been coated with either single or sequentially deposited multiple layers of these materials. Each coating has a hardness double that of hardened tool steel, a hard material in its own right. Only 5- to 10-μm (5000- to 10,000-nm)-thick layers are deposited. This coating thickness is enough to bestow considerable wear resistance to the underlying tool so that it can last 5 to 10 times longer than uncoated tools before requiring sharpening. A reactor used to deposit all three coatings is shown schematically in Fig. 5-3. Input gases react at the substrate surface forming the compound deposit of interest while gaseous products are swept out of the reactor. The chemical reactions relied upon are

$$2TiCl_4(g) + N_2(g) + 4H_2(g) = 2TiN(s) + 8HCl(g) \qquad 1000°C \qquad (5\text{-}5a)$$

$$TiCl_4(g) + CH_4(g) = TiC(s) + 4HCl(g) \qquad 1000°C \qquad (5\text{-}5b)$$

$$2AlCl_3(g) + 3CO_2(g) + 3H_2(g) = Al_2O_3(s) + 3CO(g) + 6HCl(g) \qquad 1000°C \qquad (5\text{-}5c)$$

Each reaction takes place at roughly 1000°C under approximate equilibrium conditions. Also, all of the reactants and products, with the exception of the coating denoted by (s), are gaseous; this is a general feature of CVD reactions. Several coated tools are reproduced in Figs. 5-4A and B together with the structure of a modern multilayer coating on a WC tool substrate (Fig. 5-4C).

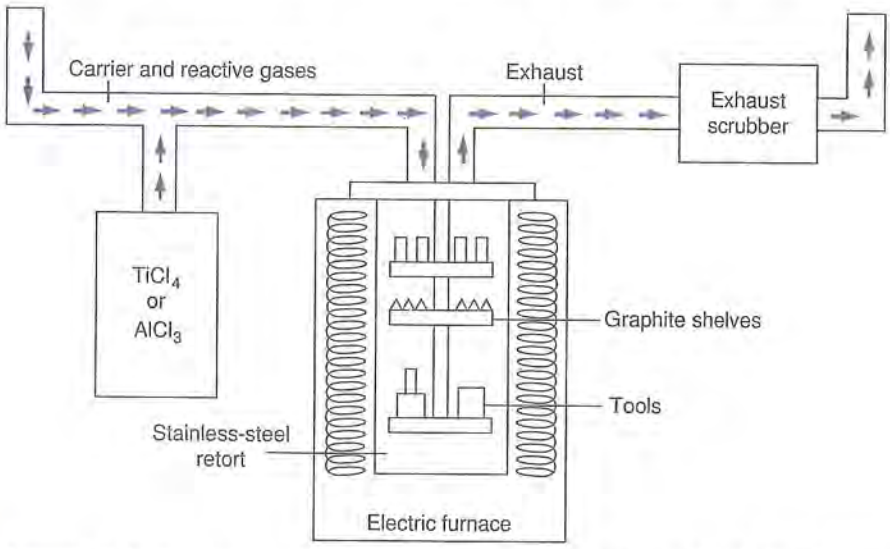

FIGURE 5-3 Schematic of chemical vapor deposition reactor used to deposit hard coatings of TiN, TiC, and Al_2O_3.

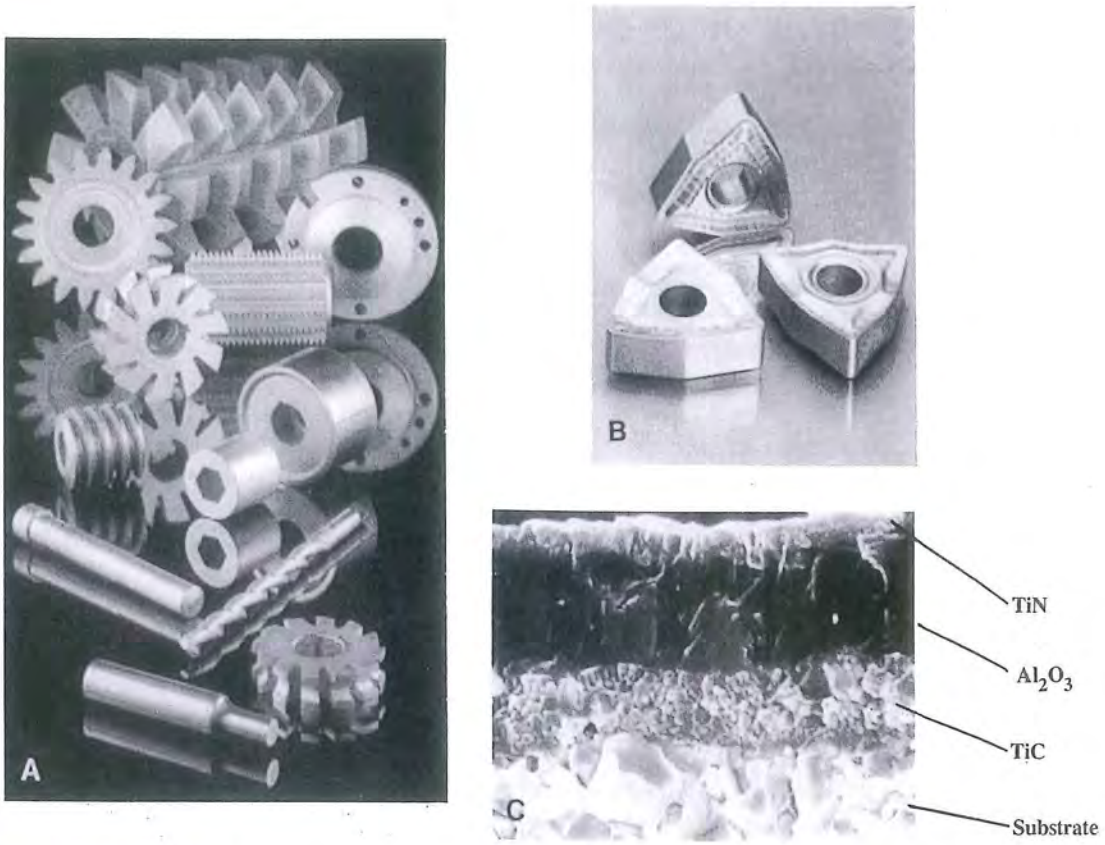

FIGURE 5-4 (A) Assorted cutting tools coated with TiN. Courtesy of Multi-Arc Scientific Coatings. (B) Multilayer coated lathe cutting tool inserts. (C) Scanning electron microscope image of a trilayer coating, deposited by CVD methods, on a WC cutting tool substrate (3500×). The TiC is hard and bonds well to the WC. Protection of the tool against excessive heating is provided by the hard but insulating Al_2O_3 layer. Finally, the hard, wear-resistant upper TiN layer is chemically stable and offers low friction in contact with the workpiece being machined. Courtesy of S. Wertheimer, ISCAR.

EXAMPLE 5-2

An important CVD reaction employed in the fabrication of Si microelectronic devices is

$$SiCl_4 + 2H_2 = Si(s) + 4HCl \qquad 1500°K \qquad (5\text{-}6)$$

Published thermodynamic data on the free energy of formation of $SiCl_4$ and HCl from the elements at 1500°K reveal

$$Si + 2Cl_2 = SiCl_4 \qquad \Delta G° = -441\ kJ/mol \qquad (5\text{-}7a)$$
$$\tfrac{1}{2}H_2 + \tfrac{1}{2}Cl_2 = HCl \qquad \Delta G° = -105\ kJ/mol. \qquad (5\text{-}7b)$$

What are $\Delta G°$ and the equilibrium constant for the reaction of Eq. 5-6 at 1500°K?

ANSWER The additive nature of energy and the simple rules of thermochemistry yield

$$\Delta G° \text{ (Eq. 5-6)} = 4\Delta G° \text{ (Eq. 5-7b)} - \Delta G° \text{ (Eq. 5-7a)}$$
$$= 4(-105) - (-441) = +21 \text{ kJ}$$

Therefore, the equilibrium constant is $K_{eq} = \exp - (21{,}000/8.32 \times 1500) = 0.19$. Crystal growth from the vapor phase is normally carried out as close as possible to $\Delta G° = 0$ or $K = 1$.

The deposition of the Si film takes place on a prior single-crystal wafer of Si. Unlike the polycrystalline structure of the hard coatings, the Si deposit is a high-quality single-crystal film. It is known as an **epitaxial film** (from the Greek *epi* and *taxis*, which means "arranged upon") because the deposit uses the substrate as a template on which to extend crystal growth. Epitaxial film growth is addressed again in Section 12.5.2.

5.3. SINGLE-COMPONENT SYSTEMS

5.3.1. Variable Pressure and Temperature (Phase Diagrams)

By **single-component systems** we mean materials possessing one chemical species that is retained in all of its phases over the broad range of temperatures (T) and pressures (P) of interest. For example, a single type of either atom (carbon) or molecule (H_2O) can constitute a single component. Thus, carbon can exist as graphite, diamond, liquid carbon, or carbon vapor, and H_2O as water, ice, or steam. Each of these recognizable homogeneous forms (solid, liquid, gas) constitutes a **phase**. A convenient way of visualizing regions of phase stability in single-component systems as a function of T and P is through phase diagrams. The widely reproduced phase diagram for H_2O is shown in Fig. 5-5. We know from experience that water, ice, and steam are individually stable over broad temperature and pressure ranges. The phase diagram, determined from careful experiment, broadly maps these limits of single-phase stability. In addition, the lines depict the special set of conditions under which two phases coexist in equilibrium. Thus, the boundary between liquid and vapor defines a set of pressure-versus-boiling point data, whereas that between the vapor and solid defines corresponding vapor pressure-versus-sublimation temperature data. Under a very restricted set of conditions, namely, 0.0075°C and 0.006 atm, all three phases of H_2O coexist in equilibrium at the triple point.

The vapor pressure–temperature data just referred to are extremely important in thin-film and coating deposition technologies. A handy representation

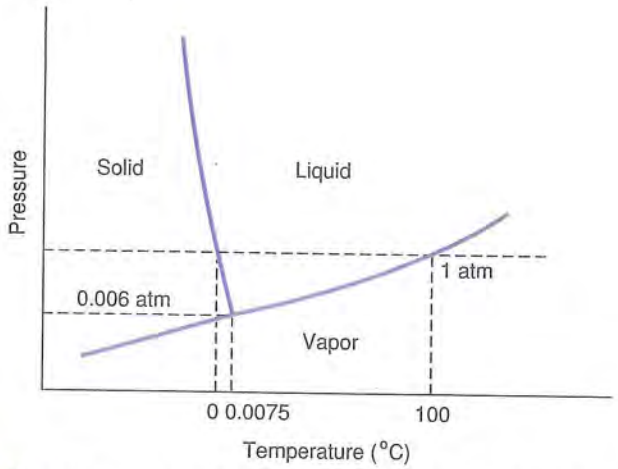

FIGURE 5-5 Pressure–temperature phase diagram for H_2O. From C. R. Barrett, W. D. Nix, and A. S. Tetelman, *The Principles of Engineering Materials,* Prentice–Hall, Englewood Cliffs, NJ (1973).

of such thermodynamic information is provided in Fig. 5-6 for a number of elements. Note that the vapor pressure for each element rises exponentially with temperature. This is not an entirely unexpected dependence because evaporation may be viewed as a reaction where the vapor (V) and condensed liquid (L) or solid (S) phases are in equilibrium. Therefore, the vaporization reaction

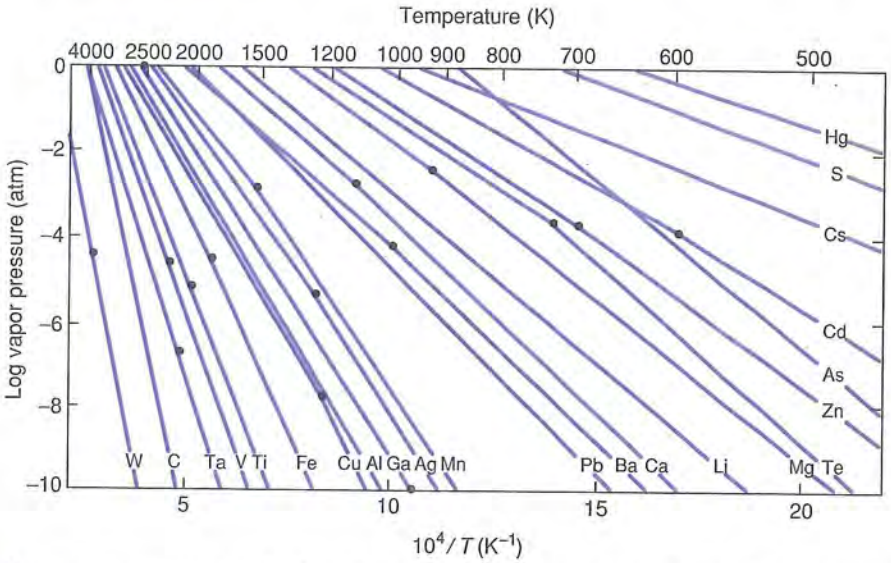

FIGURE 5-6 Vapor pressure–temperature data for selected elements. From C. H. P. Lupis, *Chemical Thermodynamics of Materials,* North-Holland, Amsterdam (1983).

for component A (from the liquid) and the corresponding equilibrium relationship are given by

$$A_L = A_V, \qquad P_A/[A_L] = \exp(-\Delta G_{vap}/RT). \tag{5-8}$$

Substitution of $\Delta G_{vap} = \Delta H_{vap} - T\Delta S_{vap}$ (Eq. 5-2) finally yields

$$P_A = [A_L] \exp(\Delta S_{vap}/R) \exp(-\Delta H_{vap}/RT) = P_0 \exp(-\Delta H_{vap}/RT). \tag{5-9}$$

In this expression ΔH_{vap} may be associated with the latent heat of vaporization and P_0, a constant, is equal to $[A_L] \exp(\Delta S_{vap}/R)$.

The phase diagram for carbon (Fig. 5-7) exhibits two triple points and contains two different solid phases, diamond and graphite. One of the most exciting quests in the history of materials science has been the synthesis of diamond. This diagram suggests that graphite might possibly be converted to diamond provided high enough pressures could be maintained at elevated temperatures. Long experimentation was rewarded with success in 1954, when the General Electric Corporation announced a process to produce diamond crystals. Typical conditions required pressures of 54,000 bars (53,500 atm), temperatures of 1430°C, and, importantly, a liquid Ni solvent from which dissolved carbon could separate out as diamond. Thermodynamic equilibrium is essentially maintained in this method for making diamond.

A no less exciting achievement of the 1980s has been the synthesis of thin films of diamond from the vapor phase under much less forbidding processing conditions. Readily accessible pressures of less than 1 atm and temperatures of 1000°C or less are required. One way to prepare such films is to reduce

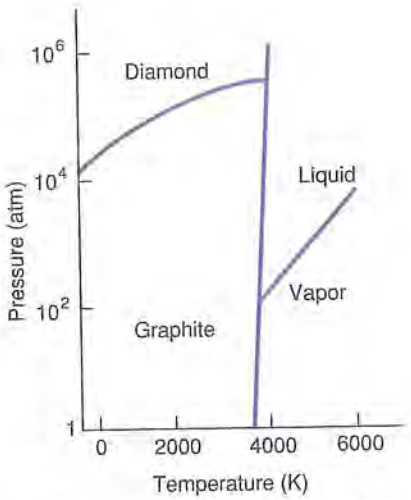

FIGURE 5-7 Pressure–temperature phase diagram of carbon. From A. L. Ruoff, *Materials Science*, Prentice–Hall, Englewood Cliffs, NJ (1973).

methane with atomic hydrogen generated in an energetic gaseous discharge or plasma. Similar discharges occur in neon signs. In this way the formation of tetrahedral sp^3 bonded carbon (see Section 2.4.4) is promoted. Examples of the resulting faceted diamond jewels are shown in Fig. 5-8. This surprisingly simple production method means that the equilibrium conditions of the phase diagram have been bypassed in favor of **metastable** synthesis. Metastability denotes a nonequilibrium state of existence that in some cases can be virtually permanent, for example, glass. If heated, glass may crystallize and more closely approach thermodynamic equilibrium. In the present case metastable diamond is retained at room temperature.

FIGURE 5-8 Diamond crystals grown by low-pressure CVD methods. Courtesy of T. R. Anthony, GE Corporate Research and Development.

5.3.2. The Gibbs Phase Rule

The celebrated *phase rule* derived by Josiah Willard Gibbs provides an interesting way to analyze not only one-component three-phase systems, but systems containing an arbitrary number of components and phases. This rule surprisingly connects the number of degrees of freedom (F) in a system to the number of components (C) and phases (ϕ) it contains, as

$$F = C + 2 - \phi. \tag{5-10}$$

Though deceptively simple in appearance, the Gibbs phase rule is arguably the most important linear algebraic equation in all of science (whole books have been written on it). By degrees of freedom or variance, we mean the number of variables (here T and P) that can be **independently** varied without altering the phase state of the system. Thus, water ($C = 1$) will remain a liquid ($\phi = 1$) even though both temperature and pressure ($F = 2$) can be independently raised or lowered over a reasonable range of values.

When water (liquid) and steam (vapor) coexist at 100°C and 1 atm, $\phi = 2$ and $F = 1$. Now assume that P is increased independently, as in a pressure cooker. The temperature must then rise in a specific, **dependent** fashion along the vaporization line to continue to preserve the water–steam equilibrium, albeit at different values of P and T. Finally, at the critical triple point, $\phi = 3$ and $F = 0$. Any change in either temperature or pressure will destroy the very precarious three-phase equilibrium and push the system into one of the single-phase fields.

5.3.3. Constant Pressure

Most frequently we are interested in systems at atmospheric pressure. Under such conditions one variable is fixed by the equation $P = 1$ atm. The variance is thus reduced by one so that the Gibbs phase rule now reads

$$F = C + 1 - \phi. \tag{5-11}$$

Thus, for one component ($C = 1$) at the melting point, both liquid and solid are present ($\phi = 2$), so that $F = 0$. This is why melting occurs at a fixed temperature.

Interestingly, some materials experience a volume expansion whereas others undergo a volume contraction upon melting. Typically the volume change is a few percent for both types of behavior. Most metals belong to the former category. Their crystal structures are tightly packed. In the case of FCC metals each atom has 12 nearest neighbors. On melting, crystalline packing deteriorates, fewer neighbors surround each atom, and separations between them extend beyond the prior solid-state lattice spacings. The resulting volume expansion is turned to a contraction upon solidification. Such shrinkage is a particularly troublesome issue during casting where it can lead to defects if not compensated for (see Section 8.2.5). In contrast, those materials that have

relatively open network structures containing stereospecific bonds frequently undergo a volume *contraction* upon heating and a corresponding *expansion* upon solidification. The excited atoms in the liquid state can now reduce their energy by forging new lower-energy bonds of shorter length. Examples of such materials include diamond cubic silicon, ice, rhombohedral bismuth, and orthorhombic gallium. In each case the solid structure is relatively loosely packed.

Another important phenomenon exhibited by certain single-component materials in the solid state is **polymorphism** or **allotropy.** The involved materials assume different crystallographic structures as the temperature changes. Iron is the outstanding engineering example exhibiting allotropy. Because it undergoes polymorphic changes we are able to harden steel by heat treatment. From below room temperature up to 910°C, α-Fe, a body-centered cubic phase ($a = 0.2866$ nm), is stable. At 910°C, α-Fe transforms to face-centered cubic γ-Fe ($a = 0.3647$ nm), and it, in turn, is stable until 1390°C. From this temperature up to its melting point (1534°C), iron exists as δ-Fe, another body-centered cubic form ($a = 0.2932$ nm). All of these phase transformations, like melting, are reversible. By Eq. 5-1, G falls with increasing T and stable phases are those that minimize the free energy as illustrated graphically in Fig. 5-9. This accounts for the existence of α-Fe below 910°C where γ-Fe and liquid Fe are metastable.

Another important example of polymorphism occurs in SiO_2 or silica. Crystalline packing of silica SiO_4^{4-} tetrahedra occurs in quartz, tridymite, and cristobalite phases, each of which exists in several modifications. Quartz trans-

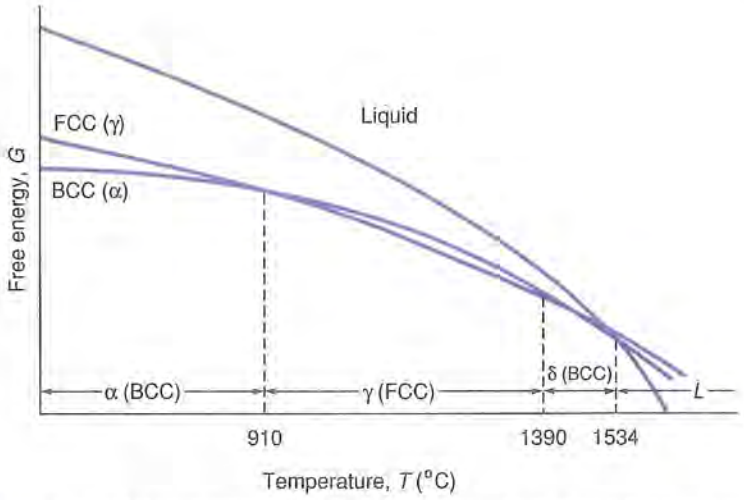

FIGURE 5-9 Free energy of phases in iron versus temperature. Phases with the lowest free energy are thermodynamically stable. After C. R. Barrett, W. D. Nix, and A. S. Tetelman, *The Principles of Engineering Materials,* Prentice–Hall, Englewood Cliffs, NJ (1973).

forms slowly into stable tridymite at 867°C. Tridymite remains stable until 1470°C when it transforms to cristobalite. These crystal forms have densities in the neighborhood of 2.65 g/cm^3, while that for amorphous fused quartz is only 2.2 g/cm^3.

5.3.4. Thermal Energy Absorption in Solids

5.3.4.1. Heat Capacity

One of the important attributes of a solid is its energy. When heat flows into a solid its temperature rises as the absorbed thermal energy (enthalpy at fixed pressure) increases. As H is a function of temperature (T) it is then possible to define the derivative of H with respect to T as the heat capacity (c_p) of the material:

$$c_p = dH/dT. \tag{5-12}$$

Because H is not necessarily linear with respect to T, c_p is generally a function of temperature. Liquids and gases also have heat capacities. Therefore, if the heat capacity of materials is measured experimentally as a function of temperature, H can be extracted through mathematical integration. By making use of other thermodynamic equations and identities, values for entropies and free energies can also be determined. This building block approach enables a consistent set of thermodynamic data for materials to be assembled for use in assorted thermochemical calculations.

Returning to our one-component solid we may well ask how thermal energy is absorbed. The core electrons are too energetic to be affected, and the valence electrons absorb relatively little energy. This leaves the atomic ion cores as the major absorber of energy. What is the probability, $P(E_i)$, that atoms can absorb a given energy E_i at a temperature T? Statistical thermodynamic considerations provide the answer to this important question. The result, given without proof, is

$$P(E_i) = \exp(-E_i/kT), \tag{5-13}$$

where k is the Boltzmann constant ($k = R/N_A$). Of the form given earlier in Eq. 5-4, the exponential is known as the Maxwell–Boltzmann factor. This equation is easily one of the most important in the book and certainly one worth remembering. Since temperature constitutes such an important variable in materials science it is significant that Eq. 5-13 accurately predicts the exponential increase in rate with temperature of a host of phenomena governed by the thermally induced motion of atoms. A partial list of examples includes rates of chemical reactions, diffusive motion of atoms, viscous flow and deformation of polymers, solid-state phase transformations, sintering of ceramic and metal powders, elevated temperature degradation, and ionic conduction in ceramics. The value of E_i differs but, remarkably, ranges from perhaps a

fraction of an electron-volt per atom (1 eV/atom = 96,500 kJ/mol) to only a few electron-volts per atom in each of these solid-state processes.

This equation can also be profitably used to describe thermal energy absorption by atoms in a solid. The latter may be viewed as being held together by a three-dimensional collection of coupled springs much like the inner spring of a mattress or trampoline. A difference, however, is that the springs are in perpetual motion. Atoms sit at the spring nodes and when thermal energy is absorbed they vibrate at higher frequencies and with greater amplitude. A spring's potential energy is half the product of the spring constant and the square of its displacement (i.e., $\frac{1}{2}k_S(r - r_0)^2$ by Section 2.5.1); its kinetic energy is the same in magnitude on average. Their sum is basically the E_i of Eq. 5-13, which is the link between the spring's mechanical and thermal energy (i.e., kT).

This classical picture is a bit simplistic. We have already seen that electrons absorb energy in discreet quanta and so do atoms. But rather than photon waves for electrons, quantized vibrational waves (phonons) are associated with lattice atoms; their energies, $E = nh\nu$, were already noted in Eq. 2-3, where ν is the vibrational frequency. What average energy can then be expected in such a complex situation? No less a person than Albert Einstein solved this problem, and for a mole of atoms, he showed that the energy E ($\sim H$) is

$$E = 3N_A h\nu/2 + 3N_A h\nu/\{\exp(h\nu/kT) - 1\}. \qquad (5\text{-}14)$$

To obtain the specific heat of the solid, this expression needs to be differentiated with respect to T. At a high temperature, where $h\nu/kT$ is small, the problem is simplified because $\exp(h\nu/kT) - 1$ can be expanded as a series and approximated by $1 + h\nu/kT + \cdots + -1 = h\nu/kT$. Therefore, $E = 3N_A h\nu/2 + 3N_A kT$. Finally, by virtue of Eq. 5-12, differentiation yields $c_p = 3N_A k$ or $3R$. Two features of this quantum calculation (note the presence of Planck's constant h) are worth noting:

1. Irrespective of material the specific heat of a solid approaches $3R$ or very nearly 25 J/mol (6 cal/mol) at elevated temperatures. This feature is illustrated in Fig. 5-10 for a number of different materials and is known as the law of Dulong and Petit.

2. Heat capacity differences between materials are reflected primarily at lower temperatures where ν does not cancel from the expressions for E and c_p. Each material has a different characteristic value of ν. In the very hard and stiff diamond lattice, atoms vibrate at a high frequency of $\sim 2.75 \times 10^{13}$ Hz. For soft lead, however, the atomic vibrational frequency is low and approximately equal to 1.83×10^{12} Hz.

5.3.4.2. Blackbody Radiation

Another phenomenon based on absorption of thermal energy is blackbody radiation. If enough heat is absorbed by a solid and it gets sufficiently hot, it begins to emit electromagnetic energy from the surface, usually in the infrared

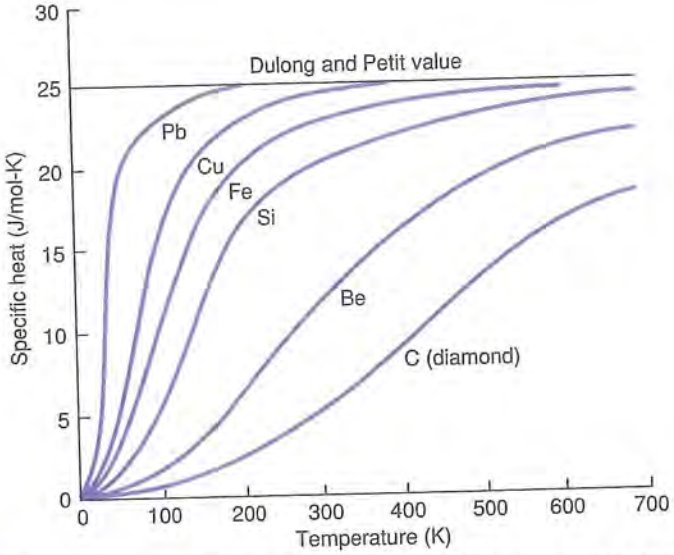

FIGURE 5-10 Heat capacity versus temperature for various solids. The upper limiting value of c_p is that predicted by Dulong and Petit. From C. Newey and G. Weaver, *Materials in Action Series: Materials Principles and Practice*, Butterworths, London (1990).

and visible regions of the spectrum. According to the formula given by Planck, the power density (P) radiated in a given wavelength (λ) range varies as

$$P(\lambda) = C_1\lambda^{-5}/\{\exp(C_2/\lambda T) - 1\} \quad \text{W/m}^2, \tag{5-15}$$

where C_1 and C_2 are constants. The mathematical similarity between Eqs. 5-14 and 5-15 is a reason for introducing this phenomenon here. As the temperature is increased the maximum value of P shifts to lower wavelengths. This accounts for the fact that starting at 500°C, a heated body begins to assume a dull red coloration. As the temperature rises it becomes progressively red, orange, yellow, and white. The total amount of heat power emitted from a surface, integrated over all directions and wavelengths, depends on temperature as T^4. This dependence is known as the Stefan–Boltzmann law.

5.4. INTRODUCTION TO BINARY PHASE DIAGRAMS

5.4.1. Phase Diagrams and How They Are Obtained

When two or more components (elements) react or are alloyed the number of possible product phases at different temperatures and pressures is limitless. Although one-element phase diagrams can comfortably fit in a book of about 100 pages, binary or two-element systems would necessitate a shelf of books

to completely account for their reactions. A library would probably be required for all of the possible ternary and higher-order systems. With the exception of several ternary alloy systems considered in Chapter 13 in connection with optical properties, these complex materials are not treated in this book.

In binary systems we are simply interested in knowing what to expect when two elements, of initially known proportions, are mixed and brought to temperatures of interest where they come to thermodynamic equilibrium. To simplify matters, only fixed pressure ($P = 1$ atm) is considered so that the Gibbs phase rule is $F = 3 - \phi$ when $C = 2$. Because it is impossible for F to be negative, three phases, at most, can coexist in equilibrium at fixed pressure. Whatever phases are present, however, can have differing melting temperatures, chemical compositions, and solubilities. Therefore, a graphic representation, that is, a binary phase diagram, that reflects this information would be very handy. In what follows the steps required to experimentally generate such a binary phase diagram by thermal analysis are described.

Consider the copper–nickel system. A series of alloys composed of different proportions by weight of Cu and Ni are prepared (e.g., 25Cu–75Ni, 50Cu–50Ni, 75Cu–25Ni), placed in separate crucibles, and then melted. A thermocouple (temperature-sensing device) is immersed in each melt and the temperature is carefully recorded as a function of time as the alloys cool from high temperatures. An extremely important assumption is that the crucible contents are in **thermodynamic equilibrium** at all times. This condition frequently means long exposure to elevated temperature coupled with low cooling rates. The individual cooling curves obtained are displayed in Fig. 5-11 together with those for pure Cu and pure Ni. In each case heat is lost to the surroundings by a combination of mechanisms that depend largely on the thermal properties (e.g., thermal conductivity, heat capacity, heat transfer coefficients) of the phases contained within the melt. At critical temperatures where new phases appear and others disappear, the cooling kinetics are strongly altered. Evolution of the latent heat of solidification and changes in the amounts and compositions of the phases present serve to pinpoint these singular temperatures; above and below them different cooling rates are frequently manifested.

Differences in cooling behavior are most pronounced in the pure metals. Both above and below the melting temperature (T_M), liquid and solid metal, respectively, cool in similar ways with time. But at T_M there is a thermal arrest that marks the transformation of liquid to solid. As there are one component and two phases, liquid (L) and solid (S), the phase rule predicts zero degrees of freedom, a condition satisfied by an **invariant** or fixed temperature.

Things are a bit more complicated in the alloys for there are no thermal arrests during solidification; instead, three regions can be distinguished. The upper and lower behaviors apparently describe cooling of either a liquid or a solid, respectively, as before. In these cases there is one phase but two components, so that $F = 2$. One of the degrees of freedom is taken up by a temperature drop as observed. In between, some combination of both liquid and solid exists

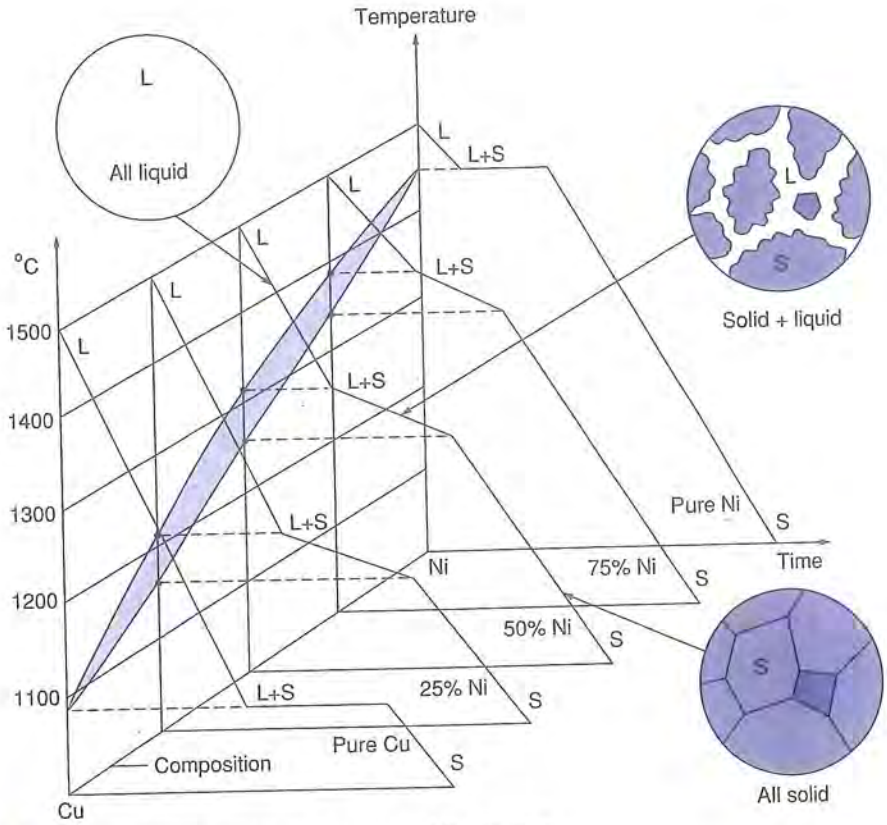

FIGURE 5-11 Temperature–time cooling curves for a series of Cu–Ni alloys.

in the crucible and the cooling behavior indicates at least one degree of freedom. If the crucible contents were stirred in this region the presence of solid pieces would be felt, but continued stirring would not dissolve them.

When corresponding sets of critical temperatures so determined are connected together for all of the metals and alloys, the resulting **equilibrium phase diagram**, depicted in Fig. 5-12, emerges for the Cu–Ni system. In the experimental technique just described, thermal property response was the vehicle used to locate critical temperatures. Although thermal analysis is the most widely employed method for this purpose, other properties sensitive to phase transformations (e.g., electrical, optical, magnetic, lattice parameter) have been used. The resulting experimentally determined phase diagrams have been compiled in books, that serve as the first references consulted when synthesizing or heat-treating materials.

The microstructure of an **equilibrated** binary Cu–Ni alloy, shown in Fig. 5-13, is not very different from that of the pure metals it comprises. Other

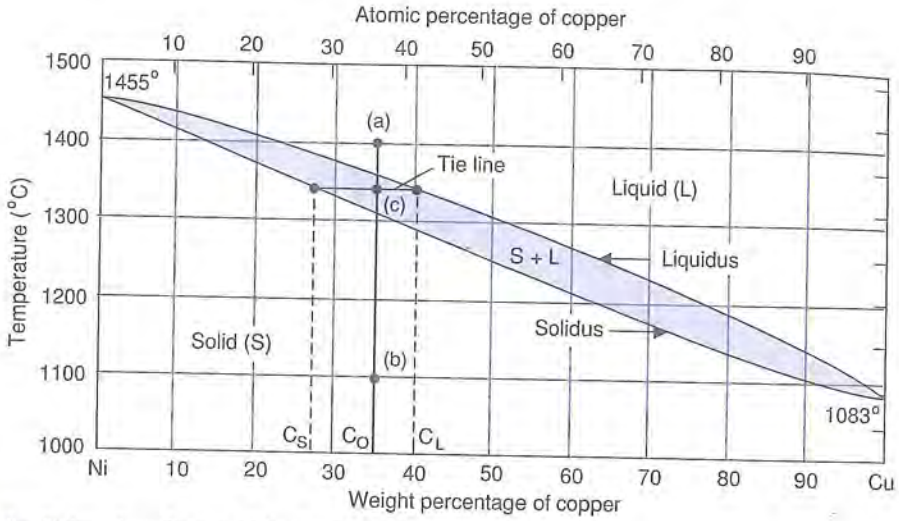

FIGURE 5-12 Equilibrium phase diagram of the Cu–Ni system.

binary combinations exhibiting similar solid solution solidification behavior include Ag–Au, Ag–Pd, Al_2O_3–Cr_2O_3, and Ge–Si, a system that is discussed further in Section 5.4.3.

5.4.2. Analysis of Binary Phase Diagrams

Phase diagrams compress a great deal of chemical and physical information about the involved element pairs into a convenient form. On the horizontal axis composition is plotted, with pure components represented at the extreme ends and alloys in between. Temperature is plotted on the vertical axis so that the intersection of composition and temperature, a point, represents a single state of the system, for example, a crucible containing a specific composition raised to the indicated temperature. In Cu–Ni alloys the possible states of the system contain either one or two phases. The former are labeled either L (liquid) or S (solid); the latter are confined to the lens-shaped region labeled L + S.

5.4.2.1. Single Phase

If a state exists in a single-phase field (in this or any other phase diagram) the **chemical** and **physical** analyses of what is present in thermodynamic equilibrium are very simple. Chemical analysis means just that—the percentage by weight or by atoms of each constituent component. Let us consider a 65 wt% Ni and 35 wt% Cu alloy (close in composition to Monel metal, which is used in petroleum refineries) and heat it to 1400°C (state a, Fig. 5-12). The alloy would melt and if we could make a chemical analysis at this temperature it would, not surprisingly, contain 65 wt% Ni and 35 wt% Cu. Physically, we

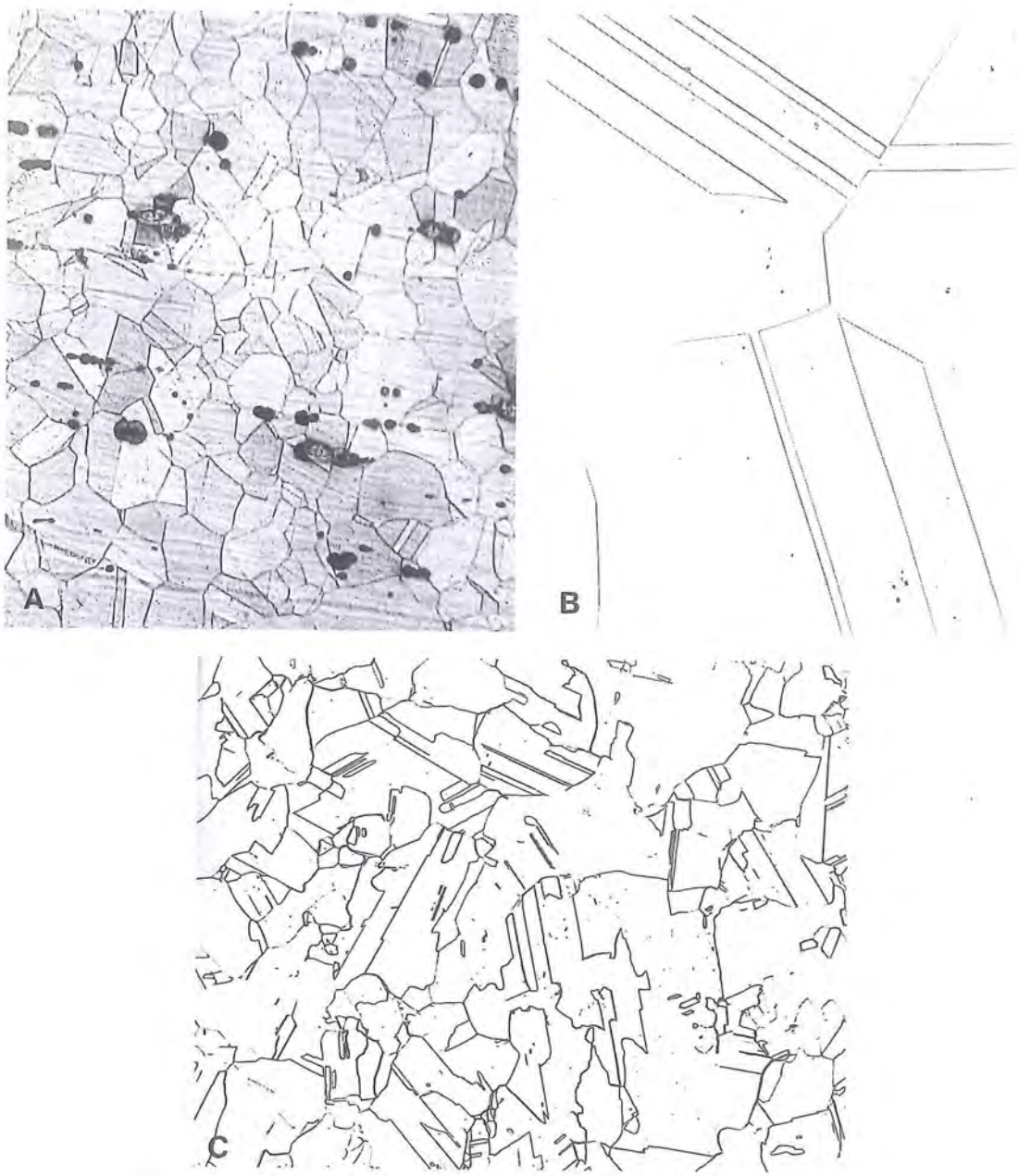

FIGURE 5-13 Microstructures of (A) 65 wt% Ni–35 wt% Cu alloy (158×), (B) pure copper (79×), and (C) pure nickel (79×). These metals are nominally single phase materials.

know that 100% of what would be present would be liquid. Similarly, if the original alloy were cooled to 1100°C (state b) we know the chemical analysis would be identical (i.e., 65 wt% Ni and 35 wt% Cu), and that physically, 100% of what would be present would be solid.

In any single-phase field of any binary equilibrium phase diagram the rules are:

1. The chemical composition is the same as that of the original alloy.
2. Physically, the alloy is either 100% homogeneous liquid or 100% homogeneous solid.
3. Single phase-alloy liquids and solids are generally stable over some range of composition and temperature.

5.4.2.2. Two-Phase Mixture: Tie Line Construction and Chemical Composition

If the system state point falls in a two-phase (L + S) field, a two-phase **physical mixture** exists. The chemical and physical analyses are now more complicated and follow rules different from those of the single-phase field. Importantly, both analyses center around the construction of a **tie line.** This line is drawn through the state point (c) and extends to the left and right until it ends at the single-phase boundaries on either side. Such a tie line is shown at 1340°C for the initial 65 wt% Ni–35 wt% Cu alloy. Tie lines are very significant because they connect two phases in **thermodynamic equilibrium.**

Mechanical equilibrium prevails because these phases coexist at the same constant pressure (1 atm).

Thermal equilibrium is assured because the tie line is drawn horizontally and not at an angle; the connected phases are thus at the same temperature.

Chemical equilibrium is also maintained but it is not as easy to visualize this. Basically the sloped lines on phase diagrams represent solubility limits. We all know, for example, that water at a given temperature dissolves as much sugar as the solubility limit allows. Below this limit, sugar dissolves in the one-phase liquid solution; above it, sugar is rejected (precipitates) out of solution to create a two-phase solid plus liquid mixture. The same considerations hold in the hot liquid and solid phases of the Cu–Ni system. The boundary line between the S and L + S fields is known as the **solidus,** and that between the L + S and L fields, the **liquidus.** Within the L + S field, chemical equilibrium requires that the composition of the solid at the solubility limit is given by the intersection point of the tie line with the solidus curve (read off on the horizontal axis). Similarly, the corresponding composition of the liquid is given by the intersection of the tie line with the liquidus curve. For example, in the 65 wt% Ni–35 wt% Cu alloy at 1340°C the solid has a composition of 27 wt% Cu–73 wt% Ni, whereas the liquid has a composition of 40 wt% Cu–60 wt% Ni. At these chemical compositions the free energy is minimized; slight increases or decreases beyond these solubility limits raise the overall free energy of this alloy relative to its minimum value.

5.4.2.3. Two-Phase Mixture: Lever Rule and Relative Phase Amounts

We are only halfway through our analysis of the two-phase mixture. Now that we know the **chemical analysis** of each phase let us perform a **physical analysis** to determine the relative proportions or weights of each phase present. The analysis is not unlike algebra word problems dealing with mixtures. Consider a portion of the phase diagram containing an alloy of A and B atoms with an initial composition C_0 expressed in terms of wt% B. Assume that two phases, α and β, coexist in equilibrium and the **chemical** composition of phase α is C_α and the composition of phase β is C_β. (It is common to identify solid phases by Greek letters.) Thus, phase α contains C_α wt% of component B and $(100 - C_\alpha)$ wt% of component A. The problem is to determine the fraction of the mixture by weight that is phase α (i.e., f_α) and the fraction that is phase β (i.e., $f_\beta = 1 - f_\alpha$). On the basis of W grams of total alloy, conservation of the mass of B atoms requires

$$WC_0 = WC_\alpha f_\alpha + WC_\beta(1 - f_\alpha). \tag{5-16}$$

The term on the left represents the total weight of B atoms in the alloy, and the terms on the right the weights of B atoms partitioned, respectively, to phases α and β. Solving for f_α and f_β yields the lever rule, which is expressed by

$$f_\alpha = (C_\beta - C_0)/(C_\beta - C_\alpha) \quad \text{and} \quad f_\beta = (C_0 - C_\alpha)/(C_\beta - C_\alpha). \tag{5-17}$$

The lever rule is so named because the fraction of a phase (f_α) multiplied by its "lever arm" $(C_0 - C_\alpha)$ is equal to the product of f_β and lever arm $(C_\beta - C_0)$. Thus, whichever phase (boundary) the initial composition is closest to is present in the greatest amount. When applied to our 65 wt% Ni–35 wt% Cu alloy at 1340°C, the fraction of solid is $f_S = (C_L - C_0)/(C_L - C_S) = 40\text{-}35/40\text{-}27 = 0.385$. For the liquid $f_L = (C_0 - C_S)/(C_L - C_S) = (35\text{-}27)/(40\text{-}27) = 0.615$.

1. Draw a horizontal tie line. (Tie lines are drawn only in two-phase fields. They make no sense in a one-phase field.)
2. The chemical composition of the two phases is given by the ends of the tie line, extended vertically down to and read off the horizontal axis.
3. The physical composition or weight fraction of each phase within the two-phase mixture is based on the tie line and given by the lever rule (Eq. 5-17).
4. Quantitative phase analyses cannot be made if the system state lies exactly on a line or boundary that separates phases. One must be either slightly above or slightly below the line to analyze the system by the above rules.

These are the rules. The rest is commentary and detail.

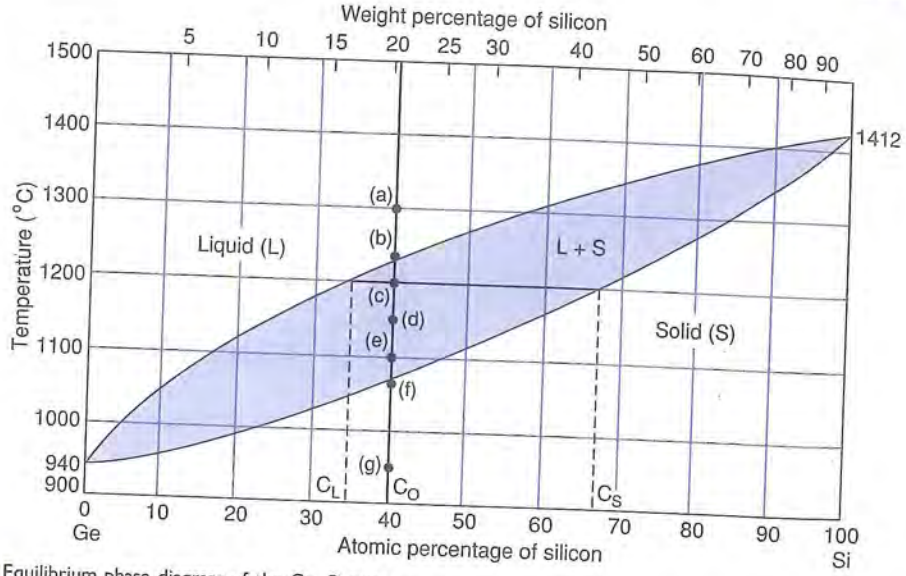

FIGURE 5-14 Equilibrium phase diagram of the Ge–Si system.

5.4.3. Analysis of an Equilibrium Cooled Alloy

We now have all the tools required to chemically and physically analyze a binary alloy system. Rather than the Cu–Ni system, which has a restricted L + S field (narrow solidification range) that makes tie line constructions difficult to read, let us consider the Ge–Si system of Fig. 5-14, which has a similar but wider two-phase field. Both phase diagrams exhibit **solid solution solidification.** The single-phase binary alloy liquid gives way to a **solid solution** upon cooling. Binary alloy liquids have many features in common with those which we imagine aqueous solutions possess. Atoms are in an agitated state of motion, sliding past each other in an amorphous medium with a density slightly different from that of the solid. These liquids are chemically homogeneous throughout and are single-phase materials because the individual randomly mixed atoms cannot be distinguished or separated. Solid solutions are similar, except that the solute atoms are randomly mixed in a crystalline matrix of solvent atoms.

EXAMPLE 5-3

An alloy containing 6×10^{22} atoms of Ge and 4×10^{22} atoms of Si is heated to 1300°C and cooled to 950°C.

a. What is the alloy composition in atomic and weight percentages?

b. At temperatures of 1300, 1230, 1200, 1150, 1100, 1070, and 950°C, what phases are present? What are their chemical compositions? How much of each phase is physically present? Assume equilibrium is attained at each temperature.

ANSWER a. The atomic percentage of Ge is

$$[6 \times 10^{22}/(6 \times 10^{22} + 4 \times 10^{22})] \times 100 = 60 \text{ at.\%}$$

Therefore, 40 at.% Si is present. The weight of the Ge atoms is

$$6 \times 10^{22} M_{Ge}/N_A = 6 \times 10^{22} \times 72.6/6.02 \times 10^{23} = 7.24 \text{ g}$$

The weight of the Si atoms is

$$4 \times 10^{22} M_{Si}/N_A = 4 \times 10^{22} \times 28.1/6.02 \times 10^{23} = 1.87 \text{ g}.$$

The wt% Ge = [7.24/(7.24 + 1.87)] × 100 = 79.5. Therefore, there is 20.5 wt% Si as noted on the upper weight percentage silicon scale. Both weight and atomic percentage notations are widely used as measures of composition.

b. The included table is self-explanatory and has the required answers.

Temperature (°C)	Phases	Chemical composition (at.% Si)	Phase amounts (atomic fraction)	Comment
a. 1300	L	40	1.0	All liquid
b. 1230	L	~40	~1.0	Solidification just beginning
	S	72	~0	
c. 1200	L	34	(67-40)/(67-34) = 0.82	Use of Eq. 5-17
	S	67	0.18	Use of Eq. 5-17
d. 1150	L	25	(56-40)/(56-25) = 0.52	Use of Eq. 5-17
	S	56	0.48	Use of Eq. 5-17
e. 1100	L	16	(47.5-40)/(47.5-16) = 0.24	Use of Eq. 5-17
	S	47.5	0.76	Use of Eq. 5-17
f. 1070	L	12	~0	Solidification almost complete
	S	~40	~1	
g. 950	S	40	1.0	All solid

An idealized picture of the solidification events during slow cooling of this alloy would first start with an amorphous melt. At 1230°C tiny Si-rich dendrites (see Section 3.6.1) would begin to form at the mold wall and perhaps in the bulk of the melt as well. With a drop in temperature the dendrites continue to grow by thickening and lengthening. Surrounding the dendrites is the remaining Ge-rich liquid which continually shrinks in amount until it effectively disappears at 1070°C, leaving grain boundaries behind.

5.5. ADDITIONAL PHASE DIAGRAMS

5.5.1. The Binary Eutectic Phase Diagram

Many pairs of elements (e.g., Bi–Cd, Sn–Zn, Ag–Cu, Al–Si) solidify in a manner similar to that of Pb–Sn, whose **eutectic phase diagram** is shown in Fig. 5-15. The eutectic is so named for the critical constant temperature or **isotherm** that dominates the phase diagram. Below this temperature (183°C in Sn–Pb) for any composition lying within the span of the isotherm (19.2–97.5 wt% Sn), liquid is no longer stable. Above the eutectic temperature, however, it is as though portions of two independent solid solution systems exist—one on the Pb side yielding Pb-rich solid solutions, the other on the Sn side giving rise to Sn-rich solid solutions. Their liquidus lines converge at a critical point, the eutectic composition (61.9 wt% Sn). This means that the liquid phase of every alloy containing between 19.2 and 97.5 wt% Sn will eventually reach the eutectic composition (61.9 wt% Sn) upon cooling from an elevated temperature to slightly above 183°C. Liquid at this very special eutectic composition then decomposes at 183°C into a mixture of two solid phases: α, a Pb-rich

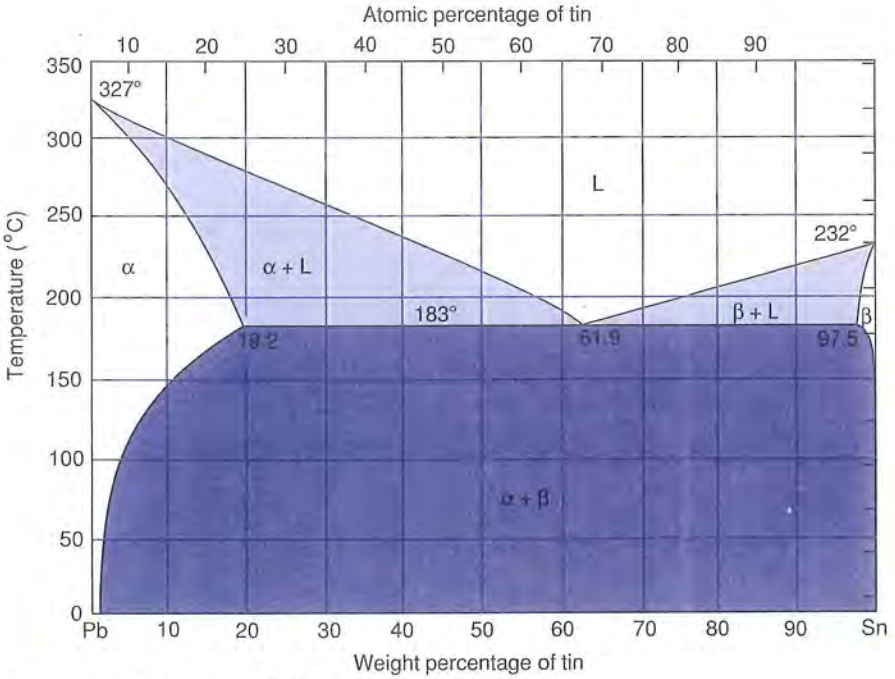

FIGURE 5-15 Equilibrium phase diagram of the Pb–Sn system.

solid solution, and β, a Sn-rich solid solution. The equation describing the decomposition of a single-phase liquid into a two-phase solid mixture at the eutectic temperature

$$L \rightarrow \alpha + \beta \tag{5-18}$$

may be taken as a definition of the generic eutectic solidification reaction. According to the phase rule, $C = 2$, $\phi = 3$ (L, α, and β); therefore, $F = 2 - 3 + 1 = 0$. Zero degrees of freedom means that the reaction is invariant; both the temperature and phase compositions remain constant during the transformation of eutectic liquid to $\alpha + \beta$. Consider now the cooling behavior of an alloy of exactly eutectic composition (61.9 wt% Sn–38.1 wt% Pb). Until the melt reaches 183°C there is the usual temperature drop. But then there is a thermal arrest at the eutectic temperature until the eutectic reaction is complete. This is followed by cooling to room temperature by the two-phase solid. If one did not know better the solidification cooling behavior of a pure metal with a melting point of 183°C might be imagined. The two-phase $\alpha + \beta$ eutectic microstructure that develops is generally characteristic of the alloy system. It often appears as a lamellar array of alternating plates of the two phases, but sometimes as a dispersion of one phase in a matrix of the other.

The rules of phase analysis in single- and two-phase fields were given previously and they will be applied once again in the example below. First, however, a few additional details of eutectic solidification should be noted. When compositions on the Pb-rich side begin to solidify, the solid α phase (in equilibrium with L) that increases in amount as the temperature drops is known as the **proeutectic** or **primary** α phase. Similarly, the solid proeutectic or primary β phase separates from the melt in Sn-rich alloys. After the eutectic reaction is completed, the eutectic mixture of $\alpha + \beta$ adds its presence to the already solidified larger crystals of proeutectic α (or β). Further cooling is accompanied by rejection of solute from proeutectic phases to satisfy solubility requirements. But solid-state reactions are often sluggish, and structural and chemical change practically ceases once the melt has totally solidified.

EXAMPLE 5-4

a. For the alloys 5 wt% Sn–95 wt% Pb, 40 wt% Sn–60 wt% Pb, and 70 wt% Sn–30 wt% Pb, identify the phases present and determine their compositions and relative amounts at 330, 184, and 25°C.

b. For a 1-kg specimen of the 70 wt% Sn–30 wt% Pb alloy, what weight of Pb is contained within the eutectic microstructure at 182°C?

ANSWER The answers are tabulated below using the tie line and lever rule in all two phase regions.

Temperature (°C)	Phases	Chemical composition (wt% Sn)	Phase amounts (weight fraction)	Comment
		5 wt% Sn–95 wt% Pb		
330	L	5	1.0	All liquid
184	α	5	1.0	All solid
25	α	~2	(100-5)/(100-2) = 0.97	(Eq. 5-17)
	β	~100	(5-2)/(100-2) = 0.03	No eutectic microstructure
		40 wt% Sn–60 wt% Pb		
330	L	40	1.0	All liquid
184	α	19.2	(61.9-40)/(61.9-19.2) = 0.51	Proeutectic α
	L	61.9	(40-19.2)/(61.9-19.2) = 0.49	Eutectic liquid
25	α	~2	(100-40)/(100-2) = 0.61	(Eq. 5-17)
	β	~100	(40-2)/(100-2) = 0.39	
Or alternatively,				
182	α	19.2	(61.9-40)/(61.9-19.2) = 0.51	Proeutectic α
	$\alpha + \beta$	61.9	(40-19.2)/(61.9-19.2) = 0.49	Eutectic mixture (Eq. 5-17)
		70 wt% Sn–30 wt% Pb		
330	L	70	1.0	All liquid
184	β	97.5	(70-61.9)/(97.5-61.9) = 0.23	Proeutectoid β
	L	61.9	(97.5-70)/(97.5-61.9) = 0.77	Eutectic liquid
25	α	~2	(100-70)/(100-2) = 0.31	(Eq. 5-17)
	β	~100	(70-2)/(100-2) = 0.69	
Or alternatively,				
182	β	~97.5	(70-61.9)/(97.5-61.9) = 0.23	Proeutectic β
	$\alpha + \beta$	61.9	(97.5-70)/(97.5-61.9) = 0.77	Eutectic mixture (Eq. 5-17)

b. In 1 kg of the 70 wt% Sn–30 wt% Pb alloy the eutectic mixture weighs 0.77 kg. Of this, 61.9% is Sn and 38.1% is Pb. Therefore, the amount of Pb = (0.77)(.381) = 0.29 kg.

Schematic microstructures of these alloys are sketched in Fig. 5-16 for the indicated alloys. They should be compared with actual room temperature microstructures of several alloys in the Pb–Sn system (Fig. 5-17). The one containing 63 wt% Sn–37 wt% Pb is common electrical solder; the 50 wt% Sn–50 wt% Pb alloy was used in plumbing. (Recently, the use of Pb in plumbing has been outlawed.)

5.5.2. Side-by-Side Eutectics

More complex phase diagrams can arise through the addition of solid solution, eutectic, and yet other solidification features in horizontal or vertical

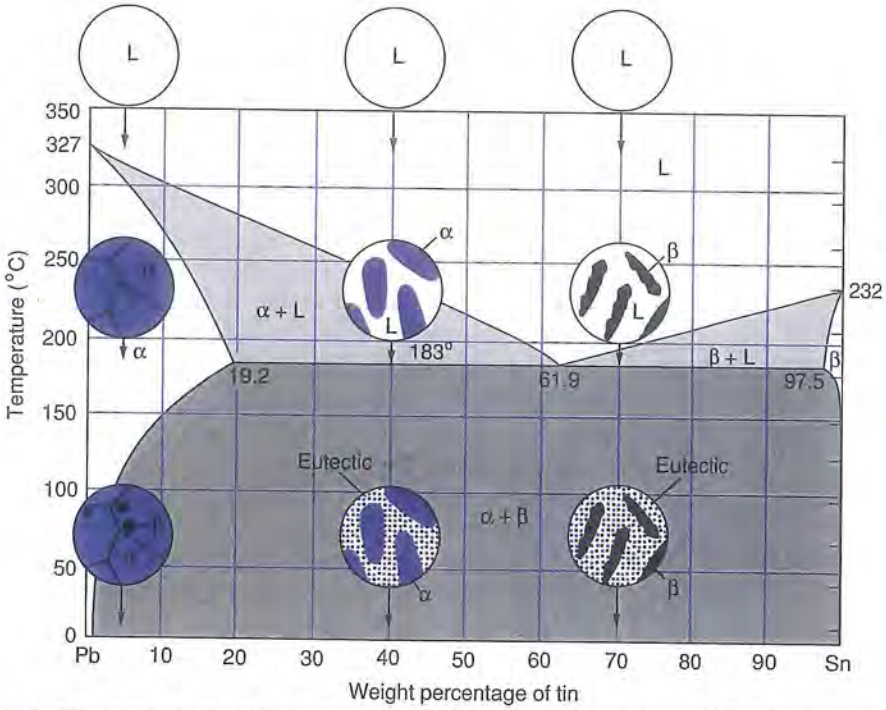

FIGURE 5-16 Schematic microstructures of three alloys in the Pb–Sn system at temperatures of 330, 184, and 25°C. The eutectic microstructure is a mechanical mixture of $\alpha + \beta$.

configurations. Phase analysis in such systems follows rules laid down earlier. Tie lines never extend beyond two-phase fields so that no more than one eutectic at a time is ever considered. Phase diagrams are like road maps; on a map of the greater New York metropolitan area one is not concerned about the neighboring states of New Jersey and Connecticut when motoring through Manhattan. In this spirit consider the Ga–As phase diagram depicted in Fig. 5-18. This system is a very important one in semiconductor technology and contains two eutectic systems stacked side by side. The eutectic compositions are so close to the respective terminal axes that they cannot be resolved on the scale of the phase diagram. A dominant feature in the phase diagram is the central compound GaAs, containing equiatomic amounts of Ga and As. It is regarded as a terminal component in the Ga–GaAs eutectic phase diagram on the left half or Ga-rich side. GaAs is also shared in common with As to

FIGURE 5-17 Optical microstructures of Pb–Sn alloys (96×). (A) 30 wt% Sn–70 wt% Pb. Dark etching, proeutectic Pb-rich α phase surrounded by light etching eutectic. (B) 50 wt% Sn–50 wt% Pb. Dark etching dendritic α phase within the light etching eutectic matrix. (C) 63 wt% Sn–37 wt% Pb. Two-phase eutectic microstructure. (D) 70 wt% Sn–30 wt% Pb. Light etching, dendritic, proeutectic Sn-rich β phase surrounded by eutectic.

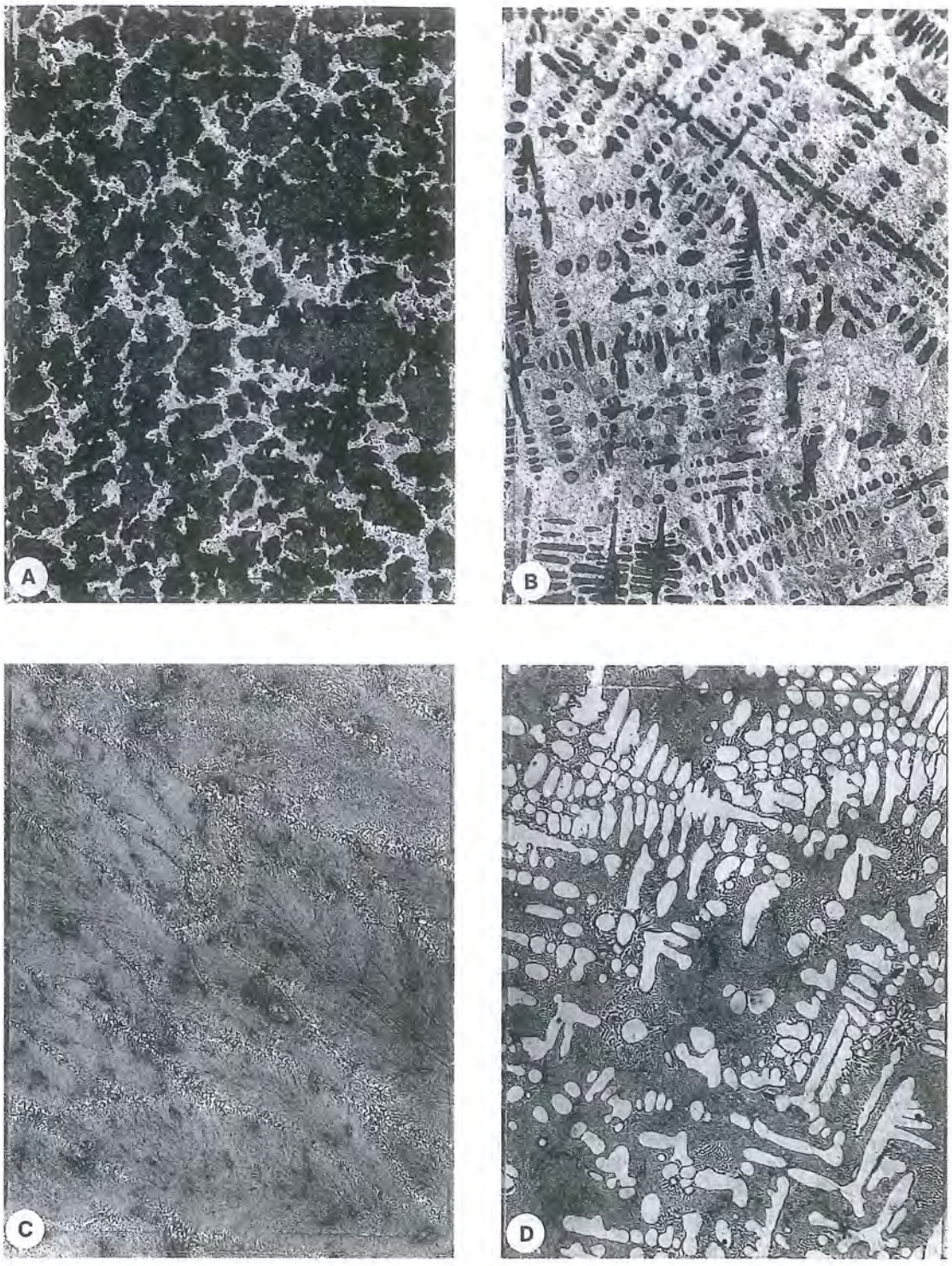
A
B
C
D

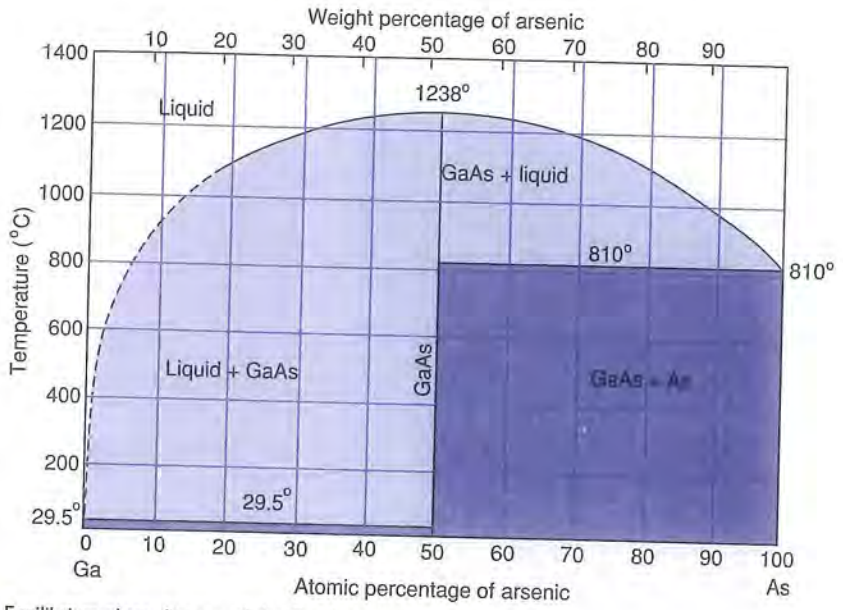

FIGURE 5-18 Equilibrium phase diagram of the Ga–As system.

generate the As–GaAs binary eutectic on the As-rich side. Compounds on phase diagrams often have well-defined stoichiometries, in this case 50 at.% Ga–50 at.% As, and are therefore denoted by narrow vertical lines.

One of the important single-crystal growth techniques employed in the fabrication of compound semiconductor lasers and diodes is known as **liquid phase epitaxy.** The technique can be simply understood in terms of this phase diagram. Consider a Ga-rich melt containing 10 at.% As that is cooled slowly just below 930°C so that it enters the two-phase L + GaAs field. A small amount of solid GaAs separates from the melt. If a single-crystal GaAs wafer substrate is placed in the melt, it will provide an accommodating surface template for the rejected GaAs to deposit on. In the process thin single-crystal epitaxial layers are grown. Readers will recognize that the crystals they grew as children from supersaturated aqueous solutions were essentially formed by this mechanism.

The combination of the ceramic materials silica (SiO_2) and corundum (Al_2O_3) yields another binary system of interest in which eutectics are joined horizontally. As shown in Fig. 5-19 one eutectic forms between SiO_2 and γ (mullite) and the other between γ and Al_2O_3. Mullite is a compound with nominal composition $3Al_2O_3 \cdot 2SiO_2$, but it apparently exists over a broader stoichiometric range than does GaAs. Alloy mixtures of these oxides are important because they are used to make refractory bricks that line high-temperature industrial furnaces.

It is interesting to note the passage from one-phase to two-phase to one-

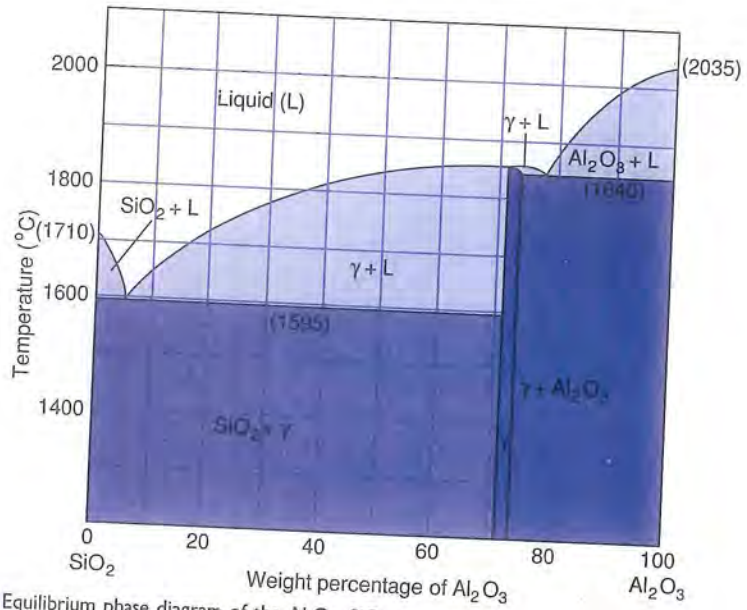

FIGURE 5-19 Equilibrium phase diagram of the Al_2O_3–SiO_2 system.

phase to two-phase to one-phase regions, and so on, across any constant temperature on the phase diagram. This 1–2–1–2–1–...–1 rule, rooted in thermodynamics, is readily illustrated by all phase diagrams.

EXAMPLE 5-5

The phase diagrams depicted in Fig. 5-20 are all thermodynamically impossible as drawn. Provide good physical arguments that specifically indicate what is wrong.

ANSWER a. The hump in the lens-shaped L + S region is incorrect. Below T_1 tie lines correctly intersect L and S fields. But above T_1 it is possible to draw tie lines that intersect only liquid fields on either side and not L + S as labeled.

b. A slanted eutectic isotherm is a contradiction in terms. It means the system is not in thermal equilibrium. Furthermore, horizontal tie lines to the slanted eutectic line connect phases that are inconsistent with the given labeling of the phase fields.

c. On the eutectic isotherm four phases—α, β, γ, and L—appear to coexist in equilibrium. But this is contrary to the phase rule (by Eq. 5-11, $F = 2 + 1 - 4 = -1$) because the maximum number of phases in a two-component system is 3.

d. The gap in composition along the eutectic isotherm is incorrect. It implies a variable composition of the eutectic liquid and negative degrees of freedom.

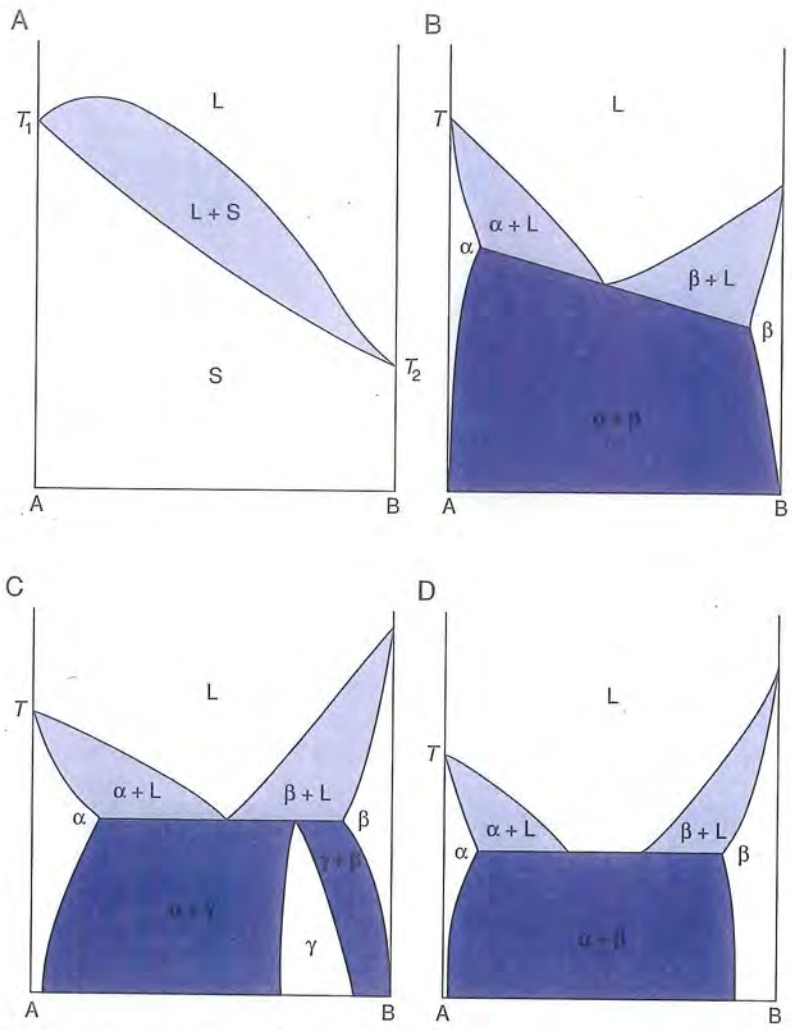

FIGURE 5-20 Four thermodynamically impossible phase diagrams.

5.5.3. Peritectic Solidification

5.5.3.1. Pt–Re

Not uncommon in the catalog of solidification sequences is the invariant peritectic reaction, which can be written in the generic form

$$L + \beta \rightarrow \alpha. \tag{5-19}$$

Peritectic reactions often occur when there is a large difference in melting point between the two components. On the phase diagram the peritectic reaction is

characterized by the prominent isotherm (zero degrees of freedom), and appears as an upside-down eutectic. There are few examples of alloy systems that exhibit only peritectic behavior over the complete temperature range. One is the platinum–rhenium system, whose phase diagram is shown in Fig. 5-21. Above the peritectic temperature of 2450°C, solid solution solidification prevails in Re-rich alloys. Below this temperature down to the melting point of Pt, liquid exists for Pt-rich compositions which also solidify as solid solutions. This is in contrast to the eutectic isotherm below which no liquid exists.

Only alloys with compositions between ~43 wt% Re and ~54 wt% Re participate in the peritectic reaction. For any alloy in this range a liquid containing ~43 wt% Re and a solid β containing ~54 wt% Re coexist just above 2450°C. The proportions depend on the initial composition and can be calculated from the lever rule (Eq. 5-17). If, for example, we consider the alloy with the critical peritectic composition, that is, 46 wt% Re, then just above 2450°C, $f_\beta = (46\text{-}43)/(54\text{-}43) \times 100 = 27\%$. Thus, 27% of the alloy is solid β, and

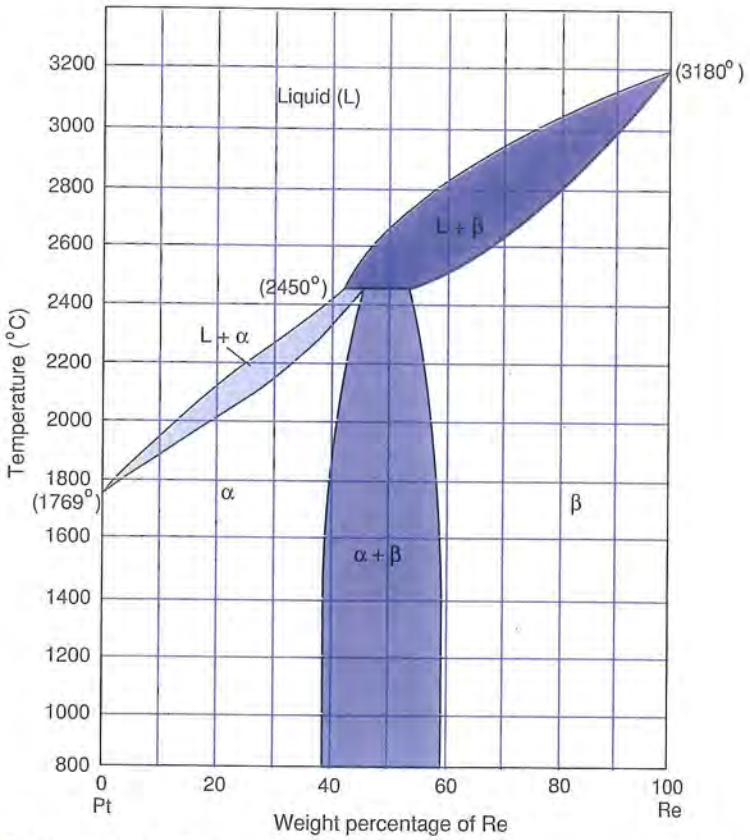

FIGURE 5-21 Equilibrium phase diagram of the Pt–Re system.

the rest is liquid. Given sufficient time, α phase will consume the prior liquid and β, as Eq. 5-19 suggests. But, as the temperature drops, β will be rejected from α and both phases will persist down to lower temperatures. Unlike eutectics, peritectics have no particularly distinguishing microstructural features.

The issue of equilibrium is an important one in peritectic solidification. As peritectic reactions are so sluggish they do not readily proceed to completion unless maintained at high temperature for long times. With practical cooling rates the peritectic reaction may be bypassed, yielding nonequilibrium phases that may not appear on the phase diagram.

5.5.3.2. Cu–Zn

One glance at Fig. 5-22 reveals a binary system with complex solidification behaviors, containing a number of phase features not yet discussed. The cop-

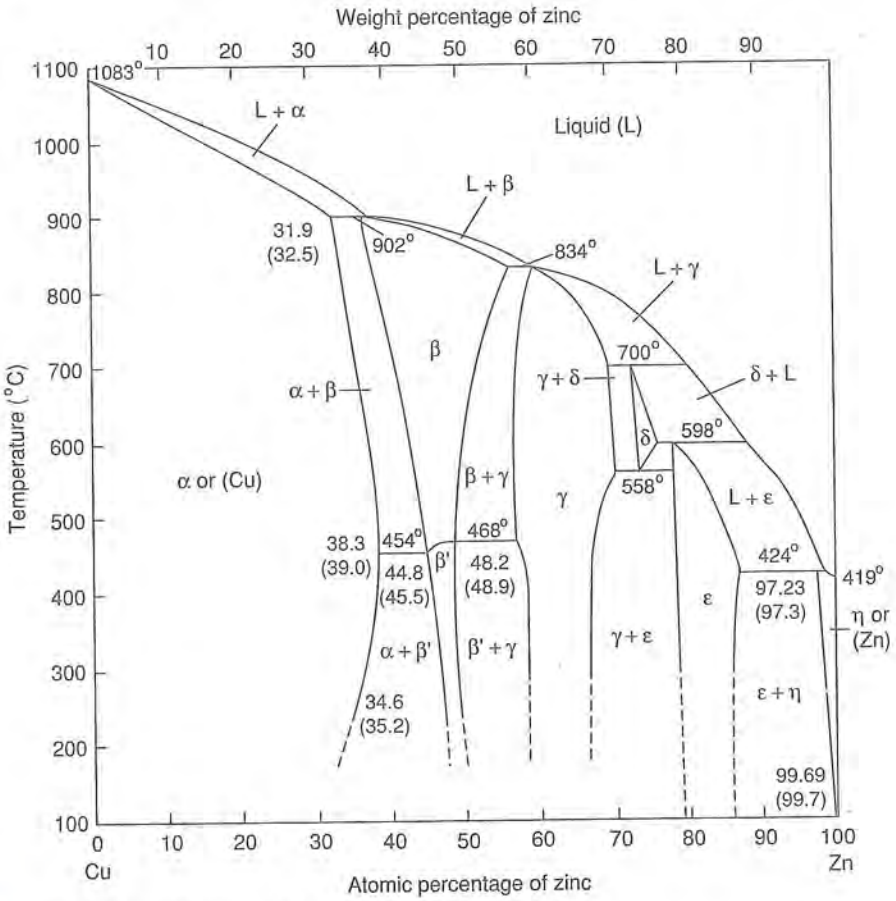

FIGURE 5-22 Equilibrium phase diagram of the Cu–Zn system.

per–zinc system includes several commercially important coppers and brasses among its compositions, for example, gilding metal (95Cu–5Zn), cartridge brass (70Cu–30Zn), and Muntz metal or β brass (60Cu–40Zn). A cascade of peritectic solidification behaviors dominates the high-temperature portion of the phase diagram for all compositions; actually there are five peritectic isotherms as well as a 558°C **eutectoid**-type reaction, whose features are discussed in the next section.

5.5.4. Fe–Fe_3C Phase Diagram

The best known and arguably most important phase diagram in metallurgy is the one shown in Fig. 5-23 between Fe and the compound Fe_3C containing 6.67 wt% C. From it much can be learned about plain carbon steels and cast irons, two of the most widely used classes of structural metals. Figure 5-23 is not a true *equilibrium* diagram, however, because Fe_3C can decompose into graphite (C) and Fe at elevated temperatures. Nevertheless, carbon steel struc-

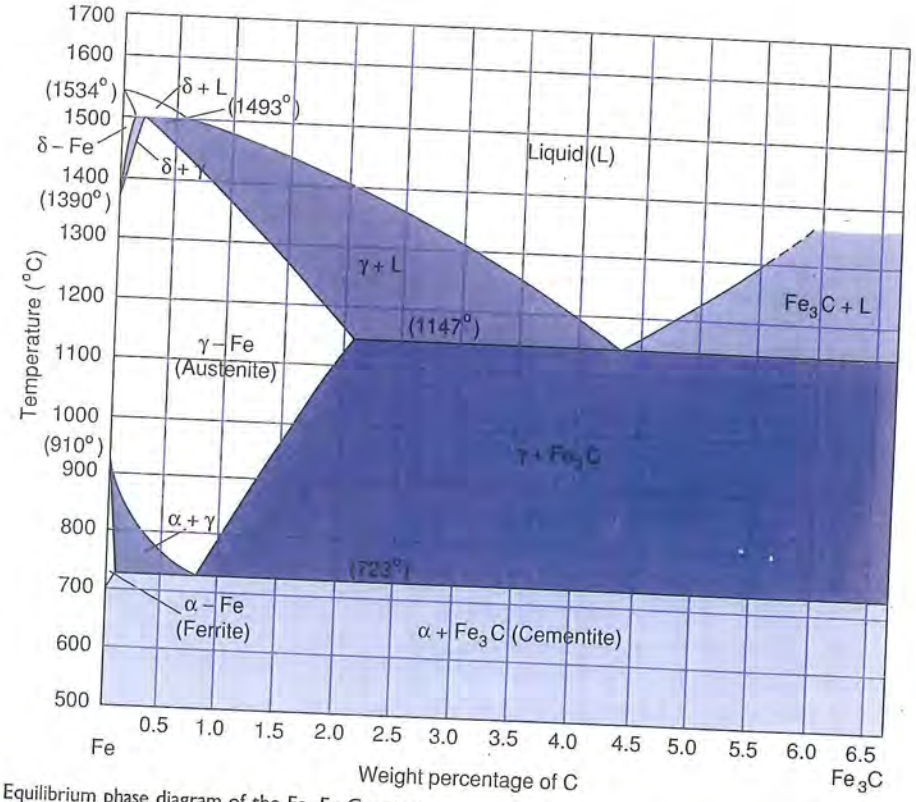

FIGURE 5-23 Equilibrium phase diagram of the Fe–Fe_3C system.

tures are not about to collapse because Fe_3C is, for all practical purposes, stable indefinitely at ambient temperatures.

It is instructive to proceed down the weight percentage C axis and indicate some of the ferrous materials commercially employed. Containing less than 0.1% carbon are the wrought irons used by railroads and in shipbuilding and decorative architectural applications (iron gratings, fences, etc.). Wrought irons also contain several percent slag (mixtures of oxides) strung out in the matrix as a result of mechanical processing. The transition to materials known as steels occurs beyond roughly 0.1 wt% C. Plain carbon steels range from ~0.1 to about 1.5 wt% C and are identified by the designation *SAE** or *AISI*† *10XY*. The last two digits refer to carbon content in hundredths of a percent.

Structural steel (1015 or 1020 containing 0.15 or 0.20 wt% C) is produced in the greatest tonnage. From roughly 0.20 to 0.60 wt% C (1020–1060) there are the medium-carbon steels, and above this, the high-carbon steels. Machine parts and tools are made from steels within these compositions. Steel containing 0.8 wt% C is at the critical eutectoid composition and is known as eutectoid steel. **Hypoeutectoid** steels contain less than 0.8 wt% C, and **hypereutectoid** steels have more than this amount of carbon. For carbon levels between ~2 and 4 wt% C we speak of cast irons. The Fe–Fe_3C phase diagram exhibits all of the solidification and transformation behaviors already discussed and one we did not yet introduce. **Solid solution** freezing is evident between the γ, γ + L, and L phase fields at elevated temperatures, **eutectic** solidification occurs at 1147°C, and there is a **peritectic** reaction at 1493°C.

The new transformation feature, the **eutectoid**, occurs at the critical temperature of 723°C and resembles a eutectic. Instead of a liquid transforming as in the eutectic, a wholly solid-state transformation occurs in which one *solid* decomposes into two different *solid* phases. The generic, invariant eutectoid reaction is

$$\gamma \text{ (solid)} \rightarrow \alpha + \beta, \tag{5-20}$$

which, in steel, is explicitly exemplified by

$$\gamma\text{-Fe (austenite)} \xrightarrow{723°C} \alpha\text{-Fe (ferrite)} + Fe_3C \text{ (cementite)}. \tag{5-21}$$

Austenite (FCC γ-Fe) dissolves as much as 2 wt% C at 1147°C, whereas **ferrite** (BCC α-Fe) can hold only a maximum of a hundredth as much or less. Partitioning of carbon between these phases at the transformation temperature plays an important role in the hardening of steel by nonequilibrium heat treatment. This important subject is discussed again in Chapter 9.

Reference to Fig. 5-24 reveals that room temperature equilibrium structures of hypoeutectoid steels are a mixture of α-Fe and Fe_3C phases. Upon cooling γ-Fe into the two-phase α-Fe + γ-Fe field, **proeutectoid** α-Fe nucleates at the

* Society of Automotive Engineers.
† American Iron and Steel Institute.

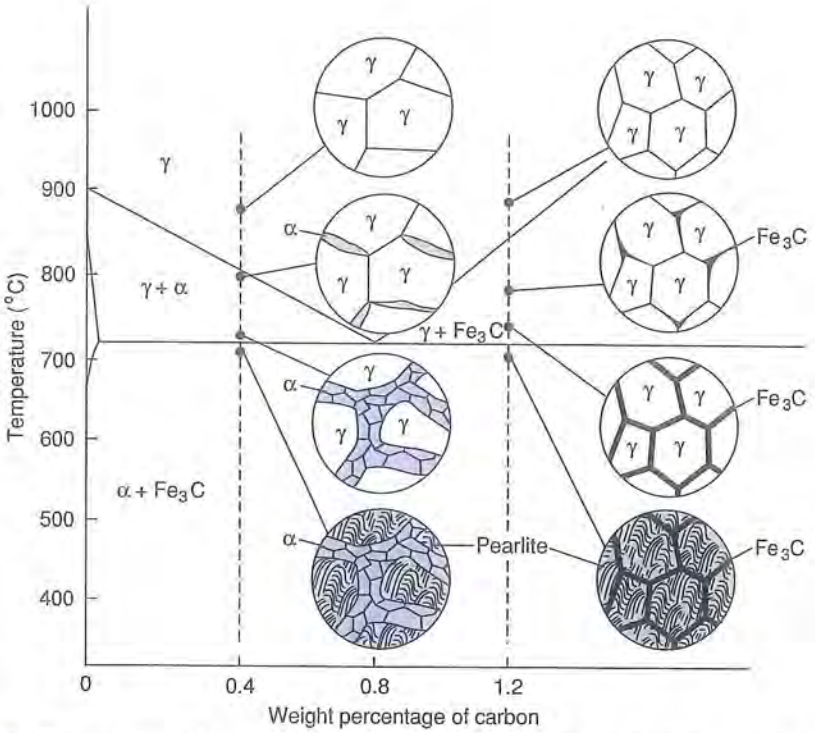

FIGURE 5-24 Equilibrium phase transformations in hypoeutectoid and hypereutectoid steels together with schematic microstructures.

prior γ grain boundaries. The situation is not unlike rejection of a proeutectic phase from a prior liquid in a eutectic system. Just above the eutectoid isotherm, the lever rule (Eq. 5-17) indicates that the amount of γ-Fe present is $(C_0 - 0.02)/(0.8 - 0.02)$, where C_0 is the initial hypoeutectoid steel composition. Below 723°C all of this γ-Fe transforms to a two-phase mixture of α-Fe + Fe_3C known as **pearlite.** Just as eutectic two-phase mixtures have a characteristic appearance, so does pearlite, whose microstructure is shown in Fig. 5-25. It consists of plates of Fe_3C (also known as **cementite**) embedded in an α-Fe matrix, so that overall, the eutectoid appears to have a fingerprint-like lamellar structure. Slowly cooled hypoeutectoid steels then contain varying proportions of ferrite and pearlite depending on steel composition.

The situation in hypereutectoid steels is complementary to that in hypoeutectoid steels. Now the proeutectoid phase is cementite, and phase fields to the right of the eutectoid composition, extending to 6.67 wt% C, are relevant. Just above 723°C there is a two-phase mixture of γ-Fe + Fe_3C, and again austenite transforms to pearlite when the steel cools below this temperature. The microstructure now consists of pearlite colonies, surrounded by a network of Fe_3C that delineates the prior austenite grain boundaries where cementite

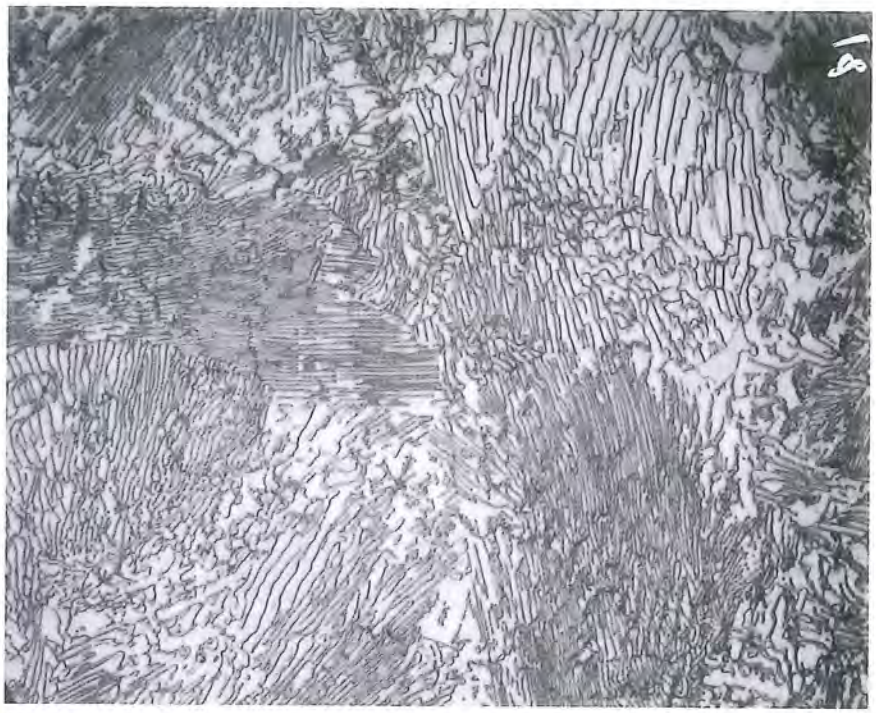

FIGURE 5-25 Microstructure of pearlite in eutectoid steel (970×). Courtesy of G. F. Vander Voort, Carpenter Technology Corporation.

nucleates. Because cementite is a hard, brittle phase it outlines potential paths for crack propagation. A coarse Fe_3C network is, therefore, viewed with concern. Heating high-carbon steels to just below the eutectoid temperature for long periods causes Fe_3C, in both pearlite and proeutectoid phases, to ball up as in Fig. 5-26. These cementite spheres are now surrounded by a softer, but more malleable, ferrite grain matrix and resemble fat globules floating in soup. Importantly, hard-to-machine tool steels are softened by this spheroidizing heat treatment. It will be clear from Section 5.7 that reduction of the Fe_3C plate surface area (or energy) is the driving force behind the spheroidization process.

5.6. STRUCTURE AND COMPOSITION OF PHASES

5.6.1. Equilibrium Phases: Solid Solutions

5.6.1.1. Substitutional Solid Solution

Binary phase diagrams usually contain an assortment of single-phase materials known as **solid solutions** and these have already been introduced in Sections 5.1 and 5.4.3. In the substitutional solid solution alloy the involved solute and

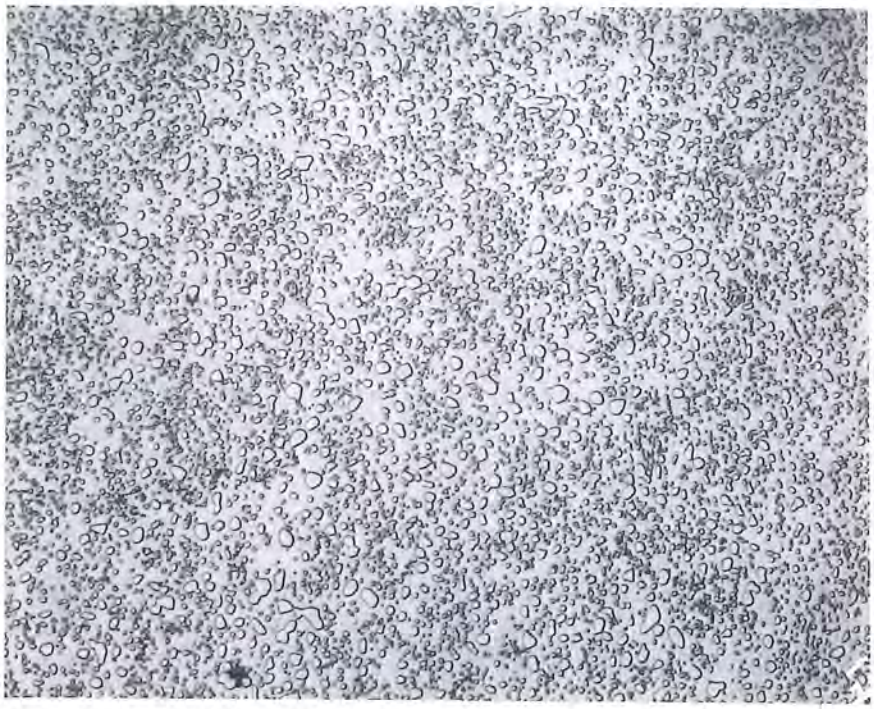

FIGURE 5-26 Microstructure of spheroidite in high-carbon steel (970×). Courtesy of G. F. Vander Voort, Carpenter Technology Corporation.

solvent atoms are randomly mixed on lattice sites. The single-phase solid alloys that extend across the entire phase diagram in the Cu–Ni and Ge–Si systems are good examples of random substitutional solid solutions. Both atoms are randomly distributed on FCC lattice sites in Cu–Ni and on diamond cubic sites in Ge–Si. In either case it makes no difference which component one starts with; the atoms mix in all proportions. A *necessary* condition for single-phase solid solution formation across the entire phase diagram is that both components have the same crystal structure. It is not a *sufficient* condition, however, because there are combinations like Ag–Cu (both FCC) and Fe–Mo (both BCC) that do not form an extensive range of solid solutions. Instead **terminal solid solutions,** so named because they appear at the ends of the phase diagram, form. The terminal α and β phases in the Pb–Sn diagram (Fig. 5-16) are examples. They are both substitutional solid solutions and display the limited solubility often exhibited by such phases. Introduction of foreign atoms into the lattice, whether by design (as dopants or solutes) or accident (as impurities), will always create dilute solid solutions which are often substitutional in nature. In fact, all "pure" materials are in effect dilute terminal solid solutions because it is thermodynamically impossible to remove all impurities.

The lattice parameter of substitutional solid solutions is usually an average of the interatomic spacings in the pure components weighted according to the atomic fractions present. This observation is known as Vegard's law. It predicts, for example, that the lattice parameter of a 25 at.% Cu–75 at.% Ni alloy will be approximately 0.25×0.3615 nm $+ 0.75 \times 0.3524$ nm $= 0.355$ nm. (See Table 3-2.)

5.6.1.2. Interstitial Solid Solution

When undersized alloying elements dissolve in the lattice they sometimes form interstitial solid solutions. Important examples include carbon and nitrogen in BCC iron, the former being the α phase on the Fe–Fe_3C phase diagram (Fig. 5-23). Rather than sit on substitutional sites, these atoms occupy the interstice in the center of the α-Fe cube faces, e.g. $(\frac{1}{2}, 0, \frac{1}{2})$. In FCC γ-Fe, carbon atoms assume the large interstitial site in the center of the unit cell. Based on a hard sphere model it is not too difficult to show that considerably less room is available for carbon to squeeze into in the α-Fe interstitial site relative to the γ-Fe site. More severe lattice bond straining in the former means that less carbon will dissolve interstitially in α-Fe compared with γ-Fe, in accord with solubility limits defined by the Fe–Fe_3C phase diagram.

5.6.1.3. Intermediate Solid Solution

Unlike terminal solid solutions that extend inward from the outer pure components, intermediate phase fields are found *within* the phase diagram. Two phase regions border either side of an intermediate phase. In the case of Cu–Zn (Fig. 5-22), α and η are terminal phases, and β, γ, δ, and ε are intermediate phases. These single phases are generally stable over a relatively wide composition range.

5.6.1.4. Ordered Solid Solution

Atoms within certain solid solutions can, surprisingly, order and give every appearance of being a compound. The resulting structure is schematically depicted in Fig. 5-1E and actually realized in 50 at.% Cu–50 at.% Zn β'-brass. In this alloy we can imagine a CsCl-like structure (Fig. 3-8) populated by atoms of Cu and Zn. Above 460°C the ordering is destroyed and a random solid solution forms. The order–disorder transformation, interestingly, bears a close resemblance to the loss of magnetism exhibited by magnets that are heated above the Curie temperature (see Chapter 14).

5.6.2. Compounds

Another very common type of solid phase that appears in phase diagrams is the compound. Elementary inorganic chemistry provides a basis for understanding compounds in many binary systems. For example, we know that salt compounds form when elements, drawn from opposite ends of the Periodic

Table, react. Further, such compounds possess well-defined stoichiometries and melting points. Cementite (Fe_3C) in Fig. 5-23 is such a compound. The oxides of iron, magnetite (Fe_3O_4), and wustite (FeO), shown in Fig. 10-19, are also compounds, but they exist over a range of oxygen content and correspondingly have varying melting points. Among the most technically important compounds are those formed between column 3A and 5A elements, for example, GaAs (Fig. 5-18). These compound semiconductors play an important role in optoelectronics and are discussed further in Chapter 13. A closer look at GaAs reveals that it can be either slightly Ga-rich or slightly As-rich, although this is not visible on the scale of the diagram. In general, most of the compounds we are concerned with have a slightly variable stoichiometry.

Although the above compounds are neither unusual nor unexpected from the standpoint of elementary chemistry, the same is not true of **intermetallic compounds**. These are composed of two metals that can, for example, stem from the same column of the Periodic Table (e.g., Na_2K), represent two different columns (e.g., $BaAl_2$), or be derived from the collection of transition metals (e.g., $MoNi_4$), The stoichiometry of these as well as the Ni_3Al intermetallic, a compound that plays an important role in commercial Ni base alloys, is not readily predictable from normal chemical valences. In this sense more complex metallic bonding issues govern the phase stability of these materials. For our purposes the following attributes of intermetallic compounds are noteworthy:

1. They often have a reasonably well defined stoichiometry (e.g., $NiAl_3$; see Fig. 5-27).
2. Just as frequently some are stable over a range of composition (e.g., Ni_3Al, NiAl).
3. Some compounds (e.g., GaAs, NiAl) melt **congruently** or maintain their composition right up to the melting point.
4. Many other compounds melt **incongruently** and undergo phase decompositions and chemical change. Examples are Ni_2Al_3 and $NiAl_3$, which display peritectic reactions at the appropriate isotherms (Fig. 5-27).

5.6.3. Some Phase Trends

Careful examination of many binary phase diagrams has led to guidelines that enable a qualitative prediction of the extent to which one metal dissolves in another when alloyed. The general relevant factors and trends they produce were summarized by Hume-Rothery, a noted British metallurgist, as follows:

1. *Atomic size.* Typically, if the two atoms differ by less than ~15% in radius, extensive solubility can be expected. For example, in Cu–Ni, a system that displays unlimited solubility, $(r_{Cu} - r_{Ni})/r_{Cu} \times 100 = 2.3\%$. Large solute atoms extend the bonds of smaller surrounding host atoms; alternately smaller

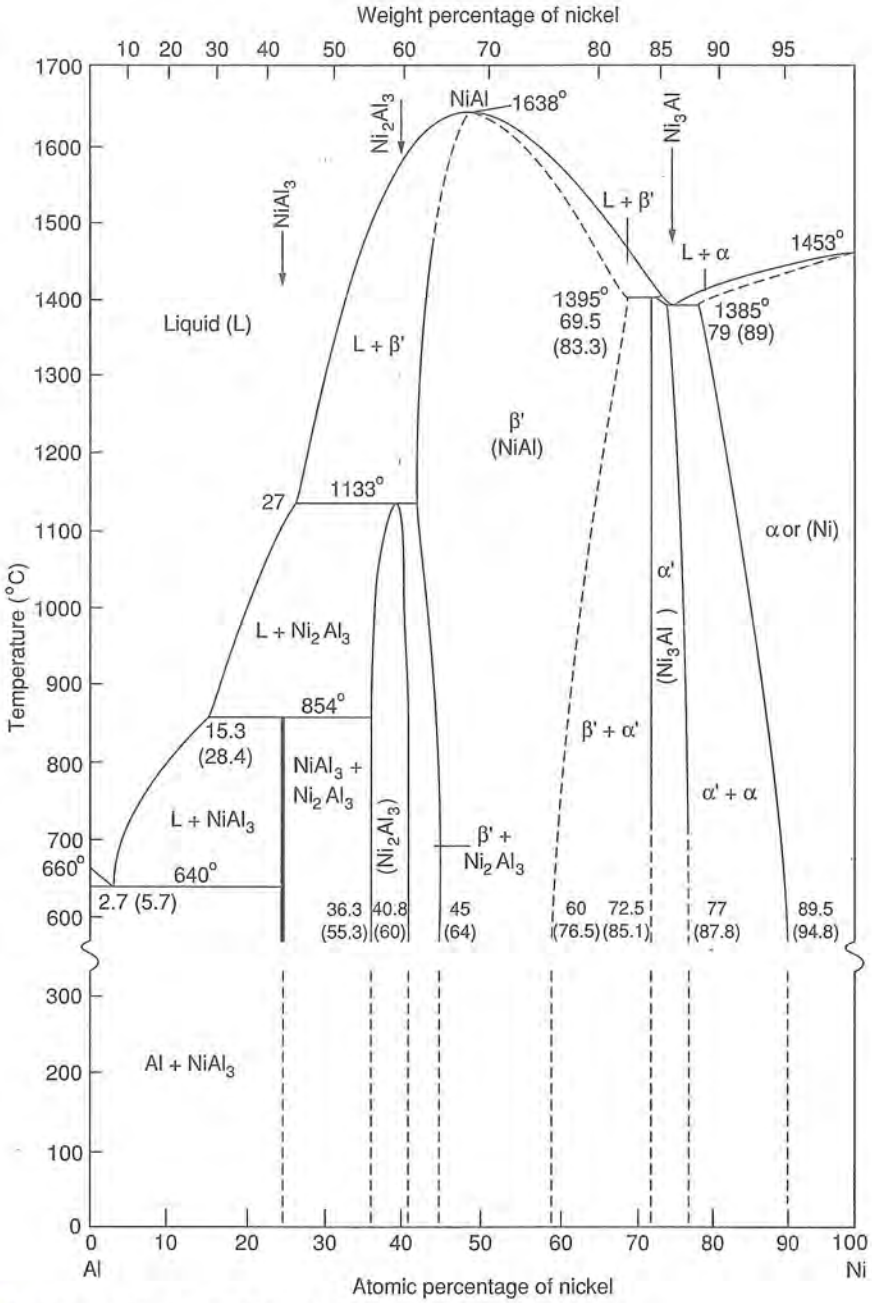

FIGURE 5-27 Equilibrium phase diagram of the Al–Ni system.

solute atoms cause a corresponding relaxation of bond lengths. In general, large differences in atomic size lead to limited solubility because strained bonds cause an unfavorable rise in their energies.

2. *Valence.* The tendency toward compound formation is greater the more electropositive one atom is and the more electronegative the other is. Under these conditions very limited solubility can also be expected. Greater solubility occurs when there is little valence difference between components.

3. *Relative valence.* Other things being equal (which they never are), a metal of low valence dissolves more readily in one of higher valence than vice versa.

5.6.4. Nonequilibrium Phases and Structures

Equilibrium is an ideal that is not often achieved in practice. Even though phase diagrams provide information on phase composition and relative amounts, they provide few clues as to their microstructure and morphology or appearance. This is all the more true of nonequilibrium phases. As properties of materials frequently hinge very strongly on phase size, shape, and distribution, as well as composition, it is important to appreciate the connections between processing and structure. Prolonged heating and slow cooling lead to equilibrium microstructures. But, relatively simple thermal treatments, such as rapid cooling from elevated temperatures, can often yield nonequilibrium microstructures and phases.

5.6.4.1. Metal Glasses

Nonequilibrium cooling of polymer and glass melts that yield amorphous structures has already been discussed in Chapter 4. An extreme example of **nonequilibrium** solidification in alloys occurs in the commercial process for the production of **metal glasses** (**Metglas**). The nonequilibrium or metastable structures in these materials evolve under conditions in which thermodynamic equilibrium is suppressed. The intent is to be as far removed from equilibrium as possible, a state achieved by quenching liquid metal alloys on cryogenically cooled surfaces. When this happens, metastable and even amorphous (noncrystalline) alloys are produced. Cooling rates of a million degrees centigrade per second are required to retain the character of the prior amorphous liquid; such rates are actually attained in shapes of small dimension (e.g., powder, thin foils less than 0.05 mm thick) because heat can be readily extracted from them. The reason that such high cooling rates are required to amorphize metals is the low melt viscosity and resulting high atomic mobility. Metal atoms do not interfere with one another when seeking to enlarge solid nuclei the way polymer and glass molecules do in viscous melts.

Continuous production of thin metal sheet, shown in Fig. 5-28, involves pouring the molten alloy on a chilled roller and removing the solidified product. A conceptually similar process is used during the very widely employed continu-

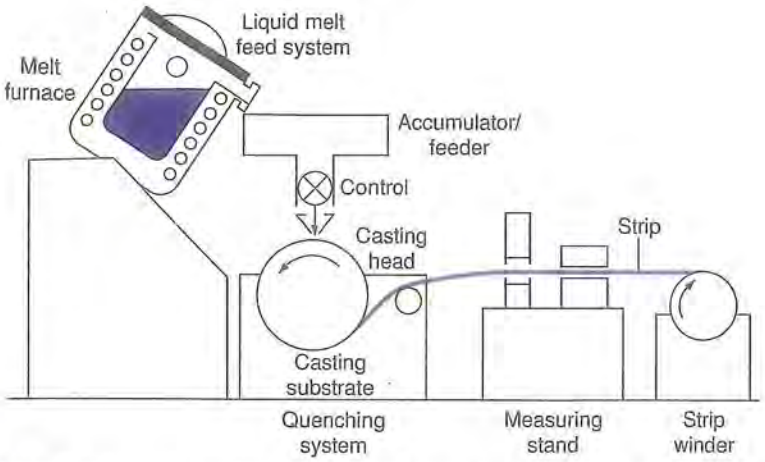

FIGURE 5-28 Diagram of the melt quenching apparatus used to produce metal glasses. Courtesy of Allied Metglas Products.

ous casting of metals. Only certain alloy compositions will yield amorphous phases. Important binary examples include combinations of transition metal and metalloid atoms (e.g., Fe–Si, Pd–Si, Fe–B). The alloys are generally strong and brittle, and some compositions display useful soft magnetic properties (e.g., Fe–B).

5.6.4.2. Cored Dendritic, Cast Structures

An important example of nonequilibrium solidification occurs during casting of metals where the luxury of very slow cooling in molds is neither feasible nor desirable. Rather, alloys are cooled relatively quickly in the foundry (but not quenched!) so that they can be processed further. What happens under these conditions can be understood with reference to Fig. 5-29. During cooling of the A–B solid solution alloy, the first solid nucleus that forms is richer in A than the overall alloy. As the temperature drops, more and more A and B atoms condense as the solid dendrite now reaches macroscopic dimensions. At each stage chemical equilibrium requires that the alloy solid have a uniform composition throughout, meaning thorough intermixing of atoms. This happens easily enough in the liquid phase but not in the solid state. Atomic diffusion, a sluggish process requiring the hopping and squeezing of atoms in between and past one another through lattice sites, does not occur readily in solids. And as the temperature continues dropping, equilibrium becomes harder and harder to achieve. Atoms are frozen in place as diffusion is further limited at low temperatures. Besides, there is physically more solid to homogenize. As a result, successive layers of increasingly richer B content surround the initial dendrite. The overall composition of the solid follows the nonequilibrium

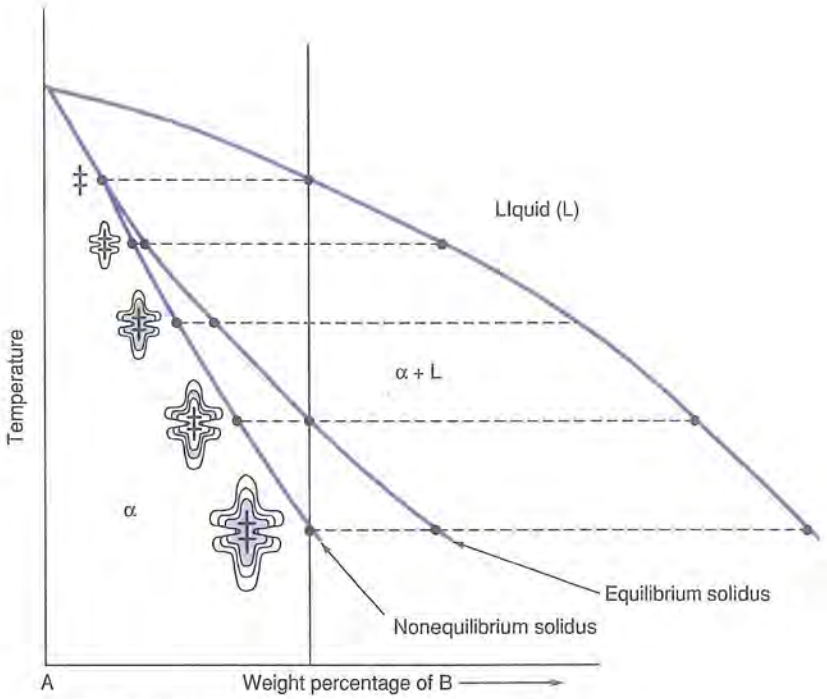

FIGURE 5-29 Illustration of dendritic coring.

solidus line rather than the equilibrium solidus line. The microstructure is said to exhibit **coring.**

Upon solidification of Cu–Ni alloys such inhomogeneous cored, dendritic microstructures develop as shown in Fig. 5-30. Undesirable properties (e.g., corrosion, lack of ductility) stem from such microstructures and they are, therefore, modified through subsequent thermomechanical processing such as hot rolling and recrystallization, which simultaneously homogenize and bring the alloys closer to equilibrium. Structural evolution considerations are generally distinct from thermodynamic ones, however, so that a better understanding of these will have to wait until some of the involved issues are addressed in Chapter 6 (also see Fig. 8-11).

5.6.4.3. Thin-Film Superlattice

As another example of nonequilibrium microstructures, this time in the Ge–Si system, consider Fig. 5-31. Shown with atomic resolution is a synthesized structure known as a **superlattice,** consisting of alternating thin-film layers of Si and a solid solution alloy of 40 at.% Ge–60 at.% Si. It was produced through careful sequential vapor deposition of the involved components an atom layer at a time. There are no visible dislocation or grain boundary defects

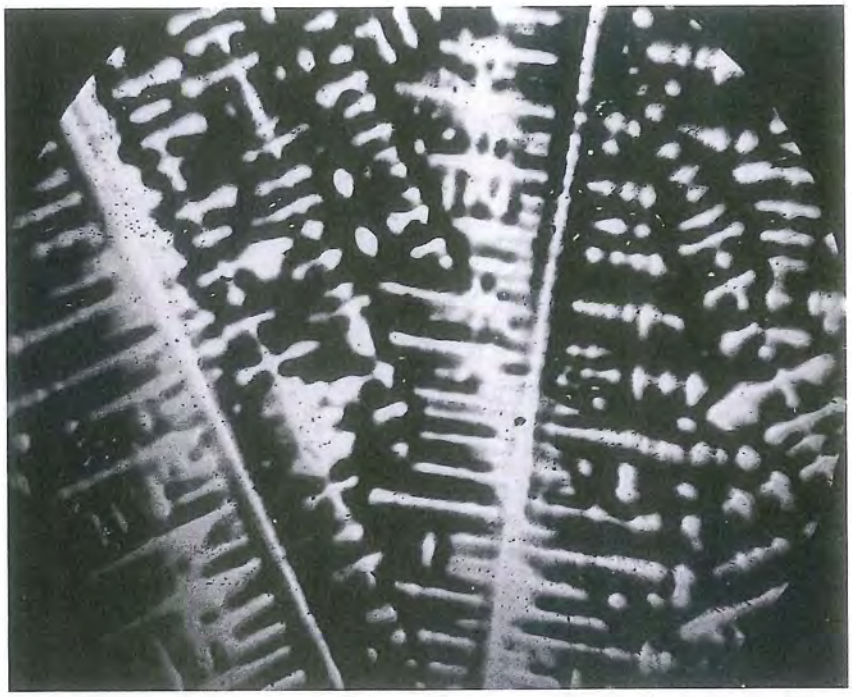

FIGURE 5-30 Dendritic cored microstructure of Monel metal (63 wt% Ni–32 wt% Cu + Fe, Si) at 50×. The light etching center of the dendrite is Ni rich; the darker surroundings are Cu rich.

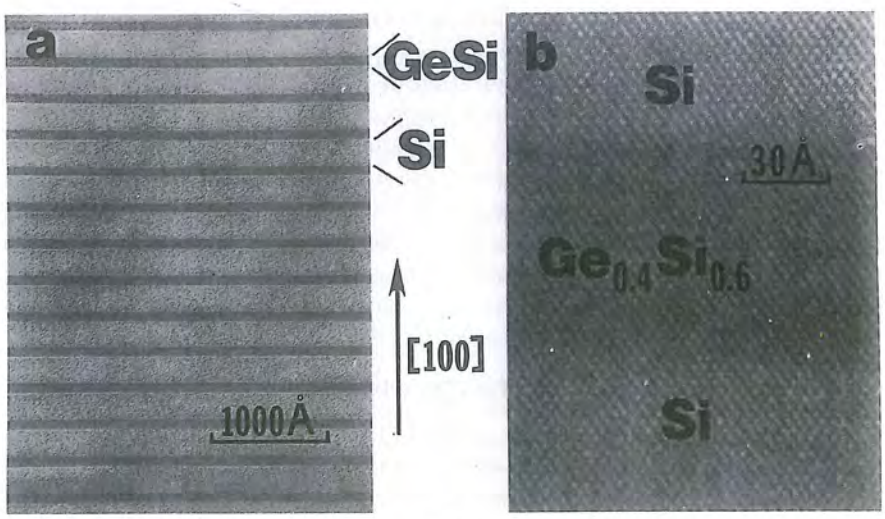

FIGURE 5-31 (A) TEM cross section of a superlattice consisting of alternating layers of pure silicon and 40 at.% Ge–60 at.% Si. (B) High-resolution lattice image of superlattice crystal. This composite structure is an uncommon two-phase, perfect single crystal. Courtesy of J. C. Bean and R. Hull, AT&T Bell Laboratories.

so the superlattice is a single crystal even though it contains atomically sharp interfaces between layered phases. The structure is in metastable equilibrium but can persist indefinitely at room temperature. Increasingly, new advanced solid-state electronic devices employ similar artificially tailored structures to achieve desired functions. But if heated to elevated temperatures, atoms will intermix and a single uniform random solid solution would replace the superlattice.

5.7. THERMODYNAMICS OF SURFACES AND INTERFACES

5.7.1. Atoms on Surfaces

Every condensed phase has a surface that is exposed not only to gases but also to other condensed phases in contact with it. All sorts of processes involving chemical reactions and atom movements occur at surfaces and interfaces (e.g., oxidation, corrosion, soldering, sintering or bonding of particles). A large fraction of atoms reside at surfaces in materials like films, coatings, and fine powders. Atoms on surfaces are more energetic than atoms in the interior of a solid. Quite simply there are fewer atoms to bond to and restrain them. Therefore, they have a greater tendency to "escape" the solid than subsurface atoms, which are effectively surrounded on all sides. The bonding curve (see Fig. 2-12) for a pair of surface atoms would lie at higher energy and be displaced to a slightly larger equilibrium spacing relative to the response for a comparable pair of interior atoms.

Interestingly, the atomic "escaping tendency" also depends on the actual *geometry* of the surface. In order of increasing reactivity are atoms on concave, planar, and convex surfaces. These respective cases are shown in Figs. 5-32A–C, and reflected by a decreasing number of interatomic bonds between the atom and the surface. It is not difficult to quantify these tendencies. First, a surface (free) energy γ has to be introduced. A sufficient definition for our purposes is the difference in energy per unit area between atoms in a surface layer relative to the same number of atoms in a layer embedded well below the surface. For practical purposes γ is known as the surface tension and values of it have been measured for both liquids and solids of many different materials. They typically range from 0.1 to 1 J/m^2. The reason that liquid mercury balls up is that surface tension effects convert some energetic surface atoms to less energetic bulk atoms during the accompanying reduction in surface area.

Let us consider a material having a spherical surface of radius r and total surface energy E_s equal to $4\pi r^2\gamma$. If the volume of an atom is Ω, then the total number of atoms (n) in the sphere of volume $4\pi^3/3$ is $4\pi r^3/3\Omega$. A convenient measure of the atomic escaping tendency or reactivity is μ, also known as the **chemical potential.** It can be defined as the rate at which surface energy changes

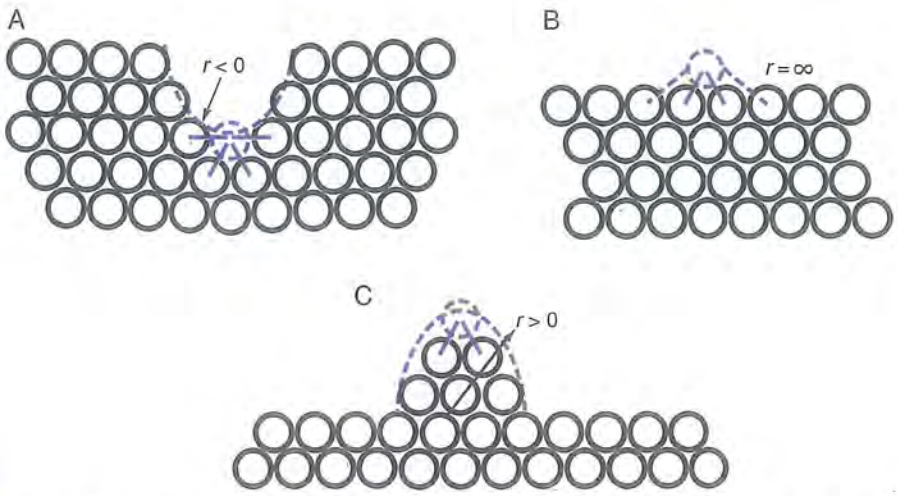

FIGURE 5-32 Atoms on (A) concave surface, (B) planar surface, and (C) convex surface. On the convex surface atoms are most reactive; on the concave surface they are least reactive.

with the addition or withdrawal of a number of atoms. Mathematically,

$$\mu = dE_s/dn = d(4\pi r^2\gamma)/d(4\pi r^3/3\Omega) = 8\pi r\gamma dr/(4\pi r^2/\Omega)\, dr$$

or

$$\mu = 2\Omega\gamma/r. \qquad (5\text{-}22)$$

Small particles have large values of μ and are thus reactive. Furthermore, for a single surface, μ is numerically largest for atoms on convex surfaces ($r > 0$) and smallest for atoms on concave surfaces ($r < 0$). In between is the flat surface where $r = \infty$ and $\mu = 0$. If particles of different size were in contact and could freely exchange atoms, then the larger particle would grow at the expense of the smaller one. Free energy is lowered in the process as equilibrium is approached.

EXAMPLE 5-6

a. What is the energy reduction that occurs when spherical particles of radii r_1 and r_2 coalesce into a single particle?

b. What fraction of the total initial surface energy is reduced when two spherical powders of equal size coalesce?

ANSWER a. The respective particle volumes are $4\pi r_1^3/3$ and $4\pi r_2^3/3$, whereas the volume of the coalesced sphere of radius r_c is $4\pi r_c^3/3$. Because mass (volume)

is conserved, $4\pi r_c^3/3 = 4\pi r_1^3/3 + 4\pi r_2^3/3$, or $r_c = (r_1^3 + r_2^3)^{1/3}$. The surface energy reduction is therefore $(4\pi r_1^2\gamma + 4\pi r_2^2\gamma) - 4\pi r_c^2\gamma$, with r_c given above.

b. The fractional energy reduction ($\Delta E/E$) is given by $(4\pi r_1^2\gamma + 4\pi r_2^2\gamma - 4\pi r_c^2\gamma)/(4\pi r_1^2\gamma + 4\pi r_2^2\gamma)$. As $r_1 = r_2 = r$, $\Delta E/E = \{1 - (2r^3)^{2/3}/2r^2\} = 1 - (2^{2/3}/2) = 0.206$ or 20.6%. Note that $\Delta E/E$ is independent of r.

Later, in Chapter 6, the *rate* at which such particles sinter together is addressed.

5.7.2. Surface Tension Effects

Why does solder sometimes ball up but flow nicely when properly fluxed? A clue to the answer can be found by considering Fig. 5-33, where a liquid (L), for example, a droplet of solder, or more generally any liquid or solid material, is in contact with a planar substrate. The surface tension is just that: a *tension,* or pull, that acts along a thin *surface* layer that is the interface between two phases. There are three such surface tensions in the system. The first is the tension at the liquid–vapor interface γ_{L-V}, and the second is that between the liquid and substrate γ_{L-S}; lastly, there is the tension between the substrate and vapor, γ_{S-V}. If the droplet is in thermodynamic equilibrium, the surface tension forces that act on it must balance. The arrows drawn in Fig. 5-33 are the directions in which these forces pull to reduce the areas of the indicated interfaces. Simple static equilibrium of forces in the horizontal direction demands

$$\gamma_{S-V} = \gamma_{L-S} + \gamma_{L-V}\cos\theta, \tag{5-23}$$

where θ is known as the wetting angle.

When θ is 0, the liquid is stretched out into a film that effectively wets or covers the surface, and $\gamma_{S-V} = \gamma_{L-S} + \gamma_{L-V}$. On the other hand, when the liquid dewets, it agglomerates into a sphere and $\theta = 180°$. Reducing γ_{L-S} is the key to enhancing wetting and is accomplished through alloying, fluxing, or the use of wetting agents.

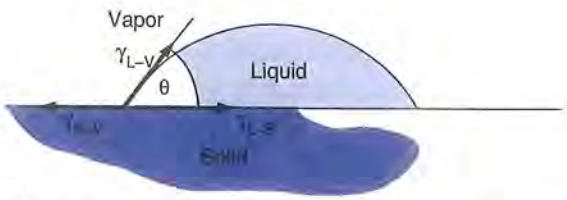

FIGURE 5-33 A liquid drop on a solid surface pulled by the various interfacial tensions.

5.8. THERMODYNAMICS OF POINT DEFECTS

What does thermodynamics say, if anything, about point defects in solids? To the extent that they behave like chemical entities they can be described in terms of the established rules of equilibrium thermochemistry. Vacancies are the defects most amenable to analysis and are the only ones discussed here. Let us start with a perfect lattice of N atoms which is taken to be the initial state. A number of vacancies (n_v) is created by extracting atoms from the lattice interior and placing them on the surface. Through the use of Eq. 5-2 we can calculate the free energy change relative to the initial state. First, energy E_v is expended in creating each vacancy and thus the total value of ΔE is $n_v E_v$.

The ΔS term is more complicated because entropy is associated not only with the internal nature of atoms and vacancies (due to lattice vibrations), but also with their locations. It makes a difference if all the vacancies are concentrated in the upper quarter, the upper half, or the lower tenth of the solid, or are distributed randomly, or in any one of an almost infinite number of other ways. Let us first start with a vacancy-free lattice; because there is only one geometric distribution, the entropy is minimum and may be taken to be zero. Then N atoms and n_v vacancies are randomly distributed on $N + n_v$ sites and the entropy can be obtained using the following statistical recipe. Consider an empty lattice of $N + n_v$ sites. The first atom can be introduced in any one of $N + n_v$ ways. If two atoms are sequentially introduced they can be accommodated in $(N + n_v)(N + n_v - 1)$ *indistinguishable* ways. Exchange of the two atoms halves this; so the number of *distinguishable* ways or combinations of placement is $(N + n_v)(N + n_v - 1)/2$. For three atoms, $(N + n_v)(N + n_v - 1)(N + n_v - 2)/2 \times 3$, and so on. For N atoms the total number of *distinguishable* distributions is $(N + n_v)!/N!\, n_v!$. The symbol $N!$, or N factorial, means $N(N - 1)(N - 2)(N - 3) \ldots 1$. A cornerstone of the science of statistical mechanics is that the statistical or configurational entropy is given by

$$S = k \ln\{(N + n_v)!/N!\, n_v!\}, \tag{5-24}$$

where k is the Boltzmann constant. The total free energy change on creating n_v vacancies, neglecting PV (Eq. 5-1), is therefore

$$\Delta G = n_v E_v - Tk \ln\{(N + n_v)!/N!\, n_v!\}. \tag{5-25}$$

Thermodynamic equilibrium implies minimization of G or $d\Delta G/dn_v = 0$. Rather than evaluate this mathematically, it is instructive to illustrate it graphically. This is done in Fig. 5-34, where the quantities ΔE and $T\Delta S$ and the sum ΔG are plotted versus n_v at two different temperatures, T_1 and T_2 ($T_2 > T_1$). At the higher temperature it is clear that the number of vacancies in equilibrium is higher because the minimum is pushed to the right. There is no reason why the vacancy concentration should not be governed by the laws of chemical equilibrium for the reaction $M_a(N) \rightarrow M_a(N - n_v) + n_v$, where M_a refers to

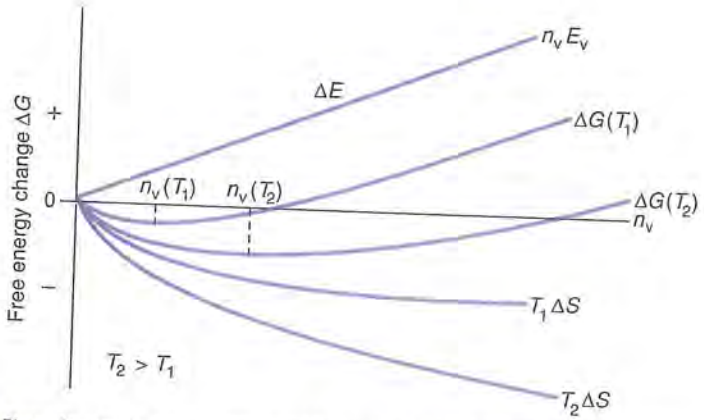

FIGURE 5-34 Plots of internal energy, entropy, and free energy as a function of the vacancy concentration. The minimum of the free energy curve graphically yields the equilibrium vacancy concentration. After C. R. Barrett, W. D. Nix, and A. S. Tetelman, *The Principles of Engineering Materials*, Prentice–Hall, Englewood Cliffs, NJ (1973).

the matrix atoms. The thermally activated concentration of vacancies given by Eq. 3-6, $C_v = \exp(-E_v/kT)$, is then not unexpected.

Values for E_v have been measured in metals by heating them to different elevated temperatures and measuring their concentrations through thermal expansion and X-ray techniques. Alternatively, they have been retained at low temperature through very rapid cooling; their numbers have then been estimated by noting the amount by which they have raised the electrical resistance of metals. Either way, values of E_v have been obtained for many metals. As already noted in Section 3.5.1, values of 1 eV per vacancy (96,500 J/mol) are typical. This is certainly true of the noble metals where $E_v = 0.98$, 1.1, and 1.0 eV for gold, silver, and copper, respectively.

Point defects in alkali halide and metal oxide compounds are also amenable to similar thermodynamic analysis. Let us consider the formation of a Schottky defect (see Section 3.5.1), a metal cation (M)–oxygen anion (O) vacancy combination, by a reaction that removes the pair of ions from the lattice and places them on the surface:

$$(M^{2+}\text{–}O^{2-})_{\text{lattice}} \rightarrow M_v + O_v + (M^{2+}\text{–}O^{2-})_{\text{surface}}. \qquad (5\text{-}26)$$

The equilibrium constant is then given by

$$(M_v)(O_v) = \exp(-E_{sv}/kT), \qquad (5\text{-}27)$$

where E_{sv} is the energy required to form an **intrinsic** Schottky vacancy (v) pair. Because of charge neutrality considerations, $(M_v) = (O_v)$, and either concentration is thus equal to $\exp(-E_{sv}/2kT)$ by taking the square root. Schottky disorder in oxides is characterized by E_{sv} values of several electron-volts. For example, in BeO, MgO, and CaO values of ~6 eV have been measured. With such a

high energy, the intrinsic point defect concentration will be negligible in ceramics except at extremely elevated temperatures. Later, in Section 11.6.1, we shall see that the presence of impurities can generate large numbers of extrinsic point defects, even at low temperatures.

It is interesting to note that, unlike vacancies, dislocations are not thermodynamic defects. Since many atoms are distributed along the line the internal energy is large; simultaneously the entropy is low because dislocation lines are constrained to assume few crystallographic orientations or configurations. As a result ΔG is large. Therefore, although dislocations can be eliminated from crystals, resulting in a free energy reduction, vacancies cannot be so removed.

5.9. PERSPECTIVE AND CONCLUSION

Thermodynamics is very definite about denying the impossible and defining limits for behavior that is possible. But, for a possible event, thermodynamics is noncommittal as to the extent to which it will occur, or even whether it will occur at all. For example, amorphous SiO_2 should crystallize and Fe_3C should thermodynamically decompose into iron and graphite at 300 K, but both can be retained indefinitely in metastable equilibrium. This is true of many other solid-state materials and reactions whether they are chemical in nature or involve physical transformations of state. Only reactions that lower the free energy of the system can proceed; and if the free energy of the system reaches a minimum and cannot be lowered further, true thermodynamic equilibrium is attained. Minimization of free energy is a cardinal principle used over and over in this book to establish the configuration of material states in equilibrium. In this chapter this one principle was expressed in different but equivalent forms and applied in the following ways:

1. ΔG° *must be negative.* For chemical equilibria (oxidation and CVD processes) a negative free energy change is required for the reaction to proceed as written. Shape changes that minimize surface energy also necessarily reduce free energy. The derivation of many important thermodynamic laws, for example, the Gibbs phase rule, stem from free energy minimization.
2. $K_{eq} = \exp(-\Delta G^\circ/kT)$. The equilibrium constant defines magnitudes of concentrations or pressures for both chemical reactions and physical transformations. Examples include the vapor pressure above condensed elemental phases and the equilibrium concentration of vacancies.
3. $d\Delta G/dn_v = 0$. When the free energy can be expressed as a function of the composition of a chemical species, for example, point defects or vacancies, this condition leads to the equilibrium concentration. This formalism also holds for the determination of the chemical potential of atoms on curved surfaces.
4. *Phase diagrams.* Phase diagrams are simply graphic displays of equilibrium solubilities in single- or multicomponent systems. The equilibrium phase

compositions and amounts for any state are those that minimize the free energy of the system. In particular, the tie line construction is rooted in thermodynamic equilibrium.

Questions of reaction rates and conditions under which equilibrium can be expected are not addressed by thermodynamics. The next chapter, on kinetics, does focus on such issues and it is to them that we now turn.

Additional Reading

ASM Handbook. Vol. 9: *Metallography and Microstructures*, 8th ed., ASM International, Materials Park, OH (1985).

A. H. Cottrell, *An Introduction to Metallurgy*, Edward Arnold, London (1967).

M. Hansen and K. Anderko, *Constitution of Binary Alloys*, 2nd ed., McGraw–Hill, New York (1958).

C. H. P. Lupis, *Chemical Thermodynamics of Materials*, North-Holland, New York (1983).

R. A. Swalin, *Thermodynamics of Solids*, 2nd ed., Wiley, New York (1972).

QUESTIONS AND PROBLEMS

5-1. An initially solid material becomes a liquid as the temperature is raised above the melting point. Explain the probable signs of the enthalpy, entropy, and free energy changes. What are the signs of these quantities as the liquid transforms back to the solid?

5-2. In Thermit welding processes aluminum reacts with iron oxide, releasing molten iron as the weld metal. If the reaction can be written as

$$2Al + 3FeO = Al_2O_3 + 3Fe,$$

what is the free energy change per mole of Al during reaction at 1600°C?

5-3. What is the minimum temperature at which it would be thermodynamically possible for carbon to reduce silica according to the reaction

$$SiO_2 + 2C = Si + 2CO?$$

Assume the effective concentrations are unity and the pressure is 1 atm.

5-4. The free energies of oxides are usually lower than those of the corresponding metals. Nevertheless, metals do not rapidly oxidize and we can comfortably rely on their long-term stability. Why?

5-5. Hydrogen is often used to reduce metal oxides (MO) at elevated temperatures. If $2M + O_2 = 2MO$ (ΔG°_{MO}) and $2H_2 + O_2 = 2H_2O$ ($\Delta G^\circ_{H_2O}$), write an expression for the equilibrium constant of the reaction $H_2 + MO = M + H_2O$ in terms of ΔG_{MO}, ΔG_{H_2O}, and the pressures of H_2 and H_2O.

5-6. Aluminum is melted at 1000°C. What is the maximum oxygen partial pressure that can be tolerated to eliminate the possibility of any Al_2O_3 formation? Practically, much higher oxygen pressures can be present without appreciable oxidation. Why?

5-7. From the data given in Fig. 5-5 determine the heat of vaporization of H_2O.
5-8. Determine the heat of vaporization for aluminum using Eq. 5-9.
5-9. On the basis of Fig. 5-5 show that ice floats on water. (The reason that aquatic life in lakes can survive winters is that water at 4°C is denser than ice and sinks to the bottom.)
5-10. A mole of lead and a mole of diamond are heated from ~4 to 700 K at atmospheric pressure. Based on Fig. 5-10 what is the approximate ratio of the heat absorbed by C (diamond) relative to that by Pb?
5-11. When the temperature of a two-phase mixture of any Cu–Ni alloy is raised, the Ni content of both the liquid and solid phases increases. Does this violate the conservation of mass?
5-12. A solder manufacturer wishes to make a batch of solder having the eutectic composition. On hand is a supply of 250 kg of electrical solder scrap containing 60 wt% Sn–40 wt% Pb and 1250 kg of plumbing solder scrap containing 60 wt% Pb–40 wt% Sn. If all of the scrap is to be melted, how much pure Sn must be added to achieve the desired 61.9 wt% Sn composition?
5-13. Gallium arsenide crystals are grown from Ga-rich melts. Can you mention one reason why As-rich melts are not used for this purpose?
5-14. A 90 wt% Sn–10 wt% Pb alloy is cooled from 300 to 0°C.
   a. What is the composition of the alloy in terms of atomic or molar percentage?
   b. Draw a cooling curve for this alloy.
   c. Upon cooling of this alloy, the degrees of freedom change from 2 to 1 to 0 to 1. List possible temperatures that correspond to these four conditions.
   d. In what ways does the equilibrium microstructure of this alloy differ from that of the 90 wt% Pb–10 wt% Sn alloy?
5-15. Consider a binary system composed of components A and B with the following features (all compositions in at.%):
   1. Melting point of A = 1500°C and melting point of B = 750°C.
   2. Melting point of intermediate phase A_2B = 1250°C.
   3. Zero degrees of freedom at a composition of 20B at 500°C.
   4. Zero degrees of freedom at a composition of 50B at 1000°C.
   5. A single solid phase of composition 50B at 900°C.
   6. Isotherms at 500 and 1000°C.

   Sketch a possible phase diagram based on this information.
5-16. The Al_2O_3–Cr_2O_3 phase diagram resembles that for Cu–Ni. The melting point of Al_2O_3 is 2040°C, whereas that of Cr_2O_3 is 2275°C.
   a. Sketch the phase diagram.
   b. How many components are there in this system?
   c. How many degrees of freedom are there in the liquid, liquid + solid, and solid phase regions?
   d. It is desired to grow a ruby single crystal with the composition 22 wt% Cr_2O_3. On your phase diagram indicate the melt composition and temperature for growth.

5-17. Suppose you have a large quantity of gallium amalgam (Ga–Hg alloy) scrap. The alloy is liquid at room temperatures and has much less value than the isolated pure metals. Suggest a physical method to separate these metals if they are initially present in equal amounts by weight.

5-18. a. In the Ga–As binary system perform total chemical and physical composition analyses for an 80 at.% Ga–20 at.% As alloy at 1200, 1000, 200, and 29°C.

b. What is different about the two two-phase fields labeled liquid + GaAs?

5-19. It is desired to pull an alloy single crystal of composition 78 at.% Ge–22 at.% Si from a binary Ge–Si melt.

a. At what temperature should the crystal be pulled?

b. What melt composition would you recommend?

c. As the crystal is pulled what must be done to ensure that its stoichiometry is kept constant?

5-20. Consider the 50 wt% Pt–50 wt% Re alloy.

a. This alloy is heated to 2800°C and cooled to 800°C. Sketch an equilibrium cooling curve for this alloy.

b. Perform complete equilibrium chemical and physical phase analyses at 2800, 2452, 2448, and 1000°C.

5-21. Make enlarged sketches of the phase regions that surround the two highest isotherms in the Cu–Zn phase diagram (see Fig. 5-22).

a. What is the name of the solidification behavior displayed in both cases?

b. Which lines on this phase diagram represent the solubility limit of Zn in the α phase?

c. Which lines on this phase diagram represent the solubility limit of Zn in the β phase?

d. Which lines on this phase diagram represent the solubility limit of Cu in the β phase?

e. Is it possible for the solubility of a component to drop as the temperature is raised?

Give an example in this phase diagram.

5-22. Perform quantitative physical and chemical phase analyses at temperatures corresponding to the four states indicated for the 0.4% C, and 1.2% C steels in the Fe–Fe_3C system of Fig. 5-24. Do your analyses correspond to the sketched microstructures?

5-23. Up until the Middle Ages iron was made by reducing iron ore (e.g., Fe_2O_3) in a bed of charcoal (carbon). Steel objects were shaped by hammering the resulting solid sponge iron that was reheated to elevated temperatures using the same fuel. As the demand for iron and steel increased, furnaces were made taller and larger. They contained more iron ore and charcoal that were heated for longer times. An interesting and extremely important thing occurred then. *Liquid* iron was produced! Why? (Molten iron issuing from the bottom of the furnace could be readily cast, a fact that helped to usher in the Machine Age.)

5-24. Give a good physical reason for the following statements:
a. Elements that are soluble in all proportions in the solid state have the same crystal structure.
b. Unlike substitutional solid solutions, interstitial solid solutions do not range over all compositions.

5-25. Distinguish between intermediate phases and compounds. Contrast metals and nonmetallic inorganic materials with respect to their tendency to form intermediate phases and compounds in binary phase diagrams.

5-26. a. A 40 wt% Al_2O_3–60 wt% SiO_2 melt is slowly cooled to 1700°C. What is the proeutectic phase and how much of it is there?
b. Furnace bricks are made from this composition. Is the melting point of these bricks higher or lower than that of pure silica bricks?
c. What is the highest melting temperature attainable for bricks containing both SiO_2 and Al_2O_3?

5-27. Gold and silver dissolve in all proportions in both the liquid and solid states. The same is true for gold and copper. Does this mean that silver and copper will form solid solutions in the solid state? Check your answer by consulting a book of phase diagrams, for example, M. Hansen, *Constitution of Binary Alloys,* McGraw–Hill, New York (1958).

5-28. A 10-g ball bearing sphere is made of a steel containing 1.1 wt% C. Suppose the ball is austenitized and slowly cooled to room temperature.
a. What is the weight of pearlite present?
b. What is the total weight of ferrite present?
c. What is the total weight of cementite present?
d. What is the weight of cementite present in the pearlite?
e. What is the weight of cementite present as the proeutectoid phase?

5-29. Cast iron weighing 1 kg and containing 3.5 wt% C (remainder Fe) is melted and slowly cooled from 1300°C. Perform a complete phase analysis (a) just below 1147°, (b) at 900°C, and (c) just below 723°C. (d) Sketch the expected microstructure at 500°C. (e) In true thermodynamic equilibrium cementite decomposes to graphite and iron. What weight of graphite would be present if all of the cementite decomposed?

5-30. The copper–oxygen system is a simple eutectic on the copper-rich side. The eutectic temperature is 1065°C and the eutectic composition contains 0.39 wt% O. Tough pitch copper, a product produced on a large scale for electrical applications, contains a few hundredths of a percent of oxygen. Sketch the microstructure of such a copper containing 0.04 wt% O if the solubility of O in Cu is nil, and (a) the eutectic mixture consists of Cu_2O particles dispersed in a nearly pure Cu matrix, or (b) the eutectic forms near the grain boundaries of primary Cu.

5-31. The fire assaying of precious metal (Au, Ag) content in alloys containing Cu and other base metals dates to antiquity, but is still the preferred method for such analysis by the U.S. Mint. In this technique known as *cupellation,* the alloy is dissolved in molten lead, a solvent for these metals. The lead and other

base metals are then oxidized at high temperature and effectively removed as their oxides are absorbed into the bone ash crucible (cupel). After complete oxidation of the lead a ball of pure unoxidized Au, Ag, or Ag–Au remains (shades of alchemy)! The solubility of Pb in the precious metals is nil. Based on this information roughly sketch features of the high-temperature Pb–precious metal phase diagram applicable in the cupellation process.

5-32. What vacancy concentration is present in gold (a) at 25°C? (b) At 1060°C? (c) Suppose Au is heated to 1062°C and then quenched so rapidly that all of the vacancies are retained at 25°C. By what fraction is the density of Au reduced?

5-33. Suppose instead of three phases, that is, solid, liquid, and vapor, equilibrated with respect to surface tensions (Fig. 5-33), we consider three grains of the same phase at a triple-joint junction. Along grain boundaries between neighboring grains there is an interfacial tension γ or force, and in equilibrium these forces balance.

a. If γ is identical between grains, sketch the force balance at the triple point. What angle exists between adjacent tensions?

b. When the three individual tensions are different, a general result of static equilibrium is $\gamma_1/\sin\theta_1 = \gamma_2/\sin\theta_2 = \gamma_3/\sin\theta_3$, where the angle θ_1 lies between the directions γ_2 and γ_3, and so on. If $\gamma_1 = 1.0$ J/m^2, $\gamma_2 = 1.0$ J/m^2, and $\gamma_3 = 1.2$ J/m^2, solve for θ_1, θ_2, and θ_3.

5-34. Consider a sphere of copper that weighs 10 g.

a. If the surface energy is 1.4 J/m^2, what is the energy associated with the surface atoms?

b. The original sphere is broken down into fine spherical grains of powders each measuring 100 nm in diameter. What is the total surface energy of all of the powder grains?

5-35. Zone refining is a process that was used to purify early semiconductor materials. Consider a long rod of solid polycrystalline silicon, containing uniformly distributed small amounts of impurities in solid solution. A narrow zone of the rod is melted at one end and the molten zone is slowly translated to the other end of the rod. At the advancing zone edge new impure solid is melted, and at the trailing edge liquid solidifies.

a. By considering that impurities typically lower the melting point of Si, what is true of the purities of solid and liquid phases in equilibrium?

b. Why is the resulting rod purer at the initially melted end and less pure at the far end?

8 MATERIALS PROCESSING AND FORMING OPERATIONS

8.1. INTRODUCTION

Engineering materials are useful only if they can be processed in quantity and fabricated in varied shapes, while meeting composition and property specifications. **Primary processing** is concerned with large-scale production of basic materials like steel and polymer precursors. This output is then sent either to **secondary processors** for alloying or blending or directly to the manufacturing industries (e.g., auto and plastic packaging companies), which additionally shape and assemble them into final products. Many variations on this theme exist and some prime producers also manufacture intermediate finished products for further assembly, for example, I beams for construction and huge rotors for steam turbines. Some companies and industries derive relatively little benefit, but others involved with semiconductors and electronics reap huge added value profits from additional processing.

In this chapter we focus on the processing associated with shaping and forming components in traditional primary and secondary manufacturing industries. A comparative approach is adopted, stressing similarities in processing methods for different materials, for example, die casting of metals and injection molding of polymers, and powder pressing and sintering of metal and ceramic powders. At the same time, differing competitive routes to production of the same component, for example, by forging, casting, or powder metallurgy, are compared. Qualitative process descriptions, engineering modeling of some of

their features, product design, and elimination of processing defects are some of the additional issues addressed.

Materials processing issues underscore a vitally important and broad subject that could easily fill a book by itself. The subject is interdisciplinary in nature. To confront it our knowledge of materials must be integrated with fundamental scientific and engineering concepts drawn largely from the fields of mechanical and chemical engineering. Solid mechanics, strength of materials, heat and mass transfer, and fluid mechanics—a substantial part of the educational core baggage borne by engineers—all play important roles in processing. For simplicity, only elementary descriptions and applications of these subjects are considered. Although processing has been benignly neglected in this book until now, it is hoped a new perspective and appreciation of materials properties will emerge from the implications of the present chapter.

Let us start with casting or, more appropriately, solidification processing.

8.2. SOLIDIFICATION PROCESSING OF METALS

Casting is a viable process because liquid metals flow readily, have a high density, and are good conductors of heat. **Fluidity**, or the ability to flow, is inversely proportional to viscosity. Liquid metals are unique in having very low viscosities (e.g., $\eta = 10^{-3}$ P or 10^{-4} Pa-s) and therefore flow readily. Coupled with high densities, liquid metals easily fill molds, whereas less dense nonmetallic fluxes, drosses, and oxide slags float to the surface where they can be skimmed off. High heat transfer rates make it possible to complete solidification rapidly, making casting production rates economical. A wonderfully diverse collection of casting processes has been developed over thousands of years. New processes as well as modifications of older ones continue to appear. The reason, as we shall see, is that solidification processing is a very attractive way to shape not only metals, but other materials as well.

8.2.1. Expendable Mold Casting

8.2.1.1. Lost Wax Method

Lost wax casting employs expendable molds that are used just once because they are destroyed in the process of making a single impression. Much can be learned about casting by considering how the bronze sculpture **Dream 1**, shown in Fig. 8-1A, was made. Except for new metal compositions and improvements in waxes and mold materials, tooling, furnaces, and other aspects, the basic process steps have not changed since antiquity. First the sculptor created an exact wax replica or pattern of what the final bronze was envisioned to look like. Then the wax was essentially removed without a trace and completely

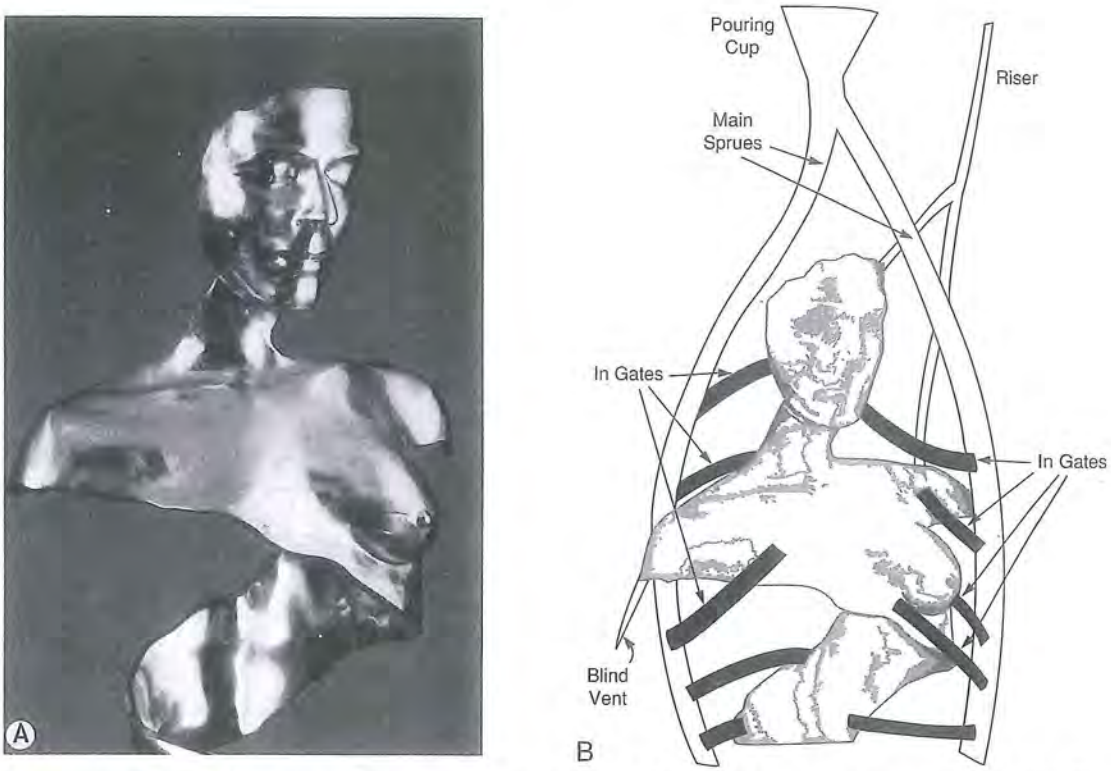

FIGURE 8-1 (A) *Dream I*, a bronze sculpture by Professor R. B. Marcus, New Jersey Institute of Technology. The sculpture is 24 in. high. (B) Schematic of the gating system used for this casting. The risers provide metal to feed shrinkage and enable gases to escape. Gates help reduce turbulent flow of the melt as it fills the mold. The blind vent ensures that voids do not form in corners.

replaced by bronze. This was not achieved by magical sleight of hand, but rather through the following time-honored series of steps:

1. Wax rods are initially attached to the wax pattern to create a type of plumbing system (Fig. 8-1B) which directs the flow of metal from the **pouring cup**, through a **sprue** and into **gates** that meter the molten metal flow into the casting. Provision must also be made to attach a wax **riser.** When filled, the riser provides a reservoir of molten metal that can flow into and fill casting cavities caused by metal shrinkage during the transformaton of liquid to solid bronze.
2. The wax and the gating system are either immersed in a plasterlike, water slurry of refractory oxide powder (e.g., SiO_2, CaO, ZrO_2, plus binders) or stuccoed over with this mold material until completely surrounded. To replicate wax copies or additional castings split or multipiece permanent molds with parting lines are used.

3. After drying, the entire mold assembly is inverted and placed in a furnace. The wax is melted, drained, and then burned out to remove the last vestiges. In the process the mold hardens and is capable of withstanding the shock of hot metal contact.

4. Molten metal is then poured into the empty cavity created by the lost wax. After solidification the mold is broken apart to free the casting. The solid gating and riser rods are sawed off and the metal surface undergoes a long finishing operation to enhance the beauty of the bronze and the artistic quality of the final sculpture.

Note that the original pattern and final sculpture are not solid but rather hollow shells with a wall typically about 0.5 to 0.75 cm thick. This not only reduces the sculpture weight but eliminates thermal and mechanical damage to the mold and lessens the probability of casting defects. **Lost wax** casting is of course not simply limited to creating bronze sculpture. All metals can be cast by this technique. In fact, it is the preferred method for producing some of the most critical, intricate, and costly shaped castings that are manufactured, for example, the prostheses in Fig. 1-10. The cobalt base alloys used to make these precise castings necessitate a high-temperature refractory ceramic (e.g., ZrO_2) mold material or investment. This is why lost wax casting is also known as **precision** or **investment casting.**

Among the most sophisticated of all castings are jet engine turbine components. Higher temperatures enable turbine blades to operate more efficiently but unfortunately accelerate thermal degradation processes due to creep. The first problem is ameliorated by incorporating fine internal passages that help cool them. To address the second problem we note (in Section 10.6) that grain boundaries are important sites for creep damage. Therefore, one strategy is to increase the casting grain size as shown in the turbine blades of Fig. 8-2 (see color plate). Ideally, single-crystal turbine blades with no grain boundaries are most immune to creep damage. This goal is achieved by first directionally solidifying the melt to induce columnar grain growth. One such grain is then isolated and constricted to form the seed onto which the single-crystal blade subsequently grows. Monocrystalline turbine blades have proven to be a significant technological advance. Other products commonly cast by lost wax techniques include tools, gold rings, and precious metal jewelry.

8.2.1.2. Sand Casting

Based on a weight criterion, more sand castings are produced than any other type. Cast iron as well as aluminum engine blocks, cast iron machine tool bases, steel machinery components of all types, stainless-steel pump housings, plumbing fixtures of all sizes, and huge bronze ship propellers are examples of some sand casting applications and the metals used. Wooden or plastic patterns of the desired shapes together with attached gates and risers are first embedded into a special casting sand contained within halves of a split mold.

This allows the pattern and its attached gates and risers to be easily removed to create the cavity, which is subsequently filled by molten metal, after the halves have been rejoined. A good idea of sand casting can be obtained from the exploded view of Fig. 8-3A.

In an important variant of sand casting known as **shell mold casting**, a thin shell (0.5–1 cm thick) of a sand–resin mixture is used as the mold. In this form split molds can be stored; when needed they are clamped together, backed by sand, and then filled with molten metal.

Another expendable mold process employs easily shaped and produced low-density polystyrene patterns of the objects to be cast. After they are embedded in sand, molten metal is poured in, rapidly vaporizing the polystyrene. Finally, metal completely displaces the original polystyrene pattern. Applications for such **full mold castings** have included aluminum cylinder heads, brake components, and manifolds for automobiles.

8.2.2. Permanent Mold Casting

8.2.2.1. Die Casting

Molds are used over and over again in permanent mold casting processes. The most widely practiced of these methods is known as die casting. Dies are extremely important manufacturing tools made of hard, tough alloy steels that enable components made of metals, polymers, and ceramics to be shaped and replicated. They not only are used as molds to contain molten metals and polymers, but find extensive applications in mechanical forming operations like extrusion, wire drawing, sheet metal forming, and the pressing of metal and ceramic powders. Because the process chamber and die steels cannot withstand lengthy elevated-temperature contact with molten metals, die casting is limited predominantly to the low-melting-point metals like zinc and aluminum alloys. In the widely used **hot chamber process**, shown in Fig. 8-3B, molten metal is first pressurized to anywhere from 14 to 35 MPa (2–5 ksi). It is then injected into the clamped, split die mold, via a gooseneck, and held under pressure until it solidifies. The die is then opened, the solidified part ejected and the cycle repeated. Production rates depend on the alloy used and shape and weight of the casting. Approximately 900 shots or injections of zinc per hour are possible.

A variant of die casting is the **cold chamber process**. Higher-melting-point metals like aluminum, magnesium, and some copper alloys can be cast this way by first ladling out metal into the shot chamber and then rapidly ramming it into the die cavity. Pressures employed range from 20 to 70 MPa (3–10 ksi) but can be even higher.

Parts made by die casting include lawnmower engine and motor housings, carburetors, hand tool housings and parts, appliance components, door handles, and zipper teeth. A collection of die castings is shown in Fig. 8-4. Most die castings weigh between 0.1 and 25 kg.

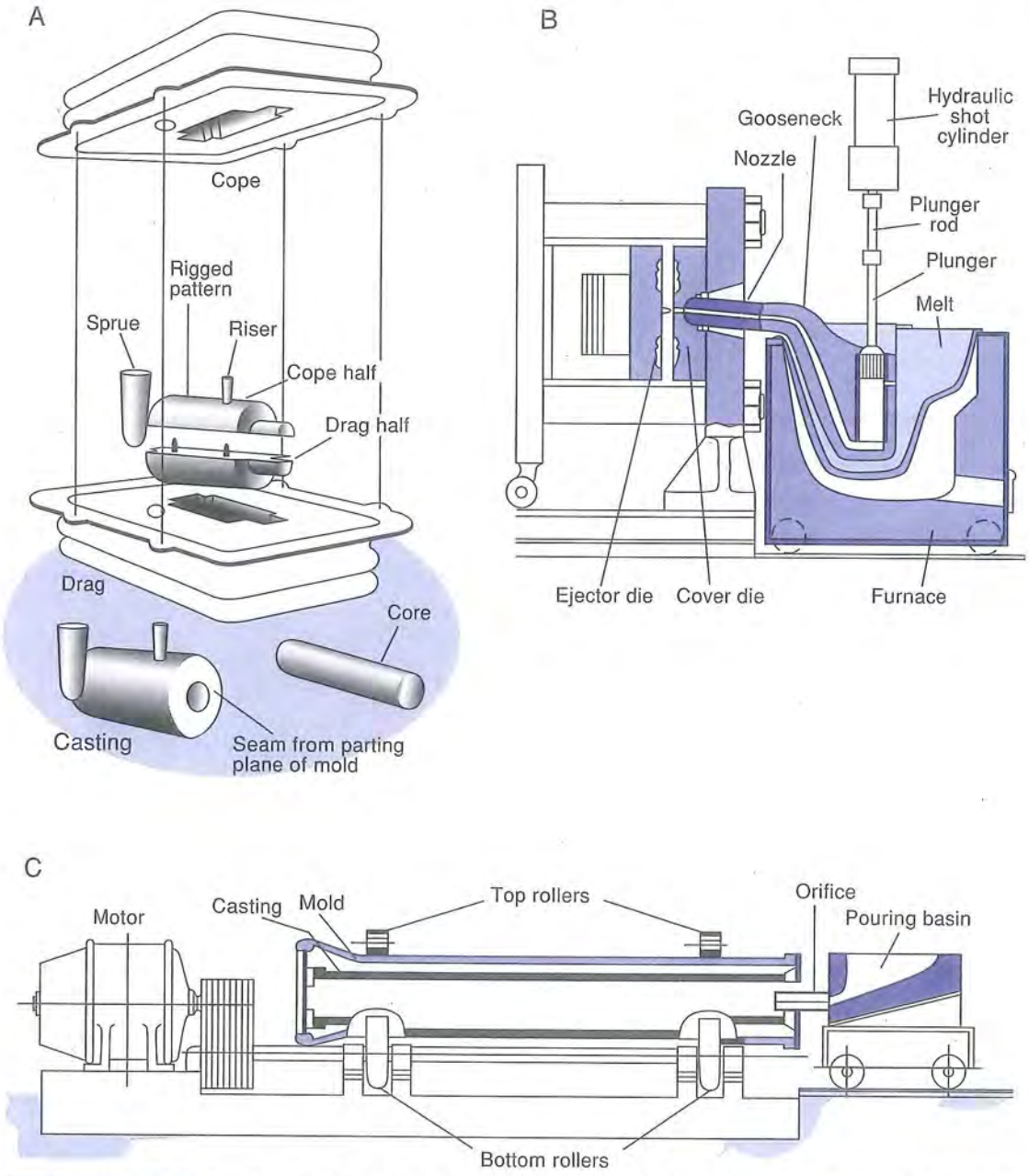

FIGURE 8-3 Casting methods. (A) Sand casting. From H. J. Heine, *Casting Design and Applications* (Fall, 1989). (B) Hot chamber die casting. (C) Centrifugal casting of pipes.

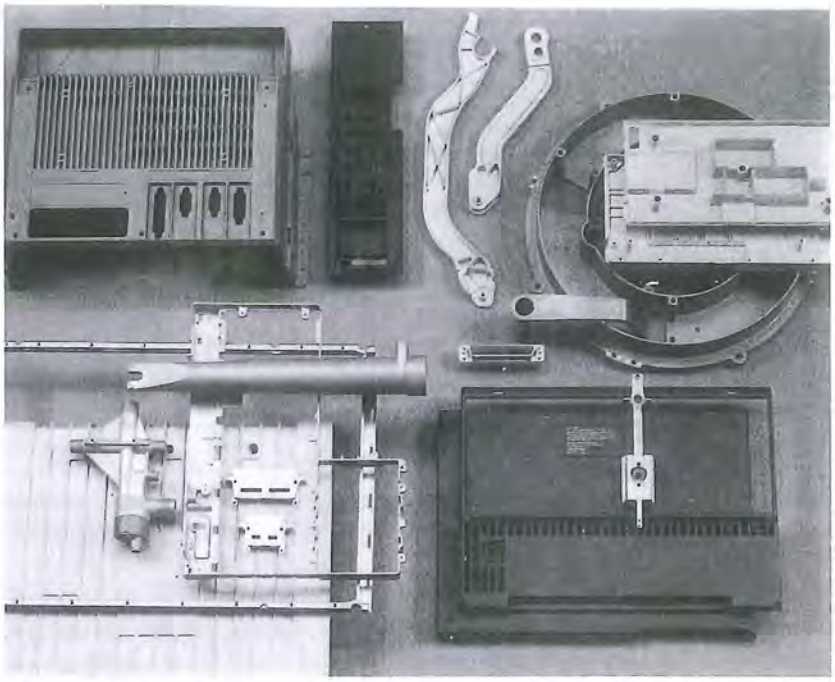

FIGURE 8-4 Assorted aluminum, magnesium, and zinc die castings. Courtesy of Chicago White Metal Casting, Inc.

8.2.2.2. Centrifugal Casting

As the name suggests, centrifugal casting (Fig. 8-3C) involves rotation to increase the inertial force that drives molten metal to fill mold cavities. By spinning permanent molds at ~1000 rpm, sounder pipes, cylinder liners, and hollow cylindrical parts of all metals can be cast while retaining good dimensional tolerances. Investment cast gold rings are often rotated about the vertical sprue axis during pouring to better fill intricately shaped molds.

Now that a number of expendable and permanent mold casting processes have been introduced, it is instructive to compare their relative merits. This is done in a self-explanatory way in Table 8-1.

8.2.3. Heat Transfer Considerations

It is important to know the temperature history at all locations within solidifying castings to identify hot spots that may become potential defect sites. There will be some discussion of how this is accomplished employing computer methods, but it is helpful first to have a physical feeling for the problem. Therefore, let us calculate the rate of solidification of the melt shown in Fig. 8-5. It is assumed that nucleation of solid from the slightly undercooled liquid

TABLE 8-1 GENERAL CHARACTERISTICS OF CASTING PROCESSES

Process	Metals cast	Weight (kg) min	Weight (kg) max	Dimensional accuracy[a]	Shape complexity[a]	Porosity[a]
Sand	All	0.05	No limit	3	1–2	4
Shell	All	0.05	100+	2	2–3	4
Investment	All (High melting point)	0.005	100+	1	1	3
Permanent mold	All	0.5	300	1	3–4	2–3
Die	Nonferrous (Al, Mg, Zn, Cu)	<0.05	50	1	3–4	1–2
Centrifugal	All	—	5000+	3	3–4	1–2

[a] Relative rating: 1 = best, 5 = worst. Variations can occur, depending on the evaluation methods used.

From S. Kalpakjian, *Manufacturing Processes for Engineering Materials*, 2nd ed. © 1991 by Addison–Wesley Publishing Company, Inc. Reprinted by permission of the publisher.

is not a problem and that the solid–liquid interface is linear. Interface motion depends on how fast heat is extracted from the melt. Initially, a relatively insulating mold contains liquid metal at its melting point T_M. As metal of density ρ_M freezes, its latent heat of fusion H (J/kg) is liberated at the interface between liquid (L) and solid (S). This heat quickly flows through the already

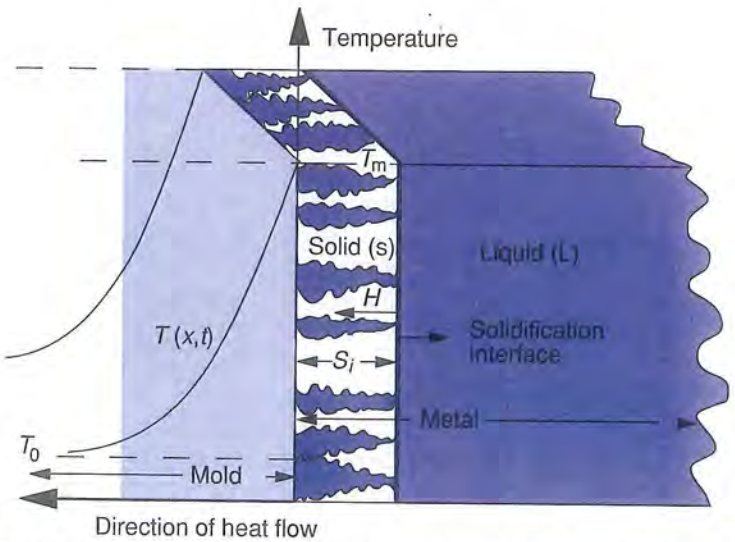

FIGURE 8-5 Model of solid metal solidification front advancing into a melt at T_M. The liberated latent heat flows through the solidified metal and into the mold.

solidified metal and enters the mold, raising its temperature. Concurrently, the amount of metal solidified increases with time. The position of the solidification front (S_i) as function of time (t) is given by

$$S_i = \frac{2}{\pi}\frac{(T_M - T_0)(\kappa c \rho_m)^{1/2} t^{1/2}}{\rho_m H}, \tag{8-1}$$

where κ, c, and ρ_m are the thermal conductivity (W/m-K), heat capacity (J/kg-K), and density (kg/m^3) of the mold material, respectively. (Derivation of Eq. 8-1 is left as an exercise in Problem 8-1.)

Conduction or diffusion of heat obeys the same physical laws as diffusion of atoms in solids. In fact, heat conduction in one dimension obeys equations similar to Eqs. 6-1 and 6-2 if C is replaced by T. Additionally, in Eq. 6-1 the mass flux J must be replaced by the heat flux Q (in units of J/m^2-s or W/m^2), and D by κ (in units of W/K-m-s). But in Eq. 6-2, the diffusion coefficient D is replaced by the thermal diffusivity α, which is equal to $\kappa/\rho_m c$; both D and α have identical units (m^2/s). Lastly, the ambient temperature is T_0. Note that S_i depends on the product of two factors, one containing metal dependent, and the other, mold dependent properties. The solidification front is seen to advance parabolically in time. This result should not be too surprising as the diffusional spreading of matter also follows a $t^{1/2}$ dependence.

Figure 8-5 reveals that S_i is equal to the volume of the solidified metal divided by the area of the planar solidification front. This result can be generalized to arbitrarily shaped solidified regions of volume (V) and (curved) surface area (A). Furthermore, if these quantities refer to the final casting volume and surface area, the time can be associated with the solidification time (t_s). Substitution of these terms in Eq. 8-1 yields Chvorinov's rule:

$$V/A = Ct_s^{1/2}; \qquad C = \text{a constant.} \tag{8-2}$$

This equation has been verified for both small and large castings in insulating molds.

8.2.4. Structural Implications of Solidification Rates

The heat flow analysis given above provides no clue as to the grain structure of the casting, an important consideration as already noted in Sections 3.6.1 and 8.2.1. Actually, dendritic growth and columnar grains are favored when the temperature gradient in the melt is small and the solid–melt interface velocity is large. When the opposite conditions prevail, as in crystal pulling (see Section 6.4.3), a planar, nondendritic solidification front develops.

In Section 9.4.2 we shall see that both higher strength and ductility of metals are associated with fine grain size. The same is true of dendritic castings, but instead of grain size the appropriate dimension of concern is the **secondary dendrite arm spacing.** Growing perpendicular to the main dendrite trunk are the secondary dendrite arms (see Fig. 5-30) and their interspacing can be reduced by cooling the melt more rapidly. In the process, undesirable composi-

tion variations due to coring are minimized. Unfortunately, heat transfer concerns limit the size of the casting whose properties can be enhanced this way. At extreme cooling rates of $\sim 10^6$°C/s the arm spacing may be effectively reduced to atomic dimensions if amorphous structures result.

EXAMPLE 8-1

Suppose solid aluminum spheres 0.2 m in diameter solidify in 30 minutes. An engineer suggests casting solid hemispheres sequentially (followed by joining) as a time-saving measure. Is this course of action wise?

ANSWER The constant C can be determined for this casting process by direct substitution of the quantities for the sphere. Therefore by Eq. 8-2,

$$C = t_s^{-1/2}(V/A) = (30^{-1/2})[(4\pi(0.1)^3/3)/(4\pi(0.1)^2)] = 6.09 \times 10^{-3} \text{ m/min}^{1/2}.$$

Assuming C is the same for casting hemispheres, the time it will take each to solidify is

$$t_s = \frac{1}{C^2}\left(\frac{V}{A}\right)^2 = \frac{1}{(6.09 \times 10^{-3})^2}\frac{[2\pi(0.1)^3/3]^2}{[2\pi(0.1)^2 + \pi(0.1)^2]^2} = 13.3 \text{ minutes}.$$

The suggestion does not appear to be wise because it will only leave $30 - 2(13.3) = 3.4$ minutes, at most, for additional preparation of two molds, double pourings, and assembly. Besides, duplicate castings are wasteful of mold material.

8.2.5. Design of Castings

Chvorinov's rule suggests that sections of the casting having a large volume-to-surface area ratio will take a long time to solidify. Such hot spots should be avoided when designing castings because they are potential sites of porosity defects. When the melt within a hot spot solidifies it contracts, leaving a shrinkage cavity that must be refilled if the casting is to be sound. If, however, neighboring thin sections solidify around the hot spot, the flow of liquid metal may be choked off, depriving the cavity of metal. Such a problem might develop when casting a metal bowling pin upright, the orientation depicted in Fig. 8-6. After the mold is completely filled, grains bridge in the neck section, restricting metal flow to the bulbous base. A mass of liquid is trapped that cannot be fed, and when it solidifies a shrinkage cavity develops. The situation is remedied by casting the pin upside down. Sufficient liquid metal will be stored above in the riser to feed the shrinkage in the casting below. The desirable progressive **directional solidification** will thus result in a sound casting.

Although the preceding example demonstrated the need for orienting the casting properly, Fig. 8-7 illustrates a number of poorly designed casting features together with recommended alternate designs. A rough but useful way

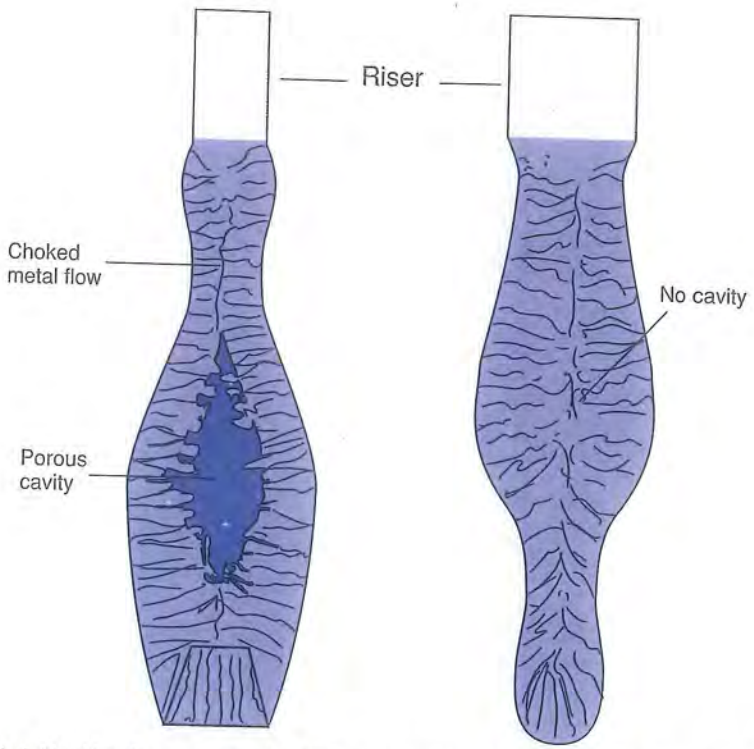

FIGURE 8-6 *Left:* Metal bowling pin cast upright. The melt flow from the riser is choked in the neck, leaving a cavity where feeding is prevented. *Right:* Bowling pin cast upside down. Directional solidification results in a sound casting.

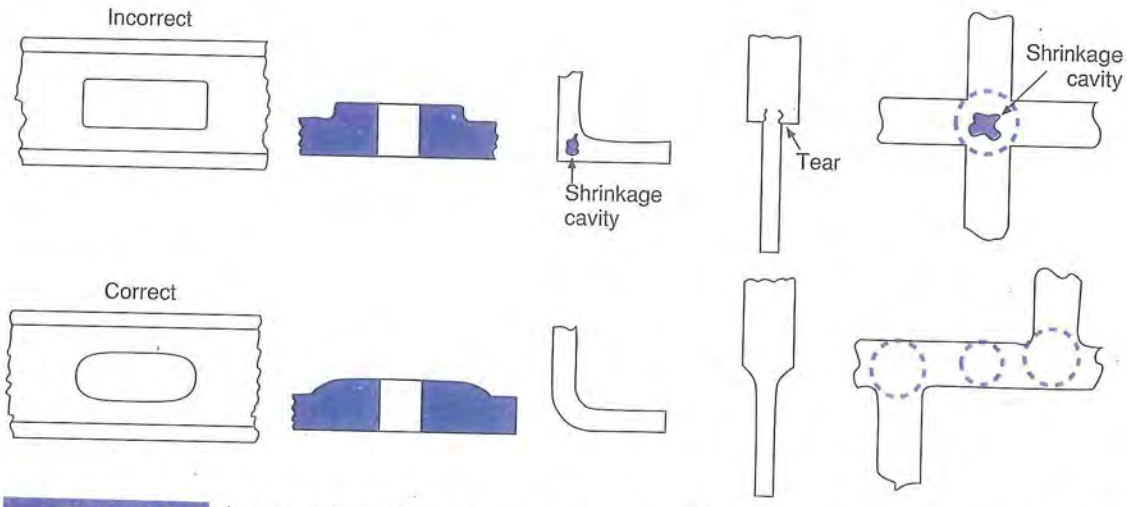

FIGURE 8-7 Incorrect and correct design geometries when casting the indicated sections. For the cross at the extreme right, spheres (circles) are inscribed to reveal casting hot spots. Shrinkage cavity formation and hot tearing effects can be minimized by modifying casting designs to eliminate hot spots, sharp corners, and nonuniform sections.

to locate hot spots at suspected sites is to find where the largest circle (sphere) can be inscribed. Large radii mean long solidification times because of the large volume-to-area ratio. On this basis, the design modifications shown reduce the probability of shrinkage defects. Sharp corners and abrupt changes in dimension should also be avoided to minimize stress concentrations. Differential thermal contraction and strength beween contiguous hotter and cooler regions of metal promote a tendency toward cracking and tearing.

8.2.6. Computers and Casting

We now consider the computer modeling of the temperature–time distribution throughout a complex shaped casting after pouring. The procedure is conceptually straightforward but rather involved in practice. First the casting, riser, and mold geometries are subdivided into a bricklike array of elements. Hundreds to hundreds of thousands of elements may be required depending on the complexity of the casting geometry. Changes in temperature of any given element caused by conduction, radiation, and convection heat transfer to it from neighboring elements are calculated by appropriate mathematical techniques. The temperature solutions are dovetailed together in three dimensions in a self-consistent manner, and the results are updated at desired time intervals. Temperature-dependent mold and metal thermal and heat transfer constants are folded into the analysis to make the simulation as accurate as possible. The power of the method is illustrated in Fig. 8-8A (see color plate), where the computer-calculated time sequence of the cooling behavior of the wheel reveals the presence of a hot spot. Note that on either side of the hot spot (void) the metal is cooler. The situation is improved by redesigning the rim to be lighter. As seen in Fig. 8-8B (see color plate), solidification now proceeds in the desired directional manner.

Computers have dramatically transformed the art of engineering design and manufacturing into a science. They enable the concurrent integration of computer-aided design (CAD) and manufacturing (CAM), involving stress (strength) and solidification analyses of the part to be cast, with the production of the required tooling (dies, molds). How this is all accomplished in the case of a lightweight automobile engine connecting rod is illustrated in Fig. 8-9.

8.3. MECHANICAL FORMING OPERATIONS

Unlike the casting of liquids that readily flow to fill molds by gravity, mechanical forming operations redistribute solid matter under the influence of applied forces. Examples of common bulk mechanical forming operations are schematically depicted in Fig. 8-10. Included are forging, rolling, extrusion, and drawing processes that one associates with the primary forming of metals. In contrast, sheet metal forming operations (treated in Section 8.3.6) are nor-

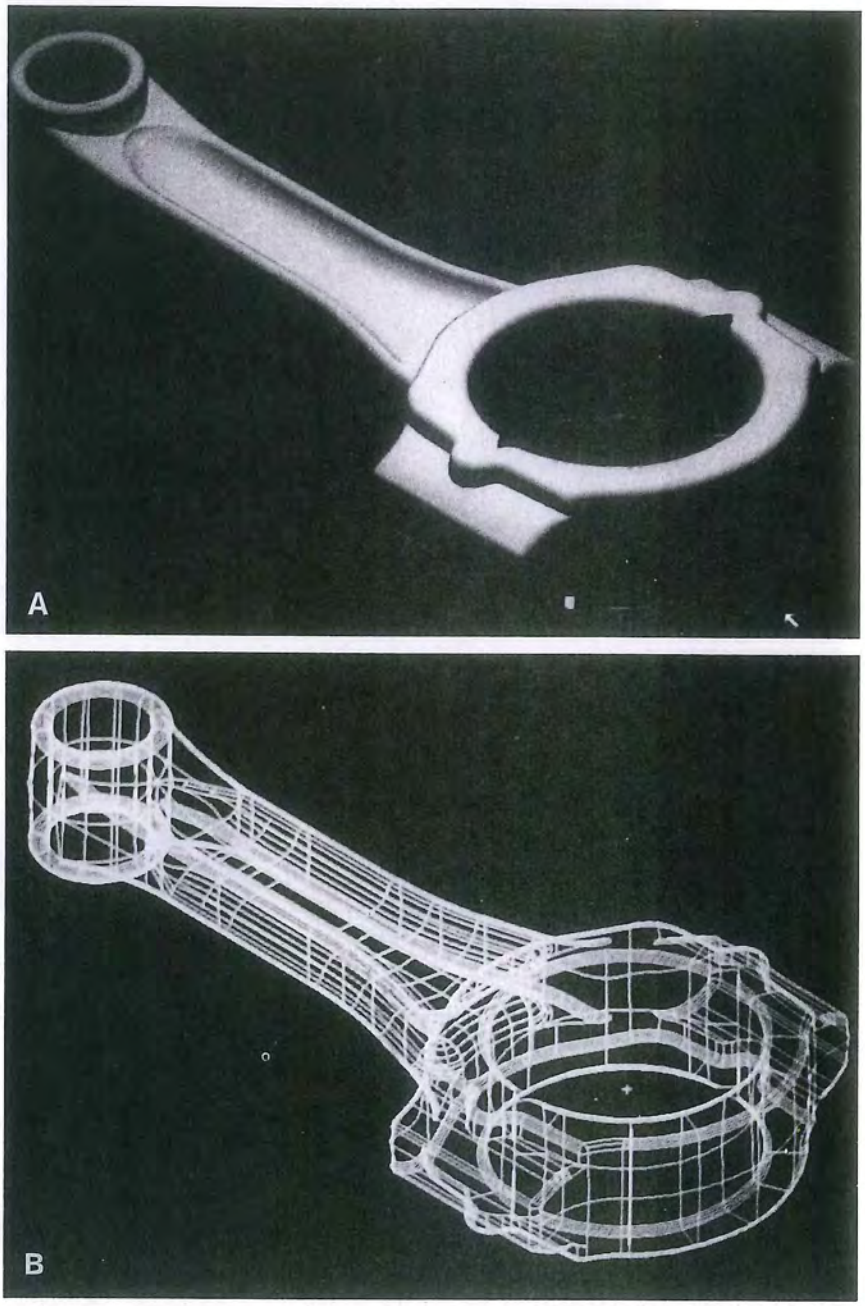

FIGURE 8-9 CAD/CAM methods used in producing a lightweight automobile engine connecting rod. (A) Shaded surface model. (B) Computerized "wireframe" model. (For parts C and D, see color plates.) (E) Computer-controlled cutter path for developing prototype tooling. Courtesy of G. Ruff, CMI International, Inc.

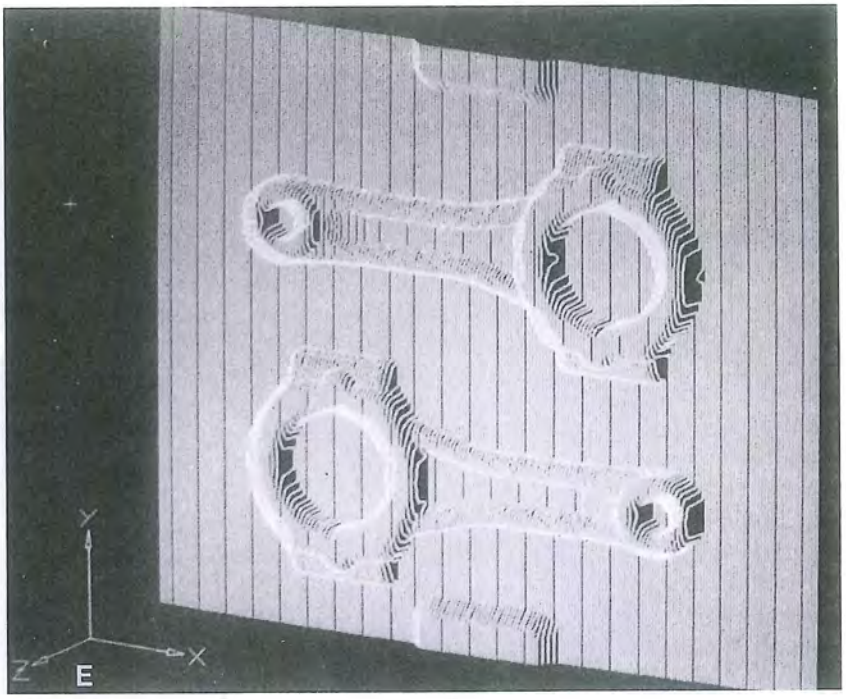

FIGURE 8-9 (*continued*)

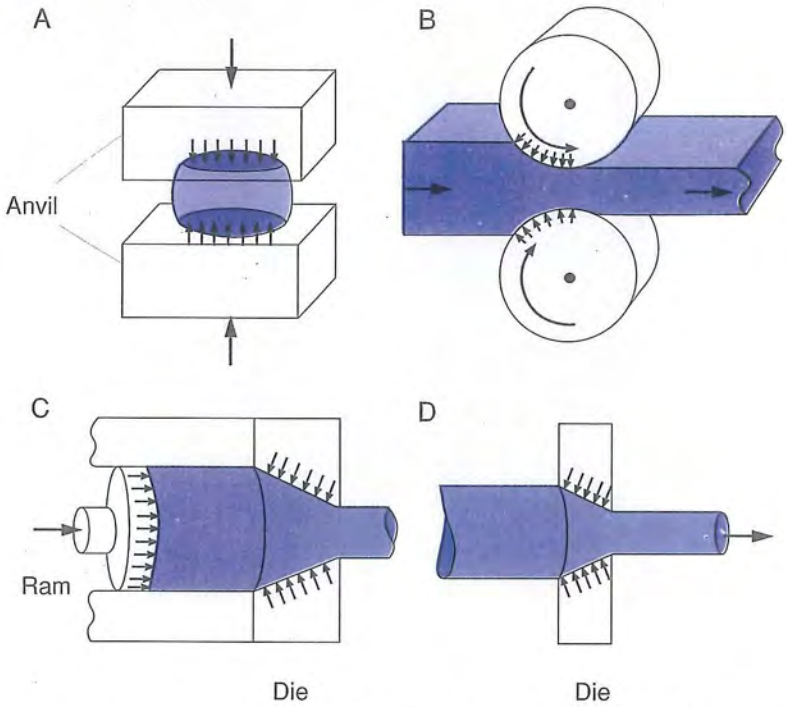

FIGURE 8-10 Typical mechanical forming methods. (A) Open die forging. (B) Rolling. (C) Extrusion. (D) Drawing. Arrows show forces on workpiece.

mally carried out in secondary manufacturing. The dividing line is not so sharp, however, and there are examples of each forming process shown in Fig. 8-10 being practiced in secondary manufacturing environments. All bulk metal forming processes can and have been carried out at room temperature, but it is more common to practice them at elevated temperatures, especially when strong, large shaped objects are involved. In this way greater ductility is achieved and lower plastic flow stresses can be capitalized on to reduce the load-bearing requirements of the forming equipment.

Mechanical forming of metals often endows them with superior mechanical properties. The traditional route of metals processing typically includes ingot casting followed by either (hot) rolling, extrusion, or forging at elevated temperatures. This causes a cast structure that is dendritic, chemically inhomogeneous, and full of shrinkage voids or porosity to be broken up by the combined effects of stress and high-temperature diffusion. The prior casting of reasonable strength but low ductility is converted into a much tougher and homogeneous material. Then the metal is frequently shaped by low-temperature forming, for example, cold rolling, where the requisite strength, ductility, and uniform grain structure are conferred for final manufacturing operations, for example, deep forming of sheet metal. These processes are illustrated in Fig. 8-11 for Monel metal. Starting with the dendritic cored structure shown in Fig. 5-30, the sequence of thermomechanical treatments progressively alters the grain structure as shown.

What is true of each forming operation in Fig. 8-10 is that the required force is usually applied in one direction; however, it invariably happens that this unidirectional force actually stresses the workpiece not only in one, but in two approximately perpendicular directions simultaneously. For example, pushing the work through the die during extrusion creates a compressive reaction from the sidewalls. And the tension applied to a wire to reduce its cross-sectional area results in a similar compressive die wall reaction on the drawn metal. Even during forging where the work appears to be simply compressed, lateral stresses are frequently generated. Frictional contact at the anvil–workpiece interface establishes forces that restrain the work from expanding laterally, and causes bulging (see Fig. 8-10A).

8.3.1. Deformation due to Biaxial Stresses

Let us expand these concepts by considering the application of mutually perpendicular forces on a solid cube as shown in Fig. 8-12. For simplicity, only the two-dimensional state of stress in the projected square section is shown. In case (A) both stresses σ_x and σ_y are tensile and assumed equal (balanced biaxial tension). Under the action of σ_x alone the deformation displaces (very exaggeratedly) the two halves of the square such that overall it extends in the x direction and contracts in the y direction. If σ_y is now sequentially applied, the square will extend in the y direction and contract in the x


A


B

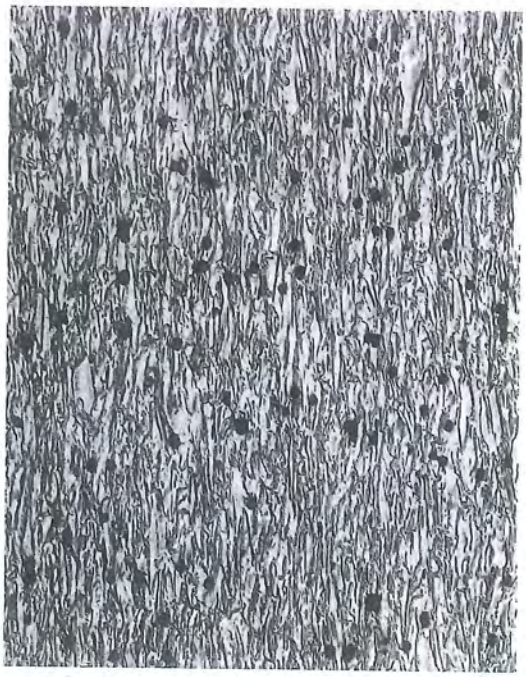


D

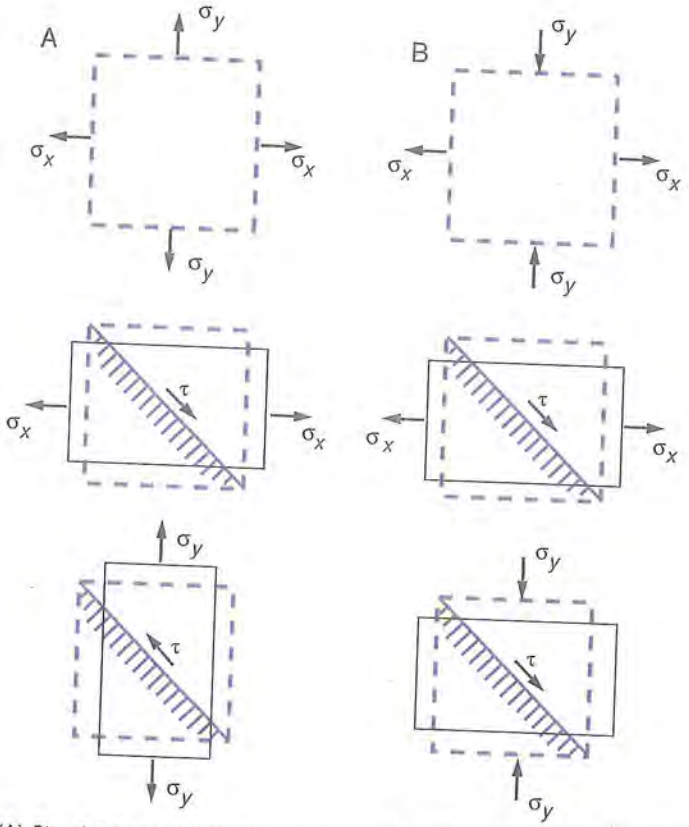

FIGURE 8-12 (A) Biaxial tension. In balanced biaxial tension or compression, superposition of the separate uniaxial stresses leads to zero net shear stress. (B) Body acted upon by mutually perpendicular tensile and compressive loads. Superposition of these uniaxial stresses leads to an enhancement of the shear stress components.

direction. A *superposition* of the two stresses will leave the square unchanged. In essence the shear stresses that act along the diagonals have vanished. If σ_x and σ_y become very large they will ideally tear the cube apart rather than plastically deform it.

Let us see what happens in case (B), where the sign of σ_y is reversed, so that it is compressive but with the same magnitude as σ_x. Clearly the deformation is doubled, as the amount produced by σ_x alone is now reinforced by a like

FIGURE 8-11 Microstructures resulting from the thermomechanical processing of Monel (nominally 63 wt% Ni, 32 wt% Cu, plus Fe and Si). The cast microstructure is shown in Fig. 5-30. Sequential treatments and microstructures: (A) Homogenized at 1120°C for 20 hours. (156×). (B) Hot forged between 650 and 1000°C (156×). (C) Cold rolled to 75% reduction in area (156×). (D) Annealed at 870°C for 1 hour (156×).

amount through the action of σ_y. Under uniaxial loading conditions it was shown in Example 7-1 that the *shear stress* on the diagonal plane has a magnitude equal to *half* that of the applied stress. Therefore, these physical results can be algebraically expressed through addition of the stresses by

$$\tfrac{1}{2}\sigma_x - \tfrac{1}{2}\sigma_y = \tau. \tag{8-3}$$

Readers familiar with the elements of structural mechanics (or Mohr's circle construction) will recognize this result; in this case σ_x and σ_y are the so-called *principal stresses.*

For our needs we must realize that forming operations involve plastic and not elastic stresses, and that Eq. 8-3 is a formula that is derived from elasticity. Nevertheless, it also applies to plasticity. If a bar of metal is pulled in uniaxial tension we know that it will plastically deform when the yield or flow stress (σ_0) is reached; when this happens the plastic shear stress τ is equal to $\sigma_0/2$. Assuming τ, σ_x, and σ_y can be associated with the corresponding plastic stresses,

$$\sigma_x - \sigma_y = \sigma_0. \tag{8.4}$$

This equation represents a criterion for the onset of plastic deformation and is known as the **Tresca condition.** Simply stated, plastic deformation can be expected when the difference between the principal (plastic) stresses is equal to the yield stress of the material. A practical implication of Eq. 8-4 is that the best way to promote plastic forming operations is to apply combined stresses that maximize the internal shear stresses. Mutually perpendicular applied tensile and compressive forces, produced by pulling and pushing the workpiece, will have the desirable effect of enhancing plastic deformation.

8.3.2. Forging

Consider the forging of a rectangular block of metal compressed between a pair of flat, parallel anvils as shown in Fig. 8-13. In practice, hammerlike impact loads are usually applied. If the yield stress is σ_0 we wish to know the compressive load required to deform the block. The presence of friction at the work–anvil interface means that tangential shear stresses exist such that $\tau/\sigma_y = f$, where f is the coefficient of friction. It also means that compressive stresses in the x direction, generated by friction forces, are distributed throughout the workpiece. The effect is cumulative. At the edges $x = \pm a$, the frictional forces are zero, but they build symmetrically to a maximum value at the center of the forging. A so-called **friction hill,** which becomes higher and steeper with increasing f, develops. The larger f is, the greater is the applied force necessary to plastically deform the block. Undesirable barrel-shaped forgings are a manifestation of work–die friction. Theory shows that the compressive stress in the y direction varies exponentially about $x = 0$ as

$$\sigma_y = -\sigma_0 \exp[2f(a - x)/h]. \tag{8-5}$$

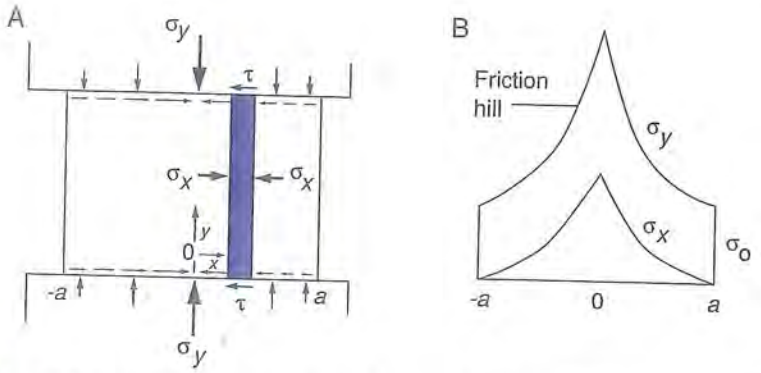

FIGURE 8-13 (A) Forging geometry in a rectangular block. Stresses acting on the interior shaded element are indicated. (B) Distribution of compressive stresses, σ_x and σ_y, versus distance. Note that vertical surfaces of the forging are stress free ($\sigma_x = 0$).

Similarly, σ_x, the compressive stress in the x direction, also reflects the symmetrical friction hill. The two stresses are related by Eq. 8-4 and their variation with x is indicated in Fig. 8-13B. Because the total area under the σ_y stress distribution is proportional to the total forging load, every effort is made to reduce f and σ_0. And since elevated temperatures reduce the yield stress, forging and other bulk metal working operations such as rolling and extrusion are carried out hot.

If f/h is sufficiently small, then the exponential term can be approximated by $1 + 2f(a - x)/h$. These are the first two terms of the series expansion for the exponential. In such a case the simpler linear formula

$$\sigma_y = -\sigma_0[1 + 2f(a - x)/h] \tag{8-6}$$

can be used. To a good approximation, Eqs. 8-5 and 8-6 also hold for forging cylinders of radius r and height h, if r is substituted for a.

EXAMPLE 8-2

A 10,000-ton (8.88×10^7N) press is used to forge Cu alloy blocks that are 0.1 m high having a square cross section equal to 0.0225 m^2. An average flow stress of 600 MPa is maintained throughout the forging process under conditions where $f = 0.2$.

a. What load is required for forging?

b. If the coefficient of friction were reduced to 0.1, what load would be required?

c. What is the largest average flow stress this press can handle if the metal is in the form of a 0.15-m-high ingot with a square cross section measuring 0.10 m^2? Assume $f = 0.1$.

ANSWER a. As $a = 0.075$ m, $2fa/h = (2)(0.2)(0.075)/(0.10) = 0.3$. Because the exponent is less than 1, we can use Eq. 8-6. The load (P) required is the product of the average value of σ_y and base area. Calculation of the peak value of $\sigma_y = \sigma_0(1 + 2fa/h)$ yields $600(1 + 0.3) = 780$ MPa, whereas the minimum value of σ_y at $x = a$ is 600 MPa. The average value of σ_y is, therefore, $\frac{1}{2}(780 + 600) = 690$ MPa. Hence,

$$F = (690 \times 10^6 \text{ Pa})(0.0225 \text{ m}^2) = 1.55 \times 10^7 \text{ N}.$$

b. If $f = 0.1$, the average stress is half the sum of $600(1 + 0.15)$ and 600 or 645 MPa. The forging load is reduced to

$$F = (645 \times 10^6)(0.0225) = 1.45 \times 10^7 \text{ N}.$$

c. In this problem we must equate the press capacity (F_p) to the load sustained in the metal. Hence, $F_p = \sigma_0[(1 + 2fa/h + 1)/2](A)$, where $A = 0.1$ m^2, $a = 0.316$ m, $h = 0.15$, and $f = 0.1$. Solving, $8.88 \times 10^7 = \sigma_0[1 + (0.1)(0.316)/(0.15)](0.1)$ yields $\sigma_0 = 7.33 \times 10^8$ Pa, or 733 MPa.

8.3.3. Forging Practice and Products

At the outset a distinction between open and closed die forging should be noted. Open die forging is the type to which the previous section applies. Large shapes such as steam turbine rotors and military cannons are forged between open die anvils of simple shapes. A blacksmith's hammer and anvil would loosely approximate open dies; however, many additional finished products like automobile crankshafts, wrenches, hand tools, turbine disks, railroad wheels, and gears have, at one time or another, been forged within shaped dies that close around the metal within. In the case of the crankshaft shown in Fig. 8-14, the steel rod is first roughly forged to bulge the metal in the right places. Then it is progressively forged between intermediate closed blocker dies which shape it further until finishing dies can be used. After several strikes a faithful impression of both die faces is made. Directed metal flow in dies confers a type of graininess to the forging, making it stronger in directions parallel to the deformation. The crankshaft emerges but with a thin flare or **flash** of steel that spreads outward from the die parting line. After the flash is ground away the finished forged shaft emerges. Since the flash is thin (h small), Eq. 8-5 indicates that the forging load rapidly mounts. Simultaneously, the flash is sufficiently strengthened so that it prevents metal in the closed die from extruding out. Friction promotes metal filling of the cavity, and without it closed die forging would not be feasible.

Metals must be ductile to be forged, but for casting purposes there is no such restriction. In general, forgings exhibit greater toughness and ductility than equivalent castings. Nevertheless, cheaper castings compete with and have replaced forgings in a number of applications including some automotive connecting rods (see Fig. 8-9) and crankshafts. For function in a car a bent

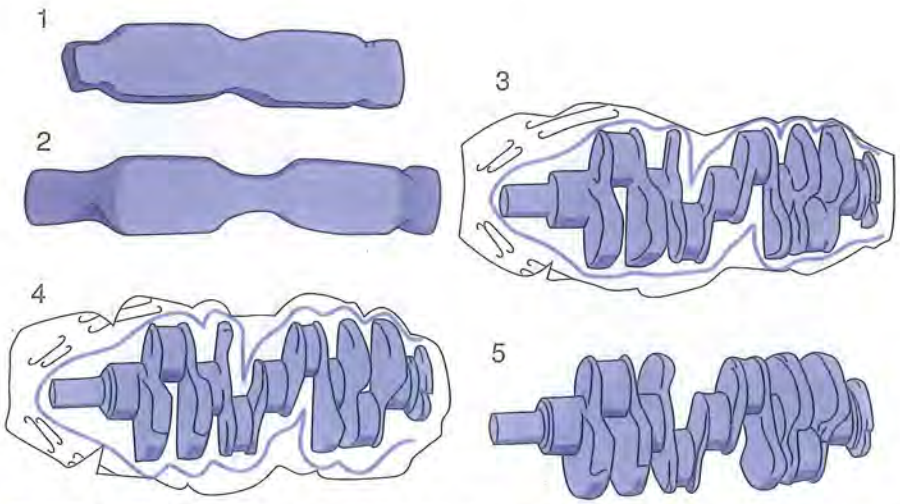

FIGURE 8-14 Stages in the closed die forging of a crankshaft. (1), (2) Preliminary roll forging. (3) Blocking in closed dies. (4) Finishing in closed dies. (5) Flash trimming. From *Metals Handbook*, 8th ed., Vol. 5, American Society of Metals, Metals Park, OH (1970).

forged crankshaft is as bad as a broken cast one. Therefore, the less tough, cast crankshafts sometimes serve just as well.

8.3.4. Rolling

Rolling of metals, a popular mechanical forming process, results in a reduction of the initial thickness as shown schematically in Fig. 8-10B. Work in the form of slabs or sheets is fed in at the left and the thinned material exits the rolls at higher speed. If the process is frozen in time, rolling is not unlike forging. A difference is that an asymmetrical stress distribution (friction hill) arises in the deformed metal because of the more complicated curved roll (anvil)–work geometry. The sheer volume of steel that passes between rolling mills dwarfs, by far, that of other metals. Irrespective of metal, however, the process is carried out at hot, warm, and cold temperatures. Hot refers to temperatures of $\geq 0.6T_M$, where T_M is the melting point in degrees Kelvin. Recrystallization of the worked matrix can occur at such temperatures. (See Chapter 9.) Between $\sim 0.3\ T_M$ and $0.6T_M$, the warm working regime is operative. Cold rolling is usually done at temperatures lower than $\sim 0.3T_M$ and most frequently at room temperature. Normalizing to the melting point of the material means that temperatures for cold working of tungsten are comparable to those required for hot rolling steel. As the rolling temperature drops, the thickness of the stock that can be rolled must necessarily decrease. Also, thinner stock is rolled at higher roll velocities and reaches delivery speeds of over a mile a minute in the case of sheet steel or aluminum foil.

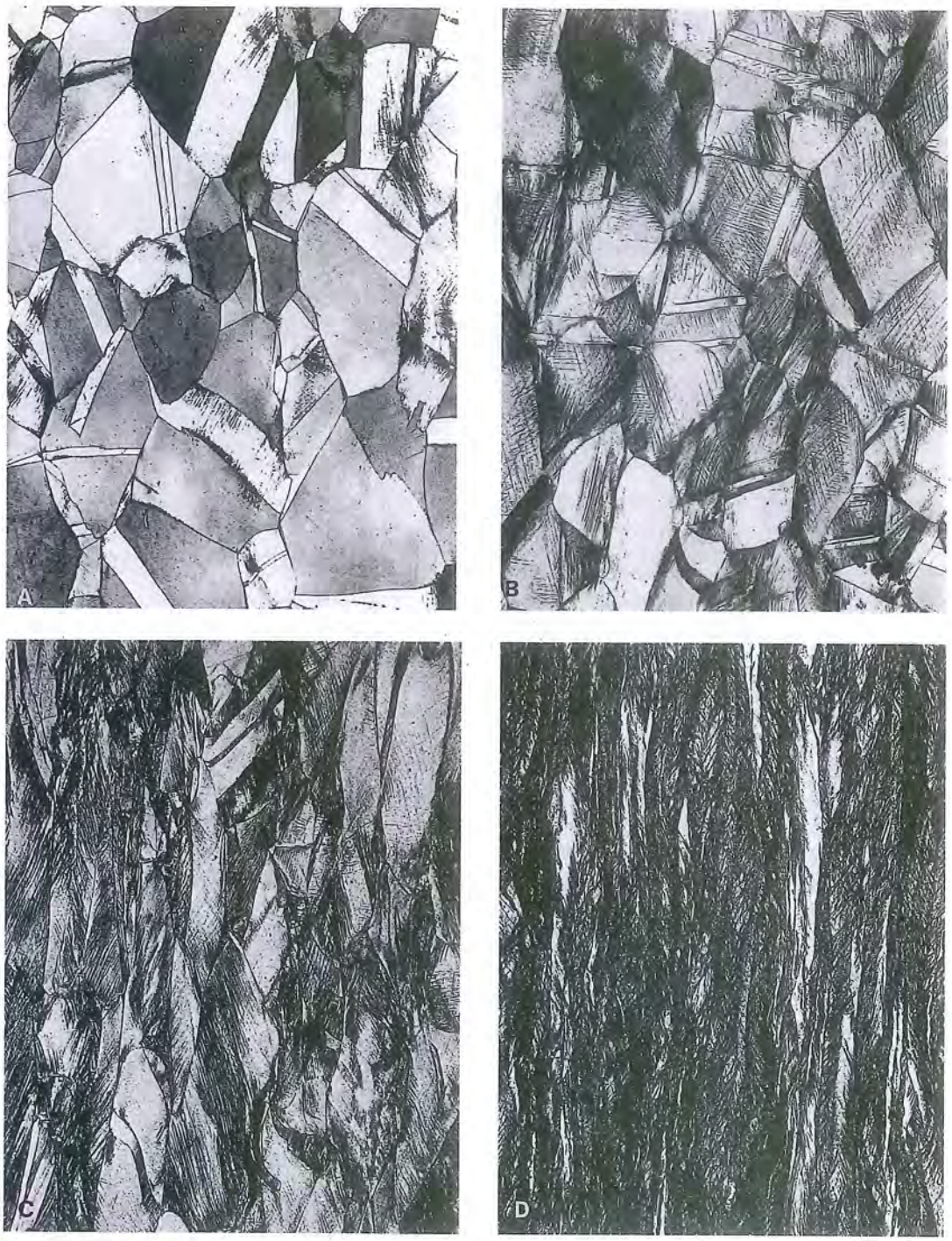

FIGURE 8-15 Microstructures of cold-rolled cartridge brass (70Cu–30Zn) starting with the undeformed metal of Fig. 3-32. (A) 15% reduction. (B) 30% reduction. (C) 50% reduction. (D) 75% reduction. 80×. Courtesy of G. F. Vander Voort, Carpenter Technologies Corporation.

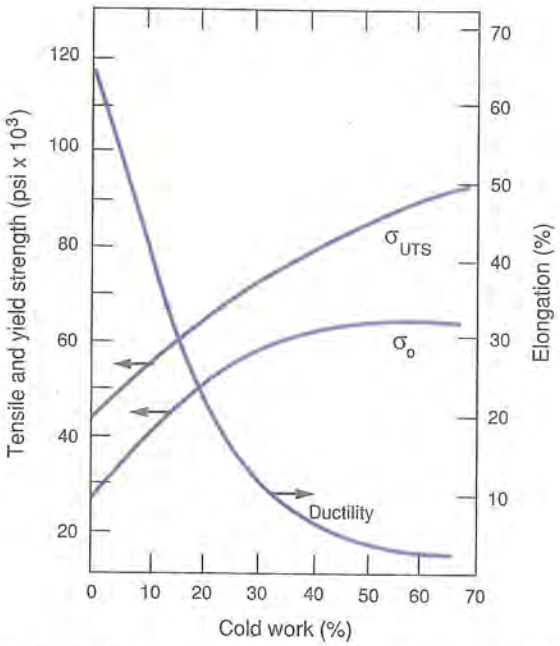

FIGURE 8-16 Effect of cold working on the yield stress, tensile stress, and ductility (percentage elongation) of cartridge brass (70Cu–30Zn).

If the initial stock has an equiaxed grain structure, cold rolling will elongate the grains and string out the grain boundaries in a distinctive manner. This is illustrated for cartridge brass in Fig. 8-15. The dislocation density grows enormously and the metal becomes harder. As shown in Fig. 8-16, strength properties increase significantly, but simultaneously, ductility measured by percentage reduction in area suffers with increasing amount of cold work. Surprisingly, these microstructural and mechanical property trends can be reversed by annealing; a metal approximating the original one prior to rolling can be regenerated through heating to elevated temperatures. Discussion of these important practical treatments is continued in the next chapter (see Section 9.4).

EXAMPLE 8-3

For a certain application, brass plate must have a tensile strength of 45,000 psi, a minimum ductility of 25% elongation, and a thickness of 0.5 in. The only plate stock available is 1.0 in. thick. Design a processing schedule that would enable the required specifications to be met.

ANSWER The total percentage reduction required is [(1.0 in. − 0.5 in.)/1.0 in.] × 100 = 50%. If the plate were rolled 50% in one pass, the tensile strength would be close to 80,000 psi but the elongation would only be about 5%. To achieve a 25% elongation, the maximum amount of cold work that can be tolerated is only 20%. Fortunately, such a deformation will produce a more than sufficient strength of ~60,000 psi. Therefore, we must ensure that the final pass involves no more than a 20% reduction. Therefore, the thickness d must be $[(d - 0.5)/d] \times 100 = 20$. Solving, $d = 0.625$ in.

Thus, the required processing could involve a single reduction from 1 to 0.625 in. [i.e., [(1.0 − 0.625)/1.0] × 100 = 37.5% reduction], followed by an annealing treatment to totally soften the brass to the original condition. This should be followed by the final 20% reduction. Alternately, several rolling passes could be initially employed to reduce the stock to 0.625 in., but the brass must then be fully annealed prior to the final 20% thickness reduction.

8.3.5. Extrusion and Drawing

Extrusion and drawing (Fig. 8-10) are normally treated together because they are analyzed in similar ways. In extrusion, materials are *pushed* through the die with a ram. Toothpaste flowing through the tube opening is an example; a shaped Playdoh extrusion is a better example. Like forging, extrusion is frequently employed to break up undesirable dendritic structures of large castings. In drawing, material is reduced in diameter by *pulling* it through a die using grips. It is a simple matter to estimate the stress required for these processes if friction between the die and work can be neglected. Suppose a billet of length L_0 and area A_0 is extruded through a die by applying uniform pressure p. The external work, W, done by the ram is the product of the force, pA_0, and the length, L_0, over which it acts. Therefore, $W = pA_0L_0$. This work is equal to the plastic deformation energy expended in the billet,

$$A_0L_0 \int_{L_0}^{L} \sigma_0 \, d\varepsilon = A_0L_0 \int_{L_0}^{L} \sigma_0 \frac{dl}{l}.$$

Direct integration yields $\sigma_0 A_0 L_0 \ln(L/L_0)$, where the final length is L. Equating, $pA_0L_0 = \sigma_0 A_0 L_0 \ln(L/L_0)$, or

$$p = \sigma_0 \ln(L/L_0) = \sigma_0 \ln(A_0/A). \tag{8-7}$$

This formula makes use of the constancy of volume ($A_0L_0 = AL$), where A is the final billet area. In extrusion, compression is involved (p negative), whereas in drawing, tension is applied (p positive). The quantity A_0/A is known as the extrusion ratio R and has values typically ranging from 10 (for Ni superalloys) to more than 100 (for Al). Required deformation pressures are seen to increase with both the material yield strength and the extrusion ratio.

EXAMPLE 8.4

a. What is the percentage reduction of area (%RA) if $R = 10$? If $R = 100$?
b. What is the maximum percentage reduction attainable during extrusion for a non-work-hardening (perfectly plastic) material?

ANSWER a. The %RA is defined by $100(A_0 - A)/A_0 = 100\ (1 - 1/R)$. For $R = 10$, the %$RA = 90\%$. If $R = 100$, the %$RA = 100\ (1 - 1/100) = 99\%$.
b. If the material does not work harden, the extrusion pressure cannot exceed σ_0. Therefore, $\sigma_0 = \sigma_0 \ln (A_0/A)$, or $\ln R = 1$. Thus, $R = e$ or 2.718, and the %RA is $100\ (1 - 1/e) = 63.2\%$.

In actuality, friction is present and materials may harden during forming. Therefore, Eq. 8-7 is too simplistic. An approximate formula that is used instead is

$$p = K_e \ln R, \tag{8-8}$$

where K_e is the extrusion constant, a quantity that incorporates many factors. Experimentally determined values of K_e for a number of metals, extruded at different temperatures, are given in Fig. 8-17. Virtually all materials, even normally brittle ceramics, can be extruded at sufficiently high temperatures because the compressive stresses of the process promote cohesion. In Fig. 8-18 the grain structure of extruded uranium dioxide fuel rods is depicted.

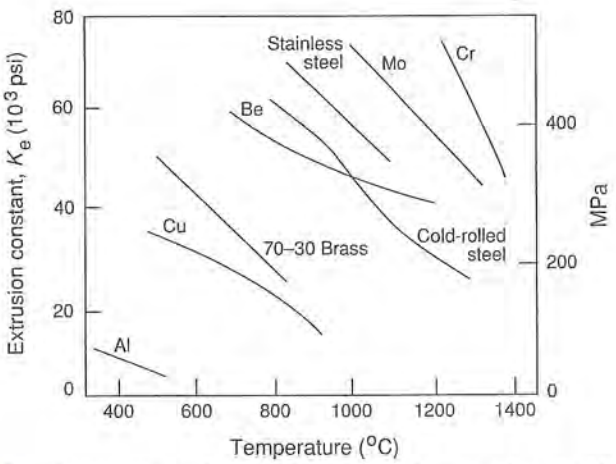

FIGURE 8-17 Extrusion constant as a function of temperature for assorted metals. After P. Lowenstein, ASTME Paper SP63-89.

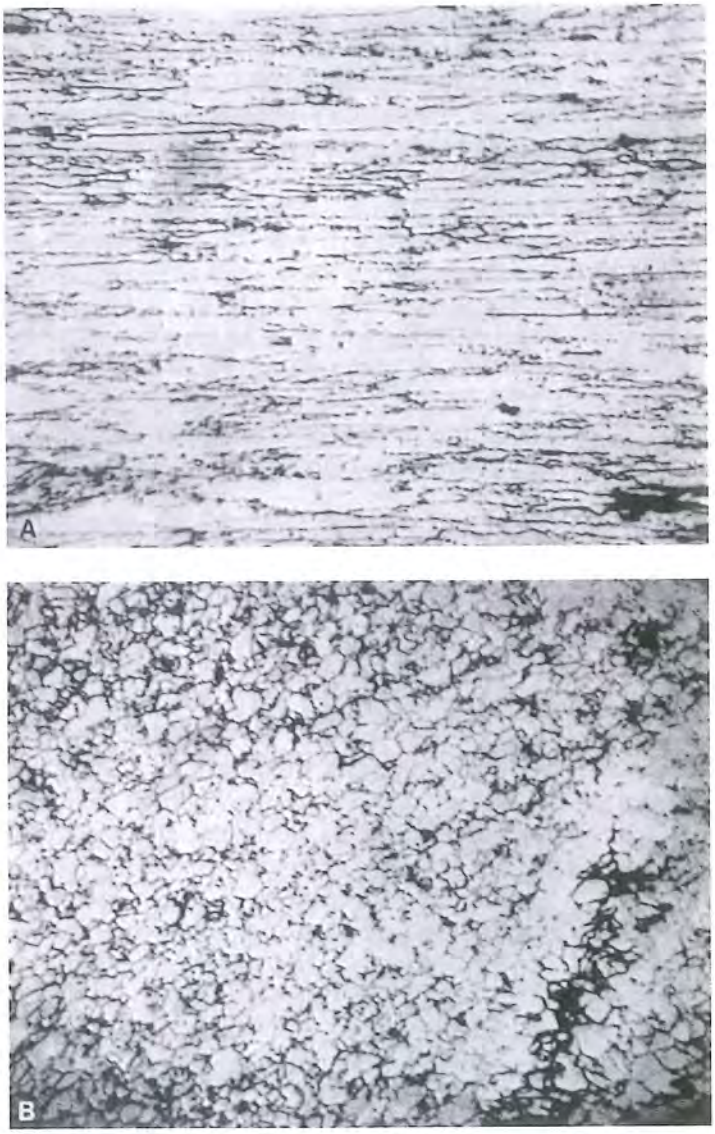

FIGURE 8-18 Microstructures of extruded UO_2: (A) Parallel to the extrusion direction. (B) Perpendicular to the extrusion direction. From Nuclear Metals, Inc.

Pressures of 1.03 to 1.38 GPa (150,000–200,000 psi) combined with temperatures above 1700°C are required before UO_2 flows plastically during extrusion.

A variant of extrusion, **coextrusion,** plays an important role in the technology of superconductors. Practical devices, for example, coils for superconducting magnets, require wire but unfortunately, virtually all of the commercially im-

portant superconductor materials are brittle and cannot be drawn without cracking. To overcome this problem, the hard, brittle materials are first incorporated into a softer, more ductile matrix. In the case of NbTi, holes are first drilled along the axis of an aluminum cylinder and cast rods of NbTi inserted. The composite is then extruded and the NbTi diameter shrinks (Fig. 8-19A). After the first extrusion the bundles are packed together in a billet for a second extrusion (Fig. 8-19B), and so on. The process is continued until a superconducting cable of required length and filament diameter is made. Similar methods have been adopted to fabricate fine-diameter, superalloy welding rods used in the repair of jet engine turbine blades. In this case, the matrix must be dissolved away to free the rods.

Among the defects encountered in extruded metals are surface cracking and internal cracking. The former are due to oxides and the latter to low-melting impurities (e.g., sulfur) which embrittle grain boundaries, a phenomenon known as **hot shortness**. A remedy for the latter in steel is to tie up S in the harmless form of MnS through small manganese additions. In addition, tailpipes (**extrusion defect**) invariably develop in the tail section or last portion to be extruded because the metal at the billet center is hotter and flows more rapidly than the metal at the outer edges. These pipes (tapered tubing) must be cut away and can account for as much as a 30% product loss. Reduction of friction, removal of surface scale, and elimination of temperature gradients help minimize the effects of this important defect.

Unlike extrusion, wire drawing tends to be a finishing operation that is generally, but not always, carried out at low temperatures. Wire and wire products are used in electrical applications, cables of all types, fencing, strings for muscial instruments, and other items. Because tensile rather than compressive stresses are involved in drawing, the metals must be intrinsically ductile and furthermore must work harden. If metals do not become stronger with deformation, they might fracture at the die exit because of their reduced cross section. Lead, for example, cannot be drawn into wire because it does not work harden at room temperature. Actually, Pb does harden, but immediately softens due to recrystallization processes (see Section 9.4), so there is no net strengthening.

8.3.6. Sheet Metal Forming

Sheet metal forming and working are among the most widely employed processes in manufacturing. Unlike the mechanical forming processes considered above where the ratio of the volume to surface area is large, the reverse is true in sheet forming. Automotive bodies, aircraft frames, major home appliance housings, and building fixtures are some of the arenas where large-area sheet products are used. But there are countless applications for smaller sheet metal parts, for example, washers, beer cans, kitchenware, and utensils.

Punches and **dies** are the basic shaping and cutting tools used in sheet forming. These tools are mounted in presses that provide the necessary forces

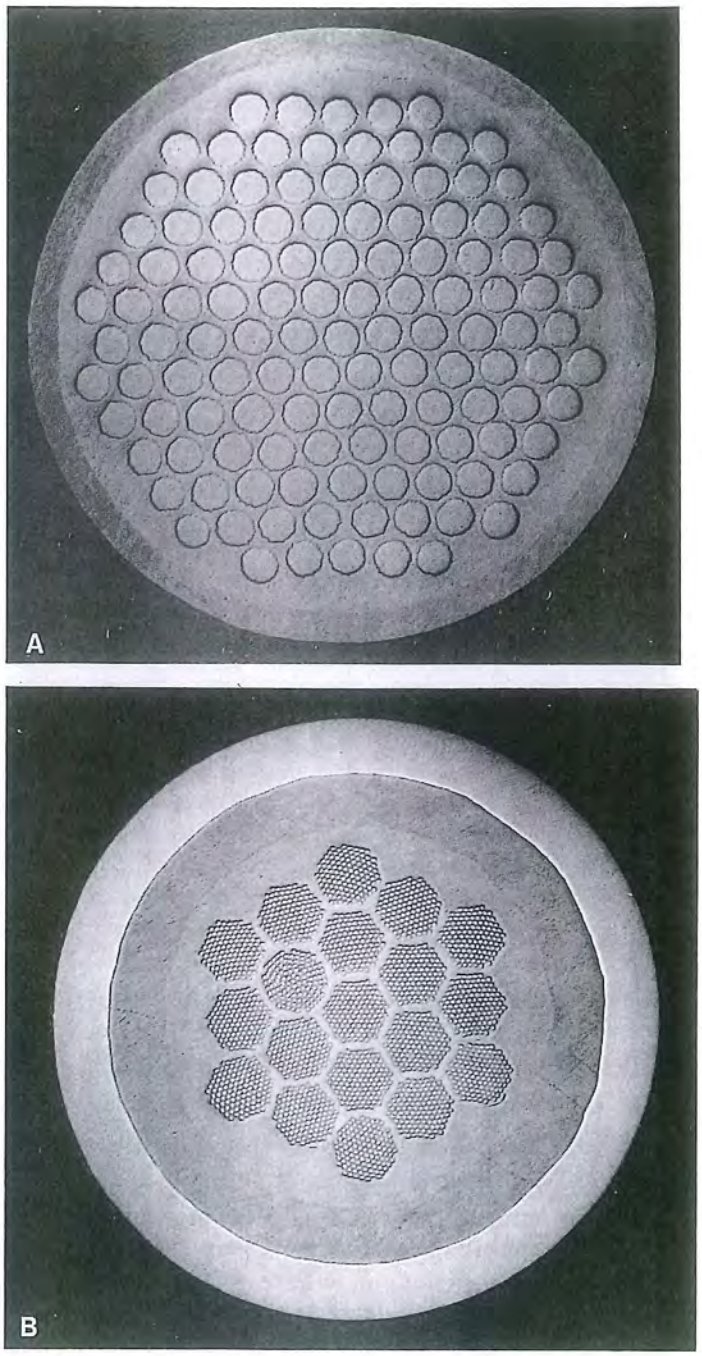

FIGURE 8-19 (A) Cross section of 121 NbTi rods in an extruded Al matrix. The initial diameter was 0.076 m and the extrusion ratio was 10 at a ram speed of 0.0085 m/s. (B) Cross section of a double-extruded superconductor structure containing 19 × 121 NbTi filaments. From AIRCO Superconductor.

to accommodate workpieces that must be sheared, simply bent, curved, deeply recessed, or impressed with a pattern in relief (coining). A couple of examples will illustrate sheet forming extremes. First consider the production of washers, perhaps the most widely produced sheet metal product. The tooling required, shown in Fig. 8-20, consists of successive (male) blanking and piercing punches and the mating (female) die. Provision must be made for feeding the sheet metal and clamping it. The basic forming operation involves shearing across a cylindrical surface. For example, in blanking a washer of thickness d with outer diameter r, a shearing force F_s (stress × shear surface area) between $\sigma_0 2\pi rd$ and $\sigma_{UTS} 2\pi rd$ is required. In practice it is typically found that

$$F_s = 0.7\sigma_{UTS} 2\pi rd. \tag{8-9}$$

At the other extreme of sheet metal forming are deep drawing or cupping operations (Fig. 8-21). Here, a circular blank sheet is held down while a punch extends the metal into the die cavity. The relatively small clearance between punch and die guides the metal that forms the cup walls. Stretching (biaxial tension) and drawing (tension–compression) modes of deformation are operative in different portions of the sheet. Deep forming makes stringent demands on metal properties. Large values of the strain hardening coefficient n are necessary to forestall necking and tearing, as noted in Section 7.3.3. It is also

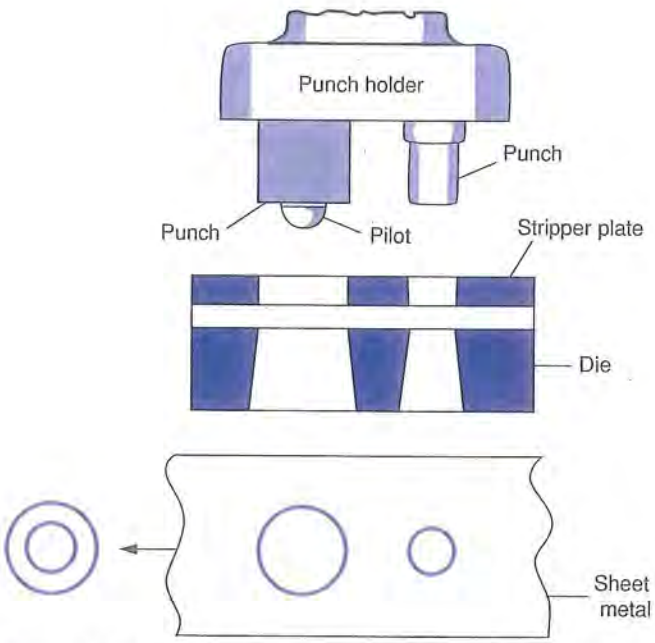

FIGURE 8-20 Schematic of the sheet metal process used to produce washers in a progressive die. From *Metals Handbook*, 8th ed., Vol. 4, American Society of Metals, Metals Park, OH (1969).

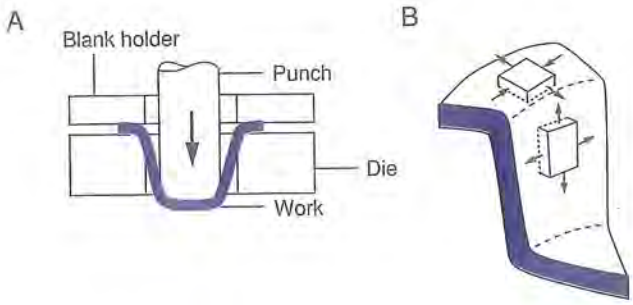

FIGURE 8-21 (A) Deep drawing of a cup. (B) Stress distribution in cup.

desirable that the metal be isotropic. Sheet metals, however, often exhibit a **preferred orientation** or **texture** that is a function of prior rolling and annealing processing. This means that a majority of indivdiual grains assume a more or less common crystallographic orientation relative to the sheet surface. Far from creating anything like a large, thin single crystal, preferred orientation produces a type of grain. The net effect is to superimpose the anisotropy of crystallographic slip on the deformation geometry. An undesirable waviness known as **earing**, which sometimes develops in the rim of formed cups, is a manifestation of this preferred texture.

8.3.7. Residual Stress

It appears paradoxical that solid bodies can be internally or residually stressed even when there are no externally applied forces. Yet this phenomenon of **residual stress** is a rather common occurrence in both solidification processing and mechanical forming operations. In fact, virtually every time materials are processed or heat treated at temperatures different from the use temperature, residual stresses are either produced or relieved. They occur in heat-treated glass, in films deposited electrolytically from solution or from the vapor phase, during welding, and in machining and assembly operations. In general, residual stresses arise from nonuniform changes in size or shape. Often it is not easy to visualize the source of the nonuniformity, much less understand or prevent its occurrence. Like a "jack in the box," residual stresses are sometimes released with disastrous consequences, as in the case of the Liberty Bell. Although they are generally harmful, sometimes residual stresses can be beneficial. By intentional introduction of residual compressive stresses through peening of the surface, materials are better able to withstand harmful applied tensile stresses that cause fracture.

To see how residual stresses are introduced into a casting consider the cooling of the initially stress-free ingot shown in Fig. 8-22A. As the outside of the ingot cools it contracts. The center is still hot, and being extended, it

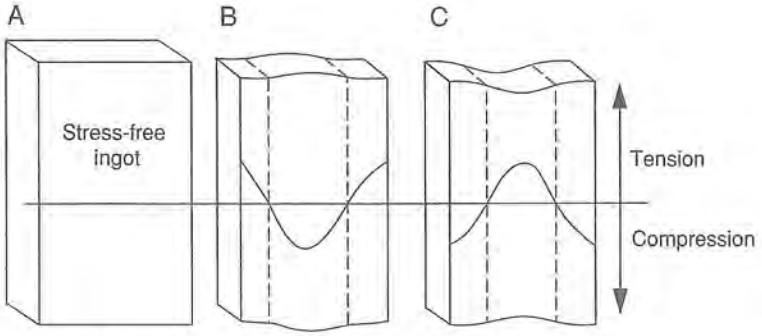

FIGURE 8-22. Illustration of how residual stresses develop in a casting.

opposes the surface contraction. Therefore the surface is stretched in tension while the core is compressed and plastically flows (Fig. 8-22B). With further cooling the core continues to contract thermally, but the surface now restrains it from shrinking. A reversal of stress ensues with the core stretched in tension while the surface winds up in compression (Fig. 8-22C). Such effects are accentuated at interfaces between solidifying sections of different sizes.

Residual stresses also occur in the absence of thermal processing. As an example consider the cold rolling of metals. During a light rolling pass of a plate, the surface fibers are stretched more than the inner metal, an effect shown in exaggerated fashion in Fig. 8-23A. Compatibility of the workpiece demands a straight cross section, however. Therefore, a compromise is struck

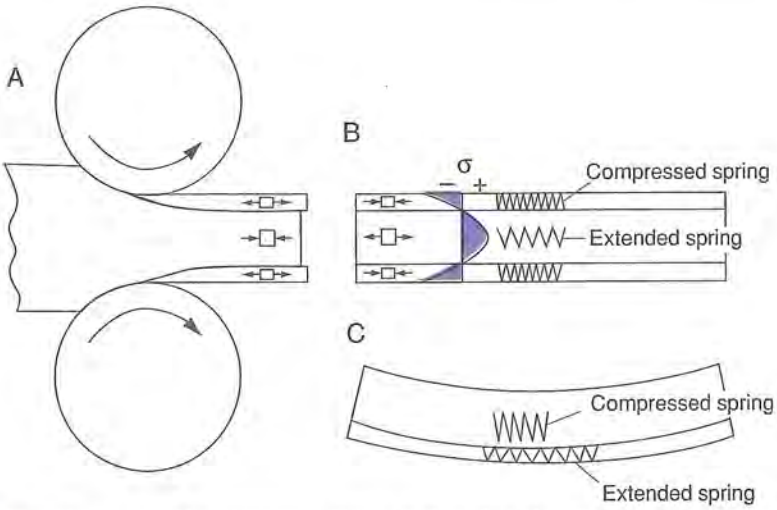

FIGURE 8-23 Development of residual compressive stresses in the surface of a lightly cold-rolled metal plate. If a thin layer is removed by machining, the plate will bow as shown.

and the surface fibers do not stretch as much as they would like to and wind up in compression. Meanwhile the interior is pulled in tension (Fig. 8-23B). In this as well as all cases of residual stress, the body is in mechanical equilibrium, and the tensile and compressive forces must balance. Now consider what happens when a strip of the rolled plate is clamped in a vice and a thin layer of metal is machined from one surface. After the plate is released, the machined surface bows distinctly concave upward (Fig. 8-23C), ruining any required tolerances. Bowing can be understood by imagining that both surfaces consist of compressed springs counterbalanced by a single stretched interior spring. Removal of one compressed spring upsets the equilibrium, causing the remaining outer spring to extend and the central spring to contract.

8.4. POWDER METALLURGY

8.4.1. Introduction

Some materials melt at too high a temperature to be easily cast, or are too hard and brittle to be plastically deformed into shape. In such cases salvation frequently comes from the powder processing route. This entails first producing powder of the material in question and then compacting it into the desired shape by pressing it in dies. Finally the compact is sintered at elevated temperatures to produce a densified, mechanically strong, finished part. Advantages of powder processing include the following:

1. Applicability to all classes of materials
2. Relatively low processing temperatures (significantly below T_M)
3. Attainment of highly homogeneous and uniform microstructures
4. Ability to create composites, mixed phases, and nonequilibrium metastable and microcrystalline structures
5. Production of precision parts with close tolerances
6. High-volume production rates, because the process is amenable to automaton
7. Absence of finishing operations like machining and grinding
8. Efficient use of material resources (no scrap)

With such an outstanding list of favorable attributes one suspects that the generally high costs of capital equipment (presses, furnaces), materials, and tooling will be disadvantages in those instances where competitive processing methods exist. Nevertheless, many metal parts are produced by the so-called **powder metallurgy** (P/M) route. Ceramic components are also fabricated this way but there does not seem to be an equivalent term for their processing.

Virtually every major industry and technology has applications requiring the use of metal and ceramic parts made by P/M. The collection of components displayed in Fig. 8-24 attests to the broad capabilities of this processing tech-

FIGURE 8-24 Assorted steel, stainless-steel, and brass powder metallurgy parts. Courtesy of Metal Powder Industries Federation.

nique. A very abbreviated list of applications includes automotive (gears, bushings, brake linings, spark plugs), aerospace (engine components), chemical (catalysts, filters), manufacturing (cutting tools, dies), and electrical (metal and ceramic magnets, contacts, relays, sputtering targets for thin film deposition). Additional technological applications use powders in the unsintered form, for example, abrasives, paint pigments, solder pastes, inks, and explosives. Making powder is a good place to start.

8.4.2. Powder Production and Properties

A number of processes including atomization, electrodeposition, and chemical reduction of oxides have been employed to make metal powders. Atomization is the most popular for metals. If molten gold is poured into water, the metal stream is broken up into shot ranging up to a few millimeters in size. This phenomenon is optimized in atomization processes (Fig. 8-25) to produce fine powder instead of shot. High-pressure jets of either gas (air, H_2, Ar) or

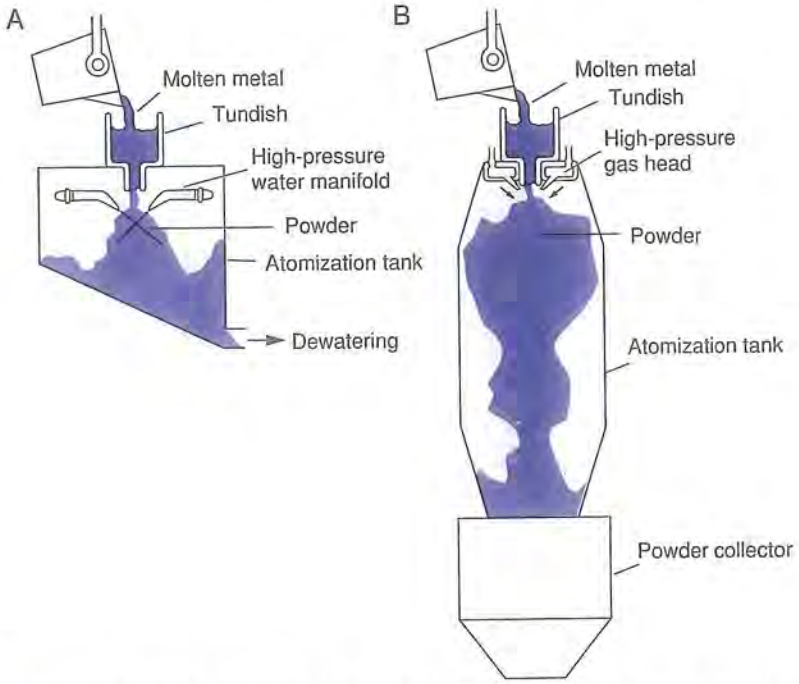

FIGURE 8-25 Schematic of powder production by (A) water and (B) gas atomization. From *Metals Handbook*, 9th ed., Vol. 7, American Society of Metals, Metals Park, OH (1984).

water are focused at molten metal streams issuing from a heated crucible. As a result the metal disintegrates in rapid order into liquid sheets, ligaments, and droplets which solidify into powder particles that are collected. The higher the kinetic energy of the H_2O or gas directed at the metal, the finer the resulting powder. Micrographs of the powder morphology of gas- and water-atomized stainless steel are reproduced in Figs. 8-26A and B.

Electrolytic powder is produced by electroplating metals onto cathodes they poorly adhere to at high current densities. Because the deposits do not stick they are easily brushed to the bottom of the plating tank and collected. In this way dendritic shaped copper, iron, titanium, and beryllium powders are produced. Crushed metal oxide particles, for example, WO_2 and MoO_2, are other sources of metal powder. When reduced by hydrogen at ~1000 to 1500°C, metal powder is liberated. In this way tungsten and molybdenum powders are produced at well over 1000°C below their melting points. Ceramic powder is usually obtained by pulverizing naturally occurring minerals of high purity. Such powder may not be suitable for some applications and may require further purification.

Powder size and shape are important variables because they influence packing, flow, and compressibility during compaction, as well as uniformity and

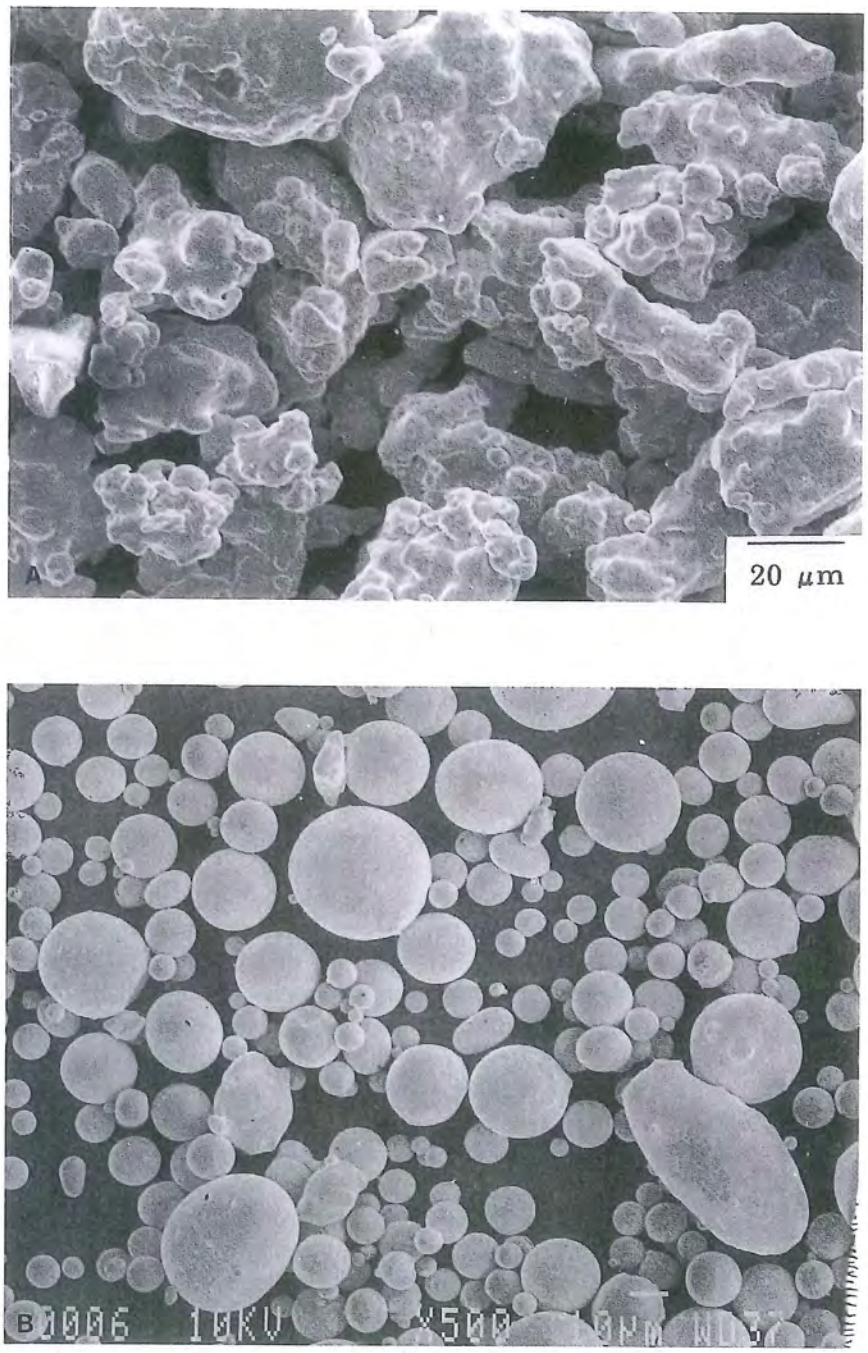

FIGURE 8-26 Morphology of stainless steel metal powder made by (A) water atomization and (B) gas atomization. Courtesy of Professor R. M. German, Pennsylvania State University.

homogeneity during sintering. Particle size is a key characteristic of powder. For a given process, particle sizes are usually statistically distributed and are measured by sieving through mesh screens with openings of different size; they typically range from ~30 to 200 μm in size. Ceramic powder can be comminuted or fractured to submicrometer (1 μm = 10^3 nm) dimensions by ball milling. In this process, steel balls continually tumble and wear the original particles by attrition upon compressive impact.

Powder shapes have descriptor names such as spherical, rounded, angular, spongy or porous, flake, polygonal, and dendritic. Both size and shape strongly influence powder friction. This property in turn determines powder flow characteristics during packaging, blending, and mixing, as well as during die filling. Not unexpectedly, smooth powder surfaces exhibit less friction. Uniform, fine, spherical powder, in particular, is in great demand for such applications as compounding solder (Sn–Pb) creams for microelectronic use and producing jet engine parts (superalloys, Ti alloys). Reasonably smooth and uniform spherical powder is produced by centrifugal atomization. In this process liquid metal streams impinge upon rapidly rotating disks, and droplets are spun off and collected as powder. The high cooling rates reduce the interdendritic arm spacing and overall compositional variations in the powder.

8.4.3. Sintering

Powders are pressed in shaped, multipiece die sets at high pressures, for example, 0.4 to 0.8 GPa (60–120 ksi), to compact them as much as possible. The resulting green compacts are like pharmaceutical pills that crumble under stress and mishandling. To eliminate porosity and strengthen them, the compacts are sintered at elevated temperatures in controlled atmospheres. The kinetics of sintering were considered at length in Section 6.6.3 and serve to design processing treatments. Sintering temperatures are obviously lower than melting temperatures, and may be hundreds to well over 1000°C lower.

It rarely happens that sintering is accomplished without enhancing its rate in some way. In one of the most common processes, **liquid phase sintering**, a liquid provides for enhanced material transport and more rapid sintering. Either low-melting powder blended into the compact or external infiltrants that penetrate the compact surface pores by capillary wicking action during sintering are the source of the liquid. For example, in the production of tungsten carbide, a very widely used cutting tool material for machining, liquid cobalt, produced at the sintering temperature, binds the WC particles together (Fig. 8-27). During sintering, the particles are first wet and may rearrange in the melt. Dissolution processes, followed by reprecipitation elsewhere, often result in better packing and densification. Similarly, infiltration of steel powder with copper base alloys is employed in the production of gears.

Beneficial changes occur in assorted properties as a function of sintering temperature as indicated schematically in Fig. 8-28. For densities ~99% of

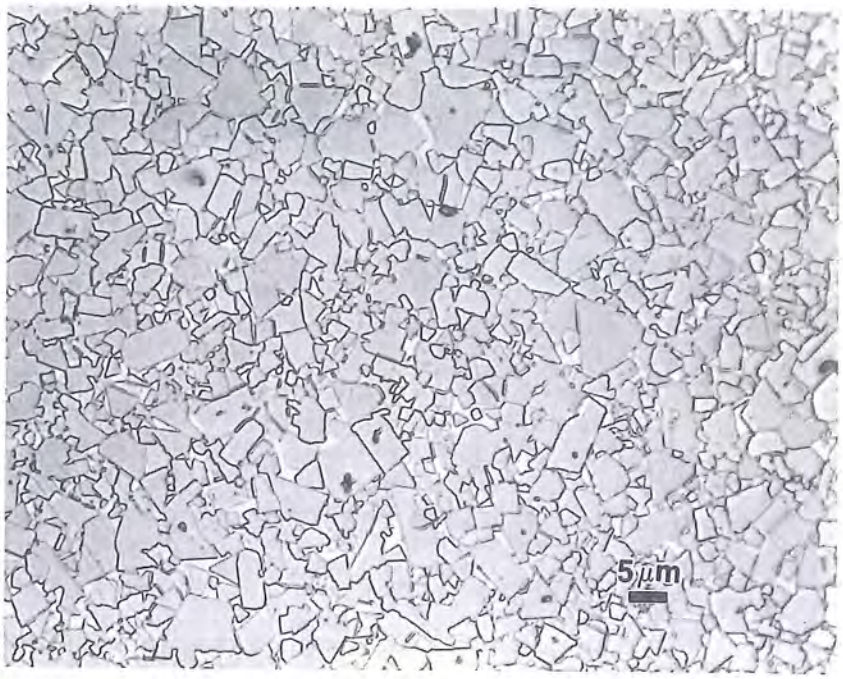

FIGURE 8-27 Microstructure of WC sintered with cobalt which surrounds the carbide particles. Courtesy of G. F. Vander Voort, Carpenter Technologies Corporation.

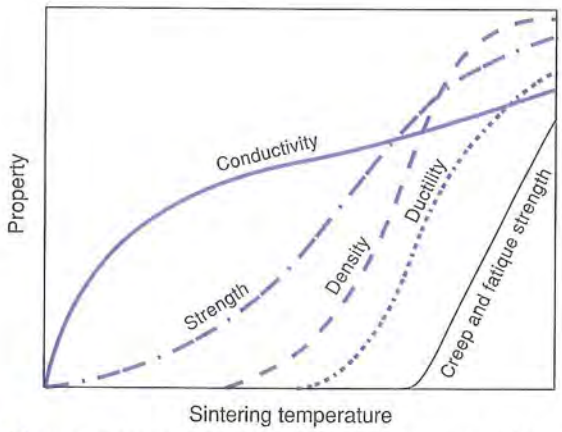

FIGURE 8-28 Schematic variation of P/M compact properties as a function of sintering temperature. After R. M. German, *Powder Metallurgy Science*, Metal Powder Industries Federation, Princeton, NJ (1984).

bulk values, mechanical properties resulting from P/M processing often exceed those in wrought (cast and mechanically worked) materials.

8.5. POLYMER PROCESSING

Polymer melts are molded or blown in the viscosity range 10^3 to 10^5 Pa-s (10^4–10^6 P), which compares with only 10^{-4} Pa-s for molten metals. Thus, pressure is generally required for polymers to fill molds, whereas metals need only be poured to be cast. A variety of extrusion and molding operations are used to process polymers. In particular, the following processing methods now enable thermoplastic products of complex shape to be produced on a very large scale: extrusion, injection molding, blow molding, compression molding, calendering, and thermoforming.

In addition there are processes employed to make reinforced polymers, and they are treated in the next chapter. Extrusion processing underlies both injection and blow molding of polymers and, therefore, is discussed first.

8.5.1. Extrusion

Extrusion of polymers resembles extrusion of metals. Lengths of tubular, sheet, and rod products possessing both simple and complex cross sections emerge from dies after pushing polymer feedstock through them. The details differ because metals do not melt during extrusion. Batch processing (one billet of metal at a time), unlike continuous extrusion of polymers, is another difference. In this sense polymer extrusion also resembles continuous casting of metals. (In continuous casting, metal is continually poured from a large, replenishable melt reservoir into an open, chilled mold, where it solidifies. Later, downstream, the solidified moving billet is cut into convenient lengths.)

Thermoplastic materials (resins) in pellet form are fed in at one end of the extruder as shown in Fig. 8-29A. Polymer feeds often contain additives, the most important of which are *lubricants,* which assist processing; *fillers and plasticizers* to modify mechanical properties; *flame retardants;* and *stabilizers* (antioxidants) to enhance degradation resistance. The polymer feed is conveyed down the extruder barrel by one (or more) long, rotating (and reciprocating) screw(s) where it is **compressed**. Through contact with the heated walls and the mechanical action of the screw, polymer **melting** occurs. In some systems polymer is pushed along by a piston. Next, melt **pumping** or **metering** under pressure through a tapered region and into a shaped die enables the product to exit. The extrudate must have a sufficiently high viscosity when it leaves the die to prevent it from deforming mechanically or even collapsing in an uncontrolled way. Therefore, water or air sprays are required to cool the product. The cooling rate must be controlled, however, because it can influence

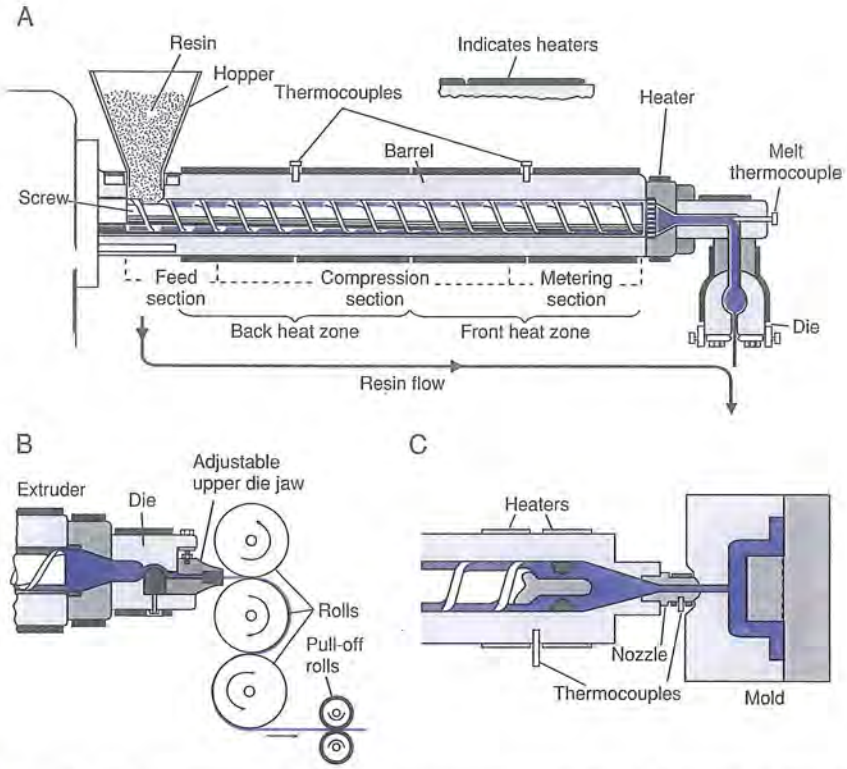

FIGURE 8-29 Polymer forming processes based on the use of a screw-type extruder: (A) Extrusion. (B) Extrusion of sheet. (C) Injection molding. Modified from R. J. Baird, *Industrial Plastics*, Goodheart–Willcox Co., South Holland, IL (1976).

the extent of crystallinity and affect mechanical properties. By use of an appropriate die and array of rollers, plastic sheet can be produced (Fig. 8-29B).

8.5.2. Injection Molding

To extend the parallels with metal processing, injection molding of shaped polymer parts closely resembles die casting. The process shown in Fig. 8-29C starts in the same way as an extrusion. Instead of being forced through a die into the unpressurized ambient, the melt is injected under pressure into a split die cavity. Injection molding is usually carried out at $\sim 1.5T_G$, where T_G is the glass transition temperature of the polymer. Pressures in the mold are typically maintained at somewhat higher levels than those employed in die casting, and range from 35 to 140 MPa (5–20 ksi). After the part cools below T_G (under pressure) the die opens and the part is ejected. The chamber is essentially a

chemical reactor that allows the mixed and heated ingredients to blend, polymerize, and crosslink during simultaneous shaping. Fibers and particles can also be introduced, enabling the production of composites.

As the sizes of parts increase so do the magnitudes of the injection pressure, and the clamping force needed to keep the dies together. To address both problems *reaction injection molding* processes have been developed. They allow polymerization reactions to occur in the dies (mold), not the chamber. Injection viscosities are then reduced by more than two orders of magnitude with a corresponding drop in back pressure. Solid and foam urethanes are the chief reaction injection molded materials.

Injection molding is a high-production-rate process with typical cycle times ranging from seconds to several minutes depending on the type of polymer and the part size. Poor heat transfer properties of polymers basically limit the speed of the process. High injection pressures mean that good tolerances and surface finishes can be maintained. Among the parts produced by injection molding are containers, housings, plumbing fixtures, gears, telephone receivers, and toys. Parts comparable in size to those produced in die casting can be injection molded. That is why polymers have increasingly replaced metals in the above and other applications.

EXAMPLE 8-5

Suppose you wish to injection mold a set of plastic toy soldiers and must determine how many can be produced during one cycle. A 100-ton (8.9×10^5-N) press is available and the die pressure required to reproduce fine die features is 100 MPa (~15 ksi). Each soldier has an average projected area of 10 cm^2 (10^{-3} m^2) and is 0.75 cm thick. How many soldiers can be molded at one time?

ANSWER If the parting plane divides the halves of the mold at the center of each soldier, the die clamping force required is the product of the pressure and die face area occupied by polymer. This force must be less than or equal to the press capacity. If n is the number of soldiers, then $(100 \times 10^6 \text{ Pa}) \times n \times (10^{-3} \text{ m}^2) = 8.9 \times 10^5$ N. Solving, $n = 8.9$. For safety, only eight soldiers should be molded during one cycle. The thickness of the part is basically immaterial in this problem.

8.5.3. Blow Molding

The combination of extrusion and air pressure makes blow molding and the production of plastic bags and bottles possible. As depicted in Fig. 8-30A, a thin-walled tube of polymer is extruded vertically and expanded by blowing through the die until the desired film thickness is produced. Plastic wrap and

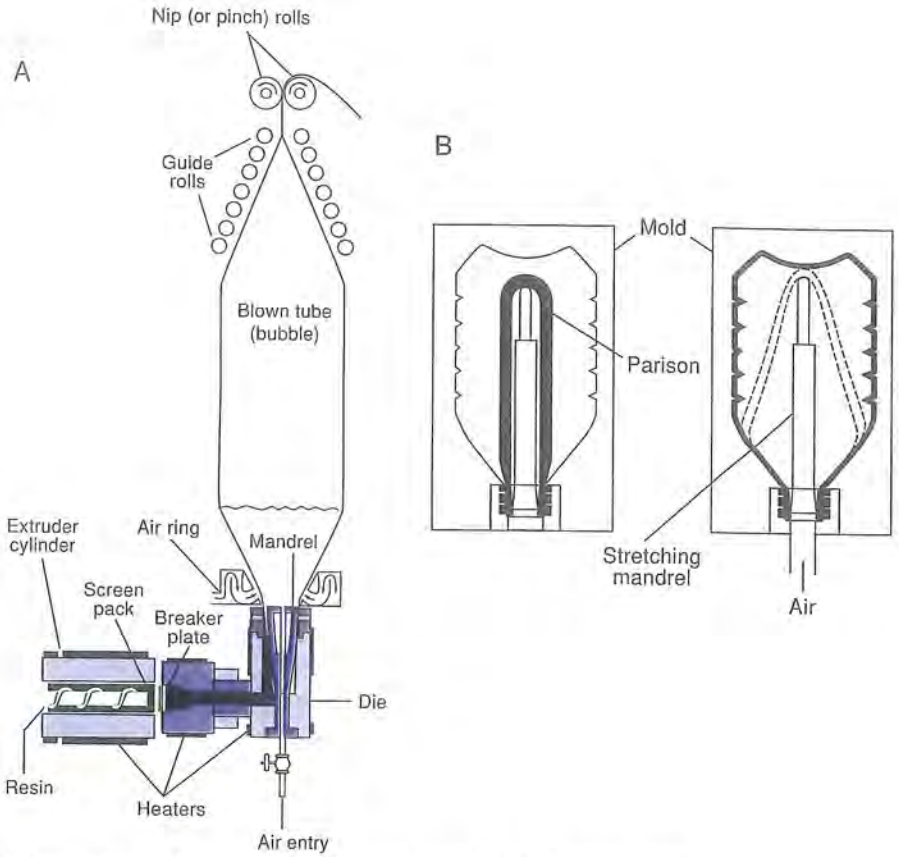

FIGURE 8-30 Polymer blow molding processes: (A) Forming blown film. (B) Forming a bottle.

bags are made continuously in variations of this process. In making beverage bottles a prior extruded tube, known as a *parison*, is pinched at one end and clamped (Fig. 8-30B) within a mold that is much larger than the tube diameter. It is then blown outward until the polymer extends to the mold wall, in a way that a balloon would if blown up within a bottle. A hot air blast at a pressure of 350 to 700 kPa (50–100 psi) is used for this purpose.

The plastic beverage bottle represents an interesting problem in materials design. For marketing purposes the bottle must be highly transparent. In addition it must be sufficiently strong (creep resistant) that it does not lose its shape on the shelf. Lastly, and importantly, it must be impermeable to CO_2 so that gas loss does not make the contents go flat. To meet these needs the polymer polyethylene terephthalate (PET) is selected and blow molded. But, if cooled rapidly, PET is amorphous. It is quite clear, but its relatively loose molecular structure makes it permeable to CO_2 and susceptible to creep. At the other

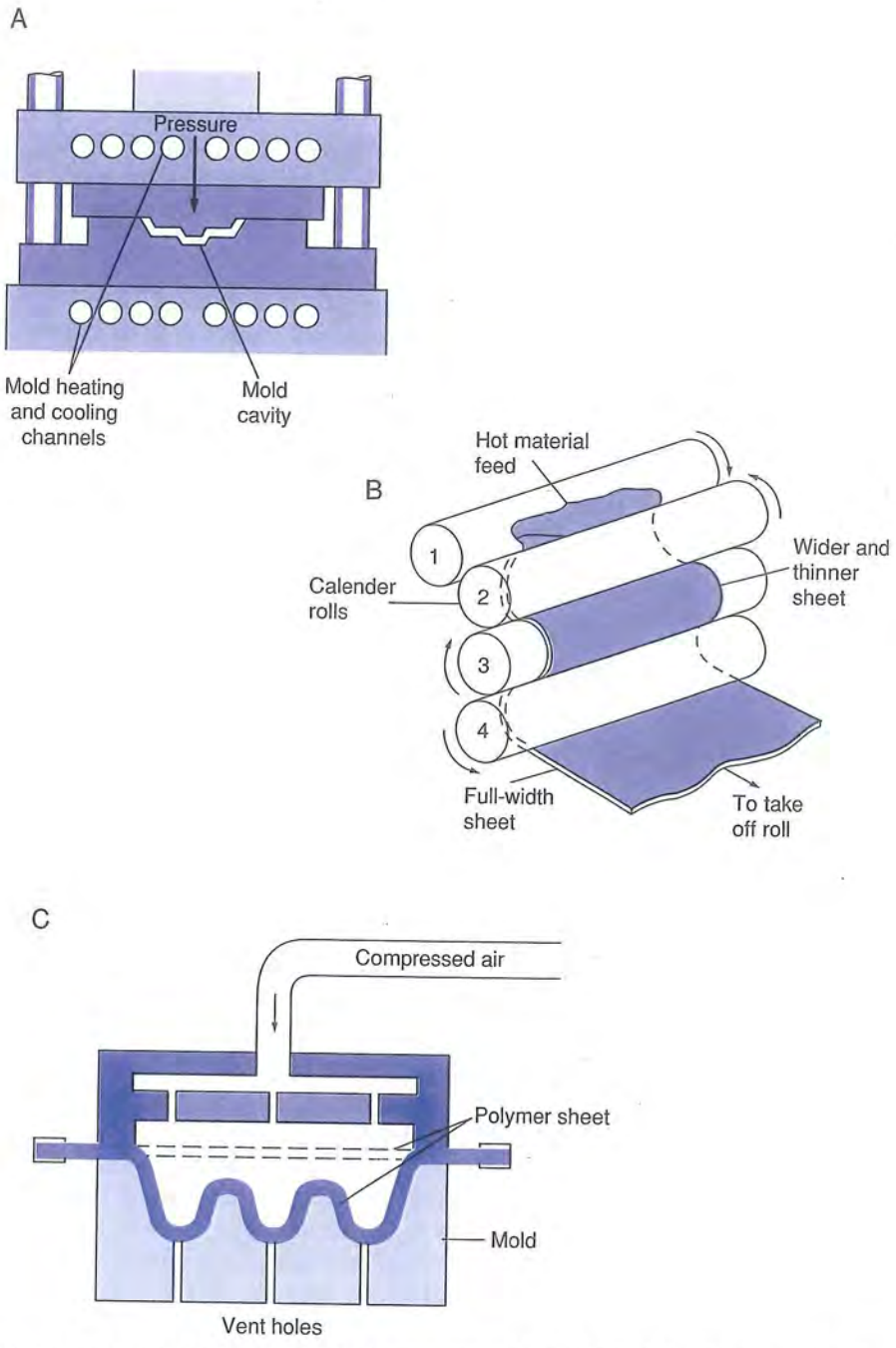

FIGURE 8-31 Additional polymer processing methods: (A) Compression molding. (B) Calendering. (C) Thermoforming. Modified from R. J. Baird, *Industrial Plastics*, Goodheart–Willcox Co., South Holland, IL (1976).

extreme of slow cooling, the polymer crystallizes. It is now strong and gastight, but opaque. The answer is first to cool the parison rapidly below T_G (340 K), where it is amorphous, and then to stretch it by blow molding at 400 K, a temperature high enough for plastic flow but too low for appreciable crystallization. Stretching a polymer induces additional crystallization and strength, and if controlled, no loss in clarity occurs.

8.5.4. Compression Molding

Where the expense of an extruder and injection molding dies is not warranted, compression molding of parts is practiced. In this process (Fig. 8-31A) premeasured volumes of polymer powder or viscous resin–filler mixtures are introduced into a heated multipiece die and then compressed with an upper plug. Thermosetting polymers and elastomers are shaped by compression molding and products include electrical terminal strips, dishes, and washing machine agitators.

8.5.5. Calendering

Polymer sheets are often made by calendering (Fig. 8-31B). In this process a warm plastic mass is fed through a series of heated rolls and stripped from them in the form of sheet. Because thermoplastics have a high strain hardening coefficient they undergo large uniform deformations, making sheet production possible.

8.5.6. Thermoforming

Thermoforming, shown in Fig. 8-31C, parallels methods used to form sheet metals. Sheet polymer (e.g., formed by calendering) is preheated and then laid over a mold having the desired shape. The applied air pressure is normally sufficient to make the sheet flow plastically and conformally cover the mold interior. Parts made this way include advertising signs, panels for shower stalls, appliance housings, and refrigerator linings.

8.6. FORMING GLASS

8.6.1. Scope

As with all materials that have been worked for a long time, many methods have evolved and been developed to form glass over the years. The important ones discussed below include pressing, blowing, casting, and rolling and float molding. These processing techniques are schematically depicted in Fig. 8-32.

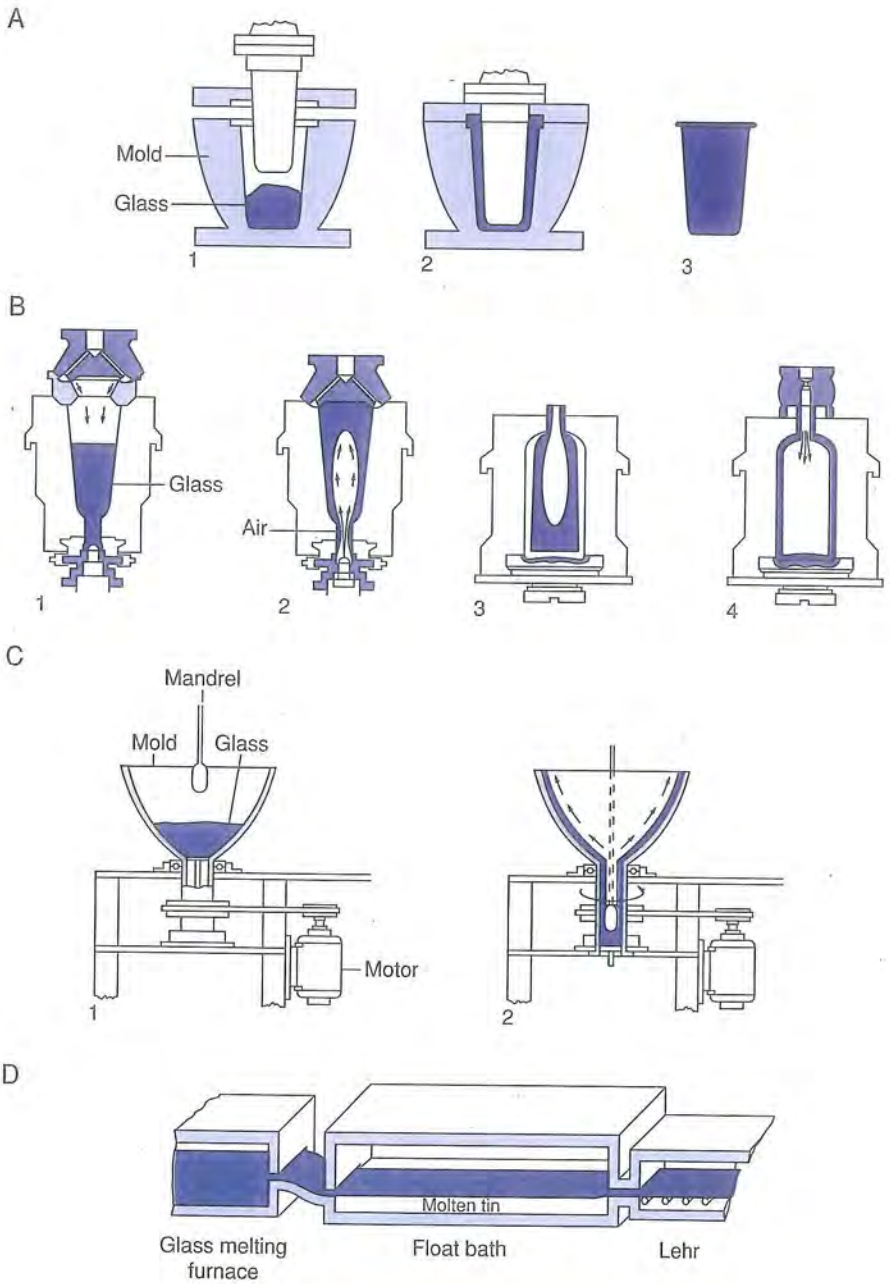

FIGURE 8-32 Processes to form and shape glass: (A) Pressing a glass container. (B) Blowing a bottle. (C) Centrifugal casting of a cathode-ray tube. (D) Plate glass manufacture by the Pilkington method. From J. R. Hutchins and R. V. Harrington, *Encyclopedia of Chemical Technology*, 2nd ed., Vol. 10, Wiley, New York (1966).

8.6.1.1. Pressing

An example of pressing involves the forming of glassware by compressing it in a mold with a plunger. The process (Fig. 8-32A) resembles closed die forging of metals and compression molding of polymers. Parts with diameters of 30 cm, depths of 10 cm, and weights of up to 15 kg are pressed using pressures of 0.69 MPa (100 psi).

8.6.1.2. Blowing

Hand blowing of glass is practiced today much as it was in antiquity. Glass is gathered on the end of an iron blowpipe and, with lung power or the use of compressed air, the glass blower shapes the "gathers." Artistic glassware is hand blown while the glass is continually rotated. The largest pieces reach weights of 15 kg, lengths of almost 2 m, and diameters of 1 m. Examples of machine-blown ware include glass containers and light bulb envelopes. Gobs of glass are delivered to the *blank* mold (1,2), where they are preformed by either blowing or pressing. After the blank is rotated, it is then blown in the *blow* mold (3,4) to finish the operation (Fig. 8-32B).

8.6.1.3. Casting

In casting, glass is poured into or on molds, tables, or rolls. One of the largest pieces ever cast is the Mount Palomar reflector, a cylinder measuring 5.08 m (200 in.) in diameter and 0.457 m thick. Other products routinely cast are radiation-shielding window blocks and television and cathode-ray tubes. The latter are centrifugally cast, and as the molten gobs are spun the glass flows up to create a uniform wall thickness (Fig. 8-32C). There is a 10^5-fold difference in viscosity between molten glasses and metals. The implication of this with respect to casting can be appreciated by comparing how honey and water pour.

8.6.1.4. Rolling and Float Molding

Both rolling and float molding are used to produce plate glass. In continuous processes, raw materials are fed in at one end of very large horizontal furnaces (with capacities of 1000 tons), where successive melting and refining of glass occur. At the other end the glass is fed into a pair of cooled rollers and the emerging ribbon of solid glass is then conveyed on rollers through an annealing lehr. Plate glass nearly 4 m wide and 1 cm thick can be rolled at rates greater than 6 m/min. The surfaces of rolled plate glass must be further ground and polished.

The revolutionary Pilkington float molding process (Fig. 8-32D) is now widely used to make plate glass. In this process soft glass is floated on the flat surface of a molten tin alloy that controls the lower glass surface temperature. The upper surface of the glass develops by gravity. As the temperature is reduced the glass stiffens and is conveyed to be annealed. This process produces a distortion-free plate glass comparable in flatness to that produced by rolling glass. A drawback of the process is incorporation of Sn into the glass.

All one has to do is look through plate glass windows of the last century to appreciate how far we have come in glass plate manufacture.

8.6.2. Viscosity

The single most important property of glass that influences these processes and subsequent heat treatments is viscosity (η). This thermomechanical property effectively combines a number of material attributes (flow resistance, fluidity, atomic diffusion) in a single constant. In inorganic glasses the temperature dependence of η is given by

$$\eta = \eta_0 \exp(E_\eta/RT), \tag{8-10}$$

where η_0 and E_η are characteristic constants that depend on composition, and RT has the usual meaning. Equation 4-5 expresses an analogous dependence applicable to polymers. The magnitude of the viscosity of glass is critical in all stages of its manufacturing and forming processes. Viscosity determines virtually all of the melting, forming, annealing, sealing, and high-temperature heat treatments of glass. Typical viscosity ranges for a number of operations are as follows:

Operation	Viscosity (Pa-s)
Glass melting and fining (bubble elimination)	5–50
Pressing	50–700
Gathering or gobbing for forming	50–1,300
Drawing	2,000–10,000
Blowing	1,000–3,000
Removal from molds	10^3–10^6
Annealing	10^{12}–10^{15}
Use	$10^{13.4}$–$10^{14.5}$

The temperatures at which these operations are carried out differ with glass composition and these are depicted in Fig. 8-33 for a number of commercial silica-based glasses. Each of the latter has a specific viscosity–temperature dependence and individual set of strain, annealing, softening, and working point temperatures. These are defined in the following ways:

Strain point. The temperature at which internal stresses are reduced significantly in a matter of hours. At this temperature the viscosity is taken as $10^{13.5}$ Pa-s.

Annealing point. The temperature at which the viscosity is about 10^{12} Pa-s and the internal stresses are reduced to acceptable commercial limits in a matter of minutes.

Softening point. At this temperature glass will rapidly deform under its own weight. For soda-lime glass this occurs at a viscosity of $10^{6.65}$ Pa-s.

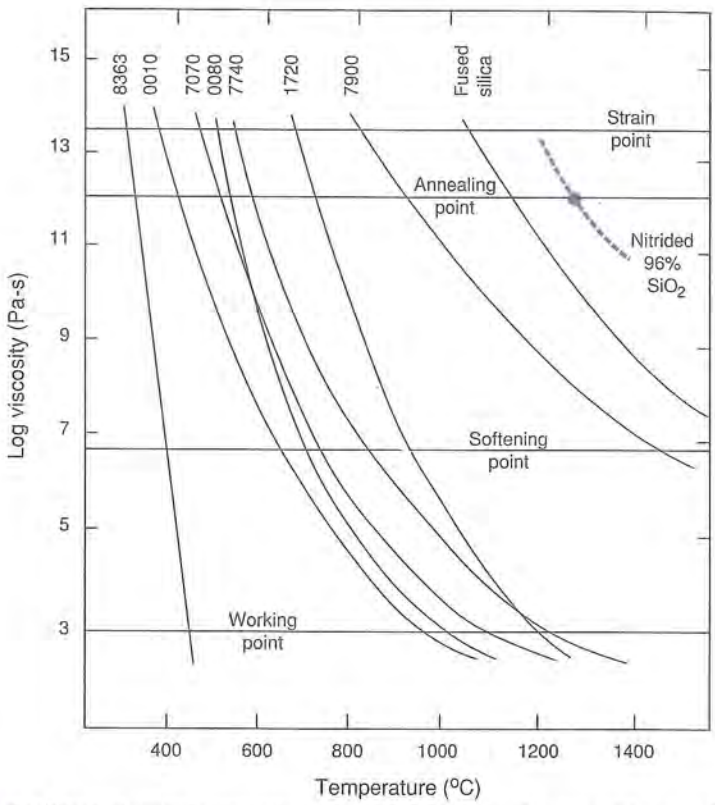

FIGURE 8-33 Coefficient of viscosity versus temperature for a number of commercial glasses. The four-digit codes refer to Corning glasses whose compositions are given in Table 4-5. From J. R. Hutchins and R. V. Harrington, *Encyclopedia of Chemical Technology*, 2nd ed., Vol. 10, Wiley, New York (1966).

Working point. At this temperature glass is soft enough for most of the common hot working processes. The working point corresponds to a viscosity of 10^3 Pa-s.

EXAMPLE 8-6

It is accurately determined that a glass has a strain point of 515°C and a softening point of 820°C. Estimate the lowest temperature at which this glass can be blown.

ANSWER In this problem we assume that Eq. 8-10 describes the viscosity of this glass as a function of temperature. Once η_0 and E_η are determined, the lowest glass blowing temperature, which corresponds to a viscosity of 3000

Pa-s, can be calculated. Using the two given pieces of information, $\eta = 10^{6.65}$ Pa-s at 820°C (1093 K) at the softening point and $\eta = 10^{13.5}$ Pa-s at 515°C (788 K) at the strain point, there are two simultaneous equations:

$$10^{6.65} = \eta_0 \exp[E_\eta/R(1093)]$$
$$10^{13.5} = \eta_0 \exp[E_\eta/R(788)].$$

Dividing the second equation by the first yields

$$10^{6.85} = \exp \frac{E_\eta}{8.314}\left(\frac{1}{788} - \frac{1}{1093}\right).$$

Solving, $E_\eta = 370$ kJ/mol. With knowledge of E_η, η_0 is calculated to be 9.27×10^{-12} Pa-s.

Finally, $3000 = 9.27 \times 10^{-12} \exp(370{,}000/8.314T)$. Solving for T, the minimum glass blowing temperature is 1332 K, or 1059°C.

8.7. PROCESSING OF CERAMICS

8.7.1. Forming the Green Body

With millennia of experience as background, many processes and variants of processes have been used to make vitreous (glass containing) ceramic products. They generally involve a number of common steps including preparing and mixing the raw ingredients (sands, clays) and binders (in a water base), forming or shaping the green body (e.g., on a potters wheel), drying it, firing the body to densify it, and finishing the product by grinding, cutting, polishing, and glazing. Shaping the green body is facilitated because the hydroplastic nature of the clay particles enables them to slide easily over one another. Upon firing, the glassy (vitreous) phase melts and coats the higher-melting clay particles, bonding them together. Most of the new ceramic (see Section 4.6.2) material processes are similar in spirit, but often there is no glassy phase. They start with powders that are generally purer. Additives to the composition may include binders (for green strength), lubricants (to reduce friction and release the body from molds), wetting and water retention agents, deflocculants (to control pH, electrostatic charge and particle dispersion), and sintering aids.

Green bodies of both traditional and new ceramics are formed by a number of methods that are enumerated below.

8.7.1.1. Slip Casting

First, a slip consisting of a suspension of clay or ceramic powder in water is prepared. This is cast into an absorbent mold as indicated in Fig. 8-34A. After sufficient water loss, the partially wet solid body is removed and dried further prior to firing. Vases as well as large and complex parts like Si_3N_4 turbine rotors have been reproduced this way.

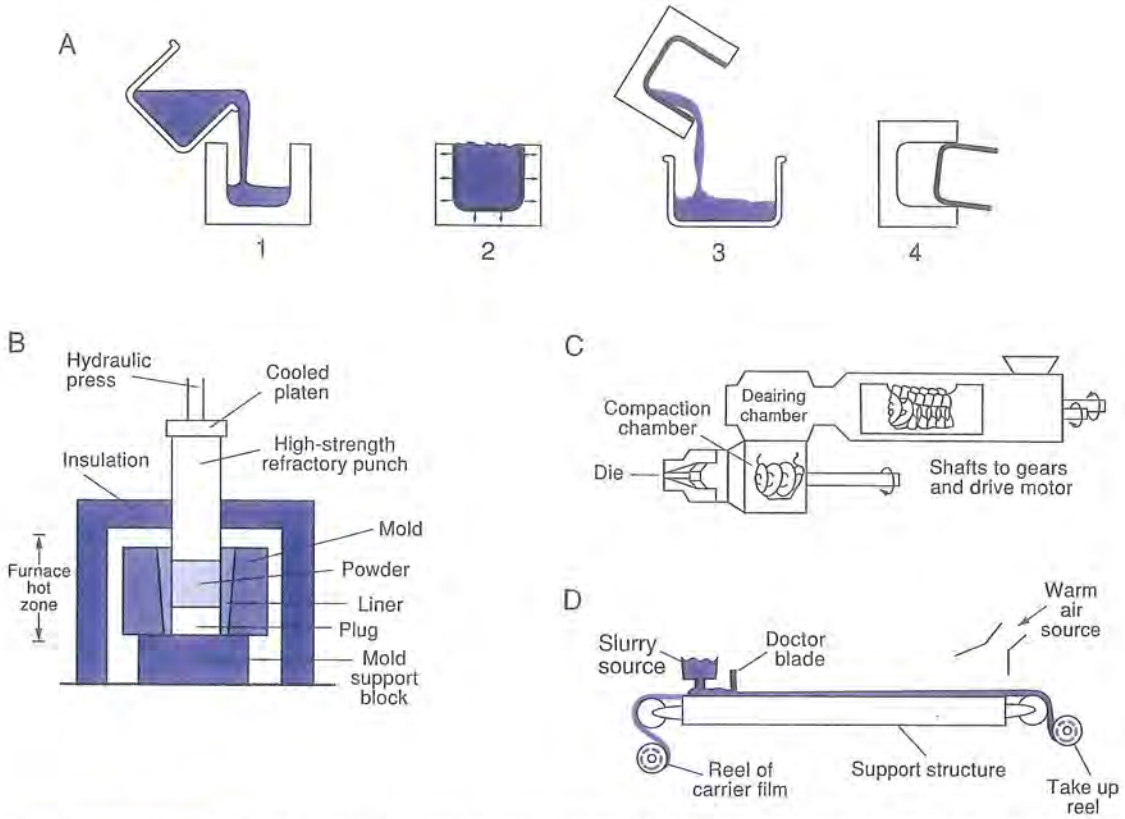

FIGURE 8-34 Several techniques used to process ceramics. (A) Slip or drain casting: (1) Pouring the clay/ceramic suspension. (2) Water absorption by plaster mold until a solid shell forms. (3) Pouring out the excess suspension. (4) Removal of body for firing. (B) Pressing. (C) Extrusion. (D) Tape forming. From S. Musikant, *What Every Engineer Should Know about Ceramics*, Marcel Dekker, New York (1991).

8.7.1.2. Pressing

The specially prepared dry powder is placed in a die and pressed under high uniaxial forces to make a green compact (Fig. 8-34B). The process is very much like pressing of metal powders in powder metallurgy dies (see Section 8-4). Only relatively small parts can be made in this way. An improvement over applying uniaxial compressive loads is to compact the powder **isostatically.** Here the part is enclosed in a flexible airtight rubber bag and immersed in a chamber filled with hydraulic fluid. Hydrostatic (uniform over all directions) pressure is applied during (cold) compaction, eliminating the complex pressure distribution throughout the die due to mold wall friction. Electrical insulators, bushings, magnetic components, and spark plug bodies are produced in this way for subsequent sintering.

Hot pressing combining compaction and sintering operations is also practiced to make a variety of highly dense ceramic components.

8.7.1.3. Extrusion

Extrusion of green bodies parallels the extrusion of polymers in that powder and screws (augers) are involved. Polymers, however, are extruded in the molten state whereas ceramic green body extrusions are created at room temperatures from pliable, powder–binder mixtures. This material is extruded through a die as shown schematically in Fig. 8-34C, and then sintered. Long tubes, rods, and honeycomb structures used to shield thermocouples or for heat exchanger applications are made in this way.

8.7.1.4. Tape Forming

Tape forming, shown in Fig. 8-34D, is used to make thin ceramic parts like alumina substrates for integrated circuit chips and special capacitors. A thin layer of slip is laid on a flat carrier which can be a paper sheet or polymer film. A doctor blade controls the slip thickness, resulting in a tape that can be stamped into small shapes. These can be stacked or coiled for subsequent sintering.

8.7.1.5. Injection Molding

In injection molding, a hybrid process, ceramic powder is mixed with thermosetting (organic) polymer binder and injected under pressure into a die or mold. The bodies are then ejected and sintered while new ones are replicated. Complex parts with excellent dimensional control can be made in this way, including many of those proposed for use in all ceramic engines.

8.7.2. Densification

8.7.2.1. Firing

As anyone who has made pottery knows, the dried green ware is next fired in a furnace to densify it into a hard body. Firing temperatures vary depending on the composition of the body, as the following brief listing indicates.

Ceramic	Approximate firing temperature (°C)
Porcelain enamels (on cast irons and steels)	650–950
Clay products (bricks, sewer pipes, earthenware, pottery)	1000–1300
Whitewares (porcelain, china, sanitary ware)	1000–1300
Refractories (alumina, silica and magnesia brick, silicon carbide)	1300–1700
Electronic and newer ceramics (aluminas, ferrites, titanates)	1300–1800

As a rough proposition highly fluxed bodies containing silica and alkali oxides are fired at lower temperatures than bodies richer in alumina and magnesia.

Note that the colored designs on the surface of ceramic ware often require application of an appropriately compounded glaze and a *second firing*. The glass that forms fills all the pores, making the body impervious to water penetration.

Reactions that occur during firing are generally complex. They have been studied in kaolin using microscopy, diffraction techniques, and calorimetry (to measure heat absorption). It is instructive to follow the sequence of events depicted in Fig. 8-35 as the temperature is raised. The kaolinite (clay) crystals remain intact until 450°C, when they decompose into a noncrystalline mass; simultaneously heat is absorbed and water is expelled. There is little shrinkage in the green body up to a temperature of ~600°C, although by this time most of the weight loss has occurred. Then at about 1000°C both alumina and mullite ($3Al_2O_3 \cdot 2SiO_2$) crystallize as heat is liberated; these reactions are accompanied by a large rate of shrinkage. At higher temperatures mullite crystals grow in size and are surrounded by the glassy (vitreous) phase that pulls the particles together by surface tension forces. At 1200°C cristobalite crystallizes from the surrounding silica-based glass, and again shrinkage and pore reduction occur at a high rate. The significant shrinkage that occurs must be accounted for in the original design of all ceramic products.

8.7.2.2. Sintering

Sintering has already been discussed on two prior occasions (see Sections 6.6.3 and 8.4.3). Only a few comments of relevance to ceramics are made here. Perhaps the chief problem associated with the sintering of ceramics is the retention of porosity. One consequence is a resultant product that is opaque because of efficient light scattering by pores. Sintering under pressure (hot

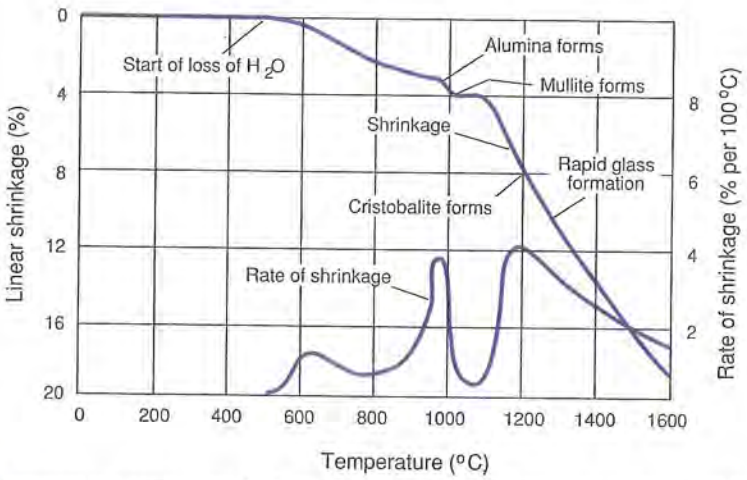

FIGURE 8-35 Processes that occur during the firing of kaolin as a function of temperature. From F. H. Norton, *Elements of Ceramics*, Addison–Wesley, Cambridge, MA (1952).

pressing) is often effective in collapsing pores. But there are systems in which pores are stubborn and cannot be easily removed because they exist in the interior of grains. If voids can be brought to grain boundaries, the resulting enhanced mass and vacancy transport there are effective in eliminating them. A strategy that will work is to limit exaggerated grain growth through suitable alloy additions. This prevents stable pores from being isolated too far from grain boundaries. In this way addition of MgO to Al_2O_3 eliminates porosity, yielding a translucent product that is used as an envelope for high-pressure sodium vapor lamps. In the same vein, 9 mol% La_2O_3 (lanthana)-strengthened Y_2O_3 (yttria) has been developed as an infrared window material (Fig. 8-36).

Together with the use of liquid-phase sintering aids to enhance pore closure, improved physical pressing and processing techniques have enabled production of denser ceramics. **Hot isostatic pressing** (HIP), schematically shown in Fig. 8-37, is one such method that goes well beyond simple isostatic pressing discussed earlier. The practice of HIPing has dramatically improved the quality not only of sintered ceramics and metals, but of cast metals as well. Parts to be HIPed are placed within a chamber that is first evacuated and then pressurized with inert gas to levels of ~3000 atm. Simultaneously, parts are heated to temperatures of up to ~2000°C. This combination of hot uniform squeezing from all directions shrinks pores and allows full density to be achieved in many cases; however, HIP equipment and operating costs are high.

FIGURE 8-36 Pore-free sintered ceramic products. Tubes in the foreground are used in sodium vapor lamps and are made of translucent Al_2O_3. The clear dome, tensile bar, and other shapes are composed of Y_2O_3 strengthened with La_2O_3. Courtesy of W. H. Rhodes, Osram Sylvania.

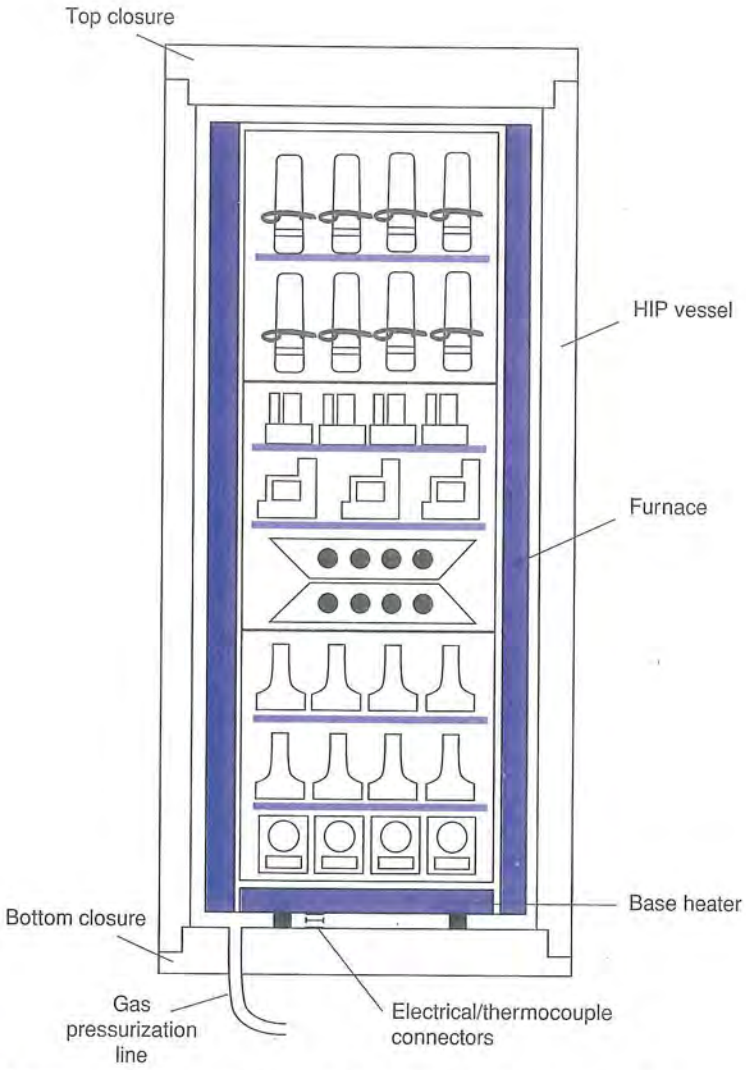

FIGURE 8-37 Schematic of a HIP system. Courtesy of HIP Division, Howmet, Whitehall, MI.

8.8. PERSPECTIVE AND CONCLUSION

When viewed from the world of processing, materials are surprisingly similar. The *micro*scopic electronic and atomic structural distinctions between materials are not directly relevant and blur somewhat when it comes to issues of shaping or forming them. Rather, the *macro*scopically linked thermomechanical flow properties of materials are capitalized on. It is the characteristic

temperatures (e.g., melting points, diffusion temperatures) and flow parameters (e.g., yield stress, viscosity) that are the important variables in shaping. If melting temperatures are easily attained, as they are in most metals, polymers, glasses, and semiconductors, then casting or solidification processing is practiced. Ceramic materials simply melt at inaccessible temperatures and, therefore, cannot be cast or otherwise be processed in the liquid state. This accounts for the extensive use of powder processing in ceramics and high-melting-point metals.

Because they are worked at the lowest as well as the highest viscosities, metals are singular with respect to materials processing. They are cast, mechanically formed, and consolidated by powder processing; no other class of material enjoys the same wide choice of possibilities. **Solidification processing** is possible because of their very low viscosity (10^{-3} Pa-s) compared with molten polymers and glasses ($\eta = \sim 10^3$ Pa-s). This combined with high density enables liquid metal to be poured easily and fill molds readily. Although heat transfer considerations determine the overall solidification rates, it is the combination of nucleation–growth effects treated in Chapter 6 that determines the size, shape, and composition of the grains within the solid. **Deformation processing** is another route to shaping metals. The most effective way to deform them is to ensure the presence of large amounts of plastic shear stresses induced by working above the yield stress. Both hot and cold plastic deformation are practiced, the former for large shapes and high-strength metals, the latter for thin stock and for finishing operations. Fortunately, metals are relatively plastic and flow sufficiently—during rolling to be reduced in thickness, during forging to fill dies, during extrusion and drawing to be reduced in area, and during sheet forming to be stretched into varied shapes.

Polymers and glasses can be liquefied but the viscosity is relatively high so they cannot be poured as easily as metals. Both are commonly shaped at viscosity levels of $\eta = \sim 10^3$ to 10^5 Pa-s, requiring simultaneous application of pressure or stress to make sure they assume the desired shape during molding or blowing operations. (Metals cannot normally be blown because viscosity levels never assume these intermediate levels.) The chief reason that polymers enjoy processing advantages relative to both metals and glasses is the very low temperatures required. For example, plastic bottles are typically blown at ~100°C compared with ~1000°C for glass bottles. In addition, polymer forming loads are often lower than those for metals. Having emphasized distinctions between polymers and metals, it is only fair that we point out similarities, for example, between injection molding and die casting, between compression molding and closed die forging, and extrusion in both materials.

Ceramics always require a two-step processing treatment: the first to form or mold them into a green product or compact, and the second to fire or sinter them. The difficulty of these steps depends on the ceramic in question. Traditional ceramics are generally easier to process than the new ceramics because the low-melting glassy phase helps to bind and consolidate particles

on firing. For new ceramics, hot pressing and sintering routes must often be followed in the quest to achieve fully dense products. High melting points and compressive strengths, coupled with low ductility, limit conventional deformation processing of ceramics.

Computer-aided design of components and control of processing methods are increasingly the keys to achieving desirable properties. The aim is to control dimensional tolerances, chemical composition and uniformity, grain size and microscopic porosity, as well as eliminate macroscopic defects such as cracks. These are generic concerns common to very different materials that are often shaped in remarkably similar ways.

Additional Reading

L. Edwards and M. Endean, Eds., *Materials in Action Series: Manufacturing with Materials*, Butterworths, London (1990).
M. C. Flemings, *Solidification Processing*, McGraw–Hill, New York (1974).
R. M. German, *Powder Metallurgy Science*, 2nd ed., Metal Powder Industries Federation, Princeton, NJ (1994).
S. Kalpakjian, *Manufacturing Processes for Engineering Materials*, 2nd ed., Addison–Wesley, Reading, MA (1991).
J. A. Schey, *Introduction to Manufacturing Processes*, 2nd ed., McGraw–Hill, New York (1987).

QUESTIONS AND PROBLEMS

8-1. Consider metal maintained at T_M initially in contact with a semi-infinite long mold at temperature T_0. As solidification occurs, latent heat (H in J/g) is released and this heat flows into the mold. The problem is like that of diffusion into a semi-infinite matrix. Therefore, by Eq. 6-3, $[T(x, t) - T_0]/[T_M - T_0] = \text{Erfc}[x/(4\alpha t)^{1/2}]$.
   a. If the heat flux (Q) is defined as $-\kappa dT/dx$, consult a calculus book to determine Q at $x = 0$. (Answer: $Q = \kappa[T_M - T_0]/(\pi\alpha t)^{1/2}$.)
   b. Show that the rate of heat production at the melt–solid interface is given by $Q_{L-S} = \rho H\, dS_i/dt$.
   c. By equating the two heat fluxes and integrating, obtain Eq. 8-1.

8-2. Metal castings of a sphere and a cube of the same metal have the same surface area. What is the ratio of the solidification times for the sphere and the cube?

8-3. Castings of a sphere and a cube of the same metal have the same volume. What is the ratio of the solidification times for the sphere and the cube?

8-4. Copper is cast into two different insulating molds of the same rectangular geometry, under identical conditions. Mold 1 is sand with the following properties: specific heat = 1150 J/kg-K, thermal conductivity = 0.6 W/m-K, density 1400 kg/m^3. Mold 2 is mullite investment with the following properties: specific heat = 750 J/kg-K, thermal conductivity = 0.5 W/m-K, density 1600 kg/m^3. What is the ratio of the times required for these two castings to solidify?

8-5. Magnesium and aluminum are poured into identical sand molds at 25°C from their respective melting temperatures. For Mg, heat capacity = 1300 J/kg-K and latent heat of fusion = 360 kJ/kg. For Al, heat capacity = 1100 J/kg-K and latent heat of fusion = 390 kJ/kg. If it takes the Al casting 10 minutes to solidify, how long will it take the Mg casting to solidify?

8-6. Design the dimensions of a cylindrical riser with height twice the diameter that would be suitable to cast the bowling pin of Fig. 8-6. Assume the riser solidification time is 25% longer than that of the casting. The pin has a volume of 1000 cm^3 and a surface area of 700 cm^2.

8-7. What casting process would you recommend to make the following items?
a. A large bronze ship propeller
b. Steel railroad wheels
c. Aluminum sole plates for electric steam irons
d. Iron base for a lathe
e. Aluminum engine block for a lawn mower
f. Steel pressure vessel tubes
g. Nickel-base alloy turbine blades
h. Large brass plumbing valves

8-8. South American natives have made beautiful jewelry containing platinum–gold alloys for centuries. How do you account for this if these alloys, bits of which are found in nature, melt at much higher temperatures than could be reached in their furnaces?

8-9. Under uniaxial tension, plastic deformation initiates in a tensile bar at a stress level of 400 MPa. It is desired to deform a plate of this material plastically by applying biaxial stresses. If one of the stresses is compressive of magnitude 220 MPa, what is the minimum stress (magnitude and sign) that must be applied in the transverse direction?

8-10. A work hardening cylinder of annealed brass 5 cm in diameter and 5 cm in height is compressed. If the true stress–true strain relationship for this metal is $\sigma = 895\varepsilon^{0.49}$ MPa, calculate the load required to compress the cylinder to half its height if there is no friction between the metal and anvils.

8-11. Derive a formula for the total forging load L on a rectangular solid of cross-sectional area $2a \times w$ by directly integrating $\int \sigma_y \, dx$ using Eq. 8-5 for σ_y. Verify the answer to illustrative Example 8-2 using this formula.

8-12. A rectangular solid block of unit depth, $a = 0.2$ m, and $h = 0.15$ m is forged with $f = 0.3$.
a. What is the fractional change in the maximum forging stress or pressure if the coefficient of friction changes by 10%?
b. What is the fractional change in the maximum forging stress if the yield stress changes by 10%?
(*Hint:* Determine $d\sigma_y/\sigma_y$ in terms of df and $d\sigma_0$.)

8-13. Show that if a steel plate enters the rolls at an initial velocity v_0 with thickness h_0 and width w, and leaves with velocity v_f, thickness h_f, and the same width, then $v_f > v_0$ (i.e., steel speeds up on the exit side).

8-14. If the diameter d of a wire is reduced 50% in length during drawing, what is the percentage reduction in area?

8-15. a. A material is reduced in area by 50% by extrusion. What is the extrusion ratio?
b. What percentage reduction in area does an extrusion ratio of 95 correspond to?

8-16. Circular disks of sheet steel 0.01 m thick and 0.15 m in diameter are punched out of a plate. If the tensile stress of the steel is 80,000 psi, what shearing force is required?

8-17. What problem do you foresee during deep drawing of metal cups:
a. If the punch used has too small a radius of curvature at the edge?
b. If there is too much clearance between punch and die?
c. If the sheet is held too loosely due to insufficient hold-down forces?
d. If the necking strain is exceeded?
e. If the sheet metal is strongly anisotropic?

8-18. Suggest possible ways of producing different powder sizes during atomization processes in metals.

8-19. Enumerate the similarities and contrast the differences in:
a. Pressing and sintering metal and ceramic powders.
b. Components made by casting and by powder metallurgy.
c. Shaping parts by forging and by powder metallurgy.
d. Extruding metals and polymers.

8-20. Why are polymers not normally shaped into parts by the powder metallurgy processes employed for metals and ceramics?

8-21. What pressure is required to extrude a bar of stainless steel at 1000°C from an initial diameter of 10 cm to 2.5 cm?

8-22. It is desired to make 4000 polymer gears per hour, each measuring 3 cm in diameter and 0.5 cm thick. What capacity press is required to injection mold them if a 120-MPa die pressure must be applied and the cycle time is 15 seconds?

8-23. Are thermosetting polymers suitable for injection molding processes? Explain.

8-24. A considerable amount of heat is generated by the interaction between the rotating auger and the churning polymer feedstock during extrusion. Suppose a 4-kW motor is used and 70% of the power goes into heating polyethylene fed at a rate of 100 kg/h. If the heat capacity of polyethylene is 1.4 J/g-°C, what will the temperature rise be in a half-hour? Assume no heat loss.

8-25. The following values were obtained for 7740 glass:

	Temperature		Viscosity (Pa-s)
	°C	K	
Annealing point	~580	853	10^{12}
Softening point	~830	1103	$10^{6.65}$
Strain point	~530	803	$10^{13.5}$
Working point	~1230	1503	10^{3}

a. From annealing and softening point data calculate E_η. Compare this value with that obtained from strain and working point data for this glass. (This shows that it is not wise to obtain E_η from only two data points.)

b. Determine a value for E_η by making an Arrhenius plot using all four sets of data.

8-26. Why is fused silica so much harder to shape than soda-lime glass?

8-27. Molten glass is compounded to flow easily during shaping or mold filling operations. Glazes and enamels are also glasses, but they must adhere to the fired ceramic or metal surface. Would you expect the compositions to differ in glasses as opposed to glazes and enamels? Mention one required property difference.

8-28. Crucibles used for melting 25 charges of silicon for single-crystal growth are made of the purest grade of fused silica and have the shape of a rounded cup with a flat bottom. The wall thickness is ~6 mm and the maximum crucible diameter is ~25 cm. Suggest a way to make these crucibles.

8-29. Tempered glass is strengthened by rapid cooling of the surface with an air blast after the glass is processed near the softening point. After cooling, the surface layers are under compression while the bulk of the interior is stressed in tension. Explain how such a state of residual stress develops.

8-30. a. A soda-lime glass has a viscosity of $10^{13.5}$ Pa-s at 570°C. If the activation energy for viscous flow is 400 kJ/mol, what is the expected viscosity at 670°C?

b. At what temperature will the viscosity be 10^9 Pa-s?

8-31. One way to strengthen surface layers of glass is to chemically diffuse in oversized alkali ions (e.g., K^+) that replace the original Na^+ ions. What state of stress develops at the surface and interior of a piece of soda-lime glass so treated?

8-32. Contrast structural and chemical differences in Al_2O_3 used for (1) substrates for microelectronic applications, (2) transparent tubes for sodium vapor lamps, and (3) furnace brick. Note any special processing requirements for these applications.

8-33. Why do ceramic bodies undergo much larger shrinkages than powder metal parts during high-temperature processing?

8-34. Porosity in ceramics is usually undesirable but there are applications where they are desired. Contrast these applications.

8-35. Why is thick ceramic ware more prone to cracking than thin ware during its processing?

8-36. A formula that describes the time (t in minutes)-dependent fractional shrinkage in length ($\Delta L/L$) of a sintered ceramic plate product is $\Delta L/L = A[\exp(-E/RT)]t^{2/5}$, where A is a constant, E is the activation energy for sintering, and RT has the usual meaning. At 1300°C and $t = 100$ minutes, $\Delta L/L = 0.05$; at 1200°C and $t = 100$ minutes, $\Delta L/L = 0.005$. Calculate A and E.

8-37. Assume that the formula $\Delta L/L = A[\exp(-E/RT)]t^{2/5}$ accurately describes the sintering of WC drawing dies. For this application the fractional shrinkage $\Delta L/L$ must be controlled to be 0.05 ± 0.003. If the sintering process is carried out at 1400°C for 60 minutes and $E = 420$ kJ/mol, what maximum variation in furnace temperature can be tolerated?
[*Hint:* Evaluate $(\Delta L/L)^{-1}\, d(\Delta L/L)/dT$.]

8-38. What is the probable method for fabricating the following ceramic objects?

a. A rare Ming dynasty vase
b. Bathroom wall tiles
c. Cups for a tea set
d. Spark plug insulation
e. A rotor for an all-ceramic engine